Characterization of vascular heterogeneity of astrocytomas grade 4 for supporting patient prognosis estimation, and treatment response assessment.

DOCTORAL THESIS

Presented by

María del Mar Álvarez Torres

Directed by

Dr. Juan M. García Gómez

Dr. Elies Fuster Garcia

Valencia, Spain

August 2022

UNIVERSITAT POLITÈCNICA DE VALÈNCIA

Abstract

Brain tumors are one of the most devastating diseases today because of the significant cognitive impairment suffered by patients, high mortality rates, and poor prognosis. Astrocytomas grade 4 bring five-year survival in approximately 5% of diagnosed patients, being the most aggressive and lethal tumors of the Central Nervous System (CNS).

Astrocytomas grade 4 continue to be an unresolved complex medical problem. Despite accounting for more than 60% of malignant brain tumors in adults, these tumors have a low relative prevalence and are considered an orphan disease, making difficult developing new drugs or treatments that might benefit patients.

The aggressiveness of these tumors is due to different characteristics, such as strong angiogenesis, necrosis, vascular microproliferation, the capacity of the tumor cells to invade and infiltrate, and a particular immune microenvironment. In addition, due to the rapid progression of astrocytomas grade 4, different specific regions coexist in the lesion area which change over time. This complex nature, along with the marked interpatient, intratumor, and longitudinal heterogeneity, makes complicate the success of a single efficient treatment for all patients.

Magnetic Resonance Imaging (MRI) represents a useful technique to characterize tumor morphology and vascularity. Using advanced and robust methods to analyze MR images collected from initial stages of patient management allows the delineation of different regions of astrocytomas grade 4, becoming useful tools for researchers, radiologists and neurosurgeons. In addition, the calculation of imaging vascular biomarkers, such as those proposed in this thesis, would facilitate tumor characterization, prognosis estimation and more personalized treatment approaches.

This thesis proposes four fundamental pillars to advance the management of astrocytomas grade 4. These include I) the multilevel characterization of the tumor to improve classifications of high-grade CNS gliomas; II) the search and development of robust biomarkers for estimating patient prognosis from the presurgical moment; III) as well as for evaluating the response to treatments and the selection of patients who may benefit from specific therapies; and IV) the design and implementation of clinical studies and protocols for long-term collecting data from internationally remarkable cohorts of patients.

To address these four pillars, an interdisciplinary approach has been used that combines medical imaging analysis, advanced artificial intelligence techniques, and molecular, histopathological, and clinical variables.

Concluding, we have addressed the influence of both interpatient and intratumor heterogeneity of astrocytoma grade 4 for tumor characterization and classification, patient prognosis estimation and predicting treatment responses. In addition, different clinical studies have been designed and implemented allowing the collection of multilevel data from international cohorts of patients with astrocytoma grade 4.

Resumen

Los tumores cerebrales son una de las enfermedades más devastadoras en la actualidad por el importante deterioro cognitivo que sufren los pacientes, la elevada tasa de mortalidad y el mal pronóstico. Los astrocitomas de grado 4 conllevan una supervivencia de cinco años en aproximadamente el 5% de los pacientes diagnosticados, siendo los tumores más agresivos y letales del Sistema Nervioso Central (SNC).

Los astrocitomas de grado 4 siguen siendo un problema médico complejo aún sin resolver. A pesar de representar más del 60% de los tumores cerebrales malignos en adultos, estos tumores tienen una baja prevalencia relativa y se consideran una enfermedad huérfana, lo que dificulta el desarrollo de nuevos fármacos o tratamientos que puedan beneficiar a los pacientes.

La agresividad de estos tumores se debe a diferentes características, como la fuerte angiogénesis, la necrosis, la microproliferación vascular, la capacidad de invasión e infiltración de las células tumorales y un microambiente inmunológico particular. Además, debido a la rápida progresión de los astrocitomas de grado 4, en la zona de la lesión coexisten diferentes regiones específicas que cambian con el tiempo. Esta naturaleza compleja, junto con la marcada heterogeneidad interpaciente, intratumoral y longitudinal, complica el éxito de un único tratamiento eficaz para todos los pacientes.

La imagen de resonancia magnética (MRI) supone una técnica útil para caracterizar la morfología y la vascularidad del tumor. El uso de métodos avanzados y robustos para analizar las imágenes de MR recogidas en las fases iniciales del tratamiento de los pacientes permite la delimitación de las diferentes regiones de los astrocitomas de grado 4, convirtiéndose en herramientas útiles para investigadores, radiólogos y neurocirujanos. Además, el cálculo de biomarcadores vasculares de imagen, como los propuestos en esta tesis, facilitaría la caracterización del tumor, la estimación del pronóstico y los enfoques de tratamiento más personalizados.

Esta tesis propone cuatro pilares fundamentales para avanzar en el manejo de los astrocitomas de grado 4. Estos incluyen I) la caracterización multinivel del tumor para mejorar las clasificaciones de los gliomas de alto grado del SNC; II) la búsqueda y desarrollo de biomarcadores robustos para estimar el pronóstico de los pacientes desde el momento prequirúrgico; III) así como para evaluar la respuesta a los tratamientos y la selección de los pacientes que pueden beneficiarse de terapias específicas; y IV) el diseño e implementación de estudios clínicos y protocolos para la recogida de datos a largo plazo de cohortes de pacientes notables a nivel internacional.

Para abordar estos cuatro pilares, se ha utilizado un enfoque interdisciplinario que combina el análisis de imágenes médicas, técnicas avanzadas de inteligencia artificial y variables moleculares, histopatológicas y clínicas.

En conclusión, hemos abordado la influencia de la heterogeneidad interpaciente e intratumoral del astrocitoma de grado 4 para la caracterización y clasificación del tumor, la estimación del pronóstico del paciente y la predicción de las respuestas al tratamiento. Además, se han diseñado e implementado diferentes estudios clínicos que permiten la recogida de datos multinivel de cohortes internacionales de pacientes con astrocitoma de grado 4.

Resum

Els tumors cerebrals són una de les malalties més devastadores en l'actualitat per la important deterioració cognitiva que pateixen els pacients, l'elevada taxa de mortalitat i el mal pronòstic. Els astrocitomes de grau 4 comporten una supervivència de cinc anys en aproximadament el 5% dels pacients diagnosticats, sent els tumors més agressius i letals del Sistema Nerviós Central (SNC).

Els astrocitomes de grau 4 continuen sent un problema mèdic complex encara sense resoldre. Malgrat representar més del 60% dels tumors cerebrals malignes en adults, aquests tumors tenen una baixa prevalença relativa i es consideren una malaltia òrfena, la qual cosa dificulta el desenvolupament de nous fàrmacs o tractaments que puguen beneficiar als pacients.

L'agressivitat d'aquests tumors es deu a diferents característiques, com la forta angiogènesis, la necrosi, la microproliferació vascular, la capacitat d'invasió i infiltració de les cèl·lules tumorals i un microambient immunològic particular. A més, a causa de la ràpida progressió dels astrocitomes de grau 4, en la zona de la lesió coexisteixen diferents regions específiques que canvien amb el temps. Aquesta naturalesa complexa, juntament amb la marcada heterogeneïtat interpacient, intratumoral i longitudinal fa que es complique l'èxit d'un únic tractament eficaç per a tots els pacients.

L'imatge de ressonància magnètica (MRI) suposa una tècnica útil per a caracteritzar la morfologia i la vascularitat del tumor. L'ús de mètodes avançats i robustos per a analitzar les imatges de MR recollides en les fases inicials del tractament dels pacients permet la delimitació de les diferents regions dels astrocitomes de grau 4, convertint-se en eines útils per a investigadors, radiòlegs i neurocirugians. A més, el càlcul de biomarcadors vasculars d'imatge, com els proposats en aquesta tesi, facilitaria la caracterització del tumor, l'estimació del pronòstic i els enfocaments de tractament més personalitzats.

Aquesta tesi proposa quatre pilars fonamentals per a avançar en el maneig dels astrocitomes de grau 4. Aquests inclouen I) la caracterització multinivell del tumor per a millorar les classificacions dels gliomes d'alt grau del SNC; II) la cerca i desenvolupament de biomarcadors robustos per a estimar el pronòstic dels pacients des del moment prequirúrgic; III) així com per a avaluar la resposta als tractaments i la selecció dels pacients que poden beneficiar-se de teràpies específiques; i IV) el disseny i implementació d'estudis clínics i protocols per a la recollida de dades a llarg termini de cohorts de pacients notables a nivell internacional.

Per a abordar aquests quatre pilars, s'ha utilitzat un enfocament interdisciplinari que combina l'anàlisi d'imatges mèdiques, tècniques avançades d'intel·ligència artificial i variables moleculars, histopatològiques i clíniques.

En conclusió, hem abordat la influència de l'heterogeneïtat interpacient i intratumoral del astrocitoma de grau 4 per a la caracterització i classificació del tumor, l'estimació del pronòstic del pacient i la predicció de les respostes al tractament. A més, s'han dissenyat i implementat diferents estudis clínics que permeten la recollida de dades multinivell de cohorts internacionals de pacients amb astrocitoma de grau 4.

Acronyms

AACR American Association of Cancer Research

AI Artificial Intelligence

AIF Arterial Input Function

α-KG α- Ketoglutaric acid

ASL Arterial Spin Labeling

BBB Blood Brain Barrier

BDSLab Biomedical Data Science laboratory

BVZ Bevacizumab

C Contribution

CD Cluster of Differentiation

CDKN Cyclin-Dependent Kinase Inhibitor

CNN Convolutional Neural Network

CNS Central Nervous System

CP Complementary Publication

CS Clinical Study

CTLA-4 Cytotoxic T-Lymphocyte Antigen 4

D Dataset

D2HG D-2-Hydroxyglutarate

DCE Dynamic Contrast Enhanced

DNA Deoxyriblonucleic Acid

DSC Dynamic Susceptibility Contrast

DWI Diffusion-Weighted Imaging

EANO European Association of Neuro-Oncology

EGFR Epidermal Growth Factor Receptor

ET Enhancing Tumor

FLAIR Fluid Attenuation Inversion Recovery

GBCA Gadolinium-Based Contrast Agent

GBM Glioblastoma

GliMR Glioma Magnetic Resonance European group

H&E Hematoxylin and Eosin

HAT High Angiogenic Tumor

HR Hazard Ratio

HTS Hemodynamic Tissue Signature

IDH Isocitrate dehydrogenase

IDO1 Indoleamine 2,3 dioxygenase 1

IPE Infiltrated Peripheral Edema

Ivy GAP Ivy Glioblastoma Atlas Project

KM Kaplan Meier

KPS Karnofsky Performance Status Scale

LAT Low Angiogenic Tumor

mAbs Monoclonal antibodies

MGMT O6-Methylguanine-DNA Methyltransferase

MMR Mismatch Repair

MR Magnetic Resonance

MRI Magnetic Resonance Imaging

MTT Mean Transit Time

Mut Mutant

MVA Microvessel Area

MVD Microvessel Density

MVP Microvascular Proliferation

NADP+ Nicotinamide Adenine Dinucleotide Phosphate

NMR Nuclear Magnetic Resonance

O Objective

OCT Optimial Cutting Temperature

OS Overall Survival

P Publication

PD Proton Density

PD-1 Programmed cell Death protein 1

PDL-1 Programmed Death-Ligand 1

PFS Progression Free Survival

PTEN Phosphatase and Tensin homolog

PWI Perfusion Weighted Imaging

qMRI quantitative MRI

RB1 Retinoblastoma Protein 1

rCBF relative Cerebral Blood Flow

rCBV relative Cerebral Blood Volume

RCT Randomized Controlled Trial

RF Radio-Frequency

RNA Ribonucleic Acid

RNAseq RNA sequencing

ROI Region of Interest

RQ Research Question

srCBV Standardized rCBV

TCIA The Cancer Imaging Archive

TE Echo Time

TMB Tumor Mutational Burden

TME Tumor Microenvironment

TMZ Temozolomide

TR Repetition Time

UPV Universitat Politècnica de València

VEGF Vascular Endothelial Growth Factor

VPE Vasogenic Peripheral Edema

WHO World Health Organization

Wt Wildtype

Contents

Chapter 1

Introduction

1.1. Motivation

Cancer is a leading cause of death worldwide, accounting for nearly 10 million deaths in 2020, representing approximately one in six deaths. Fortunately, many types of cancer can be cured if detected early, diagnosed adequately, and treated effectively. These advances are mainly due to biomedical research, clinical trials, and technology efforts during the last decades. In this context, some types of cancer, such as astrocytomas grade 4 stand out for their extremely aggressive nature, presenting one of the poorest prognoses among all human cancers, with a median patient survival of 12-14 months, and remaining as an unsolved problem.

In this context, the need to investigate the behavior of these high-grade gliomas is vital for improving the prognosis and quality of life of patients. From the diagnosis, and throughout patient treatment and follow-up, a considerable amount of multilevel data is generated (e.g., medical imaging, histopathological and molecular analysis, and clinical variables). One of the main non-invasive tools to visualize and guide doctors managing patients with brain tumors is Magnetic Resonance Imaging (MRI). This medical imaging modality allows radiologists to make a first diagnosis of the patient, and follow-up of the lesion to detect tumor recurrence during and after treatment. Following the development of artificial intelligence (AI) techniques, the information that MRI can provide has been a breakthrough.

The possibility of using automatic segmentation methodologies of the tumor and its environment, and calculating biomarkers associated with relevant clinical outcomes, has been the support for the development of this thesis. The routine acquisition of clinical MRI modalities, such as perfusion, allows the characterization of some of astrocytomas' main hallmarks, including the strong angiogenesis and high microvascular proliferation. This can be done from diagnosis and in a completely non-invasive manner. In addition, this vascular characterization through imaging allows a better classification of high-grade gliomas since it is associated with the underlying molecular and histopathological profiles.

Providing the same treatment for all patients with astrocytoma grade 4 is an inefficient strategy, revealing the need for precision therapies. Against this background, the personalization of chemo- and radiotherapy (providing optimal doses, cycles, and

timing), the provision of specific second-line treatments, or the selection of suitable patients for novel clinical trials, becomes an imperative. MRI biomarkers can be valuable tools to stratify groups of patients with similar tumor characteristics and to evaluate specific treatment responses.

This thesis confronts all the factors mentioned above. The thesis focuses on the combination of MRI vascular assessment on clinical, histopathological, and molecular data to characterize astrocytomas grade 4, support patient prognosis estimation and assess treatment responses. These premises have established this work's main motivation and goals, leading to the following research questions and objectives.

1.2. Research Questions and Objectives

After analyzing the state of the art of the medical problem exposed in the motivation, four fundamental areas of action were defined, and guided the structure of this thesis:

Part I. Tumors characterization and classification. Due to the highly variable nature of these gliomas, a deeper characterization is still needed. In addition, considering the last update of the World Health Organization (WHO) classification of CNS tumors, for a correct classification and patient monitoring, it is critical to identify the *Isocitrate Dehydrogenase* (*IDH*) mutation, and to detect and quantify the microvascular proliferation. Currently, these two factors only can be defined analyzing samples collected during tumor biopsy or surgery. Their estimation using automatic analysis of routinary MRIs would allow performing this characterization from the diagnostic time and in a non-invasive manner, allowing an early characterization and classification.

Part II. Patient prognosis estimation and stratification. Predicting the survival time of each patient is a challenging task mainly due to the marked interpatient heterogeneity. Finding robust biomarkers that could be calculated from the earliest stage may be of great value both for improving prognostic models and for stratifying patients into specific groups. In addition, due to temporal heterogeneity, it is necessary to identify the influence on survival of different hallmarks, such as vascularity, throughout follow-up.

Part III. Treatment responses assessment. Considering the lack of improvement in patient prognosis since 2005 when Stupp proposed the standard treatment, it seems evident that the *same treatment* approach for all patients is not enough. To improve patient survival times and quality of life, it is vital to personalize treatments according to tumor and patient characteristics, as well as for evaluating responses to new therapies. In this sense, non-invasive biomarkers can be useful tools for helping in treatment response assessment and selecting patients who benefit from specific therapies.

Part IV. Clinical studies design and implementation and datasets creation. To perform studies addressing the three previous parts, it is essential to collect a remarkable amount of multilevel data from patients with astrocytoma grade 4. To do so, it is needed to design and implement clinical studies and create relevant datasets.

Then, the following specific research questions (RQ) and objectives (O) were proposed for each proposed conceptual part:

Part I. Tumors characterization and classification

- **RQ1.** Are MRI dynamic susceptibility contrast (DSC) perfusion (MRI-DSC) biomarkers associated with microvascular proliferation (MVP), and therefore useful for astrocytoma grade 4 classification?
- **RQ2.** Are glioblastoma *IDH*-wildtype and astrocytoma *IDH*-mutant grade 4 different at vascular genes expression? Can be these potential differences detected by MRI-DSC biomarkers?

Part II. Patient prognosis estimation and stratification

- **RQ3.** Are the MRI-DSC biomarkers calculated at vascular tumor and edema habitats reproducible in an international multicenter setting with different clinical and MRI acquisition protocols?
- **RQ4.** Is the prognostic capability of the MRI-DSC biomarkers, calculated at presurgical stage, robust in an international multicenter setting?
- **RQ5.** Is moderate tumor vascularity beneficial in terms of prognosis in both long- and short-term survivors (LTS and STS) of astrocytoma grade 4?

Part III. Treatment response assessment

- **RQ6.** Does tumor vascularity influence patient response to Temozolomide (TMZ) treatment in terms of survival? Can MRI-DSC biomarkers determine subgroups of patients who benefits most from extending the TMZ treatment?
- **RQ7.** Can we define clinical and imaging features to select patients who can benefit from immunotherapy with programmed cell death protein 1 inhibitor (anti-PD-1)?

Part IV. Clinical studies implementation and datasets creation

- **RQ8.** Can we design and implement clinical protocols for long-term collection of biological samples from each tumor and edema vascular habitat found at astrocytoma grade 4?

The research work conducted in this thesis aims to provide answers and solutions to these questions using a interdisciplinary approach that combines knowledge from fields such as Medical Image Analysis, Molecular Biology, Histopathology or

Neuro-Oncology. To this end, different collaborations have been carried out during the development of this thesis.

According to the defined research questions, the following specific objectives were proposed for each part:

Part I. Tumors characterization and classification

- **O1.** To study the potential contribution of MRI-DSC biomarkers calculated at the presurgical stage for astrocytoma grade 4 classification by analyzing its association with MVP.
- **O2.** To evaluate the potential use of MRI-DSC biomarkers to spatially detect the presence and magnitude of microvessels in astrocytoma grade 4.
- **O3.** To analyze vascular differences between glioblastoma *IDH*-wildtype and astrocytoma *IDH*-mutant grade 4 at transcriptomic and imaging levels.

Part II. Patient prognosis estimation and stratification

- **O4.** To validate the reproducibility at multicenter and international levels of MRI-DSC biomarkers calculated at the tumor and edema vascular habitats in astrocytomas grade 4.
- **O5.** To assess the robustness of the association between vascularity, defined by MRI-DSC biomarkers calculated at tumor and edema habitats, and overall survival (OS) in patients with astrocytomas grade 4.
- **O6.** To evaluate whether a moderate vascularity is beneficial in terms of survival for both LTS and STS of astrocytoma grade 4.

Part III. Treatment response assessment

- **O7.** To analyze the combined effect of vascularity and relevant molecular alterations on patient response to TMZ in terms of survival. As well as to select subgroups of patients who could benefit from a prolonged TMZ treatment.
- **O8.** To define clinical and imaging features useful for selecting patients with glioblastoma *IDH*-wildtype who can benefit from the immunotherapy with anti-PD-1.

Part IV. Clinical studies implementation and datasets creation

- **O9.** To design and implement a clinical protocol to collect biologic samples from each vascular habitat found at astrocytoma grade 4.
- **O10.** To collect an international dataset with data of different nature (clinical, imaging, and molecular) of a remarkable number of patients with astrocytoma grade 4.

The proposed objectives enclose the main goal of this thesis: *chatacterizing vascular heterogeneity of astrocytoma grade 4 for supportinh patient prognosis estimation, and treatment responses assessment.* This goal can also be decomposed in two strands depending on the research scope and approach: *I)* the scientific goal, which intends to provide new knowledge about heterogeneity in astrocytoma grade 4, focused on tumor and edema vascularity from molecular, histopathological and imaging levels, and *II)* the clinical goal, which aims to improve clinical decision making by contributing to astrocytoma grade 4 classification, as well as improving both patient prognosis and treatment response predictive models. In this sense, the following scientific contributions support the achievement of the proposed objectives.

1.3. Thesis contributions

This section presents the main contributions derived from this thesis. First, a summary of the most relevant aspects of each contribution is presented. Next, the publications in scientific journals and congress are listed, as well as the clinical studies led, and the databases generated during the thesis. Finally, the basic information of the performed projects, and the international research stay have been also included.

1.3.1. Main Contributions

C1. The proposal of MRI-DSC biomarkers to facilitate the classification of astrocytomas grade 4 from the presurgical stage in non-invasive way. The last classification of CNS tumors proposed by the WHO in 2021 defines the mutation in *IDH* gene and the presence of MVP as the most relevant criteria to classify astrocytomas grade 4. We have analyzed the potential role of MRI-DSC biomarkers calculated from the presurgical stage as surrogate markers to identify both MVP and *IDH* mutation. Positive results derived from the performed studies have been published in scientific journals P4 and P9 and presented in the international congress P5. In addition, complementary publications CP4, CP6 and CP7 are related with tumor characterization and high-grade glioma classification (see *subsection 1.3.2*, which includes scientific publications).

C2. International multicenter validation of the prognostic capabilities of the MRI-DSC biomarkers calculated with the vascular heterogeneity assessment method. To assess the prognostic capabilities of the MRI-DSC biomarkers calculated at vascular habitats, two international multicenter studies were conducted (CS1 and CS2). The CS1 consisted of a retrospective observational study in which data from more than 300 patients with astrocytoma grade 4 was included. This constituted the first multicenter clinical studyin which the Universitat Politècnica de València (UPV) was the sponsor (registered in clinicaltrials.gov; NCT03439332). (See subsection

1.3.3. for further information about clinical studies led during this thesis). Derived results were published in P2 and presented in the international congress P6. Considering these promising results and the success of the collaboration with the seven-participating hospitals, the clinical study CS2 was initiated in March 2020 to validate prospectively the previous results (currently in patient recruitment stage).

C3. **A better knowledge of the influence of tumor vascularity over time on relevant clinical outcomes comparing between long- and short-term survivors of astrocytoma grade 4.** A study analyzing the effect of tumor vascularity over time on patient survival was performed, including independent analysis for short- and long-term survivors. The results of this study were published in P3. In addition, to get a deeper knowledge about vascularity during tumor relapse, the potential application of DSC perfusion to differentiate tumor relapse from pseudo-progression has been analyzed in a review article in collaboration with the European GliMR group (sponsored by the COST action). These reviews are published in complementary publications CP1 and CP2.

C4. **The proposal of a more personalized approach for Temozolomide treatment based on the combined effect of O6-methylguanine-DNA methyltransferase (*MGMT*) methylation and tumor vascularity.** Two studies with independent multicenter cohorts of patients with astrocytomas grade 4 were performed to evaluate differences in the response to TMZ treatment. Results of both studies were consistent and complementary. The first study concludes that *MGMT* methylation may benefit overall survival (OS) in patients with moderately vascularized astrocytomas grade 4 (P7). The second study validated the lack of benefit of extending the TMZ treatment in patients with high vascularized tumors, and propose the MRI-DSC biomarkers, together to *MGMT* methylation status, to select the optimal number of TMZ cycles for each patient (published in P1 and presented in the international congress P8). These studies were carried out with data compiled during the development of the clinical study CS1 and dataset D4 (see subsection 1.3.3. for further information of clinical studies and datasets).

C5. **The proposal of tumor laterality as a clinically relevant factor to improve the selection of patients with astrocytoma grade 4 who benefit from immunotherapy with anti-PD1.** During the international research stay at the Rabadan Lab in Columbia University (see section 1.5), a cohort of patients treated with anti-PD1 was analyzed in order to find specific profiles or characteristics which help to select patients who responds well to this immunotherapy. The related scientific publication is still in process. Results derived from this study constitutes chapter 8 of this thesis.

C6. The design and implementation of clinical studies, as well as the compilation of multilevel data from 780 patients with astrocytoma grade 4 treated at 18 medical institutions. To achieve the proposed objectives, different clinical studies have been designed and implemented in collaboration with national and international hospitals (clinical studies CS1-CS3), allowing the compilation of different datasets D1-D3. Additionally, other retrospective datasets have been compiled during the thesis (datasets D4-D7). As a transversal contribution, an entire database with information from 780 patients with astrocytoma grade 4 treated at 18 institutions has been generated at the time of writing this thesis. It is estimated that at the end of the two clinical studies that are in progress (CS2 and CS3), the number will rise to more than 1,000 patients.

C7. Participation in the registration of the software ONCOhabitats (ND-494-2021). Coauthor (10%). Software desciption: ONCOhabitats is a platform for glioma analysis based on AI and MRI. The platform contains four modules: 1. MRI image preprocessing module, which improves image quality and eliminates possible artifacts; 2. Segmentation module, capable of determining and differentiating in the image the location of the edema, tumor and necrosis of the lesion; 3. Perfusion module, which calculates vascularity biomarkers from perfusion curves; 4. regions within the lesion that describe the vascular hetereogeneity of the lesion. A more detailed description of the software is included in complementary publication CP3, as well as in section 2.6 of chapter 2 of this thesis.

1.3.2. Scientific publications

1.3.2.1. Main publications

The main scientific publications, both in journals and conferences, derived from this thesis are listed below:

P1. María del Mar Álvarez-Torres, Elies Fuster-García, Carmen Balaña, Josep Puig, and Juan M. García-Gómez. *'Lack of benefit of extending Temozolomide treatment in patients with high vascular glioblastoma with methylated MGMT.'* Cancers, 2021; 13(21), 5420. (Álvarez-Torres M. *et al*, 2021a)[1]

IF: 6,64 (JCR 2020): 51/242 Oncology (Q1).

P2. María del Mar Álvarez-Torres, Javier Juan-Albarracín, Elies Fuster-Garcia, Fuensanta Bellvís-Bataller, David Lorente, Gaspar Reynés, Jaime Font de Mora, Fernando Aparici-Robles, Carlos Botella, Jose Muñoz-Langa, Raquel Faubel, Sabina Asensio-Cuesta, Germán A. García-Ferrando, Eduard Chelebian, Cristina Auger, Jose Pineda, Alex Rovira, Laura Oleaga, Enrique Mollà-Olmos, Antonio J. Revert,

Luaba Tshibanda, Girolamo Crisi, Kyrre E. Emblem, Didier Martin, Paulina Due-Tønnessen, Torstein R. Meling, Silvano Filice, Carlos Sáez, and Juan M. García-Gómez. *'Robust association between vascular habitats and patient prognosis in glioblastoma: An international multicenter study.'* Journal of Magnetic Resonance Imaging, 2019; 51(5):1478–1486. (Álvarez-Torres M. *et al*, 2019)[2]

IF: 3,95 (JCR 2019): 23/134 Radiology, Nuclear Medicine & Magnetic Resonance Imaging (Q1).

P3. María del Mar Álvarez-Torres, Elies Fuster-García, Gaspar Reynés, Javier Juan-Albarracín, Eduard Chelebian, Laura Oleaga, Jose Pineda, Cristina Auger, Alex Rovira, Kyrre E. Emblem, Silvano Filice, Enrique Mollà-Olmos, and Juan Miguel García-Gómez. *'Differential effect of vascularity between long- and short-term survivors with IDH1/2 wild-type glioblastoma.'* NMR in Biomedicine, 2021; 34(4):e4462. (Álvarez-Torres M. *et al*, 2021b)[3]

IF: 4,05 (JCR 2020): 34/134 Radiology, Nuclear Medicine & Magnetic Resonance Imaging (Q1); 18/71 Biophysics (Q1); 6/43 Spectroscopy (Q1).

P4. María del Mar Álvarez-Torres, Elies Fuster-García, Javier Juan-Albarracín, Gaspar Reynés, Fernando Aparici-Robles, Jaime Ferrer-Lozano and Juan Miguel García-Gómez. *'Local detection of microvessels in IDH-wildtype glioblastoma using relative cerebral blood volume: an imaging marker useful for astrocytoma grade 4 classification.'* BMC Cancer, 2022; 22, 40 (Álvarez-Torres M. *et al*, 2022)[4]

IF: 4,43 (JCR 2020): 110/242 Oncology (Q2).

P5. María del Mar Álvarez-Torres, Elies Fuster-Garcia, Carmen Balaña, Josep Puig, Gaspar Reynes, Kyrre Eeg Emblem, Enrique Mollà-Olmos, Jose Pineda, and Juan M. García Gómez. *'Relative cerebral blood volume of tumor habitats can differentiate presurgical IDH-wildtype glioblastoma from IDH-mutant astrocytoma grade 4.'* Proceedings: Joint Annual ISMRM-ESMRMB & ISMRT 31st Annual Meeting, 07-12 May 2022, London, England, UK.

P6. María del Mar Álvarez-Torres, Fuensanta Bellvís–Bataller, Javier Juan–Albarracín, Elies Fuster–Garcia, David Lorente Estellés, Gaspar Reynes, Fernando Aparici-Robles, Carlos Botella, Jose Muñoz-Langa, Raquel Faubel, Sabina Asensio-Cuesta, Germán García–Ferrando, Cristina Auger, Alex Rovira, Jose Pineda, Laura Oleaga, Jaime Font de Mora, Enrique Mollà-Olmos, Antonio Revert-Ventura, Luaba Tshibanda, Didier Martin, Girolamo Crisi, Kyrre E Emblem, Paulina Due-Tonnessen,

Torstein Meling, and Juan M García-Gómez. *'Preliminary results of the ONCOhabitats Study NCT03439332: A multicenter validation of overall survival estimation of patients with glioblastoma using vascular biomarkers.'* Proceedings: AACR Annual Meeting 2019; March 29-April 3, 2019; Atlanta, GA, USA.

P7. Elies Fuster-García, David Lorente Estellés, **María Del Mar Álvarez-Torre**s, Javier Juan-Albarracín, Eduard Chelebian, Alex Rovira, Cristina Auger Acosta, Jose Pineda, Laura Oleaga, Enrique Mollá-Olmos, Silvano Filice, Paulina Due-Tønnessen, Torstein R Meling, Kyrre E Emblem, and Juan M García-Gómez. '*MGMT methylation may benefit overall survival in patients with moderately vascularized glioblastomas.'* European Radiology, 2021; 31(3):1738-1747. (Fuster-Garcia E. *et al*, 2021)[5]

IF: 5,31 (JCR 2020): 22/133 Radiology, Nuclear Medicine & Magnetic Resonance Imaging (Q1).

P8. María del Mar Álvarez-Torres, Elies Fuster-Garcia, Javier Juan-Albarracín, Josep Puig, Carmen Balaña, Jaime Capellades, Kyrre E Emblem, and Juan M García-Gómez. '*Differential effect of MGMT methylation between moderate or high vascular profile in IDH wild-type glioblastoma.'* Proceedings: AACR Annual Meeting 2021; virtual.

P9. María del Mar Álvarez-Torres, Adolfo López-Cerdán, Maria de la Iglesia Vayá, Elies Fuster-Garcia, Francisco García-García, Juan Miguel García-Gómez. *'Vascular differences between glioblastoma IDH-wildtype and astrocytoma IDH-mutant grade 4 at imaging and transcriptomic level'.* Preprint in medRxiv, 2022. https://doi.org/10.1101/2022.06.20.22276639

1.3.2.2. Complementary publications

During the completion of the thesis, the author has participated in different studies in collaboration with researchers, generating complementary publications as co-author. All of them have focused on the analysis of high-grade gliomas.

CP1. Otto M Henriksen, **María del Mar Álvarez-Torres**, Patricia Figueiredo, Gilbert Hangel, Vera Catharina Keil, Ruben E Nechifor, Frank Riemer, Kathleen Schmainda, Esther Warnert, Evita Wiegers and Thomas Booth. *'High-Grade Glioma Treatment Response Monitoring Biomarkers: A Position Statement on the Evidence Supporting the Use of Advanced MRI Techniques in the Clinic, and the Latest Bench-to-Bedside Developments. Part I: Perfusion and Diffusion Techniques.'* Frontiers in Oncology, 2022.[6]

IF: 6,24 (JCR 2020): 62/242 Oncology (Q1).

CP2. Thomas Booth, **María del Mar Álvarez-Torres**, Patricia Figueiredo, Gilbert Hangel, Vera Catharina Keil, Ruben E Nechifor, Frank Riemer, Kathleen Schmainda ,Esther Warnert, Evita Wiegers and Otto M Henriksen. *'High-Grade Glioma Treatment Response Monitoring Biomarkers: A Position Statement on the Evidence Supporting the Use of Advanced MRI Techniques in the Clinic, and the Latest Bench-to-Bedside Developments. Part II: Spectroscopy, Chemical Exchange Saturation, Multiparametric Imaging, and Radiomics.'* Frontiers in Oncology, 2022.[7]

IF: 6,24 (JCR 2020): 62/242 Oncology (Q1).

CP3. Javier Juan-Albarracín, Elies Fuster-Garcia, **María del Mar Álvarez-Torres**, Eduard Chelebian, Juan M García-Gómez. *ONCOhabitats glioma segmentation model.* International MICCAI Brainlesion Workshop, 2019; 295-303.

CP4. Eduard Chelebian, Elies Fuster-Garcia, **María del Mar Álvarez-Torres**, Javier Juan-Albarracín, Juan M García-Gómez. *Higher vascularity at infiltrated peripheral edema differentiates proneural glioblastoma subtype*. PloS one, 2020; 15(10).[8]

IF: 3,24 (JCR 2020): 26/72 Multidisciplinary Sciences (Q2).

CP5. Elies Fuster-Garcia, Javier Juan Albarracín, Ivar T Hovden1, **María del Mar Ávarez-Torres**, Alex Rovira, Laura Oleaga, Antonio J. Revert, Silvano Filice, Juan Miguel García-Gómez, and Kyrre Eeg Emblem. *The use of a DSC-MRI perfusion atlas for cerebral blood volume normalization and its impact in improving prognostic estimation.* Proceedings: Joint Annual ISMRM-ESMRMB & ISMRT 30th Annual Meeting, 2021, virtual.

CP6. Eduard Chelebian, Elies Fuster-Garcia, José Muñoz-Langa, David Lorente, **María del Mar Álvarez-Torres,** Javier Juan-Albarracín, Gaspar Reynés, Juan M García-Gómez. *Vascularity as a predictive and prognostic marker for glioblastoma patients treated with second-line Bevacizumab.* Simposio anual del Grupo Español de Investigación en Neurooncología, Madrid 2019.

CP7. Gaspar Reynés Muntaner, Jaime Ferrer Lozano, Sarai Palanca Suela, José Muñoz Langa, **María del Mar Álvarez-Torres**, Juan Miguel García Gómez, Jaime Font de Mora Sáinz. *Marcadores moleculares, inmunológicos y de imagen en glioblastoma primario. Datos preliminares.* Simposio annual del Grupo Español de Investigación en Neurooncología, Madrid 2019.

1.3.3. Clinical studies and Datasets

To achieve the proposed objectives of this thesis, biomedical data from approximately 780 patients with astrocytoma grade 4 have been collected. Public databases, including TCGA-GBM and Ivy Glioblastoma Atlas Project (Ivy GAP), have been analyzed to perform some of the included studies. However, for some of the proposed objectives, additional data was needed, and several clinical studies have been led by the Biomedical Data Science Laboratory (BDSLab) during the development of this thesis to collect it. Both, the clinical studies led and the collected private datasets, constitute a relevant transversal contribution of this thesis. Chapter 9 includes a complete description of the generation of protocols, their implementation and preliminary results derived from the *BIOhabitats* study.

1.3.3.1. Clinical studies

All the following clinical studies led by the BDSLab have been registered at ClinicalTrials.gov from the U.S. National Library of Medicine, which is the largest database of privately and publicly funded clinical studies conducted around the world.

CS1. Retrospective international multicenter study (*MTS4UP* study). ID at ClinicalTrials.gov: NCT03439332. This study included retrospective clinical and MRI data from 305 patients from seven European hospitals enrolled since 1st of January of 2012 until 1st of February of 2018. The main purposes of the MTS4UP study were: i) to validate the association between imaging biomarkers calculated at vascular habitats of the tumor and edema and patient survival, and ii) to validate the multisite reproducibility of these biomarkers. The following seven European hospitals participated in the clinical study were: Hospital de la Ribera (Alzira, Valencia, Spain), Hospital de Manises (Manises, Valencia, Spain), Hospital Clinic de Barcelona (Barcelona, Spain), Hospital Vall d'Hebron (Barcelona, Spain), Azienda Ospedaliera Parma (Parma, Italy), Oslo University Hospital (Oslo, Norway) and Hospital Center Univiersitaire de Liège (Liège, Belgium).

CS2. Prospective international multicenter study (*ALBATROSS* study). ID at ClinicalTrials.gov: NCT05229198. Prospective clinical and MRI data are being collected from patients with high-grade gliomas diagnosed from March 2020 to March 2022. The main objective of the ALBATROSS study is to validate the prognostic and patient stratification capabilities of imaging biomarkers with prospective data. The following seven European hospitals participated in the clinical study were: Hospital de la Ribera (Alzira, Valencia, Spain), Hospital de Manises (Manises, Valencia, Spain), Hospital Clinic de Barcelona (Barcelona, Spain), Hospital Vall d'Hebron (Barcelona, Spain), Azienda Ospedaliera Parma (Parma, Italy), Oslo

University Hospital (Oslo, Norway) and Hospital Center Univiersitaire de Liège (Liège, Belgium).

CS3. Clinical study for biologic validation of the vascular habitats (*BIOhabitats* study). ID at ClinicalTrials.gov: NCT05375318. In order to validate the MRI-DSC biomarkers calculated at tumor and edema vascular habitats, these must be assessed biologically, including analyses at molecular, cellular and histopathological levels. A prospective, low-interventional clinical study is being conducted including patients with astrocytoma grade 4 from two Spanish hospitals: Hospital Universitario Clinic de Valencia (Valencia) and Hospital Universitario 12 de Octubre (Madrid). The detailed protocol established, its implementation and current status constitutes Chapter 9 of this thesis.

1.3.3.2. Datasets

D1.*MTS4UP* dataset. Derived from the MTS4UP study (CS1), a dataset with information from 305 patients was collected, including basic clinical data and presurgical and follow-up MRIs (anatomical and DSC perfusion images). Participating hospitals are mentioned in CS1.

D2. *ALBATROSS* dataset. Derived from the ALBATROSS study (CS2), a dataset with information from approximately 200 patients is expected to be collected. Data includes presurgical MRI (anatomical and DSC perfusion images, clinical data, and specific molecular alterations). At this moment 40 patients have been collected. This study still in process, and the recruitment stage will finish on June 1st, 2022. Participating hospitals are mentioned in CS2.

D3.*BIOhabitats* dataset. Derived from the clinical study CS3, 42 patients have been included on May 1st. This study still in process, and the recruitment stage will finish on June 1st, 2022. Participating hospitals are mentioned in CS1. The complete protocol and data collection are included in chapter 9 of this thesis.

D4. *GLIOCAT* dataset. A collaboration with the GLIOCAT group was stablished to reuse a dataset with clinical and MRI data from 302 patients from 6 hospitals at Cataluña (Spain) that they have compiled. The participating hospitals were: Institut Català d'Oncologia (ICO) de Badalona, Hospital Clinic de Barcelona, Hospital del Mar, Hospital Sant Pau, ICO Girona and ICO Hospitalet de Llobregat.

D5. *Columbia U.* dataset. In collaboration with the Rabadán Lab (Columbia University, NY), a dataset with 42 patients with astrocytoma grade 4 treated with

immunotherapy with anti-PD-1 was collected, including clinical, genomic and transcriptomic data.

D6. *GEINO*-Mol. A collaboration with the services of Oncology and Anatomical Pathology of Hospital Universitario y Politécnico La Fe was stablished to analyze MRI and molecular data (derived from inmuhistochemestry) from 49 patients.

D7. ONCOhabitats results for public datasets. MRIs included in TCGA-GBM and Ivy GAP public databases were processed with ONCOhabitats and results are available in Zenodo (including classical segmentation, vascular habitats masks and imaging biomarkers).

D7.1. María del Mar Álvarez-Torres, Eduard Chelebian, Elies Fuster-Garcia, Javier Juan-Albarracín, Juan Miguel García-Gómez. *ONCOhabitats results for Ivy Glioblastoma Atlas Project (Ivy Gap): Segmentation and Hemodynamic Tissue Signature.* Zenodo. (https://zenodo.org/record/4704106#.YnOZU9pBw2w)

D7.2. Eduard Chelebian, **María del Mar Álvarez-Torres**, Elies Fuster-Garcia, Javier Juan-Albarracín, Juan Miguel García-Gómez. *ONCOhabitats results for The Cancer Genome Atlas Glioblastoma Multiforme (TCGA-GBM): Segmentation and Hemodynamic Tissue Signature.* Zenodo. (https://zenodo.org/record/4704090#.YnOZbNpBw2w).

1.4. Projects and partners

During the development of this thesis, the author has actively participated in several national and international projects in collaboration with different hospitals, universities, and research centers. The projects related to this thesis are listed below:

MTS4Up *Biomarcadores dinámicos basados en firmas tisulares multiparamétricas para el seguimiento y evaluación de la respuesta a tratamiento de pacientes con glioblastoma y cáncer de próstata*. Funded by the Spanish National Research Agency (DPI2016-80054-R, 2017-2018).

Objectives: O1. Improve the technology to obtain radiological signatures of the glioblastoma incorporating diffusion MRI to describe not only tumor vascularity, but also the cell density properties of the tissues. Such improvements will allow an early evaluation of tumor progression and patient prognosis. O2. To evaluate the technology in a multicenter study to ensure reproducibility and robustness when using MRIs from different hospitals, countries and acquisition protocols.

Partners: Biomedical Data Science Laboratory, Universitat Politècnica de València (Valencia, Spain).

ALBATROSS *Clinically validated decision support system based on pixel level Artificial Intelligent models for deciding treatment in glioblastoma.* Funded by National Plan for Scientific and Technical Research and Innovation 2017–2020 (PID2019-104978RB-I0).

Objectives: O1. Delineate functional habitats from multiparametric MRI relative to the growth, proliferation, infiltration and angiogenesis at the enhanced tumor and infiltrated peripheral edema. O2. Demonstrate that functional habitats at enhanced tumors and infiltrated peripheral edema show structural, cellular and molecular differences related to the heterogeneity of the tumor region and are compatible with mathematical models of glioma growth and infiltration. O3. Determine the in-vivo molecular sub-type of patients with glioblastoma from image biomarkers in functional habitats. O4. Identify groups of patients with glioblastoma presenting positive therapeutic response in terms of longer survival using image biomarkers from functional habitats. O5. Position ONCOhabitats as a clinical decision support system for the management of patients with glioblastoma.

Partners: Biomedical Data Science Laboratory, Universitat Politecnica de València (Valencia, Spain). Hospital Clinic Universitari de València (Valencia, Spain). Department of Neurosurgery and department of Pathological anatomy; Hospital Universitario 12 de Octubre (Madrid, Spain). Department of Neurosurgery. Department of Neuro-oncology.

1.5. International research stay

During the development of this thesis, the author has carried out an international research stay at the Rabadán Laboratory in Columbia University, department of System Biology (New York, United States of America).

Dates and duration: The stay took place from October 1st, 2021, to January 5th, 2022, resulting in a 94-day stay.

Objectives: To analyze clinical, imaging and molecular data derived from a cohort of patients with astrocytoma grade 4 treated with immunotherapy to find tumor/patient characteristics to evaluate treatment responses.

Results: The main results of the worked carried out during the research stay constitute chapter 8 of this thesis and contribution C5. A journal publication will be derived from this study.

1.6. Thesis outline

This thesis is structured in ten chapters that thoroughly describe the research work carried out. The chapter 1 has introduced the motivation, the research questions and objectives, and main contributions. Chapter 2 describes the thesis rationale, introducing the clinical problem addressed, as well as the background needed to get a complete understanding of the following chapters. Chapters 3 and 4 constitute part I and correspond to the works related with tumor characterization and classification. Chapter 3 focuses on the association between imaging and histopathology of vascular structures existing in astrocytoma grade 4, and chapter 4 includes the study of differences in tumor vascularity depending on mutation in *IDH* genes. Part II includes chapters 5 and 6 which present the studies related with patient prognosis estimation. Chapter 5 includes the multicenter validation of the prognostic application of the imaging biomarkers calculated at vascular habitats, and chapter 6 focuses on the effect of tumor vascularity on survival over time. Part III includes chapters 7 and 8, that present studies related with treatment selection: personalized chemotherapy and immunotherapy, respectively. Chapter 9 corresponds with Part IV which presents the clinical studies designed, including the protocol definition, its implementation and coordination, and datasets creation. Finally, chapter 10 ends this dissertation with the concluding remarks and recommendations to continue with the research developed in this thesis.

Figure 1.1 outlines the objectives, thesis contributions structured among the thesis chapters, along with the publications, research projects and collaborations developed during this study.

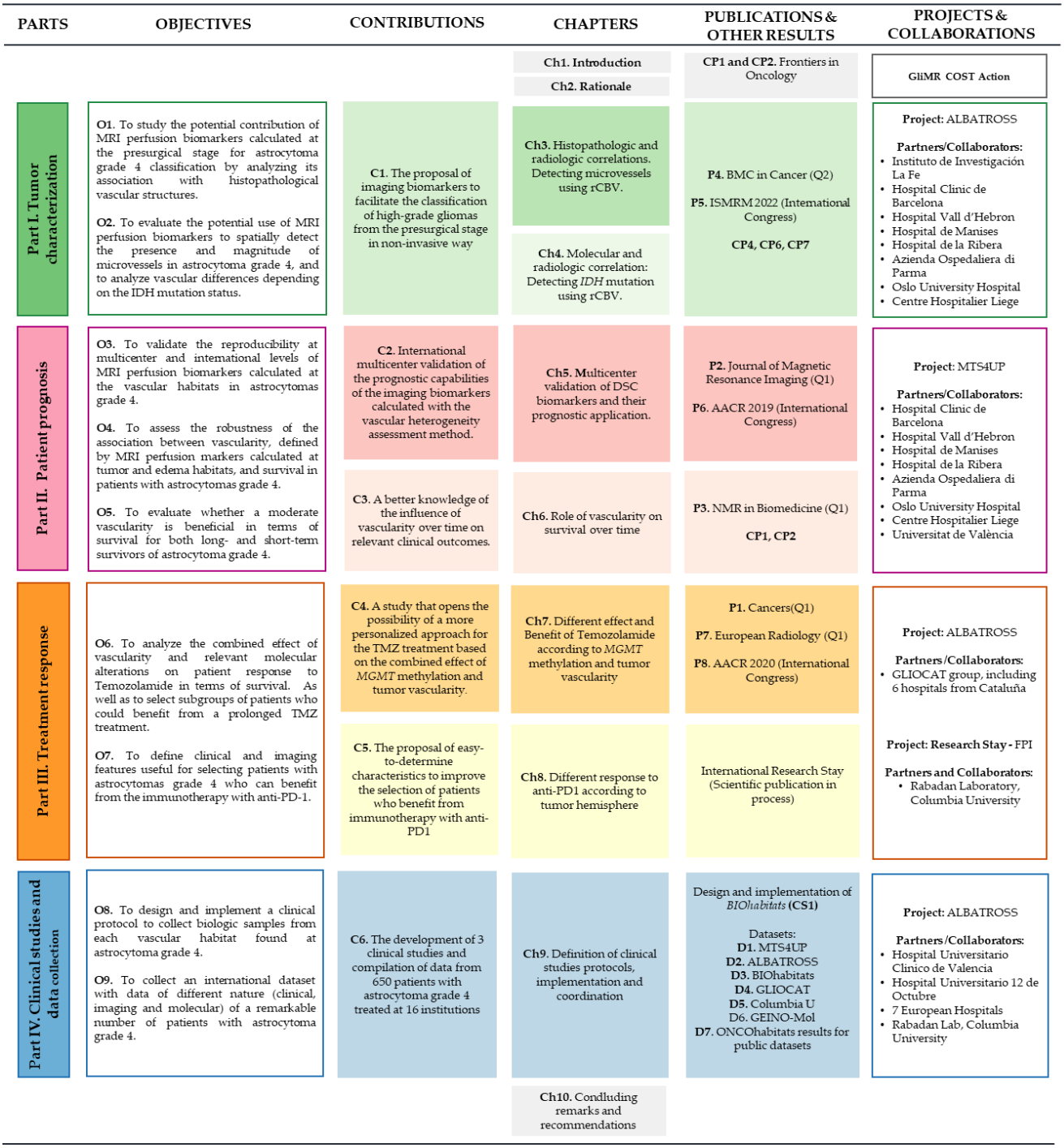

Figure 1.1. Thesis outline, including objectives, main contributions, chapters, publications, and projects.

Chapter 2

Rationale

**Explanatory note: The studies conducted during the development of this thesis were initiated in 2018. Until June 2021, the WHO classification of central nervous system tumors considers glioblastoma IDH-wildtype and astrocytoma IDH-mutant grade 4 as the sam high-grade glioma, the glioblastoma. For this reason, the scientific publications included in this thesis and most of the bibliography refer to glioblastoma without considering the IDH mutation status and the last update of the WHO classification.*

2.1. Astrocytoma grade 4

2.1.1. Astrocytoma grade 4: a particularly challenging medical problem

Astrocytomas are CNS tumors that originated in a particular kind of glial cells called astrocytes[9]. This type of tumors occurs in most parts of the brain and occasionally in the spinal cord, and they do not usually spread outside, affecting other organs. The WHO grading system assigns a grade from 1 to 4 to classify astrocytomas, with grade 1 being the least aggressive and grade 4, the most aggressive[10]. This thesis focuses on the study of astrocytomas grade 4.

Astrocytomas grade 4 are the most common and aggressive brain tumors in adults, and, unfortunately, they derive in terminal prognosis, with only 5% of patients surviving five years[10–12]. These gliomas were histologically defined for the first time in 1865 by Rudolf Virchow as malignant tumor formations with their origin in the CNS and showing apparent differences with healthy brain tissue. Figure 2.1 shows images from hematoxylin and eosin (H&E) slides including some of the main histopathological hallmarks of astrocytomas grade 4 (B and C) against healthy brain tissue (A).

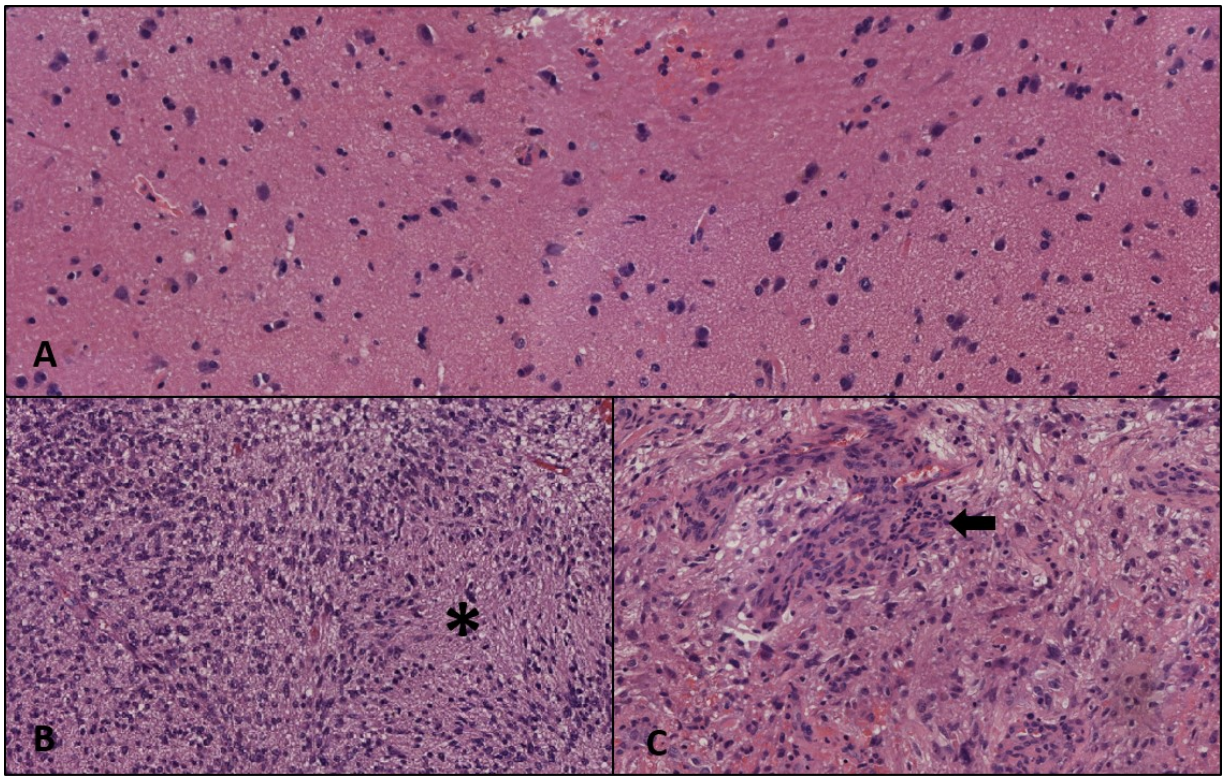

Figure 2.1. Histopathological features of healthy brain tissue and WHO grade 4 astrocytoma. A) Healthy brain tissue (H&E 200X). B-C) Hypercellularity, atypia, pseudopalisading necrosis (*) and glomeruloid proliferation of endothelial cells(➡)(H&E 100X). Images proportioned by Dr. Jaime Agustí, derived from our collaborating project *BIOhabitats* (NCT05375318).

These devastating tumors have an incidence of 2 to 5 per 100000 inhabitants in United States[12] and Europe[13], increasing their prevalence with age[12]. Unlike most aggressive neoplasms, astrocytomas grade 4 only appear to thrive in the unique brain microenvironment[12]. However, individual astrocytoma cells show an unparalleled ability to invade surrounding areas of the brain and thus exert a locally destructive influence on brain tissues and functions. These infiltrative and invasive masses are characterized by hypercellularity, pleomorphism, MVP, and high necrosis[14]. This behavior, along with the heterogeneity at intratumor, interpatient, and longitudinal levels, makes these gliomas one of the most challenging human cancers to combat[12]. Figure 2.2 includes an example of the macroscopic view of these tumors.

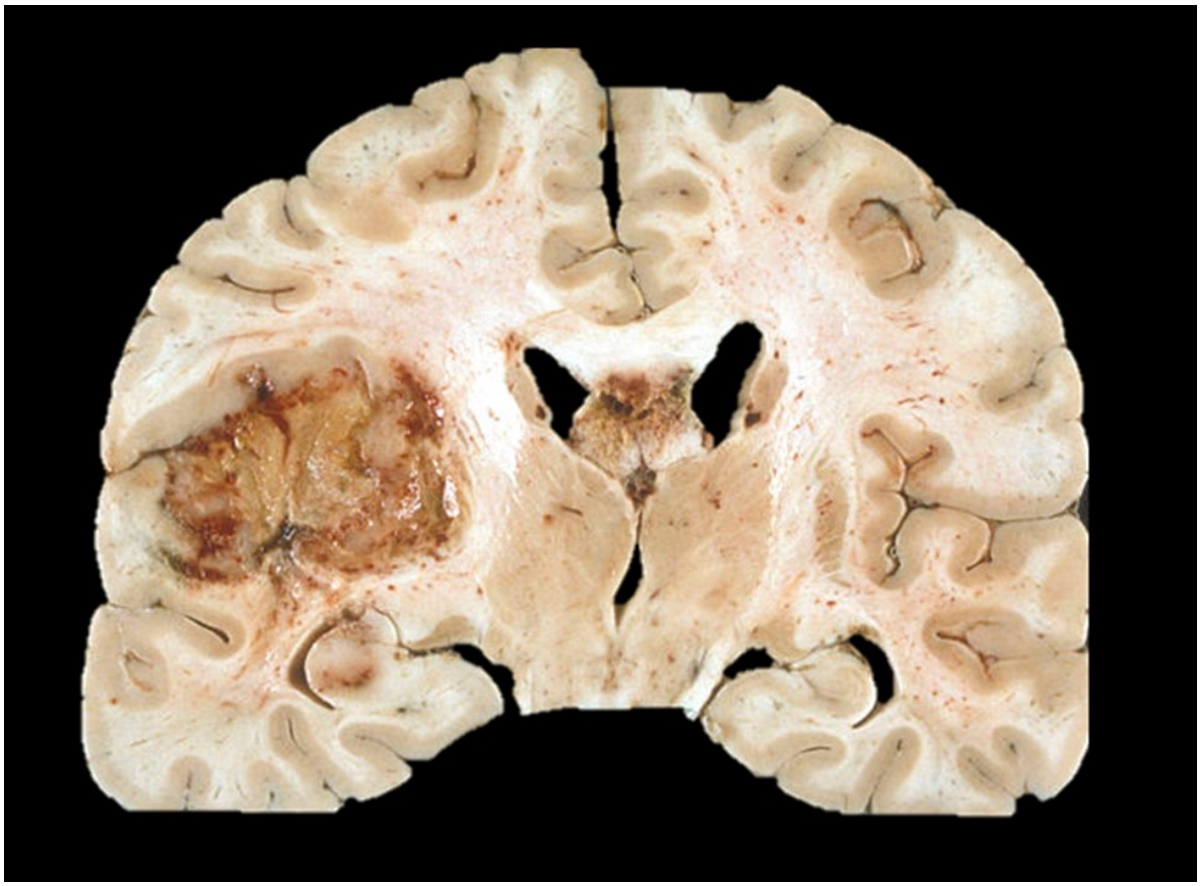

Figure 2.2. Example of the macroscopic view of a brain affected by an astrocytoma grade 4 located at the right hemisphere of the cerebral cortex (Image credit CC BY-SA 4.0; https://commons.wikimedia.org/wiki/File:Glioblastoma_macro.jpg).

As one of the most complex oncological problems to address, there have been many historical reports, including the exhaustive multidisciplinary research made regarding these tumors. Such diverse fields ranging from Neuro-Oncology, Pathology, or Molecular Biology to Radiology, Computer Science, and Physics have analyzed these brain tumors to understand their complex biology and improve patients' lives. All the derived knowledge has led to detailed descriptions astrocytomas that has given us essentially, but still not enough information to design successful treatments for patients with this disease, resulting in a very challenging problem yet to be solved.

2.1.2. Differentiating between glioblastoma IDH-wildtype and astrocytoma IDH-mutant grade 4

Astrocytoma grade 4 includes both glioblastoma *IDH*-wildtype and astrocytoma *IDH*-mutant grade 4[11,15]. In the last update (6th) of the WHO classification of tumors

of the CNS (WHO CNS5)[10], nomenclature changed from *'glioblastoma'* to more accurate terms differentiating between these two high-grade gliomas[10]. This new classification is based on the gene mutation status that encodes the enzyme isocitrate dehydrogenase (*IDH*). Molecular characterization of gliomas has supported our understanding of their origins[16–18]. It has identified somatic alterations, such as *IDH* mutation, that allow a more precise classification according to different tumor biology and patient survival times[10,11].

Glioblastoma *IDH*-wildtype and astrocytoma *IDH*-mutant grade 4 are fatal diseases, even though patients receive the complete standard treatment[11,19]. To understand the reasons for differentiating between these two high-grade gliomas, the critical differences between these two tumors have been summarized in table 2.1, noting differences in patients' overall survival.

Table 2.1. Main biological and clinical differences between glioblastoma *IDH*-wildtype and astrocytoma *IDH*-mutant grade 4.

	Glioblastoma *IDH*-wildtype	**Astrocytoma *IDH*-mutant grade 4**
Synonyms	Primary glioblastoma	Secondary glioblastoma Glioblastoma *IDH*-mutant
Precursor Lesion	Not identifiable develops de novo	Diffuse astrocytoma Anaplastic astrocytoma
Proportion of astrocytomas grade 4	~95%	~5%
Median age at diagnosis	~62 years	~44 years
Male to female ratio	1.42:1	1.05:1
Median overall survival		
• Surgery + radiotherapy	9.9 months	24 months
• Surgery + radiotherapy + chemotherapy	15 months	31 months
Necrosis at diagnosis	Extensive	Limited
TERT promoter mutations	72%	26%
TP53 mutations	27%	81%
ATRX mutations	Exceptional	71%
EGFR amplification	35%	Exceptional
PTEN mutations	24%	Exceptional

Presenting the *IDH* mutation confers a less aggressive tumor behavior, which impacts patient prognosis due to the vital role of the IDH enzymes in cellular and metabolic homeostasis of tumor cells. There are three isoforms of IDH enzymes, and

they are essential in several major metabolic processes, such as the Krebs cycle, glutamine metabolism, lipogenesis, and redox regulation[20]. IDH1 is located in the cytoplasm and peroxisomes, whereas IDH2 and IDH3 are located in the mitochondrial matrix[20]. The substrate for IDH1 and 2 is isocitrate, together with nicotinamide adenine dinucleotide phosphate (NADP+) and a divalent metal cation, usually magnesium or manganese, resulting in the formation of α-ketoglutarate (α-KG). Mutations in *IDH1* and *IDH2* genes are prevalent in human tumors[21]. These gain-of-function mutations modify the regular activity of IDH enzymes, causing a replacement of arginine residue (with a strong positive charge) with lower-polarity amino acids such as histidine, lysine, or cysteine[20]. This modification decreases the affinity with isocitrate, causing a metabolic change in which the primary reaction catalyzed is the reduction of aKG to (D)2-hydroxyglutarate (D2HG), which is NADPH-dependent[22,23]. To compensate changes in enzyme function, cells exhibit metabolic reprogramming, including the activation of non-Krebs-cycles pathways, decrease novo lipogenesis, and affect the level of hypoxia-inducible factor, among others.

Overall, the unique metabolism in astrocytoma *IDH*-mutated cells explains the slower-growing nature of this disease compared to glioblastoma *IDH*-wildtype[20]. These differences in growth and progression velocities also imply different requirements of blood supply, being involved in several mechanisms of new vessel formation, affecting the vascular architecture and behavior of these tumors[24,25].

The biological and clinical differences between these two astrocytomas, and consequently among patients, make crucial an early classification for patient management. It is relevant to acquire a better knowledge of the diseases for patient prognosis and for suggesting the possibility of developing targeted strategies for *IDH*-mutant and *IDH*-wildtype specific metabolic patterns.

2.2. Treatment of patients with astrocytomas grade 4

2.2.1. Standard treatment

Except for clinical trials, the current treatment for astrocytoma grade 4 is almost the same for all patients. Stupp proposed the standard treatment in 2005[19], and it includes the most complete tumor resection possible, followed by radiotherapy and concomitant and adjuvant chemotherapy with TMZ.
The standard treatment[19] has not been modified to distinguish between patients with these two different high-grade gliomas due to the novelty of the last WHO classification update[10] (in June 2021). However, the *IDH* mutation status is

considered in most clinical trials, being a requirement for patient inclusion/exclusion in many cases.

Despite the invasive and aggressive therapy provided, there is a tumor recurrence in practically all the cases. This is mainly due to astrocytomas grade 4 are infiltrating tumors, the remaining tumor cells that migrate after debulking are resistant to conventional, and because complete surgical resection is almost impossible.

After tumor relapse, different second-line therapies could be provided to patients for trying to contain progression. However, no standard of care is established for recurrent or progressive astrocytoma grade 4, and the option of second surgery remains controversial[26]. Although there have not been drastic changes in patient treatment since 2005, relevant advances have been made in the scientific field, which hopefully will translate into an improvement in both time and quality of life of specific patients. In this sense, the European Association of Neuro-Oncology (EANO) published a guideline in 2021 to reflect the last changes and advances[27]. The main treatment recommendations related to surgery, radio- and, pharmacotherapy, of this updated guideline are summarized as follows:

Surgical therapy. The therapeutic goal of surgery is to remove as much tumor volume as safely feasible without compromising neurological function. Several microsurgical techniques and surgical navigation systems help reduce postoperative residual tumor tissues while keeping the risk of new neurological deficits low. The extent of resection should be assessed within 24–48 hours of surgery through MRI, acquiring images without and with magnetic contrast. Whether and why the size of resection truly matters remain a controversial question. First, rather than the percentage of the extent of resection, clinicians might need to consider the absolute volume of remaining tumor tissue, including both enhancing and non-enhancing tumor tissue. Several factors can affect the completeness of the resection, being one of the most relevant to the location of the tumor in the brain.

Radiotherapy. The goal of radiotherapy is to improve local control without inducing neurotoxicity. Radiotherapy delays neurological deterioration and improve prognosis[28,29]. The timing, dosing, and scheduling of radiotherapy are determined by the disease subtype and prognostic factors, including age, Karnofsky Performance Status Scale (KPS), and percentage of residual tumor tissue. Radiotherapy should start within 3–5 weeks after surgery and is usually administered at 50–60 Gy in 1.8–2 Gy daily fractions. An MRI 3–4 weeks after completion of radiotherapy is recommended to provide a new baseline to monitor the further course of the disease.

Pharmacotherapy. Whenever possible, patients with astrocytoma grade 4 will receive chemotherapy with temozolomide, an oral deoxyribonucleic acid (DNA) alkylating agent that penetrates the blood-brain barrier. The benefit of alkylating agent chemotherapy demonstrated in various randomized controlled trials (RCT)s must be weighed against the potential long-term toxicities and the risk of inducing a hypermutator phenotype associated with a more malignant behavior. This is particularly evident in patients with astrocytoma *IDH*-mutant who have a longer life expectancy. The effect of the TMZ is hugely determined by the presence or absence of the methylation of the promotor of the *MGMT* gene. Tumor cells can reverse the alkylating effect over the DNA and, therefore, allow the progression and infiltration of the tumor. However, when the *MGMT* is methylated, the ability to repair the damage induced by the TMZ is impaired, supposing a benefit in receiving this treatment.
As a treatment choice for recurrent astrocytoma grade 4, Bevacizumab, an anti-VEGF antibody, is approved in the USA, Canada, Switzerland, and several other countries outside the European Union. Still, its use has not demonstrated a benefit in OS.

The EANO guideline[27] encourages centers to carry documentation of treatment, including laboratory results and information on complications and contraindications, and generate standard operating procedures and instructions for standardized application of chemotherapy and the management of adverse events and complications from treatment.

Considering the last update of the WHO classification of tumors of CNS[10], specific clinical pathways are recommended for patients with astrocytoma grade 4 depending on the *IDH* mutation status and other fundamental characteristics. Figure 2.3 summarizes the clinical roadmap for patients with glioblastoma *IDH*-wildtype and astrocytoma *IDH*-mutant grade 4.

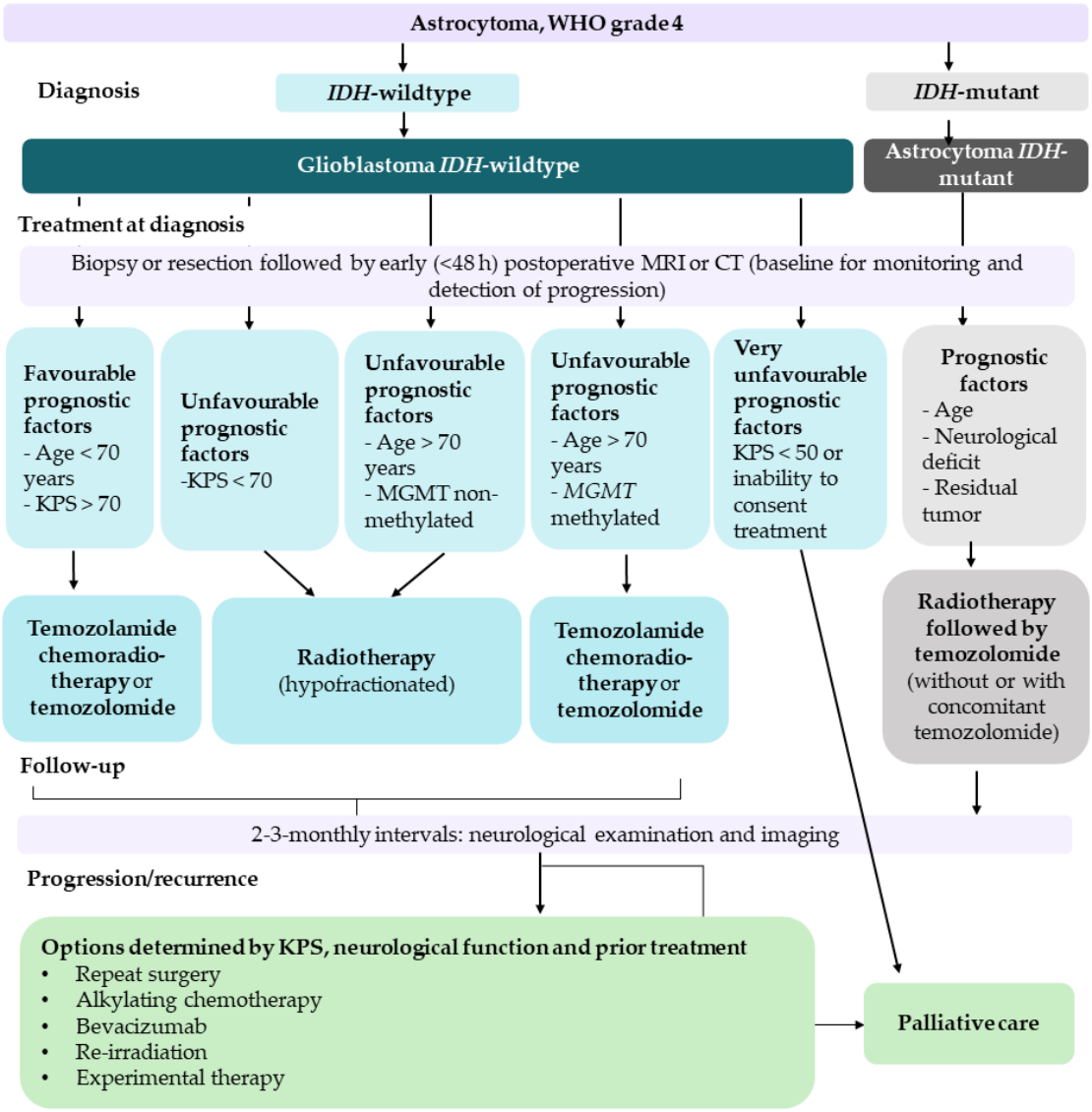

Figure 2.3. Clinical roadmap for glioblastoma *IDH*-wildtype and astrocytoma *IDH*-mutant grade 4. Scheme based on figures 2 and 3 included at the EANO guidelines[30].
*KPS: Karnofsky performance status.

Although these treatment pathways cannot be considered personalized, this guideline recommends the most appropriate choice for different groups of patients. To do this, essential characteristics such as age, KPS, and molecular alterations, including *IDH* mutation and *MGMT* methylation, must be considered. However, the definition of the status of these molecular alterations is not standardized in all clinical centers. The current situation is that in many medical centers, the same treatment is provided for every patient with astrocytoma grade 4, resulting in highly variable and inefficient therapy responses and outcomes.

2.2.2. Immunotherapies

The recent success of immunotherapy with checkpoint inhibitors has initiated a paradigm shift in preclinical and clinical investigations to combat a variety of solid tumors. The discovery of specific immune molecules, such as cell death protein -1 (PD-1) and cytotoxic T-lymphocyte antigen 4 (CTLA-4), seems to have been a potential breakthrough in therapy development in advanced melanoma[31,32], Hodgkin's Lymphoma[33,34], or non-small-cell lung cancer[35], among others. Considering the remarkable success fighting these cancer types, there has been considerable interest in utilizing immunotherapy to treat high-grade gliomas[32,36,37]. However, most attempts to incorporate these immunotherapeutics for these aggressive brain tumors have been inefficacious thus far, with only a small subset of patients with positive responses.

2.2.2.1. The brain as an immune privileged organ

Understanding the unique relationship between the brain and the immune system is key for immunotherapy in brain diseases such as astrocytomas grade 4. Historically, the brain has been considered as a hermetic organ, protected by a closely regulated blood-brain barrier (BBB) and deprived of any immunologic surveillance. Nevertheless, this idea of 'immune privilege' was questioned when it was discovered that alloantigens could provoke an immune response in the brain[38]. Advances in technology, such as intravital imaging, have revealed that immune surveillance and, specifically, the T cell priming and activation predominantly occurs in the meningeal compartment of the CNS[39]. However, the connection between CNS and the peripheral immune system has been clarified in the last decade. In 2015, two pioneering studies showed for the first time a network of functional lymphatic vessels that line the dural sinuses, which drain into the deep cervical lymph nodes, and serve as a gateway for T cell trafficking between the periphery and the cerebrospinal fluid (CSF) of the CNS[40,41]. These studies demonstrated that the idea of immune privilege is not accurate. Currently, it is appreciated that the brain receives constant immune surveillance and communication with the peripheral immune system, allowing the possibility of immunotherapy to treat diseases of the CNS. One remaining challenge for astrocytoma treatment efficacy is overcoming the BBB despite these potential opportunities. Other options are being considered, including the direct application of immunotherapy with checkpoint inhibitors in the resection cavity during su[36,42,43].

2.2.2.2. Monotherapy with PD-1/PD-L1 inhibitors

The main class of checkpoint inhibitors is monoclonal antibodies targeting the protein PD-1 or its ligand (PD-L1); this category includes pembrolizumab, nivolumab, durvalumab, and atezolizumab[44].
Commonly, the ability of high-grade gliomas to induce local and systemic immunosuppression reduces the innate defense against tumor growth and the efficacy of adaptive immunotherapy. T lymphocytes have the potential to recognize antigens, but their regular activity can be suppressed by immune checkpoints, especially by PD-1/PD-L1. Due to the binding of this protein and its ligand, activated immune cells suffer apoptosis and its regular activity is considerably limited[45], allowing tumor cells to proliferate without restrictions.
Considering the common immunosuppression induced by PD-1/PD-L1 in high-grade gliomas, a potential solution is to provide immunotherapy with PD-1 and PD-L1 monoclonal antibodies (mAbs). This therapy has relevant benefits with durable responses but only for a reduced proportion of patients with astrocytoma grade 4[44].

Several factors can affect the efficacy of PD-1/PD-L1 inhibitors, including tumor cell *PD-L1* expression[46], tumor-infiltrating lymphocytes, tumor-infiltrating myeloid cells[47], tumor mutation burden (TMB), new antigen burden, microsatellite instability, mismatch repair (MMR) system status, and polymerase epsilon mutation status[48]. In addition, patient response is also correlated with some gene alterations such as *PTEN* mutation and *MAPK* alterations[42]. Nonetheless, there is still not enough information to agree to select patients who will respond well to this monotherapy. Easy-to-determine biomarkers that predict responses would be crucial for successful clinical implementation of the anti-PD1 treatment in treating patients with astrocytoma grade 4.

2.2.2.3. Combined immunotherapies

Several preclinical studies in mouse models of high-grade gliomas involved targeting the PD-1/PD-L1 axis and other immunosuppressive inhibitors[45]. The modulation and cross-talk of high-grade gliomas with the immune system are one of the causes of tumor evolution, immune escape, resistance to therapy and tumor relapse. Immunotherapy, together with antibody-dependent cellular cytotoxicity treatment has become the standard of care for glioma patients with *PD-L1* overexpression [49,50]. Targeting tumor cell surface with antibodies against PD-1 or EGFR eradicates tumor cells by inducing antibody-dependent cellular cytotoxicity (ADCC). It is mediated mainly by natural killer (NK) cells, monocytes, neutrophils, macrophages, and complement-dependent cytotoxicity (CDC)[51]. However, abreast of the potential efficacy of these immunotherapies, only a subset of astrocytoma grade 4 patients responds to it[42]. Thus, it is essential to define the determinants driving the

effectiveness and resistance to standard immunotherapy and consider novel strategies for unresponsive tumors. Patients with *PTEN* mutations are less likely to respond to immunotherapy with anti-PD-1 antibodies therapies[42]. However, these studies have not reported the activation of other crucial immune checkpoints such as B7-H3, indoleamine 2,3 dioxygenase 1 (IDO1), or immunosuppressive cell populations. The degree of tumor-infiltrating immune cells and tumor genomics are considered determinants of immunotherapy response in other tumors[52].

Kynurenine metabolites derived from tryptophan catabolism are known biologically active immunosuppressants[53]. IDO1 is the enzyme catalyzing the first rate-limiting step of tryptophan catabolism[54]. Thus, *IDO1* overexpression by tumor cells and lymph nodes draining the tumor may result in tumor immune escape. *IDO1* overexpression is implicated in high-grade gliomas, and the efficacy of current therapies may be reduced by inhibition of effector cells by kynurenine production and tryptophan depletion IDO1[55]. In addition to the rate-limiting enzyme IDO1, the isoenzyme TDO2 constitutes another therapeutically targetable pathway of immunosuppressive tryptophan degradation in a subset of glioblastoma *IDH*-wildtype with a particularly poor prognosis. These intratumoral biomarkers are of clinical relevance as they reveal therapeutic alternatives for non-responding patients. Increasing evidence support the role of innate and adaptive immune mechanisms, and the presence of an established immunosuppressive high-grade glioma microenvironment that suppresses and/or prevents the anti-tumor host response.

2.2.2.4. Major challenges of implementing immunotherapy and potential solutions

Summarizing, most of the studies analyzing immunotherapies conclude that they have the potential to transform high-grade glioma treatment[36,37,42–50]. However, overcoming the following two main challenges is still necessary:

- *Treatment-related immunosuppression.* Standard radio- and chemotherapy provided to patients with astrocytoma grade 4 can produce drastic and persistent reductions in peripheral CD4 T cell levels, which is significantly associated with shorter survival times[56]. This may decrease the potential pool of circulating tumor-reactive T cells, which could neutralize or avoid the effect of immunotherapy[57].

- *Challenges in evaluating radiographic responses to immunotherapy.* Immunotherapies cause singular radiographic reactions that can be misclassified by traditional assessment tools such as WHO, and RANO[58]. Prior to demonstrating treatment response, such as a transient increase in tumor burden, either increasing tumor

growth or development of new lesions, can be associated with immunotherapy. These radiographic changes may represent either continued tumor growth before generating an adequate immune response or the infiltration of immune cells rather than tumor cell proliferation (with or without edema). To avoid misclassifying these responses as a progressive disease, refinements to RANO, known as immunotherapy-RANO (iRANO), have been established. If there is radiographic progression without clinical deterioration within six months of initiating immunotherapy, iRANO recommends treatment continuation with repeat MRI brain imaging after three months. If the progressive disease is still noted at repeat assessment, the patient should be retrospectively classified as having progressive disease on the date of initial radiographic progression. If repeat imaging shows the stable or improved condition, the immunotherapy should be continued.

Different studies address these limitations and propose potential solutions, including advanced delivery strategies for immunotherapies[59,60], focusing on nanoparticles and conjugates, injectable biomaterials, and implantable scaffolds[37,44]. On the other hand, the combination of functional MRI with AI techniques can be helpful in differentiating the effect on images caused by immunotherapy from natural tumor progression. A meta-analysis that studies treatment response monitoring biomarkers has recently been published, proposing advanced MRI techniques in the clinic and the latest bench-to-bedside developments[6,7]. Part 1 of this meta-analysis[6] includes the contribution of perfusion and diffusion techniques, and Part 2[7] focused on spectroscopy, chemical exchange saturation, multiparametric imaging, and radiomics. Some of these advanced MRI techniques show huge promise in treatment response assessment and may be proposed as helpful for evaluating radiographic responses to immunotherapy. Although many of these techniques are in their infancy, others have generated a larger body of evidence for clinical application, being DSC perfusion one of the most remarkable[6,7].

2.2.3 Antiangiogenic treatment

Astrocytomas grade 4 show marked angiogenesis, which represents a key histopathologic process for tumor progression and aggressiveness. It is not surprising, therefore, that tumor vascularity has been the target of drug development over the last decades. Research into this type of drugs was triggered by the disappointing outcomes with cytotoxic agents. In addition, the recognition that the extensive and rapid vascularization should make this disease potentially suitable for antiangiogenic therapy[61–63].

The mechanisms of action of antiangiogenic therapies are multiple: originally, in 1979, Folkman proposed that antiangiogenic agents confer an antitumor effect inducing endothelial cell apoptosis, inhibiting new blood vessel formation, obstructing small vessels, and decreasing tumor perfusion, resulting in decreased delivery of oxygen and nutrients ('tumor starvation')[64]. However, at initial treatment stages, antiangiogenic agents may temporarily normalize aberrant tumor vasculature by reducing blood vessel diameter and permeability. These changes paradoxically improve tumor perfusion, decrease interstitial pressure, and facilitate tumor oxygenation[65], potentially sensitizing for radiotherapy and increasing tumor exposure to cytotoxic chemotherapy[65].
The majority of antiangiogenic treatments target the vascular endothelial growth factor (VEGF) pathway, since it plays a main role in astrocytoma grade 4 angiogenesis and interact with different pathways to promote tumor growth[61–63].

2.2.3.1. Bevacizumab (Avastin)

Bevacizumab is the most typically used antiangiogenic agent for astrocytomas grade 4 and was approved by the U.S. Food and Drug Administration (FDA) for use in patients with recurrent tumors in 2009. It consists of recombinant, humanized monoclonal antibody that inhibits VEGFR-mediated cell signaling inhibitor, by sequestration of its ligand VEGF-A. Initial studies with bevacizumab in recurrent astrocytomas grade 4 showed radiographic response rates of 28–40% and 6-month progression free survival (PFS6) rates of 40–50%[66–68]. This compared favorably to prior studies in recurrent astrocytoma grade 4 in which the median PFS6 was only 15%[69].
Based on these promising results, a randomized, non-comparative phase II trial of patients with recurrent astrocytomas grade 4 was performed[70]. The combination arm (bevacizumab + irinotecan) was shown to be more effective than bevacizumab alone because of the possible normalizing effects on tumor vasculature resulting in improved delivery of chemotherapy. The APF6 was 35.1% in the bevacizumab alone arm and 50.2% in the combination therapy arm. Median OS was 9.7 months in the bevacizumab arm and 8.9 months in the combination arm with more frequent CTCAE Grade 3 toxicities in the bevacizumab and irinotecan arm (67% versus 48%). Consequently, although APF6 was better in the combination arm, the increased rate of toxicity and equivalent median OS questioned the significant benefit to combining bevacizumab with irinotecan over bevacizumab alone.
Posterior phase III trials[71,72] demonstrated an increase in PFS (10.7 and 10.6 vs. 7.3 and 6.2 respectively) but none benefit in prolong OS in patients with newly diagnosed astrocytomas grade 4 when bevacizumab is added to TMZ therapy[30].

In addition, attempts to increase the benefit of single-agent bevacizumab included studies evaluating bevacizumab combined with chemotherapy[73–79], targeted therapies[80–82] and re-irradiation[83–85]. Unfortunately, these combination treatments failed to improve outcomes beyond bevacizumab monotherapy.

2.2.3.2. Recommendations from the EANO about bevacizumab treatment

Considering results of diverse studies and clinical trials carried out, the benefit of using bevacizumab still being a matter of debate.
For newly diagnosed astrocytomas grade 4, bevacizumab is not approved, with very few exceptions, but EANO recommends its use for patients with large tumors who are highly symptomatic and who might not otherwise tolerate radiotherapy.
However, this antiangiogenic agent is one of the main choices to treat recurrent tumors, although benefit in OS has not been proven.

The potential benefit of antiangiogenic treatments probably depends on the initial vascularity, the nature of the tumor, and the phase of treatment at which it is administered. Chapter 6 of this thesis discusses the different effect of vascularity on OS of patients in both long-term and short-term survivors. A better understanding of the influence of tumor vascularity may be useful to include patients in clinical studies analyzing the effect of antiangiogenics. Treatment with bevacizumab may not be suitable for all patients or at any stage of the disease but could benefit specific groups of patients.

2.3. Heterogeneity in astrocytoma grade 4: At interpatient, intratumor, and longitudinal levels

The heterogeneity of astrocytomas grade 4 is an evidence that has been widely studied in the literature, as it affects the response to treatments and survival times[26–32]. However, it is a complex concept that can be analyzed from diverse points of view. Simplifying, heterogeneity can be studied at interpatient, intratumor, and longitudinal levels.

2.3.1. Interpatient heterogeneity

Although astrocytomas grade 4 share common features that allow their diagnosis and classification, these gliomas are highly variable from patient to patient[18,26].

Interpatient heterogeneity exists at genetic level and macroscopic scales, including tissular, vascular and structural.

2.3.1.1. Interpatient heterogeneity at the genetic level

The most key and apparent alterations that may vary between patients are mutations in *IDH* genes. As mentioned above, knowing the *IDH* mutation status is essential to classify these tumors according to the last update of the WHO in glioblastoma *IDH*-wildtype or astrocytoma *IDH*-mutant grade 4. As shown in Table 2.1, patient outcomes are highly variable depending on this gene alteration, including two-fold longer survivals in patients with the *IDH* mutation. But not only this mutation isdecisive, alterations in *EGFR*, *MGMT*, *PTEN*, *ATRX*, and *TERT* genes and the mutational burden have been extensively studied, concluding their relevance in patient prognosis and treatment responses.

2.3.1.2. Interpatient heterogeneity at the macroscopic scale

Factors such as tumor size, location, and vascular architecture are associated with tumor evolution and patient follow-up. Different studies conclude that a reduced tumor volume at the presurgical stage results in longer patient survival[33–35]. However, this factor has been a source of debate since other authors have found a correlation between the peritumoral edema on MRI and survival times, but not with the tumor volume[36–38]. Maybe the influence of tumor volume on survival is variable throughout the course of the disease.

Considerable heterogeneity in the anatomic distribution of gliomas within the brain has been shown in different studies. Figure 2.4 shows a schematic diagram of the sagittal view of the brain with the different lobes and anatomy indicated.

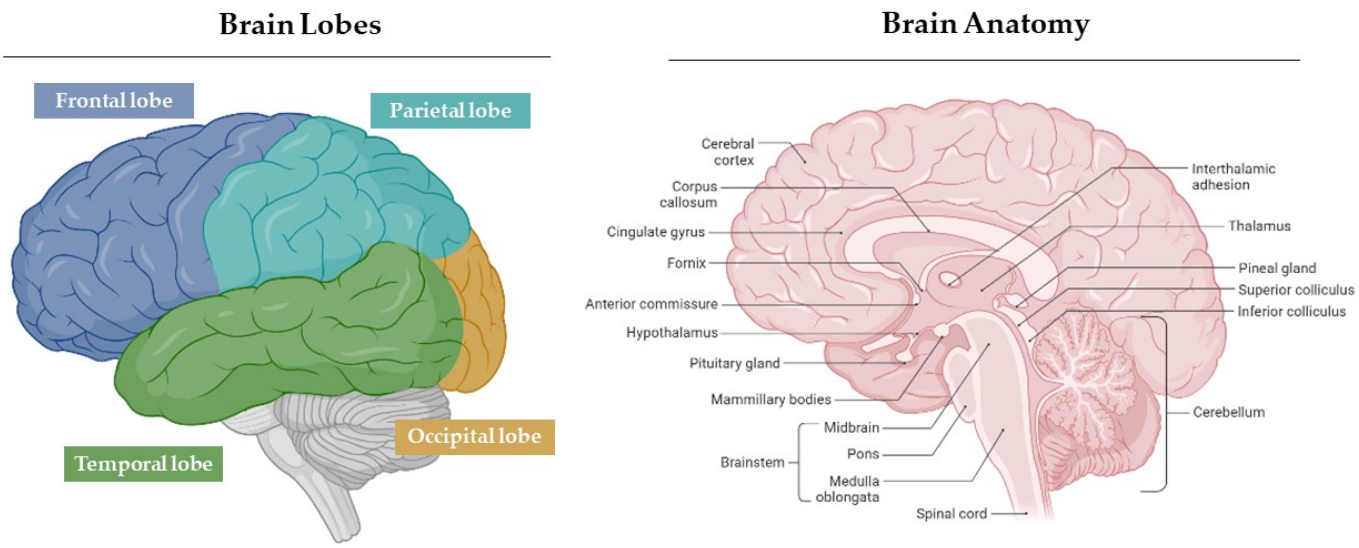

Figure 2.4. Sagittal view of brain lobes and anatomy. Created with BioRender.com

There seems to be an agreement that frontal tumors are the most prevalent[39], and they are more associated with longer survival[38,40]. This can be explained because more accessible locations in the brain allows a more complete resection during surgery than those located near the skull[38–41]. In addition, the location of the lesion affects the damage to neurocognitive functions[39]. The affection of the parietal lobe affects attention and memory functions; frontal lobe tumors involve disabilities in planning complex actions and novel problem solving, and patients with temporal lesions were more likely to have impaired memory and executive functions[42]. Furthermore, neurophysiological symptoms differ depending on the affected hemisphere, since cognitive functions are differentially represented in brain hemispheres. Aphasia is more prevalent in patients with left-sided astrocytomas. In contrast, attention deficits (more challenging to recognize for patients) are more frequent in patients with the tumor in the right hemisphere [43].

Not only does tumor size and location influence patient survival and quality of life, but differences in vascular structures and behavior play a relevant role in tumor progression and treatment response. Subsection *2.3.5 Vascular heterogeneity* of this chapter covers this aspect.

2.3.2. Intratumor heterogeneity

One of the main causes of the aggressive behavior of astrocytomas grade 4 is the intrinsic intratumor heterogeneity, conferring significant variations in diverse

hallmark functions of tumor cells. These high-grade gliomas are intricate ecosystems composed of a diversity of clonal and subclonal differentiated tumor cell populations and multiple non-tumor cells, such as endothelial and inflammatory cells, and other components of the TME both at micro- and macroscopic levels.

Astrocytomas grade 4 are also characterized by diffuse invasion of tumor cells into the healthy parenchyma using various motility patterns[31]. These results in random processes of tumor growth and in the existence of disparate tissues[29,31,32]. Although these processes can be considered stochastic, intratumor heterogeneity can be spatially defined from the core of the tumor to the periphery[12], since it also involves the peritumoral and edema regions[29]. The core of the tumor is comprised of necrotic tissue surrounded by the tumor zone, and a marked proliferation and inflammation distinguish it. In addition, the core region is more likely to be radioresistant and chemo-resistant[12]. Tumor cell density decreases from tumor core to the periphery[12], resulting in heterogenous areas within the lesion with distinctive properties.

A very high cell density implies a significant blood supply requirement for the establishment, growth, and progression of the tumor[44]. Therefore, distinct regions with variable levels of hypoxia and necrosis coexist in the same tumor[32]. This lack of oxygen triggers several mechanisms implicated in forming new vessels[24,44,45], including MVP, angiogenesis, vascular co-option, and vasculogenesis[46–48]. The result of these processes is an abundant, aberrant, and heterogeneous vascular architecture[48].

This novo-generated vasculature is formed by dysfunctional and occluded vessels that cannot maintain normoxia, hence the formation of hypoxic regions[12]. Although a hypoxic microenvironment could induce cell death in normal conditions, it also can maintain cancer stem cells (CSCs), especially in astrocytomas grade 4[49]. While actively proliferating cells are more likely to be found close to the vessels, stem-like cells lie in the core of the tumor, contributing to a CSC niche[50]. These different distributions of cells continue illustrating the marked heterogeneity of these gliomas.

Different types of data can be generated when analyzing intratumor heterogeneity, from molecular and histopathologic profiles to advanced assessment of tumor vascularity using imaging techniques. This data is complementary and can provide useful prognostic and therapy selection information. Analyzing characteristics from different regions of the active tumor and the rest of the lesion represents a historical record of alterations and changes accumulated during tumor evolution. In this regard, the study of spatial heterogeneity at microscopic and macroscopic levels may help to know the genesis and progression of individual astrocytomas[28]. As well as interpatient heterogeneity may be key for a short-term approach of precision medicine for specific groups of patients, evaluating intratumor heterogeneity will be

essential to adopt more personalized treatments in the long term, since it allows the individual analysis of each tumor.

2.3.3. Longitudinal heterogeneity

In addition to interpatient and intratumor heterogeneity, astrocytomas are influenced by tumor progression, i.e., it changes over time. On top of that, these tumors show focally varying levels of aggressiveness and an inhomogeneous genome that mutates during the pathology[30,51,52]. In addition, the aggressive treatment provided, including resection, chemo- and radiotherapy, induces important changes in tumors during patient follow up. This thesis has focused specifically on the study of presurgical biomarkers. However, the relevance of monitoring treatment management and prediction of tumor relapse has been addressed in complementary publications CP1 and CP2. The section addressing the potential solutions for theses needs using DSC perfusion biomarkers constitutes *subsection 2.7.2* of this chapter.

2.3.4. Advanced approaches to address heterogeneity

To address differences in survival and responses to standard and novel treatments, it is necessary to study in detail the heterogeneity that characterizes this disease at the three main levels described above.
In recent years, different approaches have been tried to analyze the heterogeneity of these tumors, as it represents the cornerstone for designing efficient and personalised treatments. Data derived from advanced methodologies and techniques have been used to determine specific patient and tumor profiles, including:

- *Next-generation sequencing*. Several studies have proposed that whole-exome sequencing (WES) can identify genes associated with treatment response and proposing personalized promising therapies for each patient with high-grade astrocytomas[53,54]. Despite these encouraging results, identifying clinically relevant findings from the vast amount of data produced by WES is still a substantial challenge to overcome.

- *Transcriptomics.* Transcriptome analyses have been performed to study response to specific cancer therapies[55] since they can be used to identify genes and pathways expressed in particular tumors[56]. However, validation of gene expression is needed previously to their use in daily clinical practice. Therefore, only the expression of a few genes are currently in use. In

addition, transcriptomic profiling provides information about the tumor at the time of biopsy but cannot describe the complete tumor biology or the intrinsic heterogeneity of individual cell populations. Innovative emerging methodologies, including single-cell transcriptome sequencing, will facilitate our understanding of tumor biology in individual patients[55]

- *Radiomics.* Radiomics is a computational approach to medical imaging, which aims to enhance the existing data available to researchers and clinicians through advanced mathematical analysis[57]. These methodologies have provided vital insight into high-grade gliomas' essential features, based mainly on the analyses of magnetic resonance images. Radiomics allows the establishment of associations between those characteristics derived from images and key clinical, genomic, proteomic, and transcriptomic features of the tumor. This approach may be part of the future of personalized medicine since it can provide support to physicians due to its influence on treatment selection[58]. Aftab K et al. summarized studies that had shown the potential application of radiomics in planning surgical procedures, evaluating the dose of radiotherapy, predicting the effective dose of chemotherapeutic agents and stratifying patients who will benefit from therapy[59]. In addition, the evidence of the benefit of radiomic analysis for precision medicine has culminated with studies demonstrating that specific radiomic signatures can predict T-cell infiltration and response to immunotherapies[60].

These techniques are instrumental for researchers to acquire precious knowledge about tumor biology, heterogeneity, and behavior, opening the possibility of abundant translational discovery opportunities. One of the potential applications of integrating all of this large data is to support precision medicine. Unfortunately, acquiring, processing, and combining this extensive and complex data for each patient is unfeasible for daily clinical practice because most of them are extremely time, effort, and economic-consuming.

Until the use of all this data for the design of personalized treatments becomes feasible, a shorter-term solution would be finding and developing easy-to-determine biomarkers that facilitate the selection of personalized treatments for specific patients. Some of these simpler-to-define biomarkers have been analyzed during the development of this thesis. Chapters 7 and 8 include those studies related to treatment response and patient selection using MRI-DSC biomarkers and basic clinical characteristics. In summarizing, this type of studies can help overcome the

limitation of heterogeneity and support treatment decisions for patients with high-grade gliomas without extra economic, time, and effort costs.

2.3.5. Vascular heterogeneity

Focusing on vascularity, it is also present at interpatient, intratumor and longitudinal levels. Each patient presents a unique vascular architecture and behavior (interpatient level); different regions can be found within the lesion with distinct vascular patterns (intratumor level); and the vascular structures and process are dynamics, i.e., they change over time (longitudinal level).

Although hopes have been placed on anti-angiogenic therapies for years (see subsection *2.2.3. Antiantiogenic treatment*), their promise has been held back in the case of these aggressive brain tumors. Due to the large palette of neovascularization processes and the heterogeneous vessel architectures that characterize these tumors, each tumor vascular pattern has to be analyzed to decide the best treatment choice, including selecting patients who can benefit from anti-angiogenic.

Fortunately, we can take advantage of the vascular heterogeneity of these aggressive tumors to determine and develop biomarkers with different applications for the clinical setting. One of the most valuable and convenient techniques to achieve these purposes is MRI perfusion, which allows the acquisition of perfusion studies of each patient. Subsection *2.4.2. Potential applications of DSC biomarkers* include previous studies analyzing the prognostic and monitoring functions of these vascular biomarkers. In addition, a validated vascular assessment methodology for high-grade gliomas developed by the BDSLab is described in section *2.6.*

2.4. Magnetic Resonance Imaging

In 1946, Felix Block in Stanford and Edward Prucell in Harvard discovered independently the Nuclear Magnetic Resonance (NMR) phenomenon, which earned them both the Nobel Prize of Physics in 1952. Broadly defined, the phenomenon of NMR consists in the fact that certain atomic nuclei (such as hydrogen), when subjected to the action of an intense magnetic field, can selectively absorb energy in the form of radio-frequency (RF) waves of a specific frequency (resonance phenomenon). This energy returns when returning to the equilibrium state, generating an electrical signal induced in an antenna or receiving coil that provides Magnetic Resonance (MR) images when analyzed and processed.

MRI is a medical imaging technique that provides invivo internal representations of the human body at anatomical and physiological levels. This technique used in radiology was developed in the decade of 1970 through the work of three professors. Prof. Damadian works (1971) on NMR relaxation of different tissues laid the

groundwork for many further developments in MRI. Some years later, Lauterbur (1973-1974) developed a reliable technique based on gradient magnets to generate MR images of the human body's interior, and Mansfield (1977), developed a mathematical formulation that dramatically accelerated the acquisition of the images. These works earned Lauterbur and Mansfield the Nobel Prize in Physiology or Medicine in 2003.

Since its development, MRI has been used routinely in hospitals and clinics, helping in the diagnosis, monitoring, and treating different medical problems and diseases. Compared to other imaging techniques, such as CT, MR pictures are more detailed and provide better contrast in soft-tissue imaging, e.g., in the brain. For this reason, in general, diagnosing a brain tumor usually begins with the radiologic study of MR images acquired from the patient.

2.4.1. MRI mechanism

This imaging technique is based on the magnetic properties of the hydrogen nucleus (*H*+) in tissues since a signal can be created and processed to form an image of the subject in terms of the density of those nuclei in a specific region. In a natural state of rest, all the *H*+ hydrogen nuclei of a body rotate randomly, thus neutralizing each other's angular momentum and producing a global magnetic momentum of zero spin. Under the influence of an external constant magnetic field B_0, the *H*+ nuclei align their spin with B_0 in a parallel (low energy) or antiparallel (high energy) state, producing an overall spin magnetic momentum M_z, with *z* the direction of B_0. The NMR phenomena is related to the excitation produced to the *H*+ nuclei by the effect of an additional temporal magnetic field, the RF pulses, with a direction different from B_0. When a RF pulse at the Larmor frequency is triggered at B_0, an energy exchange occurs with some *H*+ nuclei, raising them to the high-energy antiparallel state. In addition, a synchronization of the precession of all the *H*+ nuclei is induced, so they begin to precess in phase. This event causes two magnetic effects in the system: 1) a decrease in the overall spin magnetic momentum M_z due to the lifted *H*+ nuclei, and 2) the apparition of a spin magnetic momentum M_{xy} transverse to the B_0 field due to the phase coherence precession. Such transverse magnetization M_{xy} generates a magnetic signal called the NMR signal.

Once the RF pulse has ended, the system begins to relax, recovering its initial state of equilibrium, being these relaxation processes are related with the generation of the MR images. The transverse spin magnetic momentum M_{xy} begins to disappear, leading to the so-called spin-spin relaxation or transverse T2 relaxation process. Likewise, the previously lifted *H*+ nuclei return to their original low energy parallel state, restoring the longitudinal magnetization M_z to its original value. This process is called the spin-lattice relaxation or longitudinal T1 relaxation. These independent

T1 and T2 relaxation processes allow each tissue returns to its equilibrium state after the previously induced excitation.

T1 and T2 relaxation times are significantly different, with T1 a longer process than T2 (300-2000 ms vs. 30-150 ms). Depending on chemical environment, T1 and T2 relaxation emit different NMR that will in essence, determine the intensities for each tissue in the MR image. There are three main MR morphological modalities: T1-weighted, T2-weighted and Proton Density (PD) images, which are related to the so-called Repetition Time (TR) and the Echo Time (TE) times. TR is the time between successive radio-frequency pulses and affects the speed at which *H+* nuclei realign to the B_0 field, being closely connected to T1 relaxation effect. The TE refers to the time at which the electrical signal induced by the *H+* nuclei is measured and concerns the degree of dephasing of the spins of the *H+* nuclei, being more related to T2 relaxation events.

2.4.2. Anatomical MRI

Depending on the chemical context, different tissues can be visualized via the measurement of their associated electrical signals, generating images that depict the anatomical structures under study. The most common MRI study for patients with high-grade gliomas includes the following type of images:

T1-weighted: This image is useful for assessing the cerebral cortex, identifying fatty tissue, and in general, obtaining morphological information, as well as for post-contrast imaging. In presence of high-grade glioma, this sequence shows the anatomical overview of the lesion, including the soft tissues below the base of the skull.

T1$_{CE}$-weighted: This sequence is acquired after the administration of a bolus of Gadolinium-Based Contrast Agent (GBCA) to improve the visibility of internal structures. Its main objective is to assess vascular systems of the region of interest (ROI) by enhancing vessels.

T2-weighted: This image allows the visualization of a more water content. This sequence evaluates basal cisterns, ventricular system, and subdural spaces, the assessment of vasogenic edema, and good visualization of flow voids in vessels.

FLAIR-T2 weighted: Typically a Fluid Attenuation Inversion Recovery (FLAIR) T2-weighted sequence. It is a unique inversion recovery sequence with a long inversion time. It is characterized by suppressing the signal from the cerebrospinal fluid, appearing like a T2-weighted image but with the cerebrospinal fluid dark instead of

bright. Its purpose is the assessment of white-matter tumor involvement and related vasogenic edema.

Figure 2.5 includes an example of the aforementioned presurgical MR images acquired from a patient with astrocytoma grade 4 included in the *MTS4UP* study.

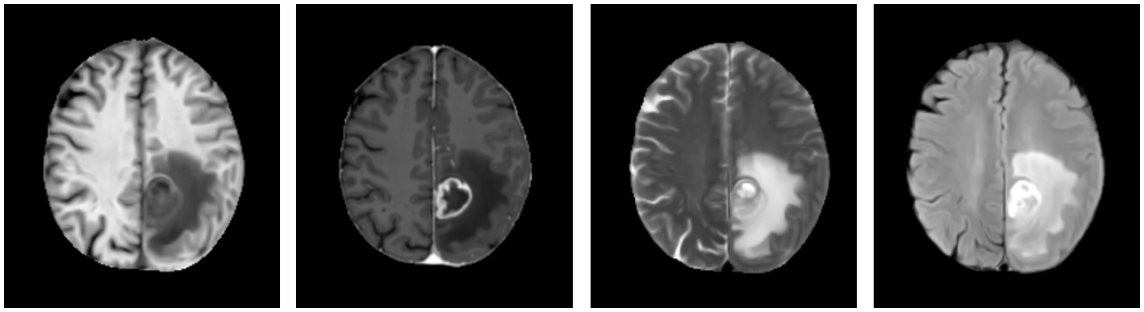

Figure 2.5. Example of anatomical presurgical magnetic resonance images typically acquired in an astrocytoma grade 4 study. From left to right: T1-weighted, T1CE-weighted, T2-weighted, and FLAIR MRI. Images were collected during the MTS4UP multicenter study.

2.4.3. DSC Perfusion MRI

As previously defined, astrocytoma grade 4 usually presents an aberrant and abnormal vascular architecture, due to its extensive MVP and marked angiogenesis. In this sense, PWI allows the measurement of hemodynamic properties through the intravenously injection of a paramagnetic contrast agent to the patient. MRI perfusion biomarkers can detect local vascular patterns of the tissues and their hemodynamic properties. There are three main PWI techniques: DSC perfusion, Dynamic Contrast Enhanced (DCE) perfusion, and Arterial Spin Labeling (ASL) perfusion, being DSC the most used PWI technique for the evaluation of high-grade gliomas[61].

With DSC-MRI, T2- or T2*-weighted images are acquired with a high temporal resolution during the bolus administration of a GBCA. The bolus passage induces a gradient of susceptibility between the intravascular and extravascular tissue compartments causing a transient decrease in the signal intensity. Most often, T2*-weighted gradient-echo (GRE) echo planar imaging (EPI) methods are used, which are sensitive to vessels of all diameters. T2-weighted images, obtained with spin-echo (SE) EPI methods, provide CBV maps primarily liable to microvessels. Subsequent descriptions will be given for GRE based methods unless otherwise noted. The same basic principles for data acquisition and processing applications for SE-based methods. The DSC signal time course, S(t) is converted to a change in the

T2* relaxation rate (DR2*(t)), where Sb is the mean of the baseline (pre-bolus) signal intensity whose integration estimates the relative cerebral blood volume (rCBV)[62].

This measure is termed *relative* because it provides a voxel wise value relative to the rest of the brain or to the contralateral white matter. Alternatively, an absolute measure of CBV can be determined from the ratio of the tissue (Ct(t)) (which is assumed equivalent to DR2*(t)) and arterial concentration-time curve (Ca(t)) first pass areas. Where k is the scale factor accounting for the density of brain tissue and the differences in hematocrit between capillaries and large vessels. As indicated, an absolute measure of CBV requires the determination of Ca(t), also referred to as the arterial input function (AIF). More often, for comparison purposes, the rCBV will be normalized by dividing the rCBV in each image voxel by the mean rCBV determined from a reference tissue ROI, such as normal appearing white matter giving normalized rCBV values. Like absolute CBV, the rCBV maps provide greater consistency for comparing rCBV across time and patients. Note that the term rCBV may be used interchangeably with normalized CBV (nCBV) in some instances, with the implicit assumption that the CBV is relative. An explicit description of the steps used to create CBV should be provided in all cases, with clear definitions of terminology. Finally, another newer *standardization* approach has been devised to calibrate the rCBV maps directly without requiring a normalizing ROI. Standardized rCBV (srCBV) has demonstrated greater consistency across time and improved repeatability compared with rCBV. Both rCBV and srCBV have been used with success in several brain tumor clinical trials[62].

Typical models for DSC quantification explicitly assume that the GBCA remains in the intra-vascular space for the duration of the perfusion acquisition. However, this assumption is not accurate for astrocytomas grade 4, since they often present disrupted BBB. Therefore, GBCA extravasates to the extravascular interstitial space producing a distortion in the signal that leads to an overestimation or underestimation of perfusion parameters if non leakage correction is performed. Numerous methods have been proposed in the literature to correct the leakage effect in perfusion, and the deviation it produces in the estimation of the perfusion markers: use of pre-dosing, double-echo acquisitions or parametric modeling. The most common and reference technique is the one proposed by Weissko et al (1994) and later elaborated by Boxerman et al[114]., which corrects the leaky signal by estimating its deviation from a non-leaky reference signal of the same patient.

2.5. Glioma segmentation methodologies

According to Duda and Hart, segmentation is *the extraction of an object of interest from an arbitrary image*[63]. For Gonzalez and Woods, it is *the subdivision of an image into its constituent parts*[64].

Often, it is of interest to know the size, volume, or in general, the properties of the parts that compose an organ or a lesion (in our case the tumor located in the brain). While the visual evaluation of images allows a qualitative analysis, image segmentation allows a quantitative analysis contributing to a more objective diagnosis of different pathologies. This, for example, is key in the diagnosis and follow-up of patients with brain tumors.

Medical imaging segmentation can be performed in three ways: manual, semi-automatic and automatic.

Manual segmentation. Manual segmentation by experts has the advantage of producing high-quality segmentations. However, it is a tedious task that requires time and a significant economic investment. In addition, manual segmentation depends on experts and their level of training, which results in high variability, i.e., it is not very reproducible[65,66]. It is not suitable for longitudinal studies or population studies in which large amounts of data must be processed consistently. This fact is compounded by the advancement of acquisition technologies that achieve high-resolution images that allow the study of increasingly smaller and more complex structures, which has caused the reliability of manual segmentation to decline and the time cost to skyrocket. To solve this problem, many semi-automatic and automatic segmentation methods have emerged over the years.

Semi-automatic segmentation. One option to reduce the time cost of manual segmentation is to use semi-automated techniques. These techniques still require the supervision of a human operator but automate some parts of the process, which reduces segmentation time and generally produces more consistent and reproducible segmentations. For example, thresholding techniques have been widely used to aid in the segmentation process since they delimit the range of intensities that discriminate between different objects in the image. Another popular way to semi-automatically select a set of pixels is a region growing. Region growing consists of the selection of a seed point from which new points are added that meet a series of conditions, such as being in contact with a previously included point and belonging to a specific range of intensities. The main advantage of this technique is the possibility of selecting regions with a similar range of intensity but different locations and connectivity.

Automatic segmentation. Countless automatic segmentation methods can be broadly classified into supervised and unsupervised categories. Supervised methods use data-class pairs (previously labeled examples) to perform a learning process after which they are applied to new data to obtain the classes to which they belong. On the other hand, unsupervised methods (clustering) use the data distribution itself to find the most coherent classification. In addition, some novel methodologies can combine both supervised and unsupervised approaches to get a more meaningful extraction of information from the MR images. This is the case of the ONCOhabitats method, developed to assess the vascular heterogeneity of high-grade gliomas.

2.6. Vascular heterogeneity assessment method: ONCOhabitats

As explained in section *'2.3.5. Vascular heterogeneity'* of this thesis, comprehending intra- and interpatient heterogeneity of astrocytomas grade 4 is one of the most relevant challenges to combat these aggressive tumors, been identified as one of the most important hallmarks of high-grade gliomas. To select effective therapies that can improve patient prognosis, an in-depth study of the aberrant vasculature, the hemodynamic behavior, and the angiogenesis mechanism of these tumors is needed. Motivated by this objective, researchers of the BDSLab of the Universitat Politècnica de València (València, Spain) developed the ONCOhabitats platform[67], which includes the Hemodynamic Tissue Signature (HTS) methodology.

The HTS methodology allows an automatic study of the discovery and delineation of differential tumor habitats by the morphology, vascular behavior, and hemodynamics of high-grade astrocytomas, only by introducing the standard presurgical MRIs (T1, T1c, T2, FLAIR and DSC perfusion) collected during the patient's diagnosis stage. The main purpose of this service, which is available in www.oncohabitats.upv.es, is to assess the vascular heterogeneity at both intratumor and interpatient levels, using advance artificial intelligence techniques.

The HTS methodology is represented in Figure 2.7, and it includes the following four stages:

1. *Image preprocessing*, incorporating correction of usual MRI artifacts, including voxel isotropic resampling of all MR images, correction of the magnetic field inhomogeneities and noise, multimodal registration, and skull stripping and brain extraction.

2. *Classical tissue segmentation*, performed by using an unsupervised segmentation method, which implements a state-of-the-art deep learning 3D convolutional neural network (CNN). It takes the morphological T1c, T2, and

FLAIR presurgical MR images as input. The current CNN is an in-house development that incorporates state-of-the-art techniques in image segmentation, such as spatial- and channel-attention blocks, deep multi-level losses, custom training schedulers, and residual- feature extraction blocks[67,68]. The backbone of our network maintains the classical U-net architecture with long-term skip-connections but adds the previously mentioned mechanisms that significantly improve the segmentation's quality. Moreover, a balanced training strategy that yields local patches of healthy, necrotic, edematous, and enhancing tumors is adopted to ensure the network is not biased towards the highest prevalent tissue in the brain. The result is the segmentation of the classical tissues, including the active tumor, the necrotic tissue and the edema.

3. *DSC perfusion quantification* calculates the hemodynamic maps derived from the DSC perfusion sequence: rCBV, relative cerebral blood flow (rCBF), mean transit time (MTT), and the extravasation coefficient (K2 permeability). All perfusion maps are normalized against contralateral unaffected white matter volume to achieve consistency and comparability across patients and cohorts. The normalization is performed automatically by a CNN trained with approximately 100 cases, detecting the contralateral unaffected white matter region with about 90% accuracy. To ensure a correct perfusion quantification and to avoid under- and over-estimation of perfusion marker, DSC perfusion quantification includes correction for contrast agent leakage effects. The HTS method implements the Boxerman leakage-correction method for T1- and T2-leakage impact and gamma-variate fitting to remove the extravasation phase and second pass of the contrast bolus.

4. *HTS habitats delineation*. In this stage, an automatic unsupervised segmentation algorithm performs the detection and delineation of four vascular habitats within the active tumor and the edema, previously segmented during the second stage. For that, the specific hemodynamic behavior of each region is considered, being these four vascular habitats unique for each patient. The vascular habitats are delineated using a DCA-SVFMM structured clustering of rCBV and rCBF maps (calculated during the third stage). The clustering includes two stages: (I) a two-class clustering of the whole enhancing tumor and edema regions and (II) a two-class clustering performed by using only the rCBV and rCBF data within the regions obtained in the first stage. To ensure the reproducibility of the HTS, both stages were initialized with a deterministic seed method.

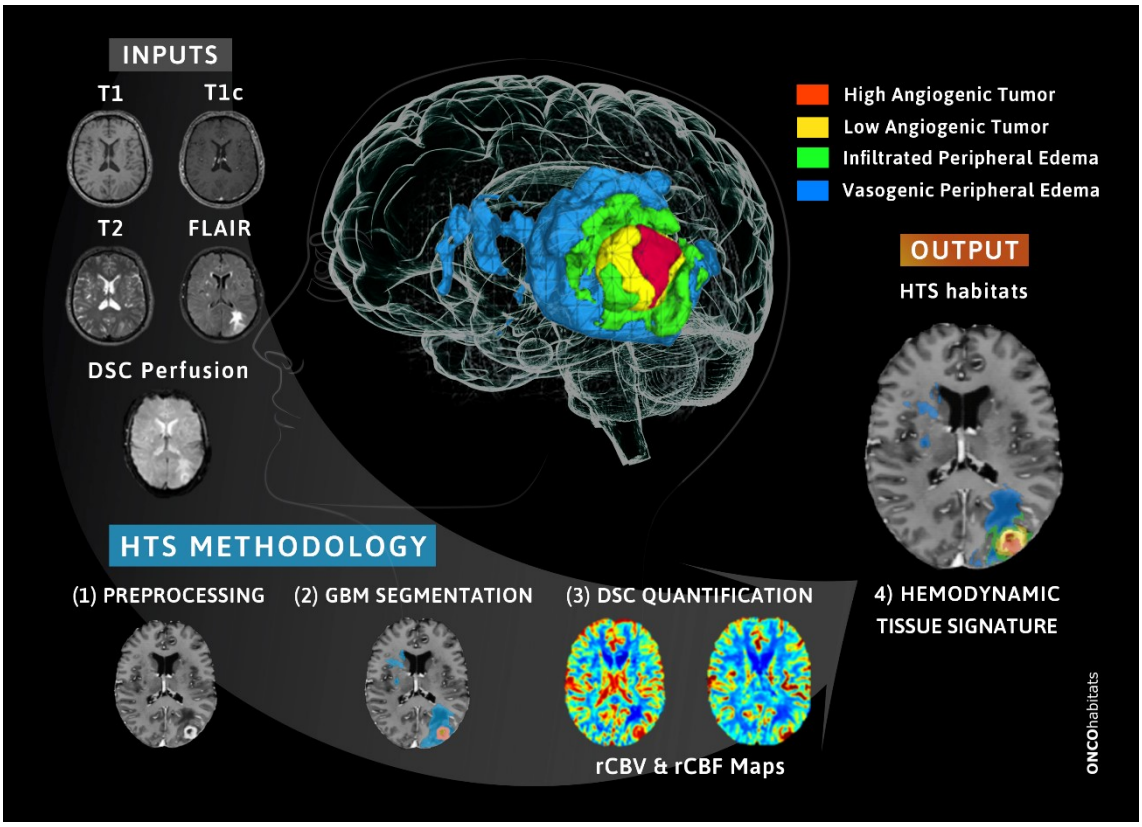

Figure 2.7. Scheme of the Hemodynamic Tissue Signature (HTS) methodology included in the ONCOhabitats platform. It consists of the following four stages.

The resulting habitats within the tumor and edema are the following: *High angiogenic tumor habitat (HAT), low angiogenic tumor habitat (LAT), infiltrated peripheral edema habitat (IPE) and vasogenic peripheral edema habitat (VPE).* Additionally, the interest of this methodology is not the possibility to segment and visualize these four habitats, but also that MRI perfusion biomarkers, such as rCBV and rCBF, can be calculated within each habitat. In a preliminary single-center study, these perfusion biomarkers were proposed as associated with patient prognosis in a preliminary single-center study[68].

The multicenter validation of the prognostic capability and the reproducibility of the MRI-DSC biomarkers calculated across different centers at international level is included in part II-chapter 3 of this thesis.

In addition, part IV of this thesis includes the design and implementation of the *BIOhabitats* study (NCT05375318), whose main objective its the biological validation of these four regions at molecular and histopathological level. The project is still in process and biologic samples of each defined habitat are being collected during standard surgeries of patients with astrocytoma grade 4 in two Spanish hospitals.

2.7. Potential applications of DSC biomarkers

2.7.1. Patient prognosis and stratification

One of the main potential applications of DSC biomarkers would be to predict patient overall survival, due to the association found between tumor vascularity and survival times[68–70]. These results are not surprising since previous studies revealed that vascularity, measured by rCBV, is correlated with tumor aggressiveness[71,72].

Despite the robustness and agreement of these results, the implementation of DSC biomarkers in clinics still being unfeasible to predict survival. One of their main limitations is the low reproducibility of its calculation due to the lack of standardized protocols for MRI acquisition, segmentation methodologies, and biomarkers computation.

In this sense, one of the main purposes for developing the ONCOhabitats methodology (presented in the previous subsection) was to overcome this limitation and provide researchers and clinicians with a robust methodology to calculate DSC biomarkers useful for patient prognosis[68].

Juan-Albarracín *et al.* demonstrated the strong correlation between overall survival and DSC biomarkers calculated in tumor habitats and in the peripheral edema habitat. This study was performed with data from 50 patients treated in a single center. The multicenter study with validation of the methodology and the DSC biomarkers to predict survival is presented in chapter 5 included in part 2 of this thesis.

2.7.2. Monitoring of treatment response and prediction of tumor relapse

**Explanatory note: The following information included in this subsection was extracted from the complementary publication CP1[6] referenced in this thesis. It consisted of a meta-analysis of the main MRI techniques for monitoring treatment response in high-grade glioma patients. The author of this thesis participated in writing the subsection related to DSC perfusion included in the CP1 publication.*

During and after treatment of patients with high-grade gliomas, *monitoring biomarkers* are measured serially and are required to detect any change in the extent of glioma infiltration or provide evidence of treatment response[73]. Subsequently, MRI has been incorporated into recommendations for determining treatment response in clinical trials. In these recommendations, treatment response assessment is based on simple linear metrics of contrast-enhancing tumor, specifically, the product of the maximal perpendicular cross-sectional dimensions (in "measurable" lesions, which are defined as > 10 mm in all perpendicular dimensions). The

recommendations are based on expert opinion informed by observational studies and derived from the biologically plausible assumption that changes in tumor size identify the progression of the disease, potentially before it becomes clinically apparent, resulting in a lead time improvement for therapeutic intervention[74]. Indeed, there may be benefits in changing management before the development of irreversible disability or before the extent of the tumor precludes intervention. Some justification for enhancement as a disease proxy has been inferred from data showing that enhancing tumor size and extent of resection are "prognostic biomarkers"[73] at both first presentation and recurrence[75,76].

A systematic review and meta-analysis of studies between 2005 and 2015 included 17 DSC-MRI studies. They concluded that individual studies, taken in an isolated form, showed encouraging results to differentiate tumor progression from treatment-related changes, with sensitivities and specificities in the 80%–90% range[7778]. Yet, widespread use has been hampered by the wide range of proposed rCBV thresholds reported (0.9–2.15). This variation is largely attributed to the statistically significant heterogeneity in how the DSC-MRI data are collected and analyzed[77]. However, the studies reviewed preceded the recently published consensus recommendation that describes how best to acquire DSC-MRI data and that a correction for leakage should be included. With the widespread implementation of this consensus acquisition, it is hoped that greater consistency in mean rCBV thresholds will follow. A recent multisite study supports this contention[78]. Several sites used their postprocessing platform to process the same DSC-MRI data whose acquisition was consistent with the subsequently published consensus recommendation regarding the acquisition. A common threshold applicable to all sites could be determined to distinguish high- from the low-grade tumor. This suggests that, with greater consistency in the acquisition of DSC-MRI data, agreement on thresholds to distinguish treatment-related effects from the residual or recurrent tumor is also possible. Using the mean rCBV determined from the enhancing lesion ROI is another often-overlooked factor that may contribute to the wide range of reported rCBV thresholds. Rarely is a lesion composed of pure tumor or pure treatment effect. Instead, an admixture of tumor and treatment effect will be unique for each patient and each cohort of patients. Yet, all studies described in the meta-analysis [77]used the mean rCBV from an ROI. Consequently, it is not surprising that each study reports a different threshold value because it comprises a unique set of patients. Even if the acquisition and post-processing methods were equivalent, it is still likely that each study would report a different threshold to distinguish tumor from treatment effect.

One proposed research solution to determining a widely accepted single threshold is to use image-localized biopsy and spatially histopathologic correlation, as described in two retrospective studies of high-grade brain tumors. Only tissue confirmed to be either pure tumor or pure treatment effect were used in these studies to determine an rCBV threshold for distinction. In both studies, the consensus acquisition protocol was used, and the rCBV threshold was determined to be the same to distinguish high-grade tumor from treatment effects. A significant difference in tumor and treatment effect was also found for standardized rCBV[79]. Biopsy-determined rCBV thresholds can be used to create voxelwise maps that distinguish tumor from non-tumor for the determination of the overall fraction of tumor burden within the enhancing lesion. These maps, referred to as fractional tumor burden (FTB) maps[80], provide a unique ability to visualize the admixture of tumor and post-treatment effects. The potential of FTB to predict response to treatment[81] and to distinguish between tumor or treatment effect, as confirmed by histopathologic examination of resected tissue samples[82], has been demonstrated. More recently, a prospective study[83] using image-localized biopsy tissue validated the ability of rCBV to predict tumor content (0–100%), demonstrating the similar performance of nRCBV and sRCBV for the creation of FTB. Given that sRCBV does not require choosing a reference ROI, this represents an important step toward workflow optimization for creating FTB maps.

2.8. Next-generation sequencing in Astrocytoma grade 4

In the early 2000's, bioinformatics began developing as a field that uses computational methods to analyze data from genomic and transcriptomic sequencing[84]. Bioinformatic techniques and molecular data emerge to understand the complexities of cancer biology including high-grade gliomas. This use of integrated genotypic and phenotypic characteristics was one of the major updates to from the 2007 WHO CNS classifications to the 2021 last updated edition[10]. Advances in genetic sequencing have also provided new insights into understanding astrocytoma grade 4 biology, TME and studying potential targets. These insights will hopefully lead to develop new treatments more efficient, but there remains a chasm between clinicians and the practical utilization of the ever-growing field of genomics and transcriptomics.

As the cost of genome and transcriptome sequencing continues to drop, the amount of data created is quickly becoming *big data*. A basic understanding of genomics and transcriptomics will be necessary to adopt an interdisciplinary approach that facilitates the treatment of such complex diseases as astrocytomas grade 4.

2.8.1. Genome sequencing

There are a large variety of technologies available to identify genetic variants and alterations. It is not the intention of this thesis to describe all of them. Chapter 8 includes a study in which genomic data was used to identify differences in immunotherapy responses depending on tumor laterality. For this work, genomic data extracted from whole exome sequencing (WES) was used. For this reason, this subsection focused on the description of this technique, as well as the relevance of this type of data in astrocytoma grade 4 research and patient management.

2.8.1.1 Basics of whole exome sequencing

WES is a genomic technique for sequencing all the exome, i.e. all the protein-coding regions of genes of genome. It consists of two main stages:

1) *To select only the exons through target enrichment strategies.* Target-enrichment methods allow to selectively capture genomic regions of interest from a DNA sample before sequencing. Different target-enrichment strategies have been developed since the original description of the direct genomic selection method in 2005[85]. Although several techniques have been proposed for targeted capture, only two of these have been mainly extended to capture whole exomes. The first strategy was the array-based hybrid capture method, developed in 2007, in which reactions occur on a solid support, but the use of in-solution capture has increased in last years.

2) *Sequencing.* There are a large number of sequencing platforms available, from classical Sanger sequencing methodologies, that involves electrophoresis and is based on the random incorporation of chain-terminating dideoxynucleotides by DNA polymerase during in vitro DNA replication, to Next Generation Sequencing (NGS) methods. They include Roche 454 sequencer and Life Technologies SOLiD systems, the Life Technologies Ion Torrent and Illumina's Illumina Genome Analyzer II (defunct) and subsequent Illumina MiSeq, HiSeq, and NovaSeq series instruments, all of which can be used for massively parallel exome sequencing. These 'short read' NGS systems are particularly well suited to analyze a high number of relatively short stretches of DNA sequences, as found in human exons.

2.8.1.2 Relevance of genomic data in astrocytoma grade 4

Astrocytoma grade 4 was the first tumor to be studied by the Cancer Genome Atlas Research Network with the analysis of 206 samples in 2008. Genetic alterations identified in three main signaling pathways (RTK/RAS/PI-3K, p53, and RB) allowed for elucidation of gliomagenesis[86,87]. It is a fact that advances in sequencing methodologies have allowed the sequencing on formalin fixed paraffin embedded (FFPE) tissue, making tumor genetics clinically essential for clinicians. This allows genetic sequencing to be part of the routine pathological analysis of tissue samples following surgical resection, facilitating the identification of patients who may qualify for targeted therapy and/or clinical trials.

As a result of collaborative efforts, a remarkable amount of genomic sequences from astrocytoma grade 4 samples are now publicly available and can be analyzed using bioinformatic strategies. This collaborative analysis detected differential gene expression levels that were associated with astrocytoma grade 4 tissues, in comparison to healthy tissue samples, that were found to significantly affect prognosis[88].

Mutations in *IDH*, *PTEN*, *EGFR*, *CDKNA/B*, *RB1*, as well as *MGMT* methylation are some of the alterations considered in the studies including in this thesis, since they are demonstrated as critical in tumor progression and classification and patient survival. These aforementioned genetic biomarkers in astrocytoma grade 4 have primarily been due to the improvements in technology that have reduced cost and accelerate the speed of genetic sequencing techniques. With this new situation, analysis of large enough numbers of tissue samples to give statistically significant results is now possible.

2.8.2. Transcriptome sequencing

As well as genomic sequencing techniques, there are a variety of transcriptomic technologies available to quantify gene expression levels. Chapter 8 includes a study in which transcriptomic data derived from ribonucleic acid (RNA) sequencing (RNAseq) was used to compare gene sets differentially enriched in tumors located in left and right brain hemispheres, since they were associated to treatment response. For this reason, this subsection only includes a description of basics of RNAseq, and the relevance of transcriptomic data in astrocytoma grade 4 research.

2.8.2.1 Basics of RNA sequencing

RNA-seq with NGS is a powerful methodology to reveal the presence and to quantify of the expression level of genome-wide genes in a biological sample at a

given moment. Compared with DNA microarray, which has been widely used to evaluate the expression of a wide range of genes, RNA-seq does not require previously prepared probes, thus enabling the evaluation of unknown gene expression and the identification of unknown fusion genes or various alternative splicing. In addition, without the risk of non-specific hybridization, it can also evaluate the expression level of transcripts of very low abundance[89].

2.8.2.2 Relevance of transcriptomic data in astrocytoma grade 4

Several studies have identified different astrocytoma grade 4 subtypes considering trancriptome profiles. In 2010, Verhaak *et al.*[90] proposed four subtypes: proneural, neural, classical and mesenchymal. Although these subtypes present distinct molecular patterns, their association with survival is ambiguous except for patients with astrocytoma grade 4 *IDH*-mutant[91]. More recent studies have found other transcriptomic patterns related with overall survival[91–93] or with therapy responses. Currently, there is not an agreement to stablish a gene expression-based classification of astrocytoma grade 4, however it seems a fact that this information is critical to predict therapy responses[94] and for patient stratification[90–92].

During the development of this thesis, specific alterations have been considered, such as *IDH* mutation (in chapters 3 and 4) and *MGMT* methylation (in chapters 6 and 7), and their associations with vascularity, measured by DSC perfusion.
In addition, for last studies of this thesis, genomic and transcriptomic data of patients with astrocytoma 4 were analyzed in order to find specific patterns correlated with tumor location, defined by MRI, and response to anti-*PD1* treatment (chapter 8).

2.9. Survival Analysis

In many medical studies, the main outcome to assess is the duration of time until one event occurs, typically patient death or tumor relapse[95]. The branch of statistics for analyzing data when the outcome variable of interest is *time until an event occurs* is Survival Analysis.

Survival data trend to follow specific statistical distribution. They are non-negative and often subject to bias depending on the timing at which events are occurring. More importantly, they are typically subject to censoring (incomplete or missing data)[96].

Two related statistical parameters are used to describe survival data: the survival probability and the hazard probability. The survival probability, also known as the survivor function S(t), is the probability that an individual survives from the time origin (e.g. diagnosis of tumor) to a specified future time t. The hazard, denoted by h(t), is the probability that an individual who is under observation at a time t has an event at that time.

The main survival analyses to work with this particular data are Kaplan Meier (KM) plots, log-rank tests, and Cox regression (proportional hazards ratios (HR))[95].

2.9.1. Type of events

In most of cancer studies, time to death or to tumor relapse are the events of interests. The generic names to define these times are overall survival (OS) time and progression free survival (PFS) time, respectively. It is important to state what the event is and when the period of observation starts and finishes. To define OS in patients with astrocytoma grade 4, the typical initial point is the date of the MRI_0, i.e., the first MRI used to make the working diagnosis by the radiologist, and the final point the date of exitus (death). In case of PFS, the final point is the date in which tumor relapse is radiologically detected.

Censoring

In a clinical trial context, it may not be possible to observe an event for each patient, thus survival analysis techniques must be able to account for missing data. [96].

Particular difficulties related to survival analysis arise mostly from the circumstance that only some patients have experienced the event (for instance, death) and, consequently, survival times will be unknown for a subgroup of the cohort. This phenomenon is called censoring and it may arise in three main ways: 1) a patient has not (yet) experienced the outcome of interest, such as relapse or death, by the time of completing the study; 2) a patient is lost to follow-up during the study period; 3) a patient suffers a different event that makes future follow-up not possible. These censored survival times underestimate the real (but uncertain) time to the outcome. Displaying the survival course of a patient as a time-line, its event (assuming it were to occur) is beyond the end of the follow-up period. This scenario is often referred to as right censoring[95]

When standard methods of survival analysis, , such as KM and Cox analysis, are performed, it is commonly accepted that censoring is non-informative of survival. However, if it is known that many dropout is due to patients becoming too ill to participate or no longer needing treatment (due to being cured) then this is

indicative of future survival and therefore missing data methods (e.g. imputation) may be required[96].

2.9.2. Kaplan Meier survival estimate

KM test is a statistic method to nonparametrically estimate the survival probability from observed survival times, both censored and uncensored.

Considering that k patients have events during the follow-up period at different times $t_1<t_2<t_3<t_4<t_5<\ldots<t_k$. As outcomes are assumed to occur independently one of each other, the probabilities of surviving from one interval to the next may be multiplied together to provide the cumulative survival probability. More formally, the probability of continuing alive at time t_j, $S(t_j)$, is calculated from $S(t_{j-1})$ the probability of being alive at t_{j1}, n_j the number of patients alive just before t_j, and d_j the number of events at t_j, by the following formula:

$$S(t_j) = S(t_{J-1})\left(1 - \frac{d_j}{n_j}\right)$$

Where $t_0 = 0$ and $S(0) = 1$, and being S(t) constant during period time between events, and therefore the estimated probability is a step function that varies value only at the time of each event. This test allows each patient to contribute data to the estimatios for as long as they are known to be event-free. If all individuals experience the event (i.e. no censoring), this estimator would simply calculate the ratio of the number of event-free individuals at time t divided by the number of patients included at the study. The KM survival curves are plots illustrating the KM survival probability along time, providing a useful representation of the data that can be used to estimate measures such as median survival time. The large skew found in the distribution of most survival data is the reason that the mean is not commonly used[95].

Figure 2.8 includes an example of KM plot including resulting curves of analyzing a cohort of patients with astrocytoma grade 4 considering if patient age is superior or inferior to 55 years old.

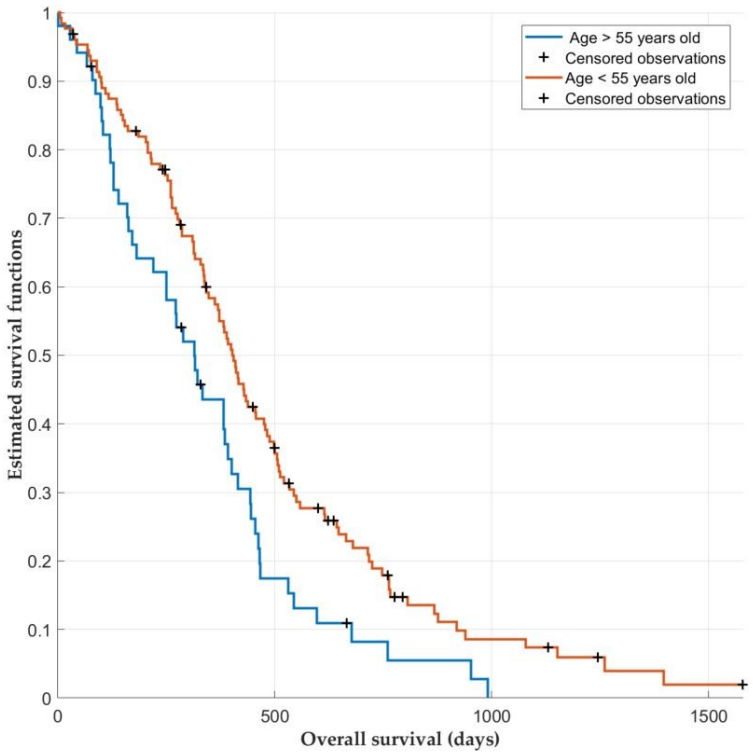

Figure 2.8. Example of Kaplan Meier curves for a multicenter cohort of 184 patients with astrocytoma grade 4 stratified according to age (in particular, if patients were younger or older than 55 years old at the diagnosis moment). Younger patients present higher probabilities of being alive in each time point. Censored observations (patients without date of exitus) are marked with +.

2.9.3. Log-rank test

The log-rank test is the most used nonparametric method to compare two or more KM survival curves. The groups may be treatment arms (different treatments vs. control arm) or prognostic groups (e.g. groups of age, presence/absence of a genetic alteration, etc). The method calculates at each event time and for each defined group, the number of expected events since the previous event if there were no difference between the groups. These values are summed over all event times to obtain the total expected number of events in each group, being E_i for group i. The log-rank test compares observed number of events, say O_i for group i, to the expected number by calculating the following statistic:

$$X^2 = \sum_{i=1}^{g} \frac{(O_i - E_i)^2}{E_i}$$

This value is compared to a X^2 distribution with (g-1) degrees of freedom, where g is the number of groups. Considering this, a p-value can be calculated to prove statistical significance of the differences between the survival curves.

2.9.4. Cox regression (proportional hazards)

The Cox proportional-hazards is essentially a regression model typically used statistical in medical research for analyzing the association between patients survival times and one or more variables[97].

In comparison with the above-mentioned methods, Kaplan-Meier curves and log-rank tests, which are examples of univariate analysis, Cox regression model can extend survival analysis to evaluate simultaneously the influence of several risk factors on survival[95,96].

Furthermore, Kaplan-Meier curves and log-rank tests are useful only when the predictor variable is categorical and different subgroups of patients are defined. However, they don't work easily for quantitative predictors. An alternative model is the Cox proportional hazards regression analysis, which works for both quantitative predictor variables and for categorical variables[95,96].

Summarizing, the main objective of the Cox model is to evaluate the influence of one or more factors simultaneously on survival. The model is expressed by the hazard function and it can be estimated as follow:

$$h(t) = h_0(t) \cdot exp(b_1x_1 + b_2x_2 + ... + b_px_p)$$

where t represents the survival time, $h(t)$ is the hazard function defined by p covariates (x_1, x_2 ,…, x_p), and the coefficients (b_1, b_2, ..., b_p) measure the magnitude (i.e., the effect size) of covariates.

The quantities $exp(b_i)$ are called hazard ratios (HR). A hazard ratio above 1 indicates a covariate that is positively associated with the event probability, and thus negatively associated with the length of survival.

In summary,

HR = 1: No effect

HR < 1: Reduction in the hazard

HR > 1: Increase in Hazard

PART I

Tumor Characterization and Classification

Chapter 3

Local detection of microvascular proliferation using MRI-DSC biomarkers

The gold standard diagnosis and grading of astrocytomas is made by the histopathological analyses of biological samples collected during surgery or biopsy. This implies that the patient starts being treated under the working diagnosis done by the radiologist.

For the correct classification of an astrocytoma grade 4, one of the first criteria to be evaluated during histopathological analysis, in addition to necrosis, is the presence and abundance of microvessels generated by microvascular proliferation (MVP). In addition, the new update of the classification of CNS tumors proposed by the WHO considered glioblastoma *IDH*-wildtype and astrocytoma *IDH*-mutant grade 4 as different tumors.

The spatial detection of microvessels from presurgical MRIs, as well as an early detection of *IDH* mutation status, would allow a more accurate initial diagnosis by the radiologist. Moreover, it could be of vital relevance to correctly classify those tumors that cannot be operated on or biopsied.

This chapter assess the local association between histopathology and medical imaging at the vascular level from the pre-surgical stage in astrocytomas grade 4. Furthermore, differences in MRI-DSC biomarkers values between glioblastoma *IDH*-wildtype and astrocytoma *IDH*-mutant grade 4 have been analyzed. Positive results derived from these studies may be relevant to improve the classification models of glial tumors using non-invasive biomarkers from the first diagnostic stage.

The contents of this chapter were published in the journal publication P4 (Álvarez-Torres M, BMC in Cancer, 2022) – thesis contribution C1.

3.1. Introduction

Glioblastoma *IDH*-wildtype is the most lethal and common tumor of the CNS, resulting in a median prognosis of 12–14 months[11,98] and being characterized by its high and heterogeneus vascularity[24,25]. Blood supply is required for the establishment, growth, and progression of the tumor; and several mechanisms are implicated in the formation of new vessels[24,25]. One of the results of these mechanisms is MVP, which generally occurs in the core of glioblastoma by sprouting new vascular microvessels from pre-existing ones, depending on the presence of hypoxia[24].

These pathologic heterogeneity features, including vascular proliferation, robust angiogenesis and extensive microvasculature heterogeneity could vary depending on *IDH* mutation status in high-grade gliomas[99]. In fact, the last update of 2020 CNS glioma classification and grading differentiates between glioblastoma *IDH*-wildtype and astrocytomas *IDH*-mutant grade 4 (previously named as glioblastomas *IDH*-mutant) as different type of gliomas, with different prognosis and vascular characteristics.

MVP is together to necrosis, the first criterion in the last update of 2020 CNS glioma classification and grading[98]. It is marked by two or more blood vessels sharing a common vessel wall, and interactions between tumor cells and blood vessels during MVP seem to facilitate tumor growth[99–101]. The result of MVP is the formation of large-lumen microvessels, usually with a glomeruloid appearance, that represent one of the main histopathologic hallmark of glioblastomas [27]. Considering the relevance of this vascular process, the microvessel area (MVA), i.e., the total area covered by the microvessels in the tumor sample, and microvessel density (MVD), i.e., the number of microvessels per volume unit, have been previously investigated[27,72,102–106]. Different studies suggest that MVD poorly describes the morphometric diversity of these microvessels in high-grade gliomas[27,102,103]. However, MVA may provide a more robust clinical biomarker, useful for prognosis and grading [27,102,103,107–109]. Regardless of this evidence, the histopathological quantification of MVA is still used exclusively in the research setting. Relevant limitations, including time and cost-expending, labor intensity, and invasiveness make it challenging for routine clinical practice.

A complementary approach to overcom1e the limitations in MVA quantification is perfusion MRI[27,79]. Some studies found that measures of relative rCBV positively correlate with microvascular structures in different glioma tumors[27,72,103–106]. However, these studies are few and present important limitations such as animal-based studies[72,103], small cohorts of glioblastoma patients [79,104–106], low number of analyzed histopathological specimens [79,104–106], or analysis with non-spatial coregistered data[72,110]

The integration of advanced and automatic techniques capable of calculating robust imaging markers, including rCBV, could help in high-grade glioma classification,

including the diagnosis of glioblastomas *IDH*-wildtype and astrocytoma *IDH*-mutant grade 4. Besides, the complementary use of rCBV would involve important advantages since calculations derived from routine presurgical MRIs can be performed through automatic and robust methodologies, such as ONCOhabitats methodology. [2,67,68].

In this context, we hypothesize that MVA could be directly associated with the rCBV in glioblastoma *IDH*-wildtype and this correlation can be measured using a robust MRI processing service. The areal density of microvessels on sections is an unbiased estimator of the volume density of microvessels according to the Delesse principle [111], and we hypothesize that the volume of microvessels can be related to the rCBV. Since the typical spatial resolution, DSC sequences is 2-mm in-plane × 5-mm slices[112], the calculation of rCBV would be reliable when it is calculated in areas larger than 2 mm.

In addition, we hypothesize that rCBV could be useful to find vascular differences between glioblastomas *IDH*-wildtype and astrocytoma *IDH*-mutant grade 4[99], and therefore, supporting the new glioma classification, which differentiates between these two tumors, providing an imaging method based on routinary presurgical MRI and AI techniques.

The general purpose of our study is to evaluate the potential use of rCBV, calculated with the ONCOhabitats methodology, to detect the presence or absence of microvessels in different regions of glioblastoma *IDH*-wildtype, and to find differences in vascularity between glioblastoma *IDH*-wildtype and astrocytoma *IDH*-mutant grade 4.

The study's specific objectives are 1) to analyze the histopathologic and radiologic correlation between the imaging markers ($rCBV_{mean}$ and $rCBV_{max}$) with the local MVA in glioblastomas *IDH*-wildtype; 2) to study whether these imaging markers can differentiate regions of the tumor with presence or absence of microvessels 3) to analyze the capacity of the rCBV to differentiate between glioblastoma *IDH*-wildtype and astrocytoma *IDH*-mutant grade 4 samples.

3.2. Material and Methods

3.2.1. Clinical data collection

The Ivy GAP database (www.glioblastoma.alleninstitute.org)[112] was used for this study since it includes: (i) Presurgical MRI data, including DSC perfusion sequences, (ii) histopathological data labeled, including microvessel area, (iii) images of the complete resected tumors with the blocks marked, and (iv) information about *IDH* mutation status. This public database includes 41 verified patients with astrocytoma

grade 4, with a total of 42 tumors, with the following information per tumor: 1) images of the resected tumor (Figure 3.1A.I) divided into tissue blocks (Figure 3.1A.II); 2) histopathological images at a cellular resolution of hematoxylin and eosin-stained sections (collected from the tissue blocks) annotated for anatomic structures, including areas of microvessels (Figure 3.1A.III and Figure 3.1B), and 3) pre-surgical MRI studies of the patients: including pre and post-gadolinium T1-weighted MRI, T2-weighted MRI, FLAIR and DSC T2* perfusion-weighted MRI (Figure 3.2A).

3.2.3. Patient and Tumor selection

Inclusion criteria

Inclusion criteria for patients participating in the study were: i) histopathological confirmation of astrocytoma grade 4 (glioblastoma *IDH*-wildtype or astrocytoma *IDH*-mutant grade 4); ii) access to complete MRI studies, including pre and post-gadolinium T1-weighted (T1 and T1c, respectively), T2-weighted, FLAIR T2-weighted, and DSC T2* perfusion sequences (Figure 3.2A); iii) access to the resected tumor image (Figure 3.1A); and iv) approval by an expert radiologist and histopathologist of the correct overlay/registration of the image of the resected tumor and the MRI of each patient (Figure 3.2).

According to 2021 update classification of the CNS[10], we consider glioblastoma *IDH*-wildtype or astrocytoma *IDH*-mutant grade 4 as different tumors.

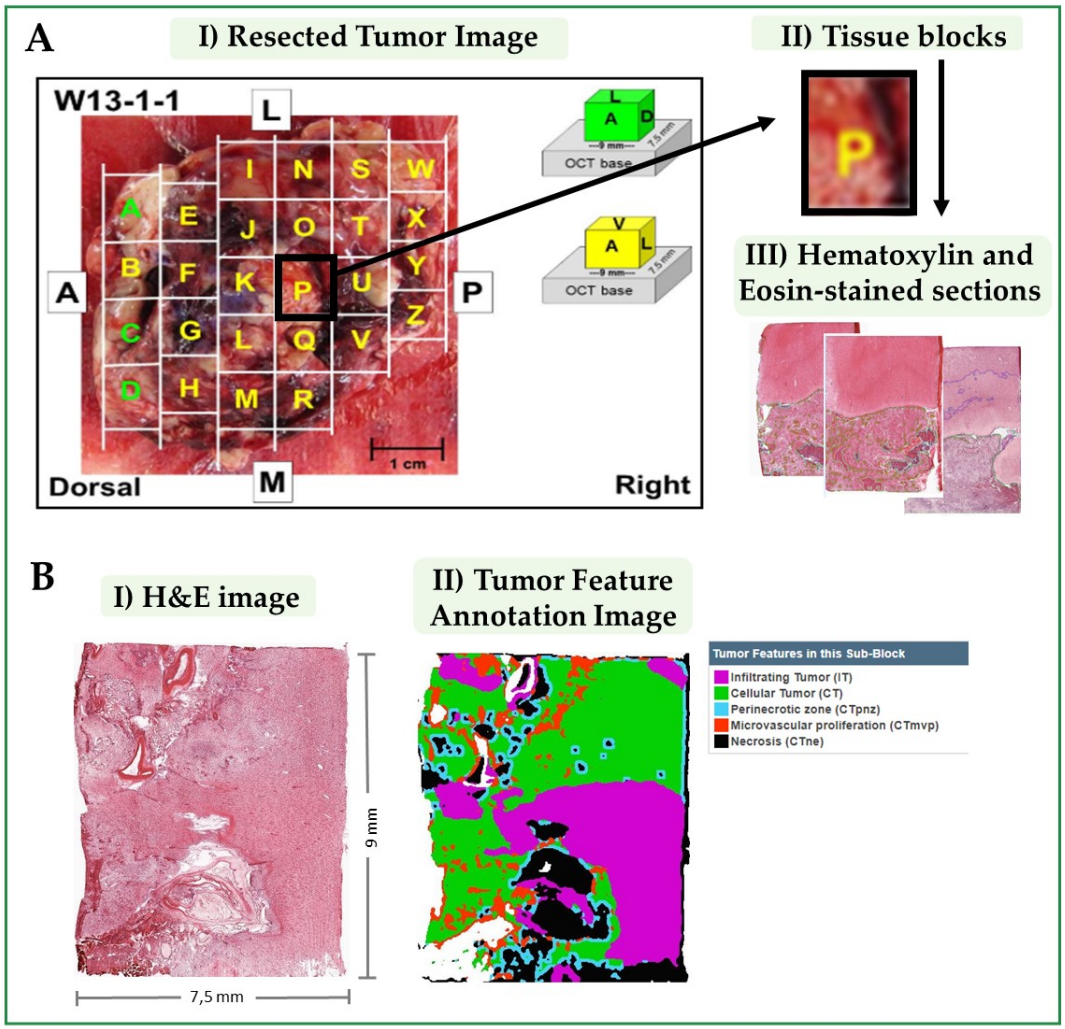

Figure 3.1. A: Included information in the Ivy Glioblastoma Atlas Project (Ivy GAP) database: I) Resected Tumor Image II) divided in tissue blocks; and III) Histopathological images at cellular resolution of hematoxylin and eosin-stained sections. **B**: I) Example of an H&E image of a slide from a resected block. II) The same image labeled with the different tissues and structures. Microvascular proliferation corresponds with areas in red color. (Images from Ivy GAP database, patient W55, block F, slice F.02). * OCT: Optimal Cutting Temperature compound. The term 'OCT base' is used to refer to the formed block after frozen and before sectioning.

Exclusion criteria

Exclusion criteria for patients were: i) inability to correctly overlay the image of the resected tumor over the MRI; ii) tumor tissue segmentation error during the processing; iii) to present extensive hemorrhage that could affect to a correct quantification of perfusion maps.

3.2.3. MRI acquisition and processing

MR images were obtained on a 3.0 or 1.5 T scanner (18 and 1 patients, respectively). More information about MRI data is included in Table S3.1 of the Supporting Information included in appendix A, and it is publicly available in The Cancer Image Archive (TCIA)[113]. MRI processing was carried out using the ONCOhabitats platform[67], freely available in https://www.oncohabitats.upv.es. The ONCOhabitats analysis included the following automatic stages (Figure 3.2):

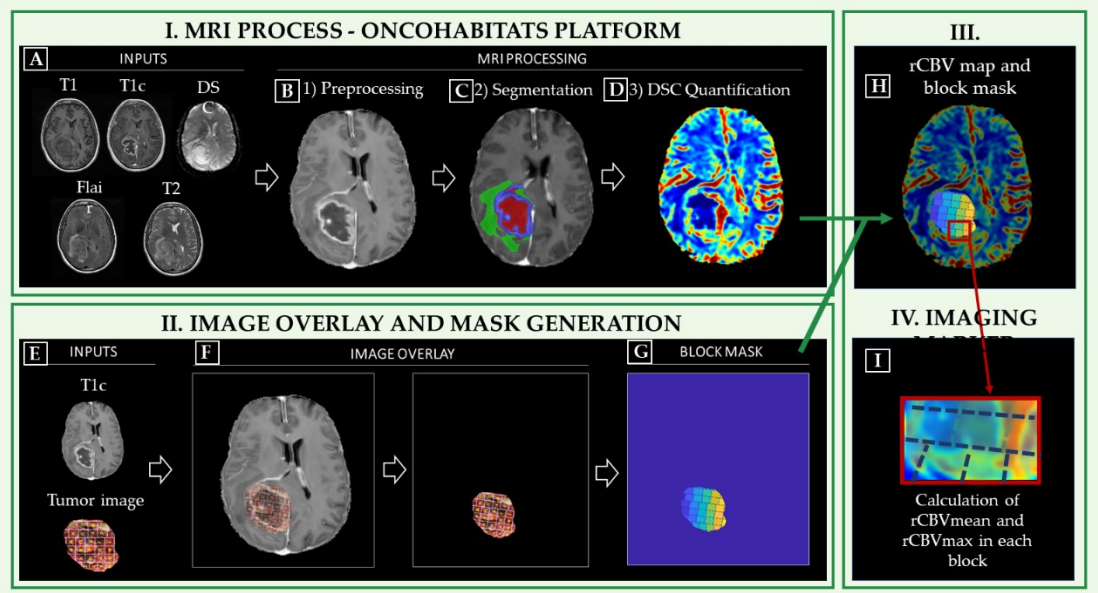

Figure 3.2. Stages of methodology: **I)** MRI Process conducted by the Segmentation Service included in the ONCOhabitats platform; **II)** Image overlay and mask generation; **III)** Coregistration and **IV)** Calculation of imaging markers. **A)** Required inputs for the MRI process (T1, T1c, T2, Flair and DSC); **B)** Preprocessing of the MRIs; **C)** Classic segmentation of the lesion into tumor, edema and necrosis; **D)** DSC perfusion quantification and rCBV map calculation. **E)** Inputs to generate the block mask; **F)** Image overlay process for mask generation; **G)** Block mask; **H)** Overlay of the rCBV map and block mask; **I)** Calculation of imaging markers ($rCBV_{mean}$ and $rCBV_{max}$) in each tissue block.

1. MRI Preprocessing (Figure 3.2B), including voxel isotropic resampling of all MR images, correction of the magnetic field in homogeneities and noise, rigid intra-patient MRI registration, and skull-stripping (Figure 3.2A).

2. Astrocytoma grade 4 tissue segmentation (Figure 3.2C), performed by using an unsupervised segmentation method, which implements a state-of-the-art deep-learning 3D CNN, which takes as input the T1c, T2, and Flair MRI. The current CNN deployed in ONCOhabitats is the next iteration of our previously published one[68]. Therefore, right now it is an in-house development that incorporates to our previous networks the current state-of-the-art techniques in image segmentation, such as

spatial- and channel-attention blocks, deep-multi-level losses or both custom training schedulers and residual- feature extraction blocks. The backbone of our network maintains the classical U-net architecture with long-term skip-connections but adding the previously mentioned mechanisms that significantly improve the segmentation's quality. Moreover, a balanced training strategy that yields local patches of healthy, necrotic, edematous and enhancing tumor is adopted to ensure the network is not biased towards the highest prevalent tissue in the brain.

This method is based on Directional Class Adaptive Spatially Varying Finite Mixture Model, or DCA-SVFMM, which consists of a clustering algorithm that combines Gaussian mixture modeling with continuous Markov random fields to take advantage of the self-similarity and local redundancy of the images.

All the used networks are trained and tested with the public BRATS dataset (available at https://www.med.upenn.edu/sbia/brats2018/data.html), which currently consist of a corpus with more than 380 astrocytomas grade 4 manually segmented by several expert radiologists. An evaluation oracle is also available to send the segmentation results over a test set to assess the quality of the network. Currently our results in term of Dice score are: 0.90 in the whole tumor segmentation (necrosis + edema + enhancing tumor), 0.83 in the tumor core (necrosis + enhancing tumor) and 0.86 in enhancing tumor segmentation[67].

3. DSC perfusion quantification (Figure 3.2D), which calculates the rCBV maps, as well as rCBF or MTT, for each patient. In this phase, T1-weighted leakage effects are automatically corrected using the Boxerman method[114], while gamma-variate curve fitting is employed to correct for T2 extravasation phase. rCBV maps are calculated by numerical integration of the area under the gamma-variate curve. The AIF is automatically quantified with a divide and conquer algorithm.

A more detailed description of the methodology is included in[67], and the results of a multicenter study demonstrated its robustness in included in [2].

3.2.4. Tissue Processing and Histological Staining

All the information included in this section was collected from the Ivy GAP white paper, available in the Ivy GAP database (https://glioblastoma.alleninstitute.org/).

Tissue acquisition, subdivision, and freezing

Immediately after en bloc resection, each tumor was set on a surgical towel, rinsed with saline, and subdivided into 9 x 7.5 x 18 mm high (tumors W1-W12) or 9 x 7.5 x 9 mm high (tumors W13-W55) tissue blocks. Using custom-fabricated L bars, each

block was supported for freezing from the bottom of the L bar assembly (top of tissue block) on a dry ice isopropanol bath. As the block was rapidly frozen, an optimal cutting temperature (OCT) base was formed with a disposable cryomold, added to the bottom of the tissue block, and frozen with a freeze aerosol (Figure 3.1A). The 18 mm high blocks were divided into two 9 mm pieces on a refrigerated dissection table (-15C). The bottom (block .1) contained the original OCT base, whereas the top (block .2) was embedded in OCT at the chopped interface. Blocks were stored at -80C before processing.

Cryosectioning for Standard In Situ Hybridization (ISH) and Hematoxylin and Eosin (H&E)

Fresh frozen tissue blocks were removed from -80°C, equilibrated at -15°C in cryostats, mounted on chilled chucks, and sectioned at 20µm with object temperature of -10°C or -11°C to reduce chatter through the necrotic areas and folds on the leading edge that contacted the blade first.

ISH Image Acquisition and Processing

Whole slides were scanned directly to SVS file format at a resolution of 0.5µm/pixel without downsampling on ScanScope® scanners (Aperio Technologies, Inc; Vista, CA) equipped with a 20x objective and Spectrum software. The raw image files of ~5 GB per image were archived after converting to JPEG 2000 file format. The preprocessed images were flipped along the horizontal axis, white balanced, and compressed at a rate of 0.8 to ~400 MB per image. During post-processing, colorized expression values or heat masks showing ISH signal intensity were generated, and the closest H&E stained image of the same specimen was calculated for each ISH section.

During the review of images, the automated bounding box overlay was manually adjusted if necessary, so that each of 8 bounding boxes per slide was placed over the corresponding tissue section, and images of slides with focus or image tile stich misalignments were re-scanned. Images were failed if artifacts compromised data analysis (e.g., mechanical damage, mounting medium bubbles, hybridization bubbles, and NBT/BCIP precipitated aggregates) associated with the corresponding tissue section.

3.2.5. Image overlay, mask generation, and image markers

To compare the information obtained from the rCBV maps and the MVA obtained from histopathological images, we overlaid the T1c MRI images to the images of tumor resected pieces, including the histopathology blocks' location (Figure 3.2E) provided in the Ivy GAP dataset. This 2D registration was performed manually using the following methodology (Figure 3.2F):

a) Localizing the lesion on the MR images based on the hyperintensity of the T1 contrast and with the help of the segmentation masks, which includes the delineation of the active tumor, the edema and the necrotic tissue.

b) Defining the orientation of the resected tumor and its blocks using the photograph provided at the Ivy GAP along with the parameters of orientation, position, and axial slice provided as reference.

c) Refining the position by taking into account the necrosis masks and vascularity values in the blocks.

d) Validation of the proposed overlay by expert radiologist (FAR), oncologist (GR) and histopathologist (JFL).

Additionally, we remove the background and generate a block mask with each block area delimited (Figure 3.2G).

To evaluate the accuracy of the co-registration technique, we used the Intersection over Union method, i.e. we measured the area proportion overlap between the resected tumor image and the MRI image. We achieved a mean accuracy of 88.8%, and a TRE of 11.2%. In all cases the % was higher than 75.0%, being 76.1% the minimum and 98.1% the maximum.

Once the blocks were coregistered with the MRI space (Figure 3.2H), we could obtain the imaging markers $rCBV_{mean}$ and $rCBV_{max}$ for each independent block (Figure 3.2I). We used the rCBV markers based on previous studies[2,5,67] in which it has been demonstrated that rCBV is the most robust DSC-perfusion marker, as well as it is the most used to find correlations with clinical outcomes.

The ONCOhabitats processing results for the patients with complete pre-surgical MRI (T1, T1Gd, T2, FLAIR and DSC perfusion) are publicly available in Zenodo (https://zenodo.org/record/4704106#.YJu8GagzY2w)[115]. For each patient, we included a report containing an analysis summary; two folders with the resulting morphological and perfusion images in MNI and native spaces; and a third folder with the transformation matrices.

3.2.6. Study variables

From each tissue block, several slides with an area of approximately 9 x 7,5mm were collected with their corresponding hematoxylin and eosin (H&E) images of the IVY Gap database. The areas of different histopathological tissues were delimited in these images (Figure 3.1B) and quantified data was available, including the mean value of MVA per block and the total area of each section of the block.

In order to normalize the MVA according to the area of each section of the tumor, the MVA value was divided by the area of the section. In addition, each block contains information from different sections; therefore, for the statistical analyses, we used the normalized mean value of MVA for each block, calculated with the following formula (where MVAbs is the MVA present in the section s of one particular block b where n sections are available):

$$\mathrm{MVA_b} = mean\left(\frac{MVA_{b1}}{Area_{b1}}, \dots, \frac{MVA_{bs}}{Area_{bs}}, \dots, \frac{MVA_{bn}}{Area_{bn}}\right) \mathrm{mm^2}$$

Besides, each block was classified into two groups: (1) blocks with presence of microvessels (MVA>0) and (2) blocks with absence of microvessels (MVA=0). An example of the microvessels generated by MVP derived from the tumor progression, as opposed to normal vessels, is illustrated in Figure 3.3.

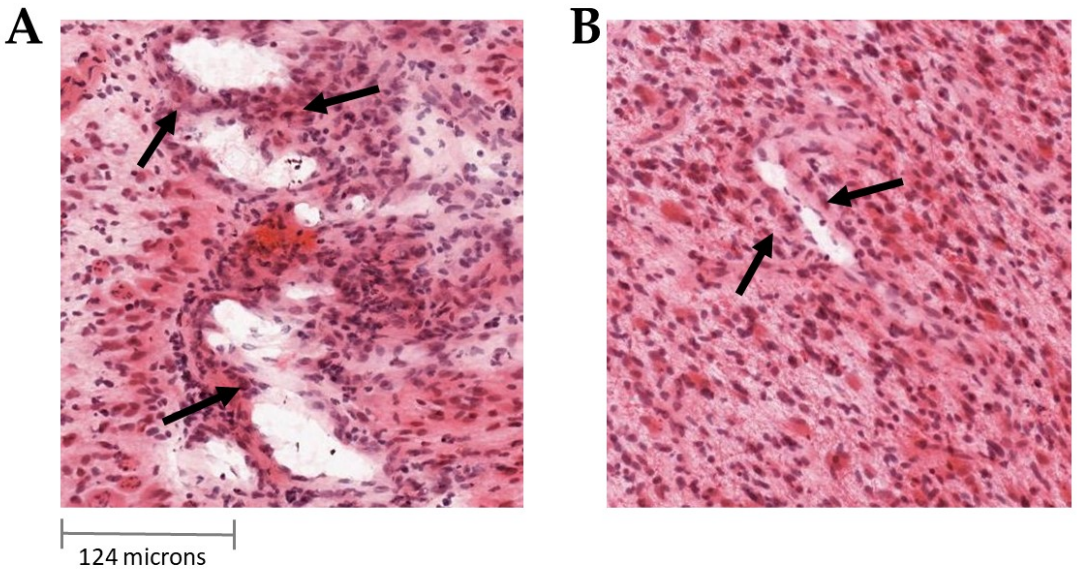

Figure 3.3. A) Aberrant vessels generated by microvascular proliferation sharing common vessel walls of endothelial and smooth muscle cells. **B)** Normal vessels. (Images from Ivy GAP database).

3.2.7. Histopathological and Radiologic correlation between MVA and rCBV in IDH-wildtype glioblastoma

Spearman's correlation test was performed to study the association between the $rCBV_{mean}$ and $rCBV_{max}$ with the MVP area (numeric continuous variable). Spearman coefficients and derived p-values were calculated, and descriptive measures of both $rCBV_{mean}$ and $rCBV_{max}$ among the whole block samples (mean, standard deviation, median, and range).

3.2.8. Differences of rCBV according to the presence or absence of microvessels in IDH-wildtype glioblastomas

Mann-Whitney tests were conducted to analyze the differences of $rCBV_{mean}$ and $rCBV_{max}$ between the group with presence of microvessels, and the group with absence of microvessels. The descriptive measures of rCBV (mean, standard deviation, and range) for each MVP and non-MVP groups were included.

3.2.9. Differences in rCBV between IDH-mutant astrocytoma and IDH-wildtype glioblastomas

Mann-Whitney tests were conducted to find the differences of $rCBV_{mean}$ and $rCBV_{max}$ between *IDH*-wildtype and *IDH*-mutant glioblastoma blocks. The descriptive measures of rCBV (mean, standard deviation, and range) for each IDH population were included.

Kaplan Meier curves were represented to analyze differences in survival between patients with glioblastoma *IDH*-wildtype and patients with astrocytoma *IDH*-mutant grade 4. In addition, Log rank test was carried out to study the significance of this difference ($p < 0.005$).

3.3. Results

3.3.1. Included Patients

From the 41 patients included in the Ivy GAP database, 3 of them presented astrocytoma *IDH*-mutant grade 4 (W10, W31, and W35); and the 38 remaining patients presented glioblastoma *IDH*-wildtype.

Glioblastomas *IDH*-wildtype

From 38 glioblastomas *IDH*-wildtype, 14 were not included because of incomplete MRI studies (W04, W06, W16, W19, W20, W21, W26, W27, W28, W32, W39, W45, W53, and W54); From the 24 included patients, 3 patients were discarded due to inability to correctly overlay the image of the resected tumor over the MRI (W08, W09, and W11). The remaining 21 patients were processed with the ONCOhabitats platform. Of these 21 cases, 3 were excluded due to tumor tissue segmentation errors (W01, W03, and W22); and 1 patient was excluded because of extensive hemorrhage that prevented a correct quantification of perfusion maps in DSC-MRI (W50). Finally, 17 glioblastomas *IDH*-wildtype were included in the study.

Astrocytomas *IDH*-mutant grade 4

From 3 astrocytomas *IDH*-mutant grade 4, 1 was not included because of defective T1c image, not allowing a correct process with the ONCOhabitats platform. Finally, 2 astrocytomas *IDH*-mutant were included in the study.

Demographic, clinical and MRI-related data of the total of 19 patients is included in Table S3.2 of the Supporting Information included in appendix A.

3.3.2. Included Blocks

Glioblastomas *IDH*-wildtype

A total of 124 blocks with complete information from the 17 glioblastomas *IDH*-wildtype were initially considered. To develop the statistical analyses, only those blocks with more than twenty-five percent (> 25%) of tumor, defined by imaging segmentation, were selected. This criterion was based on the existence of blocks that mostly contain necrotic tissue and therefore were not suitable for the study due to their lack of vascularization. Seventy-three (73) tissue blocks formed the final study sample of glioblastoma *IDH*-wildtype.

***Astrocytomas IDH*-mutant grade 4**

Thirteen (13) blocks were initially considered from 2 astrocytomas *IDH*-mutant grade 4. Following the same criterion than for *IDH*-wildtype tumors, finally 7 blocks formed the final study sample of astrocytomas *IDH*-mutant grade 4.

3.3.3. Histopathological and radiologic correlation between MVA and rCBV in IDH-wildtype glioblastomas

Table 3.1 includes the calculation of mean, standard deviation, median and range for $rCBV_{mean}$ and $rCBV_{max}$ for the 73 tissue blocks from glioblastomas 17 *IDH*-wildtype. The results of the Spearman correlation analyses between the MVA and each imaging marker ($rCBV_{mean}$ and $rCBV_{max}$) are also included in Table 3.1.

Both $rCBV_{mean}$ and $rCBV_{max}$ showed a significant positive correlation with MVA. That is, regions of the tumor with higher rCBV present significantly larger microvessel areas.

Table 3.1. Descriptive measures of $rCBV_{mean}$ and $rCBV_{max}$ (mean ± standard deviation, median and range) for the whole sample (71 blocks) and Spearman correlation results of these imaging markers with the microvascular proliferation area.

IDH-wildtype glioblastomas	**Mean ± standard deviation**	**Median**	**Range [min, max]**	**Spearman correlation with MVA (Coefficient; pvalue)**
$rCBV_{mean}$	4.91 ± 270	4.60	[1.07, 13.42]	C = 0.38; **p = 0.0008***
$rCBV_{max}$	9.52 ± 4.95	8.55	[2.35, 24.41]	C = 0.42; **p < 0.0002***

MVA: microvessel area

Figure 3.4A shows an example (patient W33) of both rCBV and MVA maps to illustrate these two variables' correlation. The white blocks did not present histopathological information, including the MVA data. It can be seen that blocks with areas with higher rCBV correspond with those with larger areas of MVA and vice versa.

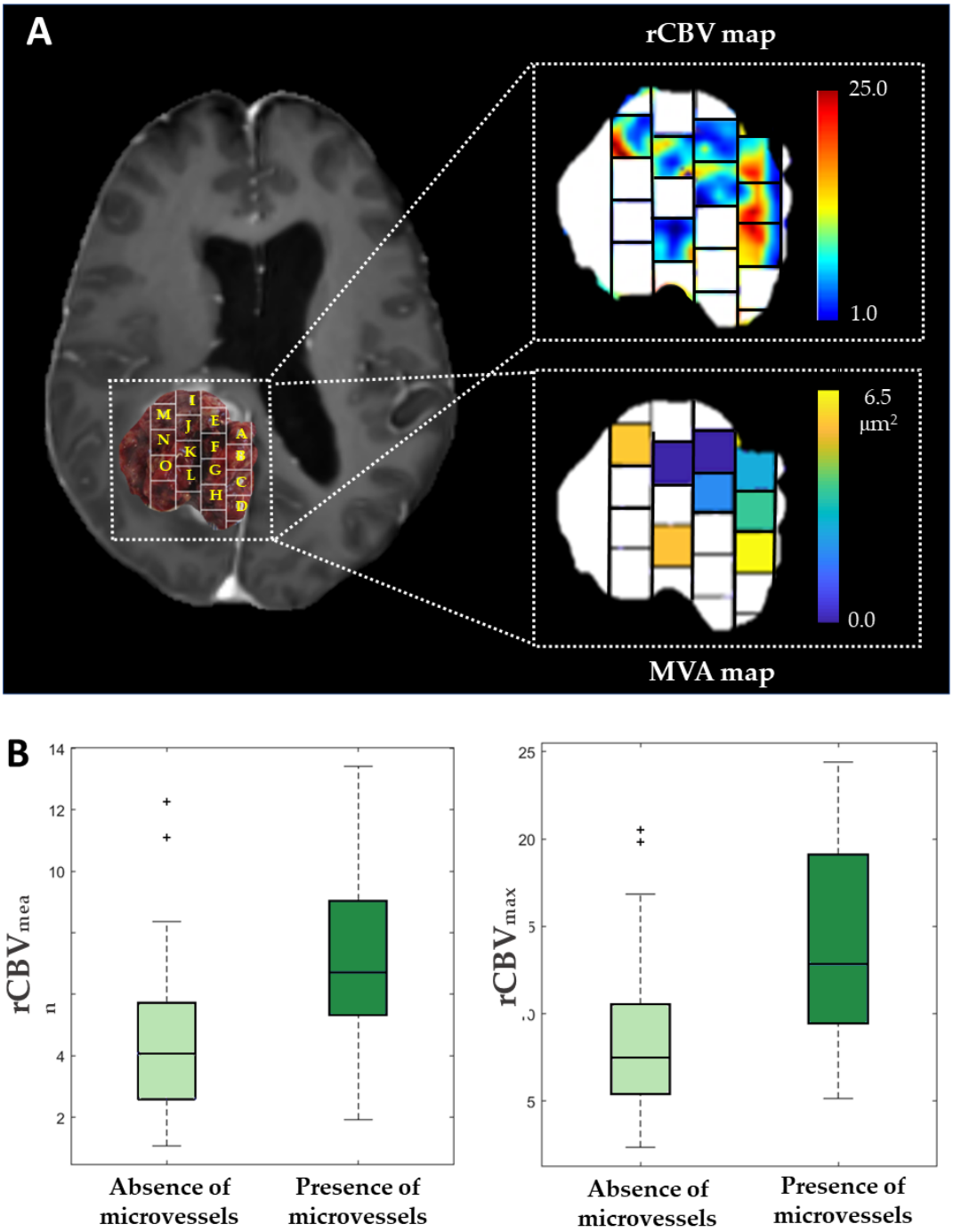

Figure 3.4. A) Post-gadolinium T1-weighted MRI overlaid with an image of the resected tumor including the delineation of the tissue blocks (left), example map of rCBV values (with a range of 1 to 25) of the areas occupied by the analyzed tumor blocks (top right), and example color map representing the MVA values (with a range from 0.0 to 6.5µ2) present in each analyzed block (below right). Blank blocks are not included due to lack of histopathological information. Example of patient W33 from the Ivy GAP database. **B)** Boxplots showing the significant differences of mean rCBV (left) and maximum rCBV (right) between the group with presence of microvessels and the group with absence of microvessels.

3.3.4. Differences in rCBV according to the presence or absence of microvessels in IDH-wildtype glioblastomas

Table 3.2 shows the descriptive measures of $rCBV_{mean}$ and $rCBV_{max}$ for the blocks corresponding to the groups with presence and absence of microvessels, and the Mann-Whitney test results. All the measures (mean, minimum and maximum) of $rCBV_{mean}$ and $rCBV_{max}$ were higher in the group of blocks with presence of microvessels, presenting values two times higher than to the group with no evidence of microvessels.

Table 3.2. Descriptive measures of $rCBV_{mean}$ and $rCBV_{max}$ (mean ± standard deviation and range) for the sample divided in groups according to the presence or the absence of microvessels, and Mann Whitney tests results from analyzing the differences of these imaging markers between these two groups are included.

***IDH*-wt glioblastomas**	***Presence of Microvessels* (n = 14 blocks, 5 patients)**		***Absence of Microvessels* (n = 59 blocks, 12 patients)**		**Mann-Whitney test**
	Mean ± std	Range [min, max]	Mean ± std	Range [min, max]	p-value
$rCBV_{mean}$	7.08 ± 2.99	[1.92, 13.42]	4.40 ± 2.31	[1.07, 12.25]	0.0016*
$rCBV_{max}$	14.15 ± 6.04	[5.15, 24,41]	8.43 ± 3.98	[2.35 20.50]	0.0005*

The Mann-Whitney test yielded significant differences ($p<0.05$) between the $rCBV_{mean}$ and the $rCBV_{max}$ of the groups generated by the presence or absence of microvessels in glioblastomas *IDH*-wildtype. The $rCBV_{mean}$ and $rCBV_{max}$ can differentiate those regions of the tumor with microvessels.

Figure 3.4B shows the boxplots which illustrate these differences of the $rCBV_{mean}$ and $rCBV_{max}$ between the group with presence of microvessels (lower values) and the groups with absence of microvessels (higher values).

3.3.5. Differences in rCBV between IDH-wildtype glioblastomas and IDH-mutant astrocytoma

Table 3.3 includes the Mann-Whitney test results, as well as the descriptive measures of $rCBV_{mean}$ and $rCBV_{max}$ for the tissue blocks corresponding to *IDH*-wildtype and *IDH*-mutant astrocytoma. Mean, median and maximum of $rCBV_{mean}$ and $rCBV_{max}$ were higher in the *IDH*-wildtype tissue blocks, presenting values more than two times superior to *IDH*-mutant tissue blocks. In addition, the Mann-Whitney test yielded significant differences ($p<0.05$) in $rCBV_{mean}$ and $rCBV_{max}$ between *IDH*-wildtype and *IDH*-mutant glioblastomas.

Table 3.3. Descriptive measures of $rCBV_{mean}$ and $rCBV_{max}$ (mean ± standard deviation and range) for *IDH*-wildtype and *IDH*-mutant glioblastomas and Mann-Whitney tests results from analyzing the differences of these imaging markers between these two groups are included.

	***IDH-wildtype tissue blocks* (n = 73)**			***IDH-mutant tissue blocks* (n = 7)**			**Mann-Whitney test**
	Mean ± std	Median	Range [min, max]	Mean ± std	Median	Range [min, max]	p-value
$rCBV_{mean}$	4.91 ± 2.66	4.60	[1.07, 13.42]	2.29 ± 0.83	2.12	[1.49, 3.82]	0.0032*
$rCBV_{max}$	9.52 ± 6.04	8.55	[2.35, 24,41]	3.98 ± 1.56	3.41	[2.56, 7.30]	0.0004*

Figure 3.5 shows the boxplots which illustrate the differences of the $rCBV_{mean}$ and $rCBV_{max}$ between the *IDH*-wildtype tissue blocks (higher values) and the *IDH*-mutant tissue blocks (lower values).

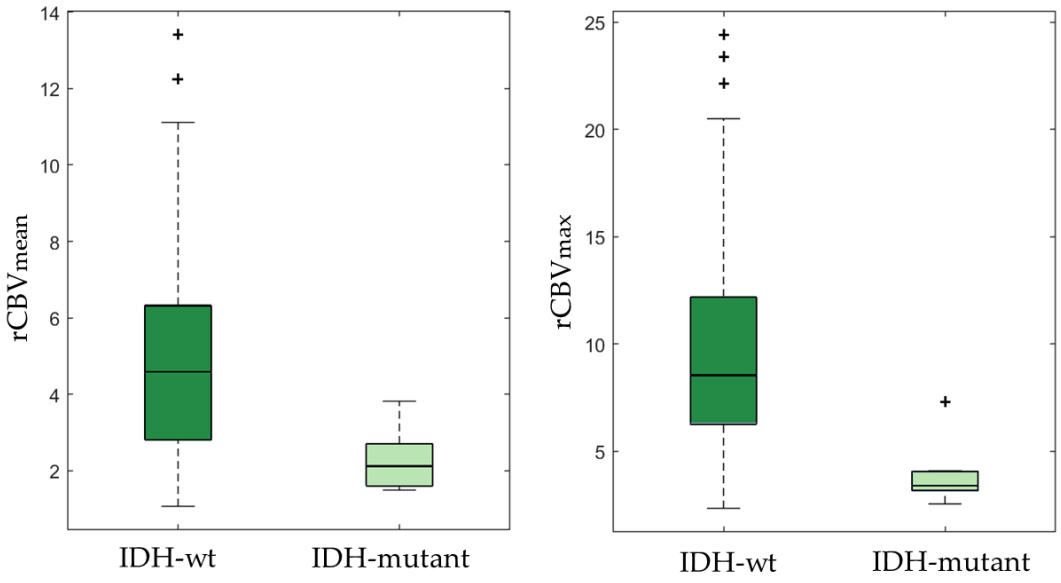

Figure 3.5. Boxplot showing the significant differences of mean rCBV (left) and maximum rCBV (right) between 73 *IDH*-wildtype tissue blocks from 17 patients and 7 *IDH*-mutant tissue blocks from 2 patients.

The Kaplan Meier curves with the estimated survival functions for patients with glioblastomas *IDH*-wildtype and astrocytomas *IDH*-mutant grade 4 are included in Figure S3.1 in Appendix A Although differences in survival did not yield statistical significance (p = 0.099) between groups, estimated survival curves are completely separated, suggesting a substantial difference in survival times between patients with glioblastoma *IDH*-wildtype and astrocytoma *IDH*-mutant.

3.4. Discussion

MVP is one of the main histopathologic hallmarks of astrocytomas grade 4, being key for the current glioma classification[10,11]. In addition, microvessel area can be considered as an independent prognostic biomarker according to previous results, in which authors reported significant longer survival in patients with astrocytoma grade 4 lacking the presence of new microvessels [103,116]. Those works suggested that tumoral microvasculature is associated with survival differences among tumors with identical histologic grades [27,103,116]. However, despite its clinical potential value, direct MVA quantification is clinically unfeasible due to its time-consuming and labor-intensive nature.

By contrast, imaging markers derived from routinary MRI protocols, such as rCBV, present several advantages since they are fast to calculate, it does not represent any

extra cost, and it is non-invasive compared with MVA. However, although rCBV is used for the assessment of brain tumors, it is not widely considered as a biomarker for clinical decision-making yet, probably due to the difficulty to normalize the rCBV values, which can generate confusion about prospective clinical guidelines, but also due to the lack of robust studies using spatially localized histologic correlations[79].

In this sense, here we investigated the association between the imaging markers $rCBV_{mean}$ and $rCBV_{max}$, calculated with the validated method ONCOhabitats [2,67,68]and the MVA in samples from glioblastoma *IDH*-wildtype. Moreover, we analyzed the differences of rCBV between those areas of the tumor with the presence of microvessels from those regions of the tumor without evidence of microvessels.

We found significant correlations between $rCBV_{mean}$ and $rCBV_{max}$ and MVA when analyzing 73 tissue samples derived from 17 human glioblastomas *IDH*-wildtype. Also, we found significant results when we evaluated the differences of both $rCBV_{mean}$ and $rCBV_{max}$ between tissue blocks with presence of microvessels from those blocks defined by the absence of microvessels. MVP is, together to necrosis, the first criterion in the last update of 2020 CNS glioma classification and grading, since it is considered as one of the main hallmarks of high-grade gliomas (including glioblastoma *IDH*-wildtype and astrocytoma *IDH*-mutant). Therefore, its correlation with rCBV, makes it also a potential candidate useful in glioma classification. Despite the few similar studies conducted[27,72,79,102–104], our results are consistent with those previously reported, finding a significant positive correlation between rCBV and MVA and significant differences in rCBV in those regions of the tumor with presence or absence of microvessels. In previous studies developed with human data and which analyze continuous variables (MVA or MV)[104,105], similar correlation coefficients were found ($\varrho = 0.42$[104] ; $\varrho = 0.46$[105] vs. $\varrho = 0.43$ in the present study). However, in previous studies, only 2 and 4 glioblastoma patients were enrolled, versus the 73 samples derived from 17 patients used in the current study. Increasing the interpatient heterogeneity in our study resulted in not higher correlation coefficients. Nonetheless, the analyses are more robust and p-values more significant. A more detailed comparison with previous studies can be found in Table S3.3 of the Supporting Information included in appendix A.

Furthermore, in this study we have investigated the differences in rCBVmean and $rCBV_{max}$ among samples glioblastoma *IDH*-wildtype and astrocytoma *IDH*-mutant grade 4. We found that blocks from glioblastoma *IDH*-wildtype present almost 2.5 times higher rCBV values than blocks from astrocytoma *IDH*-mutant grade 4. These represent promising preliminary results to propose the rCBV, calculated with ONCOhabitats, to predict with a non-invasive method the *IDH* status in these gliomas and a complementary method for diagnosis.

This study has some limitations. Firstly, the manual registration between morphologic MRI images and the resected tumor image could be affected by deformations of the tumor tissue morphology when resected and/or the difficulty of finding matchings between both image features. Also, the number of independent analyzed samples is not much higher despite it being higher than in other previous studies. In addition, the results derived from the comparation between *IDH*-wildtype and *IDH*-mutant samples should be considered with caution, since only 7 blocks from 2 patients were included for the *IDH*-mutant group.

The results derived from this work suggest the potential of imaging vascular markers calculated with the ONCOhabitats platform for helping in unmet challenges in high-grade glioma management, including glioma classification and prediction of *IDH* mutation status, with a non-invasive method and from the initial stage of diagnosis. We consider that the rCBV is a clinically relevant option for decision making in management of patients with astrocytoma grade 4[2,27,68], since it could be a complementary tool to histopathology for analyzing intratumor vascular heterogeneity at both temporal and spatial levels in a non-invasive way[68]. This marker could be especially relevant for inoperable tumors, for which an exhaustive histopathological analysis cannot be performed. An early diagnosis, a correct classification and a more precise and personalized analysis of the glioma will have a positive impact on the patient's treatment. Furthermore, this study opens up the possibility of evaluating tumor vascularity more correctly after antiangiogenic treatments, in addition to other prognostic/predictive markers related to tumor vascularization.

In addition, we consider useful to provide the ONCOhabitats results for Ivy GAP dataset with the purpose of enabling researchers investigating other relevant correlations between imaging-based biomarkers and histopathology for prognostic/predictive applications in high-grade astrocytoma. These results are publicly available for viewing and downloading in Zenodo (https://zenodo.org/record/4704106#.YJu8GagzY2w)[115].

3.5. Conclusions

The main conclusion of this study is the demonstration of a significant histopathological and radiologic correlation between the MVA and the rCBV in local regions of glioblastoma *IDH*-wildtype. The ONCOhabitats method allows a spatial location and detection of different regions of the tumor with presence of microvessels since the first diagnostic stage in a non-invasive way. In addition, significant differences in the rCBV values are found between glioblastomas *IDH*-wildtype and

astrocytomas *IDH*-mutant grade 4, supporting the last update of glioma classification, which consider these high-grade gliomas as different tumors[10,11,98].

Chapter 4

Vascular differences between glioblastoma *IDH*-wildtype and astrocytomas *IDH*-mutant grade 4 at imaging and transcriptomic levels.

A global agreement in CNS tumors classification is essential in order to decide treatment correctly, predict prognosis, evaluate treatment response, compare outcomes, and select adequate patients for clinical trials at international level.
The last update of the WHO of CNS tumor classification and grading 2021 considered for the first time glioblastoma *IDH*-wildtype and astrocytoma *IDH*-mutant grade 4 as different tumors. *IDH* mutation produce a metabolic reprogramming of tumor cells, thus affecting the processes of hypoxia and vascularity. The differences in the aggressiveness of these gliomas, which affect patient survival, are evident, with significative longer survival times for those patients who present *IDH* mutated tumors.

Estimating the presence of this genetic alteration at an early stage is crucial to improve prognostic models. Furthermore, it will be crucial for treatment selection and evaluation. Although currently the standard treatment for patients with astrocytoma grade 4 does not change, *IDH* mutation status is a selection criterion in most clinical trials.
Previous chapter of this thesis includes preliminary studies proposing differences in vascularity in astrocytoma grade 4 samples depending on the presence/absence of the *IDH* mutation. That sub-study focused on localized spatial analysis and included several samples per patient. However, it only includes samples from two patients with astrocytoma *IDH*-mutant grade 4. To further analyze the ability of MRI-DSC biomarkers to detect this genetic alteration and to improve patient classification from an early stage, a study with a larger multicenter cohort has been performed. This study constitutes chapter 4 of this thesis.

The contents of this chapter were published as a preprint in P9 (Álvarez-Torres M, 2022) and presented in P5 (ISMRM-ESMRBM, 2022)– thesis contribution C1.

4.1. Introduction

Astrocytomas grade 4 includes two different tumors since 2016, when the *CNS tumors classification and grading of the WHO* incorporated new entities according to both histology and molecular features[10,11]. This difference is maintained in the new WHO of CNS 2021[10], and in addition, it is accentuated, having also changed its nomenclature to glioblastoma *IDH*-wildtype and astrocytoma *IDH*-mutant grade 4 (instead of only *glioblastoma*). Glioblastoma *IDH*-wildtype represents about 95 % of astrocytomas grade 4 and predominates in patients over 55 years of age. Astrocytoma *IDH*-mutant grade 4 (about 5 % of cases) is more frequent in younger patients or in those with a history of prior lower grade diffuse glioma[10,11,117].

Relevant differences are found between these two astrocytoma types at clinical level, since they cause different patient survival rates[117–120] as well as distinct therapy responses[20,121,122]. Therefore, it is evident that an early-stage classification considering the *IDH* mutation is necessary to get an adequate prognostic evaluation and a more personalized treatment of patients with astrocytomas grade 4.

Despite its important role, the definition of full *IDH* evaluation can differ according to patient age[11], clinical protocols, and centers. The absence of R132H *IDH1* and *IDH2* mutations in astrocytomas from patients over about 55 years old suggests that sequencing may not be needed in the setting of negative R132H *IDH1* immunohistochemistry in those patients. Since protocols do not include full sequencing for every patient, alternative biomarkers could be useful and complementary to get a more reliable classification. In this sense, MRI-based methodologies could be key because they are non-invasive, could be used from the presurgical moment, and do not suppose additional economical or effort costs.

In 2020, Hao Wu *et al.* [123] evaluated the potential clinical impact of the Hemodynamic Tissue Signature (HTS) method for predicting *IDH* mutation status in patients with glioma tumors. They analyzed the association between the relative cerebral blood volume (rCBV) at the high angiogenic tumor (HAT) habitat and the *IDH* mutation status. A significant decreased rCBV for the *IDH*-mutant group was found. They concluded that "the HTS method was proven to have high prediction capabilities for *IDH* mutation status in high-grade glioma patients". Despite the great interest in these results, it only includes 25 patients with astrocytoma grade 4. In addition, the molecular basis of these vascular differences between these two high-grade tumors still unsolved.

The main purpose of this work is to evaluate and validate the association between MRI-DSC biomarkers and *IDH* mutation status in high-grade astrocytomas. In addition, to get a deeper understanding of the vascular differences, we aim to study

the transcriptomic bases of these vascular differences between these two high-grade astrocytomas.

4.2. Material and Methods

4.2.1. Study cohorts

Patient cohort with MRI data

The study cohort includes 299 patients with MRI data, 16 of them presented astrocytoma *IDH*-mutant grade 4, and the rest 283 presented glioblastoma *IDH*-wildtype. To collect this cohort, both public (35 patients from TCGA-GBM, 19 patients from Ivy GAP and 10 from CPTAC-3) and private datasets (108 patients from *MTS4UP* dataset, 20 from *GEINO-mol* dataset, and 107 from *GLIOCAT* dataset) were used. Public datasets are available to download in The Cancer Imaging Archive (https://www.cancerimagingarchive.net/). Subsection 1.3.3. of this thesis includes further information about the private datasets.

Public dataset with RNAseq data

To analyze differences in gene expression between these two types of high-grade astrocytomas, two public datasets have been used, including 99 patients from CPTAC3 and 151 patients from TCGA-GBM.

4.2.2. MRI data

Presurgical MRI studies were collected from all the included datasets, including pre- and post-gadolinium T1-weighted, T2-weighted, FLAIR and DSC T2*-weighted perfusion sequences obtained by standard of care protocols using 1.5 or 3.0-T.

MRI processing and perfusion markers calculation

To process the MRIs and to calculate the imaging vascular biomarkers, we used the HTS method[2,68], included in the ONCOhabitats site (www.oncohabitats.upv.es)[67]. The HTS method is illustrated in figure 4.1 and includes the following stages:

a. **Preprocessing**. In this stage, common MRI artefacts such as magnetic field in homogeneities and noise, multimodal registration, brain extraction, or motion correction are corrected.

b. **Glioma segmentation**. A state-of-the-art deep learning 3D convolutional neural network is implemented to segment the enhancing tumor, the edema, and the necrotic tissue. It is based on the directional class adaptive spatially varying finite mixture model (DCA-SVFMM), which is a clustering algorithm that combines Gaussian mixture modelling with continuous Markov random fields to make use of the self-similarity and local redundancy of the images. This methodology uses the unenhanced and GBCA-enhanced T1-weighted sequences, the T2-weighted sequence, and the fluid-attenuated inversion-recovery T2-weighted sequence combined with atlas-based prior knowledge of healthy tissues to delineate the regions.

c. DSC perfusion quantification. During this stage, the hemodynamic maps derived from the DSC perfusion sequence are calculated, including rCBV, rCBF, MTT, and K2 permeability. All perfusion maps are normalized against contralateral unaffected white matter volume to achieve consistency and comparability across different datasets. The normalization is performed automatically by a convolutional neural network, which detects the contralateral unaffected white matter region with 90% accuracy. To ensure a correct perfusion quantification and to avoid under- and over-estimation of perfusion marker, DSC perfusion quantification includes correction for contrast agent leakage effects. The HTS method implements the Boxerman leakage-correction method[114] for T1- and T2-leakage effects, as well as gamma-variate fitting to remove the extravasation phase and second pass of the contrast bolus.

d. Hemodynamic Tissue Signature (HTS) habitats. In this final stage an automated unsupervised segmentation algorithm performs the detection of the four vascular habitats within the tumor and edema. Each delineated habitat presents its specific hemodynamic behavior. They are named as: the High Angiogenic Tumor (HAT) habitat, the Low Angiogenic Tumor (LAT) habitat, the Infiltrated Peripheral Edema (IPE) habitat, and the Vasogenic Peripheral Edema (VPE) habitat. HTS habitats are delineated using a DCA-SVFMM structured clustering of rCBV and rCBF maps. The clustering includes two stages: (I) a two-class clustering of the whole enhancing tumor and edema regions and (II) a two-class clustering performed by using only the rCBV and rCBF data within the regions obtained in the first stage. To ensure the reproducibility of the HTS, both stages were initialized with a deterministic seed method.

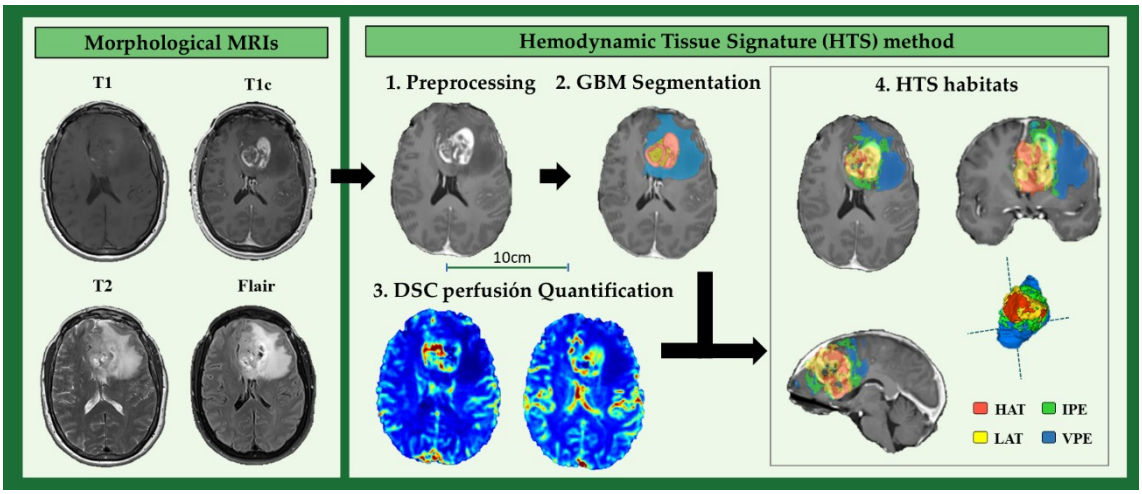

Figure 4.1. Hemodynamic Tissue Signature (HTS) method, including the four stages: (1) preprocessing, (2) glioma segmentation in classical tissues: active tumor, edema and necrosis, (3) DSC perfusion quantification, and (4) HTS habitats: High Angiogenic Tumor (HAT), Low Angiogenic Tumor (LAT), Infiltrated Peripheral Edema (IPE), and Vasogenic Peripheral Edema (VPE).

4.2.3. RNA data

Data Download and Normalization

For both datasets, we retrieved the HT-Seq mRNA read counts from the TCGA Database. Samples without *IDH* status information were filtered out to define two experimental groups: *IDH*-mutant and *IDH*-wildtype. Read counts were filtered by expression, removing genes with low counts across all samples. Normalization factors were calculated for each dataset using the Trimmed Mean of M-values (TMM) method.

Differential Gene Expression Analysis

We determined the Differential expressed genes (DEGs) in both datasets by fitting a quasi-likelihood negative binomial generalized log-linear model, implemented in the *edgeR* R package[124]. P values were corrected using the Benjamini-Hochberg procedure to control type I errors when conducting multiple comparisons. Genes having an adjusted p-value lower than 0.05 and an absolute value of log Fold-Change greater than 1 were considered as differentially expressed.

4.2.4. Statistical Analyses

Study cohort description

To analyze the correlation between the demographic and clinical variables with overall OS, independent Uniparametric Cox regression analyses were used. To

evaluate the differences in survival between both groups of patients, Kaplan Meier analyses and Log Rank test were performed.

Correlation between MRI-DSC biomarkers calculated at vascular habitats with IDH mutation

We evaluated the significant correlation between each MRI-DSC biomarker with OS to select the optimal biomarkers to find differences among astrocytoma types.

Differences in the imaging vascular biomarkers between glioblastoma *IDH*-wildtype and astrocytoma *IDH*-mutant grade 4 were assessed with Mann Whitney U test, as well boxplots were performed to illustrate differences.

Differences in transcriptome between high-grade astrocytoma types

Results from DEG were functionally annotated using the Biological Processes ontology from the Gene Ontology database[125,126]. First, we selected the GO terms related to vascular processes by matching a list of vascular key terms with their descriptions (table S4.1 of Supporting Material, included in appendix B) Then, we selected all genes mapping with these matched GO terms as our vascular genes set. Most significant vascular and non-vascular DEGs were plotted in heatmaps to illustrate the differences between expression profiles across experimental groups.

Finally, we assessed overall functional differences between astrocytoma types by performing a Gene Set Enrichment Analysis (GSEA) on Differential Expression Analysis results using the *fgsea* R package[127]. Genes were pre-ranked according to their log fold-change values. Gene sets with an adjusted p-value < 0.05 were considered significant.

4.3. Results

4.3.1. Detection of relevant prognostic demographic and clinical variables

We analyzed the correlation between OS with the following demographic and clinical characteristics: age, sex, tumor resection type, tumor location (hemisphere), *IDH* mutation and *MGMT* methylation. Results are included in figure 4.2A, resulting the *IDH* mutation as the variable most correlated with longer survival rates (with the lowest hazard ratio), followed by methylated *MGMT* and total tumor resection.

4.3.2. Cohorts' description

Proportions of each type of astrocytoma in this study dataset are coherent with previously published in literature[10,11,118], representing the population with *IDH*-

widltype glioblastoma a 95% of the entire cohort (Figure 4.2B). In addition, the number of patients from each dataset with *IDH*-mutant astrocytoma and *IDH*-wildtype glioblastoma were compared, showing these proportions differences among datasets (Figure 4.2C).

Differences in OS between these two groups were studied, demonstrating significantly longer survival times for the group of patients with *IDH*-mutant astrocytoma grade 4 ($p = 0.001$, Log rank test). Kaplan Meier curves are included in figure 4.2D, illustrating a median difference in OS of 267 days among the two populations.

Differences in the main demographic, clinical and molecular features between the two populations were analyzed and results are included in table 4.1.

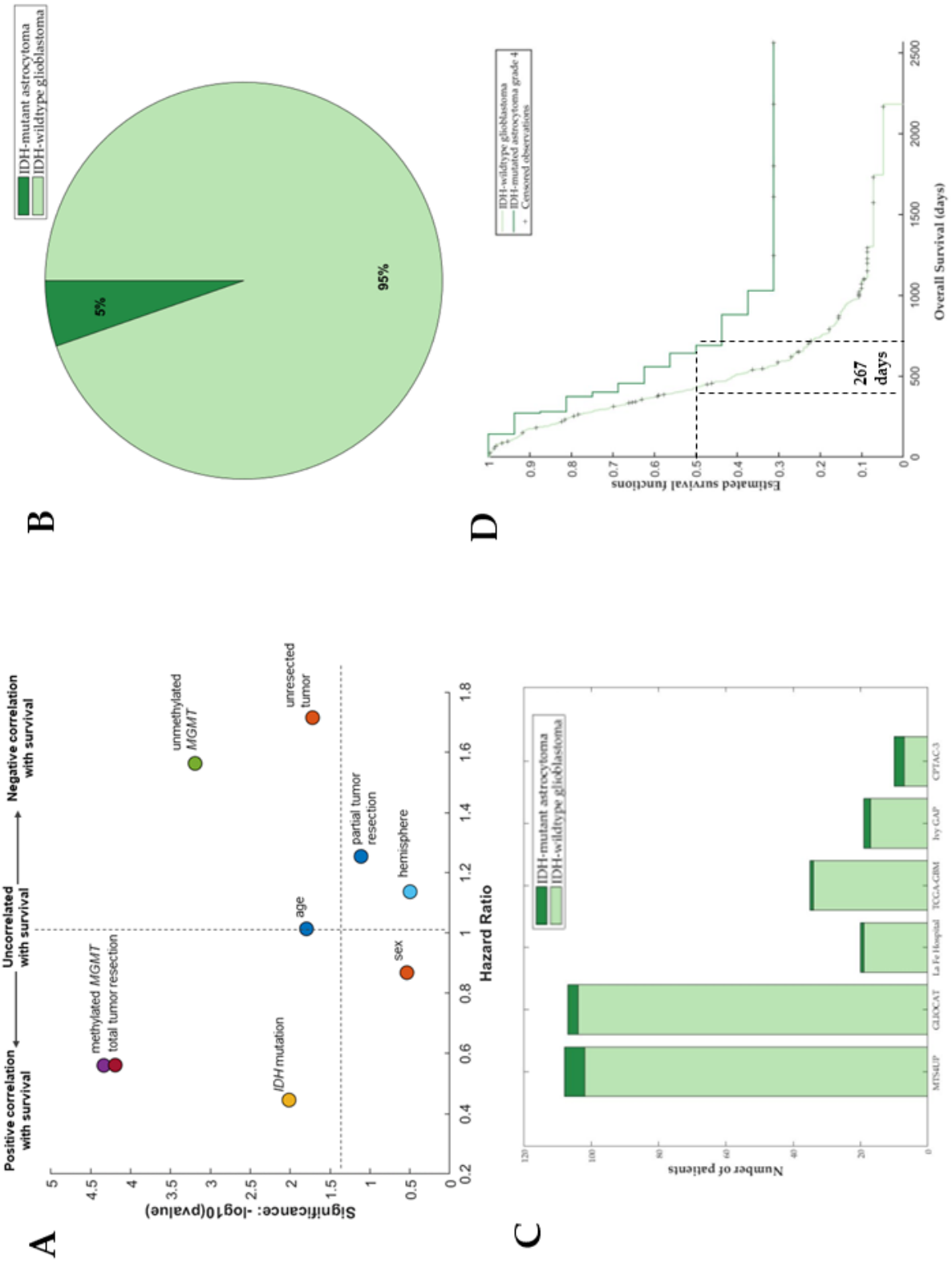

Figure 4.2. **A)** Scatter plot with the correlation between the main demographic and clinical characteristics and overall survival. **B)** Proportion of patients of the studied cohort with *IDH*-mutant astrocytoma and *IDH*-wildtype glioblastoma. **C)** Number of patients from each dataset with MRI data with. **D)** Kaplan Meier curves showing the survival differences between patients with astrocytoma *IDH*-mutant grade 4 (n = 16) and glioblastoma *IDH*-wildtype (n = 287).

Table 4.1. Demographic, clinical, and molecular features for the cohort with *IDH*-mutant astrocytoma (n = 16) and for the cohort with *IDH*-wildtype glioblastoma (n = 287). P-values resulting from the Mann Whitney test are also included.

	***IDH*-mutant astrocytoma grade 4**	***IDH*-wildtype glioblastoma**	**p-values (Mann Whitney test)**
#patients (% of entire cohort)	16 (5.3%)	287 (94.7%)	-
Sex (% Females)	56.2%	35.3%	0.1339
Mean Age at Diagnosis	49	60	0.0007*
Resection type (#patients)			
- Total	5	92	0.9183
- Partial	6	122	0.6609
- Biopsy	0	24	0.2265
- Unknown	5	49	0.1106
MGMT methylation (#patients; %)			
-Methylated	6 (37.5%)	93	0.7032
-Unmethylated	5 (31.2%)	111	0.5262
-Unknown	5 (31.2%)	83	0.7746

Only the median age of diagnosis was significantly different between groups, being lower for the group of patients with astrocytoma *IDH*-mutant grade 4 (49 vs 60 years old).

4.3.3. *Correlation between imaging vascular biomarkers and overall survival*

rCBV and rCBF markers at each vascular habitat (HAT, LAT, IPE and VPE) and for each metric (mean, median and maximum) were calculated, resulting in 24 markers. We studied the potential prognostic capacity of these markers, analyzing their correlation with *IDH* mutational status.

Figure 4.3 shows the correlation coefficient and the significance for each MRI-DSC biomarker with overall survival. We can see that the 12 markers related with the HAT and LAT habitats are the most significantly correlated ($p<0.05$), but only the rCBV markers yield a coefficient higher than 0.2. The selected markers to develop the following analyses were HAT-$rCBV_{mean}$, HAT-$rCBV_{median}$, HAT-$rCBV_{max}$, LAT-$rCBV_{mean}$, LAT-$rCBV_{median}$ and LAT-$rCBV_{max}$.

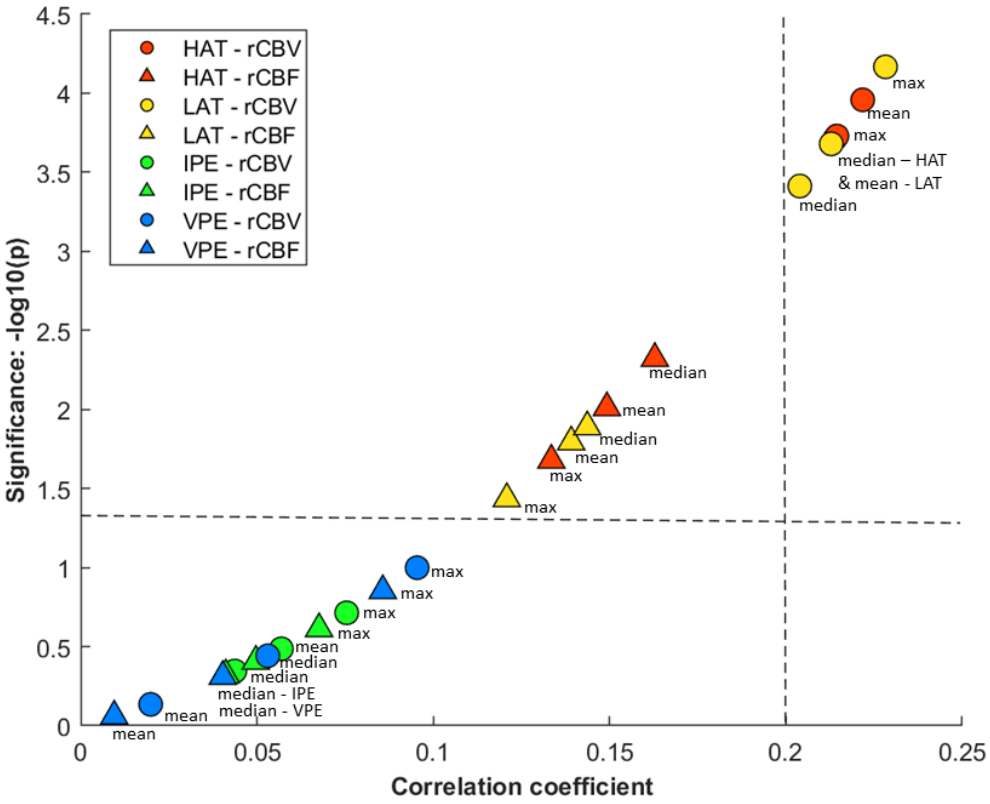

Figure 4.3. Scatter plot with the correlation results (correlation coefficients and significance) between MRI-DSC biomarkers and overall survival for the entire cohort (n = 299). Circle markers show rCBV and triangles show the rCBF. Each habitat is represented with a color, HAT in red, LAT in yellow, IPE in green and VPE in blue, and different metrics are also indicated (mean, median and maximum).

Significant differences (Mann Whitney, $p<0.05$) in $rCBV_{max}$ in HAT and LAT between *IDH*-mutant astrocytomas grade 4 and *IDH*-wildtype glioblastomas were found and are illustrated in figure 4.4. Figure S4.1 includes boxplot for $rCBV_{median}$ and $rCBV_{mean}$ at HAT and LAT habitats. For all the selected MRI-DSC biomarkers, the median value and the minimum and maximum range were higher for the *IDH*-wildtype glioblastoma group, suggesting a significantly higher vascularity for these tumors in comparison with *IDH*-mutant astrocytomas grade 4. Table S4.2 of Supporting Material (appendix B) includes the exact values of each biomarker for the group of *IDH*-wildtype glioblastoma and *IDH*-mutant astrocytoma grade 4.

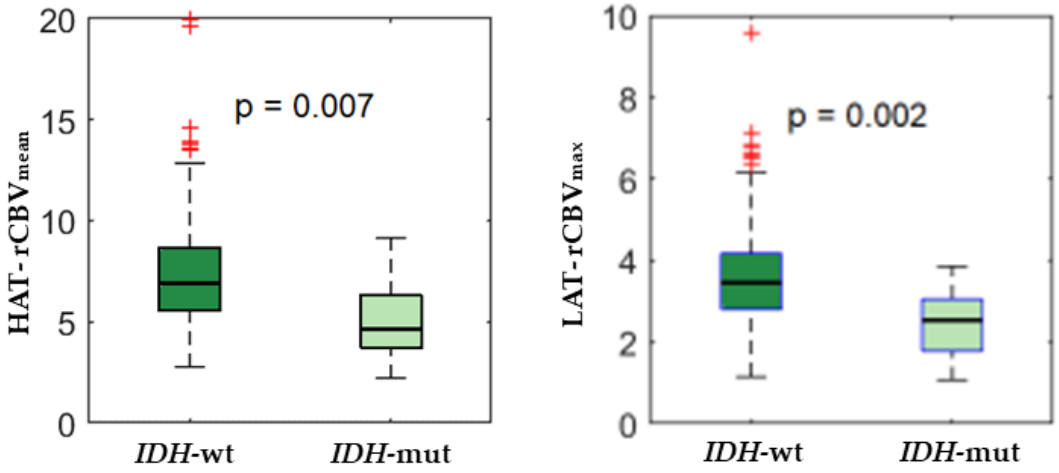

Figure 4.4. Boxplot showing differences in perfusion ($rCBV_{max}$ at HAT and LAT habitats) between glioblastomas *IDH*-wildtype and astrocytomas *IDH*-mutant grade 4.

4.3.4. Distinct transcriptome between IDH-wildtype glioblastoma and IDH-mutant astrocytoma grade 4

Differential expression analysis revealed considerable transcriptomic variations between glioblastoma *IDH-wildtype* and astrocytoma *IDH*-mutant grade 4. The total number of significant DEGs (adjusted p-value < 0.05 and absolute log Fold-Change > 1) was consistent across datasets (2568 and 2056 DEGs from CPTAC and TCGA, respectively, with an intersection of 879 DEGs).

We detected 1313 (CPTAC) and 1262 (TCGA) overexpressed genes in the *IDH*-wildtype group. A considerable fraction of these DEGs were considered part of the "vascular" functional gene set (143 and 123, respectively, with an intersection of 75 DEGs).

Also, we determined that a total of 1345 (CPTAC) and 794 (TCGA) genes were overexpressed in the *IDH*-mutant group. A total of 30 and 37 DEGs, respectively, were labeled as "vascular" genes, having in common a group of 11 DEGs.

Figure 4.5. includes the heatmaps showing different gene expression between glioblastoma *IDH*-wildtype and astrocytoma *IDH*-mutant grade 4 performed with two public datasets. Vascular genes are marked in different color.

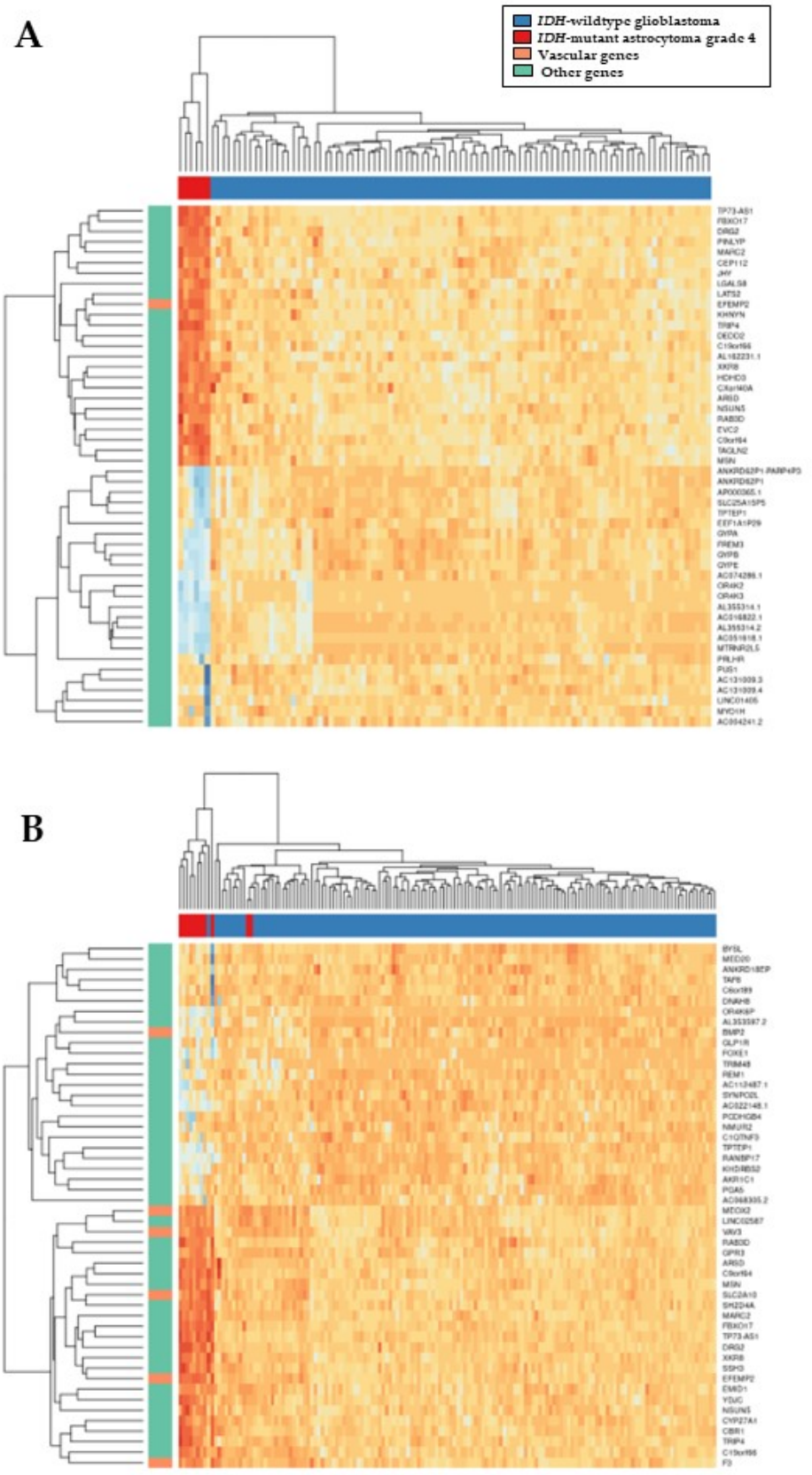

Figure 4.5. Heatmaps showing different gene expression between *IDH*-wildtype glioblastoma and *IDH*-mutant astrocytoma grade 4 performed with two public datasets: **A)** CPTAC3 (n = 93, and 6 respectively) and **B)** TCGA-GBM (n = 140, and 11 respectively)

All significant DEGs, labeled as vascular or nonvascular, are included in table S4.3. of the Supporting Material included in appendix B. This table also contains the adjusted p-values and the log Fold Change values for each gene.

GSEA on differential expression analysis results showed significant differences between the two groups at the biological processes level. On the one hand, a total of 169 (CPTAC) and 39 (TCGA) GO terms showed significant overrepresentation in IDH-wildtype Glioblastomas. A core subset of 33 GO terms was present in both sets of significant functions.

On the other hand, we only detected 1 (CPTAC), and 3 (TCGA) significantly overrepresented GO terms in *IDH*-mutated Astrocytomas. There was not any coincident function between sets.

4.4. Discussion

With this study we have demonstrated that *IDH*-wildtype glioblastoma and *IDH*-mutant astrocytoma grade 4 present different vascular patterns both in high- and low-angiogenic tumor habitats, defined by the automatic ONCOhabitats method. These differences can be detected using MRI-DSC biomarkers, such as rCBV and rCBF calculated from the presurgical stage, since they are correlated with the presence of the *IDH* mutation. These results are obtained with a multicenter cohort of 299 patients and validate those found in a previous study[123].

The association between tumor and edema vascularity and OS has been previously analyzed in literature[2,68,70,128]. There is a consensus that higher values of vascularity, measured by DSC perfusion biomarkers, result in shorter survival times. These important differences in survival may be due in part to different vascular behavior, resulting in quicker progression and greater aggressiveness of *IDH*-wildtype glioblastomas[24,25,44]. With this work, we have validated this hypothesis, demonstrating significantly higher rCBV values for *IDH*-wildtype glioblastomas. The clinical relevance of this finding is that opens the possibility to use the MRI-DSC biomarkers as complementary tools to support the first diagnosis made by the radiologist from the presurgical stage.

In addition, to acquire a deeper understanding of vascular differences between these two high-grade astrocytomas, we analyzed gene expression patterns of two public datasets that include RNAseq data. We focused on analyzing genes related to vascular processes and structures. We found that 75 genes related to vascularity were up-regulated in both datasets for the group of *IDH*-wildtype glioblastoma, versus only 11 vascular genes up-regulated in the group of *IDH*-mutant astrocytomas grade

4. This finding supports our hypothesis, that stronger vascular processes occur during the establishment and progression of *IDH*-wildtype tumors.

In glioblastomas *IDH*-wildtype, we found overexpression of several genes previously reported as associated with vascular remodeling and arterial abnormalities in high-grade gliomas. Some of these genes are *EGF-containing fibulin-like extracellular matrix protein 2* (*EFEMP2)*[129], *solute carrier family 2 member 10 (SLC2A10)*[130], *midkine (MDK)*[131] and *transmembrane BAX inhibitor motif-containing 1* (*TMBIM1)*[132]. They also have been proven as associated with poor progression, which seems coherent since a higher vascular supply allows quicker tumor progression.

On the other hand, there were 11 vascular genes overexpressed in astrocytomas *IDH*-mutated grade 4 compared with glioblastomas *IDH*-wildtype. We can remark on the relevance of *bone morphogenetic protein 2 (BMP2),* which has been previously defined as relevant for prognosis estimation[133], since the higher the expression of *BMP2*, the better the prognosis of patients. In addition, we found an overexpression in *STOX1*, which was previously associated with younger patients and with gliomas of lower grades and less aggressive[134]. The correlation of higher expression of these genes with the presence of *IDH* mutation can be due to the metabolic reprogramming that suffers tumor cells with this alteration.

4.5. Conclusions

In conclusion we have validated the association between the *IDH* mutation with tumor vascularity, measured by DSC perfusion biomarkers at HAT and LAT habitats. Astrocytomas *IDH*-mutant grade 4 present lower rCBV and rCBF, and longer survival times, which can be partly explained by a slower tumor progression, due to less vascularity.

We have assessed the potential relevance on vascularity of specific genes overexpressed in glioblastomas *IDH*-wildtype, such as *EFEMP2*, *SLC2A10*, *MDK* and *TMBIM1*, and in *IDH*-mutant astrocytomas grade 4, such as *BMP2* and *STOX1*. Although it is needed deep analyses, these genes can be proposed as targets for specific novel therapies for each type of high-grade astrocytoma.

This constitutes the first study analyzing vascular differences both at MRI and transcriptomic levels between *IDH*-wildtype glioblastoma and *IDH*-mutant astrocytoma grade 4. We propose DSC biomarkers automatically calculated with the ONCOhabitats method as useful to estimate the *IDH* mutation status in astrocytomas grade 4 from the presurgical stage. Moreover, we suggest the key role of specific genes overexpressed in glioblastomas *IDH*-wildtype as determinant for presenting

stronger vascularity; and the clinical relevance of *BMP2* and *STOX1* for astrocytomas *IDH*-mutant grade 4.

PART II

Patient Prognosis Estimation and Stratification

Chapter 5

Multicenter validation of calculation and prognostic application of MRI-DSC biomarkers of vascular habitats

Researchers and clinicians are increasingly demanding non-invasive biomarkers to improve decision making in the management of patients with high-grade gliomas. Although there are robust studies proposing MRI-DSC biomarkers with prognostic application, there are two important gaps that must be overcome to validate and implement them in clinical practice. The first one is related to the requirement of a multisite validation, this is, multiple centers have to be involved in the clinical study and robust results have to be yielded when using data from different centers. The second gap is referred to the need of a biological validation of the biomarkers through its characterization (this point has been addressed in part 1 of this thesis).

In this chapter, it is addressed the multicenter validation of MRI-DSC biomarkers calculated at vascular habitats with an automatic methodology and data from seven European hospitals with different MRI and clinical acquisition protocols. The main purposes of this chapter are: 1) the validation of the robustness of the methodology to process MRIs that the MRI-DSC biomarkers are comparable among centers; and 2) to validate the prognostic application of the MRI-DSC biomarkers calculated at the tumor habitats and the peripheral edema habitat defined by the vascular assessment method (ONCOhabitats methodology).

The contents of this chapter were published in the journal publications P2 (Álvarez-Torres M. JMRI, 2019) and presented in P6 (AACR 2019) – thesis contribution C2.

5.1. Introduction

Glioblastoma is the most aggressive malignant primary brain tumor in adults, with a median survival rate of 12–15 months[11,135]. It still carries a poor prognosis despite aggressive treatment, which includes tumor resection followed by chemoradiotherapy[32,135,136]. One of the main factors thought to be responsible for glioblastoma aggressiveness is its vascular heterogeneity[26,32], mainly defined by strong angiogenesis, which supplies the glioblastoma's metabolic needs and accounts for its rapid progression[25,44]. The tumor vascular profile is strongly associated with the molecular characteristics of the lesion[44]. Thus, the vascular

conditions of the early tumor stages and its environment are both associated with glioblastoma progression[25].

A negative association between patient survival rates and vascular features, extracted from perfusion magnetic resonance imaging (MRI), has been widely analyzed in the literature[32,70,137]. In these studies, perfusion indices such as relative cerebral blood volume (rCBV) or capillary heterogeneity were found to have prognostic capabilities. The methodologies employed to assess these perfusion indices range from manually defined regions of interest (ROIs), which introduce high uncertainty and lack repeatability, to more up-to-date techniques based on artificial intelligence methods able to analyze tumoral heterogeneity[138–142].

In 2018, Juan-Albarracín *et al.*[68] proposed the hemodynamic tissue signature (HTS) methodology (publicly accessible at ONCOhabitats site: https://www.oncohabitats.upv.es) to characterize glioblastoma's vascular heterogeneity by means of delineating the vascular habitats. The HTS technique defines four habitats within the lesion with different hemodynamic behavior: the HAT, LAT, IPE and VPE habitats. The prior study of Juan-Albarracín *et al* found a significant correlation between overall survival (OS) and HTS markers in the high and low angiogenic habitats[68]. In 2018, Fuster-Garcia *et al* demonstrated the ability of these imaging markers to improve the prognosis of conventional models based on clinical, morphological, and demographic features[143]. Both studies included a limited number of patients from a single hospital.

Although both researchers and clinicians are increasingly demanding imaging markers to improve decision making[144], two translational gaps have to be overcome to validate them in clinical practice (O'Connor *et al*. [145]): The first requires to use preclinical or clinical datasets from a single or only a few expert centers. The second requires that multiple centers be involved in the study, together with the biological validation of the biomarkers. Although previous studies[68,143] overcame the first translational gap, to validate the vascular markers from the HTS habitats and demonstrate the generalization of the methodology required an extended multicenter study. The main aim of this work was to validate the prognostic capacities of HTS markers calculated from vascular habitats in glioblastoma. To this end, we analyzed the possible association between these markers and patients OS, as well as their capability for stratification in groups of patients. Furthermore, including a large heterogeneous international cohort, our aim was to assess the robustness of the HTS methodology against MRI acquisition variability among centers.

5.2. Material and Methods

5.2.1. Patient Selection

The following seven European clinical centers participated in the study: the Hospital Universitario de La Ribera, Alzira, Spain; Hospital de Manises, Manises, Spain; Hospital Clinic, Barcelona, Spain; Hospital Universitario Vall d'Hebron, Barcelona, Spain; Azienda Ospedaliero-Universitaria di Parma, Parma, Italy; Centre Hospitalier Universitaire de Liège, Liège, Belgium and the Oslo University Hospital, Oslo, Norway. A Material Transfer Agreement (MTA) was approved by all the participating centers and an acceptance report was issued by the Ethical Committee of each center. The managing institution review board also approved this retrospective study and the requirement for patient-informed consent was waived.

The inclusion criteria for patients participating in the study were: (a) adult patients (age > 18 y.o.) with histopathological confirmation of glioblastoma diagnosed between January 1, 2012 and January 1, 2018; (b) access to the preoperative MRI studies, including: pre- and post-gadolinium T1-weighted, T2-weighted, FLAIR and DSC T2*-weighted perfusion sequences; and (c) patients who underwent standard Stupp treatment[19] with a minimum survival of 30 days.

5.2.2. MRI

Standard-of-care MR examinations were obtained with 1.5T or 3.0T scanners. Pregadolinium and post gadolinium-based contrast agent enhanced T1-weighted MRI, as well as T2-weighted, FLAIR T2-weighted, and DSC T2* perfusion MRI sequences were collected from each center. Table S5.1 of Supporting Information (appendix C) summarizes the MRI acquisition protocols grouped by center, including the magnetic field strength, repetition time, echo time, matrix size, slice thickness, field of view, and the number of temporal acquisitions of the perfusion MR sequence.

5.2.3. GBM Vascular Heterogeneity Assessment Through HTS Habitats

The HTS methodology from the ONCOhabitats platform was used to analyze the MRI studies. This methodology comprises the following stages:

1. Preprocessing, including correction of common MRI artifacts such as magnetic field in homogeneities and noise, multimodal registration, brain extraction, and motion correction.

2. Glioblastoma tissue segmentation, which implements a state-of-the-art deep-learning 3D CNN that segments the enhancing tumor, edema, and necrosis tissues.

3. DSC perfusion quantification, which calculates the hemodynamic maps derived from the DSC perfusion sequence (relative cerebral blood volume (rCBV), relative cerebral blood flow (rCBF), MTT, and K2 permeability.

4. Hemodynamic tissue signature map, in which an automated unsupervised segmentation algorithm performs the detection of the HAT, LAT, IPE, and VPE habitats each with its specific hemodynamic behavior. Following a previous study[146], for each habitat we define its HTS marker as the $rCBV_{max}$, computed as the 95th percentile of the rCBV distribution at the corresponding habitat. Accordingly, these four habitat-specific HTS markers describe the overall glioblastoma vascular heterogeneity of a patient.

A more detailed description of the HTS method is included in chapter 2, section 2.4.3.

5.2.4. Association Between Patient OS and HTS Markers (Entire Cohort)

Cox proportional hazard regression analysis was used to quantify the associations between patient OS and HTS markers. The proportional hazard ratios (HRs) with a 95% confidence interval (CI) were reported, as well as the associated P-values corrected for multiple hypothesis testing by the false discovery rate (FDR) method ($\alpha = 0.05$). Kaplan–Meier analyses were performed to study the capabilities of the HTS markers to stratify the population into "moderate-vascular" and "high-vascular" groups. We define "moderate-" and "high-vascular" as the two groups of patients generated by the Kaplan–Meier test when dividing the whole population using a cutoff threshold for each HTS marker. The "moderate-vascular" group includes the patients with an $rCBV_{max}$ lower than the threshold, and the "high vascular" group includes the patients with an $rCBV_{max}$ higher than the threshold. The optimum cutoff threshold for each perfusion index and habitat was determined by the C-index method. The C-indexes for the final cutoff thresholds were also reported. The log-rank test was used to determine any statistical differences between the estimated survival functions of the groups defined by the HTS markers.

5.2.5. Intercenter Association Between Patient OS and HTS Markers

Similarities between the HTS markers distributions among the clinical centers with different MRI protocols were evaluated to determine the degree of agreement in describing tumor vascular heterogeneity. To this end, we conducted a pairwise

Mann–Whitney U-test to compare the distributions of the HTS markers of each center (α = 0.05), followed by a post-hoc Tukey's honest significant difference criterion test.

As in the analyses for the whole cohort, Cox regression analyses were conducted to assess whether the association between patient OS and HTS markers differed among the centers. Kaplan–Meier analyses were performed after dividing the population of each center using the cutoffs for each HTS marker previously calculated for the entire cohort. In addition, we evaluated the differences among centers in terms of age and gender using an analysis of variance (ANOVA) test and post-hoc comparison. All statistical analyses were performed with MatLab R2017b (MathWorks, Natick, MA).

5.3. Results

5.3.1. Description of patient cohort

From the initial cohort, consisting of 196 glioblastoma patients, four cases were excluded due to HTS processing errors; five cases were excluded due to noise or MR artifacts that precluded DSC quantification (gamma variate R2 goodness of fit <0.95); one case was excluded due to inability to differentiate between tumor vascularity and reactive meningeal enhancement; and two cases were excluded due to defective perfusion images. The final study cohort included 184 patients. Supporting Information Table S5.2 describes the number of patients of each center. Those who were still alive during the study were considered censored observations. The date of censorship was the last date of contact with the patient or, if not available, the date of the last MRI exam. Table 5.1 summarizes the most important demographic and clinical characteristics of the studied population. The results of analyzing the differences among centers in terms of age and gender are included in Table S5.3 of the Supporting Information (appendix C).

Table 5.1. Demographic and clinical data of the 184 patients included in the study.

	HR[a]	**HM[b]**	**CB[c]**	**HV[d]**	**AO P[e]**	**CH Liège[f]**	**OUH[g]**	**Total**
	Sex (F/M)							
- # of patients	6/1	5/9	10/15	14/19	12/28	11/22	8/24	66/118
	Age at diagnosis (years)							
- Mean	49	65	56	60	61	58	63	60
- Range	[24,67]	[39,79]	[35,74]	[30,81]	[35,76]	[32,77]	[40,81]	[24,81]
	Overall survival (months)							
- Mean	14.6	14.4	10.3	15.2	11.7	15.3	15.4	13.7

- Median	9.1	12.8	9.6	13.0	12.9	14.5	12.6	12.6
- Range	[3.4,52.6]	[3.4,38.4]	[1.3, 26.9]	[4.1,40.0]	[1.1,30.7]	[2.5,41.0]	[3.0,36.9]	[1.1,52.6]
Resection (# of patients)								
- Total	3	3	0	12	19	22	11	70
- Sub-total	1	4	10	10	15	6	21	67
- Biopsy	1	7	6	11	2	5	0	32
- Unknown	2	0	9	0	4	0	0	15
Tumor location (# of patients)								
- Frontal	2	4	7	10	18	11	12	64
- Parietal	2	0	5	7	4	9	3	30
-Temporal	3	7	11	13	12	9	14	69
- Occipital	0	2	1	2	2	0	1	8
- Other /Unknown	0	1	1	1	4	4	2	13
IDH1 mutation status								
- Mutated	2	0	4	0	0	0	1	6
- Wild type	2	0	4	32	30	34	31	99
- Unknown	3	14	17	1	10	0	1	79

Hospital de la Ribera[a]; Hospital de Manises[b]; Clinic de Barcelona[c]; Hospital Vall d'Hebron[d]; Azienda Ospedaliero-Universitaria di Parma[e]; Centre Hospitalier Universitaire de Liège[f]; Oslo University Hospital[g]

5.3.2. Association Between Patient OS and HTS Markers (Entire Cohort)

Table 5.2 shows the Cox proportional hazard analysis between HTS markers and patient OS. Significant negative associations were found between $rCBV_{max}$ at HAT, LAT, and IPE habitats and patient OS (α = 0.05, FDR adjusted). The IPE marker showed the highest HR (1.28). Thus, a variation in IPE $rCBV_{max}$ would increase the risk more of occurring the event "exitus" than a variation of the same magnitude in the rest of the studied markers. The HR of VPE (1.19), despite being the second highest, showed a large variance, thus resulting in being not significantly different.

Table 5.2: Cox regression analysis for $rCBV_{max}$ of the vascular habitats to predict overall patient survival. * Indicates significant difference ($p<0.05$).

HTS markers	Hazard Ratio	95% Confidence intervals	P-value	P-value (FDR adjusted)
HAT	1.05	[1.01, 1.09]	0.0115*	0.0174*
LAT	1.11	[1.02, 1.20]	0.0131*	0.0174*
IPE	1.28	[1.05, 1.55]	0.0122*	0.0174*

VPE	1.19	[0.89, 1.60]	0.2502	0.2502

HTS: Hemodynamic Tissue Signature; HAT: High Angiogenic Tumor; LAT: Low Angiogenic Tumor; IPE: Infiltrated Peripheral Edema; VPE: Vasogenic Peripheral Edema

The Kaplan–Meier results are summarized in Table 5.3, including estimated optimal cutoff thresholds, number of patients per group, estimated C-index, median OS calculated per group, and log-rank test results (P-values). Again, significant differences in OS between moderate and high vascularity, as defined by rCBVmax, were found in HAT, LAT, and IPE, but not in VPE. Those patients with a moderate $rCBV_{max}$ in HAT, LAT, and IPE presented a higher median survival rate. The Kaplan–Meier curves for the populations divided by high and moderate $rCBV_{max}$ in the vascular habitats are shown in Figure 5.1. The capability of the HTS markers to stratify patients in groups can be seen to coincide with higher or shorter median OS, depending on the vascular group.

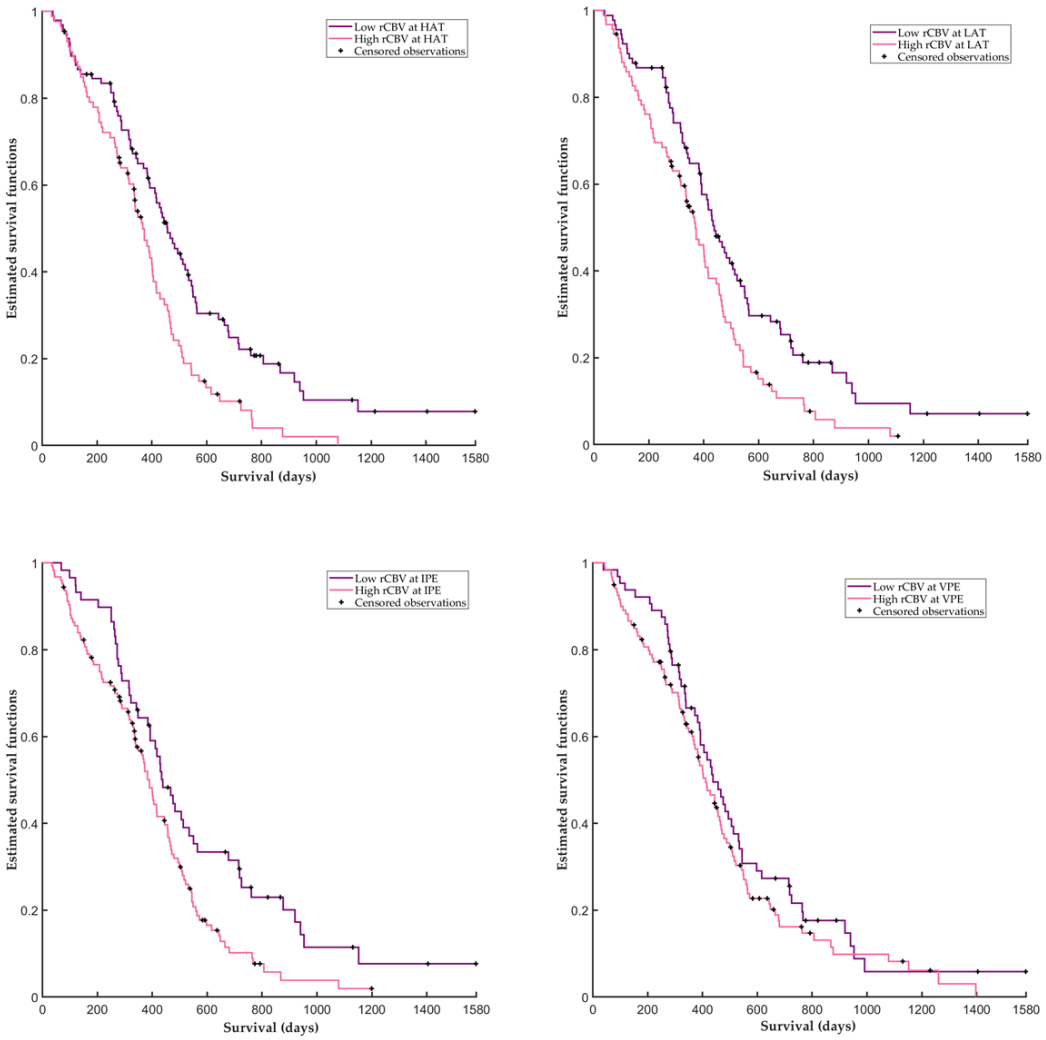

Figure 5.1. Kaplan–Meier estimated survival functions for the populations stratified into groups according to high or low $rCBV_{max}$ in HAT (top left), LAT (top right), IPE (down left), and VPE (down right) habitats.

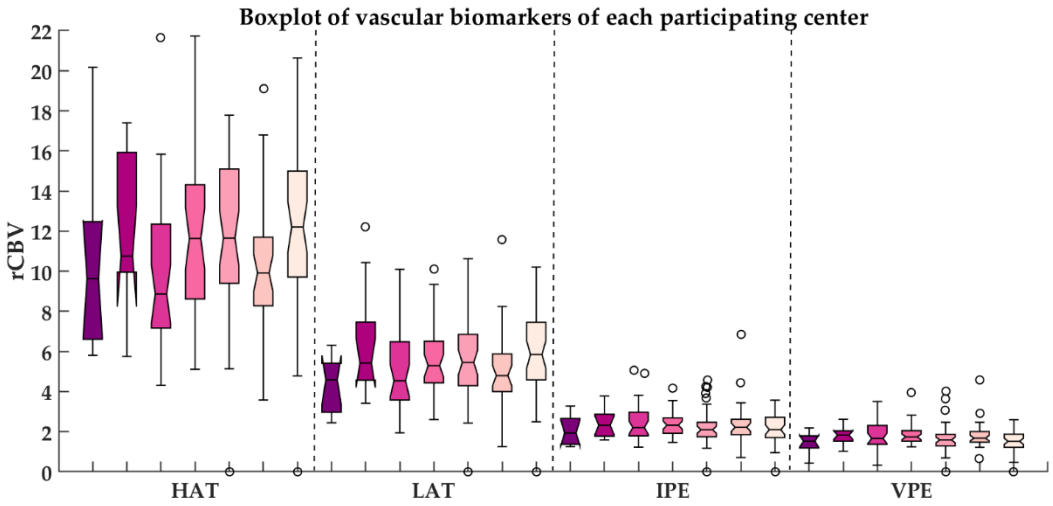

Figure 5.2. Boxplot of the HTS markers ($rCBV_{max}$ at HAT, LAT, IPE, and VPE) of glioblastoma patients of each participating center.

5.3.3. Intercenter Association Between Patient OS and HTS markers (per center)

No significant differences were found between the $rCBV_{max}$ values of the habitats between most of the centers ($\alpha = 0.05$) (Supporting Information Tables S5.3.1, S5.3.2, S5.3.3, and S5.3.4). We highlight that none were found for the IPE marker; most correlated with OS in the whole cohort study. This can be observed in the box-and-whisker diagram in Figure 5.2, where the $rCBV_{max}$ intervals for each hospital overlap.

Table 5.3: Kaplan Meier and Log Rank test results for $rCBV_{max}$ in HAT, LAT, IPE and VPE to stratify patient in groups by low and high vascularity.

	Cut-off threshold	Patients per group	AUC (c-index)	Median OS per group	P-value
$rCBV_{max}$		Low High		Low High	
HAT	11.06	[97, 87]	0.606	[14.3, 11.3]	0.0014*
LAT	5.31	[91, 93]	0.605	[13.9, 11.3]	0.0085*
IPE	1.92	[59 125]	0.634	[14.3, 11.4]	0.0101*
VPE	1.67	[100, 84]	0.599	[13.8, 11.2]	0.1356

HTS: Hemodynamic Tissue Signature; $rCBV_{max}$: Maximum relative Cerebral Blood Volume; HAT: High Angiogenic Tumor; LAT: Low Angiogenic Tumor; IPE: Infiltrated Peripheral Edema; VPE: Vasogenic Peripheral Edema; AUC: Area under the curve

Table S5.4 of the Supporting Material (appendix C) shows the results of the Cox regression analysis, depicted by hospital, of those HTS markers that yielded a

significant association with OS (Table 2). Given the reduction of the sample sizes, CIs tended to be larger, especially in those centers with a small sample size. However, the results are, on average, consistent with those in the entire cohort study which, in addition, counting a larger sample size leads to results that are more precise. Figure 5.3 contains a graph of the HTS markers that yielded significant results in the Cox analyses with the whole cohort. The figure shows an unambiguous overlap between CIs for most of the centers, suggesting no significant differences among them in calculating HAT, LAT, and IPE markers. Therefore, the results of the association of these markers and OS per hospital are consistent with those obtained for the entire cohort.

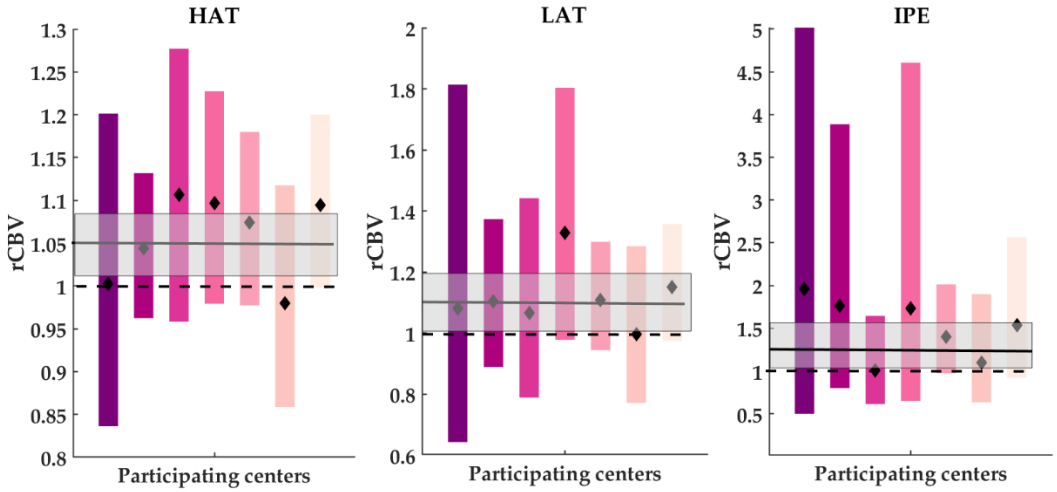

Figure 5.3. Plot with the HRs and 95% CIs to study the association between the overall survival and the HTS markers at HAT, LAT, and IPE for each center. The continuous black line and the gray band correspond respectively to the value of HR and CIs obtained by performing the Cox analysis with data from all centers and for each HTS marker. The black markers are those of the HR obtained by performing the Cox analysis with the data from each center and each HTS marker.

Figure 5.4 show the Kaplan–Meier plots for the stratification of the population per hospital in high and moderate vascular glioblastomas, using the optimal C-index thresholds. For the sake of clarity, this figure only gives the results of the HAT marker (ie, the HTS marker in the HAT habitat), as this showed the clearest differences between the populations.

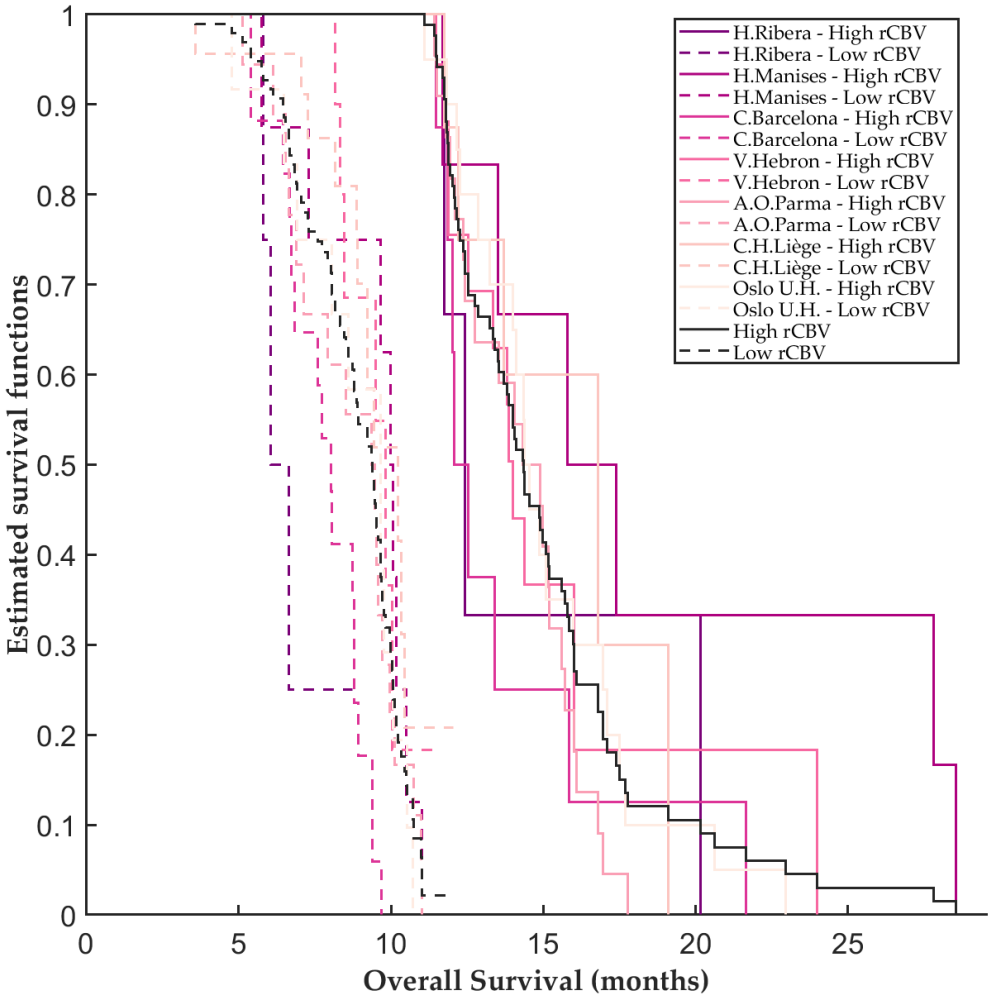

Figure 5.4. Kaplan–Meier estimated survival functions for the populations of each center stratified into groups according to high or low $rCBV_{max}$ in HAT, divided by the threshold calculated with the data of all centers (cutoff threshold of 11.6).

5.4. Discussion

Using data from seven European centers, significant negative associations were found between patient OS and the HTS markers in the HAT, LAT, and IPE habitats. These results agree with a previous single-center study[68] in which significantly longer survival rates were found for patients with lower $rCBV_{max}$. Overcoming the intercenter variability in calculating imaging markers is not easy. Other authors have pointed out the uncertain or low reproducibility of some MRI markers, especially across centers[144,145,147,148]. A manual definition of ROIs and the interpretation of images by several experts may be other sources of variability, making it difficult to validate new imaging markers[147].

Although the current study involved a cohort with large variations in terms of patient demographics, as well as image acquisition protocols, we did not find any relevant differences among the distributions of the HTS markers calculated from MRIs from different centers. Only for a small number of cases were significant differences found for the HAT and LAT markers among centers. These results suggest that the proposed method is robust against intercenter variability in calculating vascular habitat HTS markers, especially the IPE marker. Furthermore, the results of the Cox and Kaplan–Meier analysis per center show a robust association between patient OS and the HTS markers, regardless of the center of origin. The proposed thresholds were also effective in stratifying patients from different centers into "moderate-" and "high-vascular" groups, presenting these two groups with a different median OS.

Having demonstrated the influence of early-stage vascularity on the prognosis of glioblastoma patients, we suggest using this factor in any clinical study that includes population randomization. The authors consider that the HTS method will help to overcome the current limitations and improve patient recruitment and randomization by initiating a route map to avoid the second translational gap cited above[144].

The HTS method segments the enhancing tumor into two habitats with different vascular profiles: HAT and LAT. Since HAT is the most vascular region in the tumor, the HAT $rCBV_{max}$ is quite similar to $rCBV_{max}$ in the whole enhancing tumor. In this regard, the correlation between high perfusion values in the HAT habitat and shorter OS is compatible with previous studies[70,149,150] that found a relationship between the perfusion parameters in the enhancing tumor region and the patient's survival rates.

We also found that the LAT habitat in the enhancing tumor has a strong association with OS and high stratification abilities. Sawlani *et al.*[128] suggested the potential of the mean rCBV ($rCBV_{mean}$) of the enhancing tumor as a predictive marker. The $rCBV_{mean}$ values obtained here for the whole tumor are comparable with the $rCBV_{max}$ in the LAT habitat. In 2005, Hambardzumyan and Bergers defined different glioblastoma niches based on different cell constituents and the functional status of the vasculature[151]. They distinguished between the perivascular niche, with vigorous and abnormal angiogenesis leading to a heterogeneous organization of blood vessels, and the hypoxic niche, with lower blood volume and flow values. Even though these regions could be consistent with the HAT and LAT habitats proposed here, we have gone a step further and identified a new important region within the tumor that provides automatic reproducibility in calculating valuable prognostic imaging markers.

One of the most important of our findings is the correlation found between long-term OS and lower $rCBV_{max}$ in the IPE habitat, which yielded the highest HR by developing the Cox regression analyses. This result implies that a variation in the $rCBV_{max}$ in IPE increases the risk more of exitus than a variation of the same magnitude in the HAT or LAT markers. These results agree with the previous study[68], which yielded decreasing HR from IPE to HAT markers.

Edematous tissue has received much less attention than the active tumor in previous studies, although there is evidence that the vascularity in this area can influence tumor evolution and patient prognosis[152]. In 2014, Jain *et al.*[70] showed that the edema rCBV generally provided relevant prognostic information. Artzi *et al.*[152] described differences between the vasogenic and peripheral edema at the metabolic and vascular levels, while we found the HTS method can automatically delineate the infiltrated edema area, ie, IPE. The clinical implications are given by the strong association between the IPE marker, patient prognosis, and the ability to stratify patients in groups with differences in the tumor vascularity, opening up new presurgical treatment options.

The main limitation of our study is the lack of homogeneity in the number of patients per hospital. Although the whole cohort size is large enough to be a study with glioblastoma patients, some of the participating centers included a small number of patients. In particular, two of the participating centers included fewer than 15 patients. In addition, we evaluated the differences among centers in terms of age and gender, and we found significant differences for the Oslo Hospital and those with a very reduced number of samples, due to the consequent increased uncertainty.

5.5. Conclusions

Since the influence of the molecular markers on patient prognosis has been demonstrated[11,153] it may be of interest to add them as cofactors in survival models. The present multicenter study focused on the robustness of the HTS markers in dealing with images from multiple centers. In future studies we hope to analyze the possible association between molecular and imaging markers and their prognostic possibilities. In addition, it may be of great interest to analyze the potential of the combination of markers in different habitats.

Chapter 6

Effect of tumor vascularity on patient survival over time. Comparison between long- and short-term survivors

The previous chapter discussed the prognostic relevance of vascular behavior in specific tumor and edema habitats. One of the main conclusions was the robust association between lower values of MRI-DSC biomarkers calculated from diagnosis and longer patient survivals. However, it is well known that astrocytomas grade 4 undergo significant macro- and microscopic changes during patient follow-up and treatment. Tumors are dynamic systems that change over time. This evidence, combined with the invasive alterations caused by resection during surgery, can drastically affect the initial architecture and vascular patterns present at the pre-surgical stage.

There are other factors that may be more decisive than tumor vascularity at the time of diagnosis in predicting patient survival. For example, age or the existence of chronic diseases or comorbidities. On the other hand, others, such as *MGMT* gene methylation will be decisive in the chemotherapy phase, as it is associated with better acceptance of Temozolomide treatment.

Considering that different factors may have a greater or lesser influence on survival at different times of follow-up, in this chapter we address the prognostic effect of vascularity in short and long survivors of astrocytoma grade 4. For this purpose, the cohort can be stratified according to patient survival times and analyze the association with vascularity independently. Finding out when vascularity has the greatest influence can be useful for establishing biomarkers cut-offs and taking it into account in randomized clinical trials.

The contents of this chapter were published in the journal publication P3 (Álvarez-Torres, NMR in Biomedicine, 2021b) – thesis contribution C3.

6.1. Introduction

Glioblastoma *IDH*-wildtype is the most lethal and common tumor of the CNS[154], with patient median survival rates of 13-14 months [11,154], and represents about 90% of the cases of glioblastoma[11]. Inter-patient tumor heterogeneity makes notable

differences to the OS of glioblastoma patients, with angiogenesis being one of the most relevant processes involved in tumor heterogeneity[25,26,32].

This process can be studied using non-invasive techniques, such as MRI, from the time of tumor diagnosis[27,138,140–142]. Hence, functional MRI techniques allow researchers and clinicians to study relevant vascular markers with prognostic, predictive and stratification capabilities. In particular, the relative cerebral blood volume (rCBV) which is the most consistently recognized independent predictor of survival [27,138,140–142]. For this, the hemodynamic tissue signature (HTS), a machine learning technology, is able to automatically define regions of interest within the tumor and the edema based on the morphologic and perfusion analysis of the MRI of the patient. It also allows calculation of perfusion metrics within each habitat to study associations with patient OS[2,68]. These habitats are regions with different vascular behaviours that represent the HAT part of the enhancing tumor, the LAT part of the enhancing tumor, the IPE and the pure VPE. On the other hand, despite having demonstrated the robustness of these vascular markers[2], biological and clinical factors, which are not static with time, can affect the effectiveness of the prognostic image markers. We hypothesize that the influence of vascularity on the aggressiveness of the tumor can vary during the treatment of the glioblastoma. To address these issues, we consider it relevant to evaluate the usefulness and accuracy of these vascular markers in different groups of patients with time, to assess for any potential clinical benefit. In particular, we have focused on the HAT habitat, i.e. that region of the active tumor with higher levels of blood volume and flow, since it is the habitat that has been shown to be most capable of predicting survival in previous studies [2,68].

Different studies have evaluated the molecular differences between long-term survivor (LTS) and short-term survivor (STS) groups of glioblastoma patients in relation to tumor angiogenesis, because of their relevance to improve patient prognosis and to decide on the correct therapeutic target[25]. Burgenske *et al.*[155] analyzed the gene expression profile of glioblastoma *IDH-wildtype* patients and split their patients into LTSs and STSs to elucidate which variables were associated with differences in survival. Their results showed apparent similarities between the two groups.

Despite those results, it was observed that LTSs presented a higher proportion of methylated *MGMT*, and for that group an enrichment of the genes of sphingomyelin metabolism was detected, which has been related to a decrease in tumor growth and angiogenesis [155]. In addition, Michaelsen *et al.* analyzed the molecular profile of LTS and STS to identify cluster of differentiation 34 (CD34) mRNA level (regulator of glioblastoma angiogenesis by promoting new blood vessel networks[156]) as prognostic for glioblastoma patient survival[157]. Moreover, clinical factors, such as

initial performance score[158], tumor size and location[159] and completeness of tumor resection[160] may also determine the likelihood of a patient becoming an LTS.

The evident efficacy of the rCBV has already been proven when dealing with clinical challenges such as diagnosis, non-invasive characterization of molecular profile and prediction of prognosis, amongst others[27], but the influence of this marker for LTSs and STSs has not yet been fully assessed. To elucidate this, we analyze in our work the prognostic and stratification capabilities of $rCBV_{mean}$ at the HAT habitat for the LTS and STS groups, independently. In the current study, we evaluate whether the beneficial effect of having moderate and functional vascularity is constant with time and if it is presented in both LTS and STS groups.

6.2. Materials and Methods

6.2.1. Patient information

This is a sub-study of the approved multicentre retrospective clinical trial NCT03439332. For this study, 99 glioblastoma *IDH*-wildtype patients from five clinical centres were included. Participating centres were Hospital Universitario de La Ribera, Alzira, Spain; Hospital Clinic, Barcelona, Spain; Hospital Universitario Vall d'Hebron, Barcelona, Spain; Azienda Ospedaliero-Universitaria di Parma, Parma, Italy and Oslo University Hospital, Oslo, Norway.

A material transfer agreement was approved by all the participating centres and an acceptance report was issued by the ethical committee of each centre. The managing institution (Universitat Politècnica de València, Valencia, Spain) review board also approved this study.

The criteria to include patients in this study were: (a) adult patients (age > 18 years) with histopathological confirmation of glioblastoma *IDH*-wildtype[10] diagnosed between 1 January 2012 and 1 January 2018; (b) access to the complete preoperative MRI studies, including pre- and post-gadolinium T1-weighted, T2-weighted, FLAIR and DSC T2*-weighted perfusion sequences; and (c) patients with a minimum survival of 30 days (since shorter survival is generally associated with incidents during the surgery or previous severe pathologies, and could generate misleading results).

The study cohort was divided in two groups as previously reported[161,162]: LTSs were defined as those patients with an OS equal to or greater than 400 days and STSs were defined as those patients with an OS less than 400 days. Because this value is close to the median survival of the study population (384 days), it allows the number of patients in the two groups to be balanced. Patients still alive at readout were

considered removed observations. The date of removal was the last date of contact with the patient or, if not available, the date of the last MRI examination.

6.2.2. MRI

Standard of care MR examinations were obtained for each patient before surgery, including pre- and post-gadolinium-based contrast-agent enhanced T1-weighted MRI, as well as T2-weighted, FLAIR T2-weighted and DSC T2* perfusion MRI. A detailed description of the acquisition parameters used at each institution is shown in Table 6.1.

Table 6.1. Summary of the magnetic resonance imaging (MRI) acquisition parameters per centre.

	MFS		**TR (ms)**	**TE (ms)**	**Matrix (mm)**	**Slice thickness (mm)**	**FOV (cm^2)**	**Number of Dynamics**
H Ribera[a]	1.5T	T1	25	4.6	268x268	0.9	24x24	-
		T2	2000	120	320x199	5.0	23x18.3	-
		FLAIR	1100	140	256x164	6.0	23x18.3	-
		DSC	1650	40	116x116	2.2	24x24	80
C Barcelona[b]	3.0T	T1	12	4.68	256x256	1.0	24x24	-
		T2	3000	80	256x256	5.0	24x24	-
		FLAIR	9000	164	256x256	5.0	24x24	-
		DSC	1550	32	128x128	5.0	24x24	50
H Vall d'Hebron[c]	3.0T	T1	253	2.64	320x180	4.0	22x16.5	-
		T2	6100	91	512x326	4.0	22x17.5	-
		FLAIR	9000	68	320x288	4.0	22x19.8	-
		DSC	1450	45	128x128	5.0	23x23	60
AO Parma[d]	3.0T	T1	8.18	8.18	256x256	1.0	24x24	-
		T2	6500	65.90	160x160	4.0	24x24	-
		FLAIR	12000	96.72	384x224	4.0	24x24	-
		DSC	1500	30	128x128	4.0	24x24	60
Oslo UH[e]	3.0T	T1	5.2	2.3	512x512	1.0	25.6x25.6	-
		T2	3800	84	896x896	3.0	22.0x22.0	-
		FLAIR	4800	325	512x512	0.9	25.6x25.6	-
		DSC	1500	25/105	128x128	5.0	25.6x25.6	100

Hospital de la Ribera[a]; Clinic de Barcelona[b]; Hospital Vall d'Hebron[c;] Azienda Ospedaliero-Universitaria di Parma[d]; Oslo University Hospital[e]. MFS: Magnetic Field Strength; TR: Repetition Time; TE: Echo Time; FOV: Field of View; T1: pre gadolinium T1-weighted; T1c: post gadolinium T1-weighted; T2: T2-weighted, FLAIR: FLuid-Attenuated Inversion Recovery; DSC: Dynamic Susceptibility Contrast

6.2.3. Processing of MRI and vascular markers

We used the HTS method, freely accessible at the ONCOhabitats platform at www.oncohabitats.upv.es, to process MR images and calculate the rCBV. The HTS is an automated unsupervised method to describe the heterogeneity of the enhancing tumor and edema tissues by delineating four vascular habitats.

a. Preprocessing, incorporating correction of usual MRI artefacts such as magnetic field in homogeneities and noise, multimodal registration, brain extraction, or motion correction.

b. Glioblastoma segmentation, which implements a state-of-the-art deep learning 3D CNN that differentiates the enhancing tumor, the edema, and the necrotic tissue. It is based on the DCA-SVFMM, which is a clustering algorithm that combines Gaussian mixture modelling with continuous Markov random fields to make use of the self similarity and local redundancy of the images. The methodology includes the unenhanced and GBMCA-enhanced T1-weighted sequences, the T2-weighted sequence, and the fluid-attenuated inversion-recovery T2-weighted sequence combined with atlas-based prior knowledge of healthy tissues to delineate the segmentation.

c. DSC perfusion quantification, which calculates the haemodynamic maps derived from the DSC perfusion sequence (rCBV, relative cerebral blood flow (rCBF), MTT, and K2 permeability. All perfusion maps are normalized against contralateral unaffected white matter volume to achieve consistency and comparability across patients and cohorts. The normalization is performed automatically by a CNN trained with about 100 cases, which detects the contralateral unaffected white matter region with about 90% accuracy. To ensure a correct perfusion quantification and to avoid under- and over-estimation of perfusion marker, DSC perfusion quantification includes correction for contrast agent leakage effects. The HTS method implements the Boxerman leakage-correction method for T1- and T2-leakage effects, as well as gamma-variate fitting to remove the extravasation phase and second pass of the contrast bolus.

d. HTS. In this phase, an automated unsupervised segmentation algorithm performs the detection of the four vascular habitats each with its specific haemodynamic behaviour: the HAT habitat, the LAT habitat, the IPE habitat, and the VPE habitat. HTS habitats were delineated using a DCA-SVFMM structured clustering of rCBV and rCBF maps. The clustering includes two stages: (I) a two-class clustering of the whole enhancing tumor and edema regions and (II) a two-class clustering performed by using only the rCBV and rCBF data within the regions obtained in the first stage. To ensure the reproducibility of the HTS, both stages were initialized with a deterministic seed method.

A more detailed definition of the methodology is included in [68]. The robustness of the HTS method, used to process the MR images and to calculate the rCBV from different hospitals and with different acquisition parameters, was demonstrated in the previous multicentre study[2]. The results obtained in this study, which included 184 patients from seven different international centres, demonstrated that the HTS standardization and quantification tools are robust to changes in MRI acquisition protocols, scanners, and MR techniques. In this sense, we employ this technology to ensure a robust analysis of the MRI, mitigating any potential bias introduced by the different acquisition protocols.

The vascular biomarker used in our study was the $rCBV_{mean}$[70,163,164] calculated in the HAT habitat, which was shown to be a relevant prognostic marker in previous studies[2,68].

6.2.4. Statistical analyses

We described the main demographic, clinical, and molecular variables for the LTS and STS groups and for the entire cohort. Possible differences in the distributions of these variables for the LTS and STS groups were assessed using Mann-Whitney and Fisher exact tests in MATLAB R2017b (MathWorks, Natick, MA). The significance level used in all the statistical analyzes was 0.05.

To analyze the time-dependent influence of the vascular biomarker ($rCBV_{mean}$ at HAT) on patient survival, we used Aalen's additive regression model included in the library "survival" for R software. This model allows plotting of time-varying effects of covariates on patient survival[165].

To analyze the association between $rCBV_{mean}$ at HAT and patient survival, we used both uniparametric and multiparametric Cox proportional hazard regression analyzes with the entire cohort, and independently with LTS and STS groups. The proportional hazard ratios (HRs) with a 95% confidence interval (CI), as well as the associated p-values, are reported. The multiparametric analysis includes *MGMT* methylation status as a covariable, as this factor could influence patient survival and affect the results of the uniparametric test.

In addition, the stratification capability of the $rCBV_{mean}$ at HAT was evaluated with the Kaplan-Meier test. The analyzes were performed with the entire cohort, as well as independently with the LTS and STS groups. For all tests, we evaluated the capability of the $rCBV_{mean}$ at HAT to stratify the population into moderate vascular and high vascular groups, and we analyzed if these two vascular groups presented different survival rates.

We define moderate and high vascular as the two groups of patients generated by dividing a population using the optimum cutoff threshold according to the vascular marker. We calculated the optimum vascular cutoff threshold using the $rCBV_{mean}$ at HAT and determined by the C-index method previously used[2] which consists in analyzing the effectiveness of each possible threshold by maximizing the C-index or area under the curve (AUC). The moderate vascular group included patients with an $rCBV_{mean}$ lower than the calculated cutoff, and the high vascular group included patients with an $rCBV_{mean}$ higher than the cutoff.

The log-rank test was used to determine any statistical difference between the estimated survival functions of the vascular groups. The optimal threshold, the number of patients included in each vascular group, the median OS rates of each group, the estimated C-index, and the p-value are reported.

6.3. Results

6.3.1. Description of the entire cohort, and the LTS and STS groups

A total of 99 glioblastoma *IDH*-wildtype patients complied with the inclusion criteria and formed the entire cohort of the study. This population was divided into (I) the LTS group, which includes 45 patients (seven removed), and II) the STS group, which includes 54 patients (eight removed). The information related to the entire cohort and the LTS and STS groups is summarized in Figure 6.1.

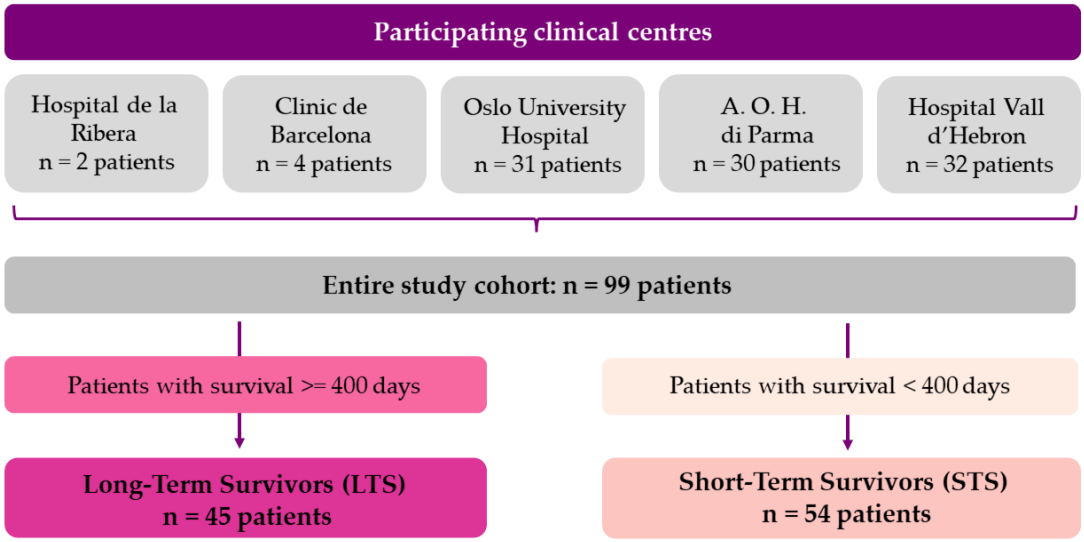

Figure 6.1. Distribution of patients that conforms the entire study cohort and both long- and short-term survivors.

Table 6.2 summarizes the most relevant demographic, clinical, and molecular features of the entire cohort and patients included in the LTS and STS groups.

Table 6.2. Demographic, clinical and molecular features of the patients included in the study (whole cohort) and for each group (long- and short-term survivors). P-values resulting from the Mann Whitney and Fisher's exact tests are also included. N: number of patients; RT-CT: radiochemotherapy.

	Long-Term Survivors	**Short-Term Survivors**	**Entire cohort**	**p-values (Mann Whitney test)**
N (%)	45 (45.5)	54 (54.5)	99 (100)	-
% Females	31.1%	35.2%	33.3%	0.6732
Mean Age at Diagnosis	59	61	60	0.5043
Type of resection (N)				
- Total	22	18	40	0.1191
- Partial	17	25	42	0.3978
- Biopsy	6	10	16	0.4909
- Unknown	0	1	1	-
RT-CT (N)				
-Complete	24	23	47	0.2574
-Incomplete	2	6	8	
-Unknown	19	25	44	-
***MGMT* methylation status (N)**				
-Methylated	14	11	25	
-Unmethylated	14	19	33	0.4267
-Unknown	17	24	41	-

No significant differences ($p > 0.05$) in gender, age, resection status, chemoradiation, *MGMT* methylation status, or $rCBV_{mean}$ at HAT were observed between the LTS and STS groups (Mann-Whitney and Fisher exact tests).

6.3.2. Differences between LTSs and STSs and the effect of rCBV on patient survival

The studied variables of the LTS and STS groups displayed similar distributions (Table 6.2), as did the mean rCBVs of the two groups (Table 3). However, we found a different effect of $rCBV_{mean}$ at HAT on the patients' OS in the LTS group compared with the STS group. A significant negative association between the $rCBV_{mean}$ level

and OS was found for the LTS group (p = 0.0140) but not for the STS group (p = 0.3543). Results of the uniparametric Cox analysis are shown in Table 6.3. The highest HR (1.19) found for the LTS group implies an increase of one unit in the $rCBV_{mean}$ at HAT, which will be equivalent to a 19% higher risk of death. This result suggests that, for the LTS group, patients with lower $rCBV_{mean}$ in the HAT habitat had significantly longer survival. For the entire cohort, the beneficial effect of having moderate vascularity in the HAT habitat was close to statistical significance at p = 0.06.

Table 6.3. Uniparametric Cox analysis of the association between the vascular marker ($rCBV_{mean}$ at HAT) and the survival for the entire cohort and for the long- and short-term survivor groups.

Variables	**Long-term survivors (n = 45pts)**		**Short-term survivors (n = 54pts)**		**Entire cohort (n = 99pts)**	
Mean HAT rCBV ± standard deviation	7.49 ± 2.39		7.48 ± 2.41		7.45 ± 2.39	
	HR [95% CI]	p-value	HR [95% CI]	p-value	HR [95% CI]	p-value
HAT $rCBV_{mean}$	1.19 [1.04, 1.38]	**0.0140***	1.06 [0.94, 1.20]	0.3543	1.09 [1.00, 1.20]	0.0601

Table 6.4 depicts the results of the multiparametric Cox analyzes, including the *MGMT* methylation status as a covariable. We did not have the *MGMT* methylation status information of 41 patients, so for those cases we used a mean imputation method. Collectively, combining *MGMT* methylation status and $rCBV_{mean}$ at HAT was significantly associated with OS for the entire cohort. Patients with lower $rCBV_{mean}$ at HAT and methylated *MGMT* had longer OS. Again, the influence of the combination of these two variables on OS is higher for the LTS group compared with the entire population (HR: 1.22 versus 1.10 for $rCBV_{mean}$; 2.68 versus 1.80 for *MGMT* methylation status). Additionally, the statistical power of the results for the LTSs was the highest (with the lowest p-values). No significant result was found for the STS group when analyzing the association between the HAT $rCBV_{mean}$ and the *MGMT* methylation status with the OS.

Table 6.4. Multiparametric Cox analysis of the association between the vascular marker ($rCBV_{mean}$ at HAT) and the *MGMT* methylation status with survival for the entire cohort, the long-term group and short-term survivor group.

Variables	**Long-term survivors**	**Short-term survivors**	**Entire cohort**

	(N = 45 patients)		(N = 54 patients)		(N = 99 patients)	
	HR [95% CI]	p-value	HR [95% CI]	p-value	HR [95% CI]	p-value
HAT $rCBV_{mean}$	1.22 [1.05, 1.42]	0.0085*	1.05 [0.92, 1.19]	0.4777	1.10 [1.00, 1.21]	0.0468*
MGMT methylation status	2.68 [1.15, 6.26]	0.0230*	0.45 [0.18, 1.13]	0.0898	1.80 [1.01, 3.22]	0.0471*

The effect of the vascularity on OS is also shown using Aalen's additive regression model. Figure 6.2 shows the marked incremental effect of both *MGMT* methylation status and $rCBV_{mean}$ at HAT on OS from 400 days after diagnosis. Again, the influence of the $rCBV_{mean}$ at HAT on OS is revealed for the LTS group. In addition, the patient baseline conditions (represented by the intercept) start to be relevant from 400 days after diagnosis, and relate to a beneficial effect on survival.

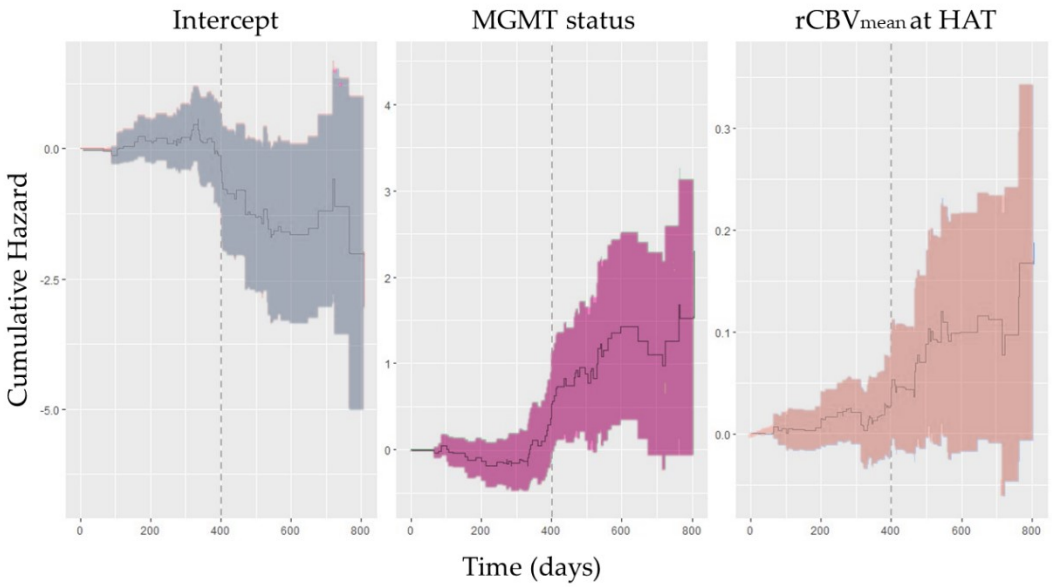

Figure 6.2. Curves of Aalen's Additive Regression Model that illustrate the incremental effect of the variables *MGMT* methylation status (in green), the $rCBV_{mean}$ (in blue) and the intercept (in grey) at over time.

The results of the Kaplan-Meier analysis are summarized in Table 6.5, including estimated optimal cutoff thresholds (used to define the different groups—moderate and high vascular), number of patients per vascular group, estimated C-index, median OS calculated per each group, and log-rank test results (p-values).

Table 6.5. Kaplan Meier and Log-rank test results for the vascular marker ($rCBV_{mean}$ at HAT) and the overall survival for the entire cohort and the long- and short-term survivor groups (LTS and STS, respectively).

Group	rCBV threshold	Patients per group	AUC (c-index)	Median OS per group	Δ OS (days)	P-value
$rCBV_{mean}$ HAT		[Moderate, High]		[Moderate, High]		
Entire cohort	6.30	[35, 64]	0.605	[13.8, 12.1]	1.7	**0.0275***
LTS	8.97	[33, 12]	**0.690**	**[18.7, 15.8]**	**87**	**0.0343***
STS	6.32	[16, 38]	0.415	[10.6, 9.6]	30	0.5149

We found a significant stratification capacity of the $rCBV_{mean}$ when analyzing the entire cohort (n = 99 patients) and when analyzing the LTS group (n = 45 patients). However, the stratification in vascular groups related to survival was more robust when we analyzed the LTS group, which yielded the highest C-index or AUC (0.690). Additionally, for the LTS group, we found the greatest difference in OS, 2.9 months, between the moderate vascular group (patients with an $rCBV_{mean}$ at HAT lower than 8.97) and the high vascular group (patients with an $rCBV_{mean}$ at HAT higher than 8.97). For the entire cohort, the test yielded a difference of only 1.7 months between these vascular groups. For the STS group, the OS was similar for the moderate and the high vascular groups and the log rank test did not yield significant results.

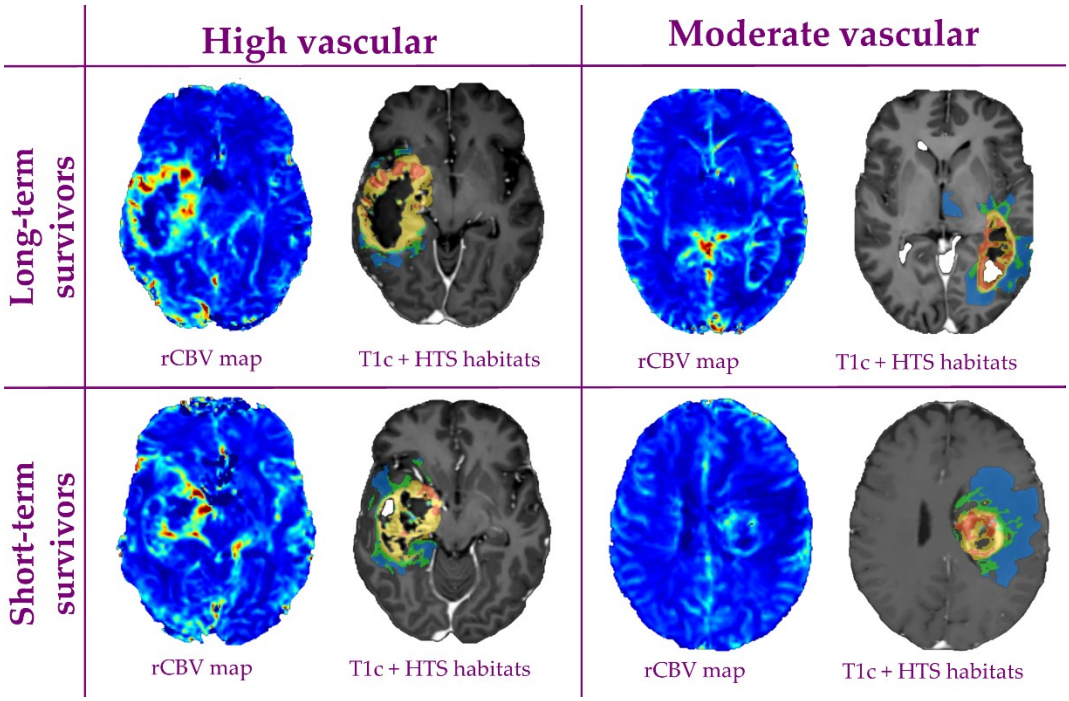

Figure 6.3. Example of rCBV maps and HTS habitats for each group.

Figure 6.3 shows an example of rCBV map and HTS habitats for a patient of each group (LTS—low vascular; LTS—high vascular; STS—low vascular, STS—high vascular). These differences between the LTS and the STS groups in the efficacy of the vascular marker, when using the optimal cutoff threshold calculated for the entire cohort (6.30), are also illustrated with the Kaplan-Meier curves for both groups (LTS and STS) in Figure 6.4. For the STS group, the survival curves of the high vascular and moderate vascular groups are overlapping, indicating no apparent differences in survival time for patients included in the STS group, independently of their $rCBV_{mean}$ at HAT. However, for the LTS group, the vascular marker is capable of stratifying survival according to the level of $rCBV_{mean}$ in the HAT habitat.

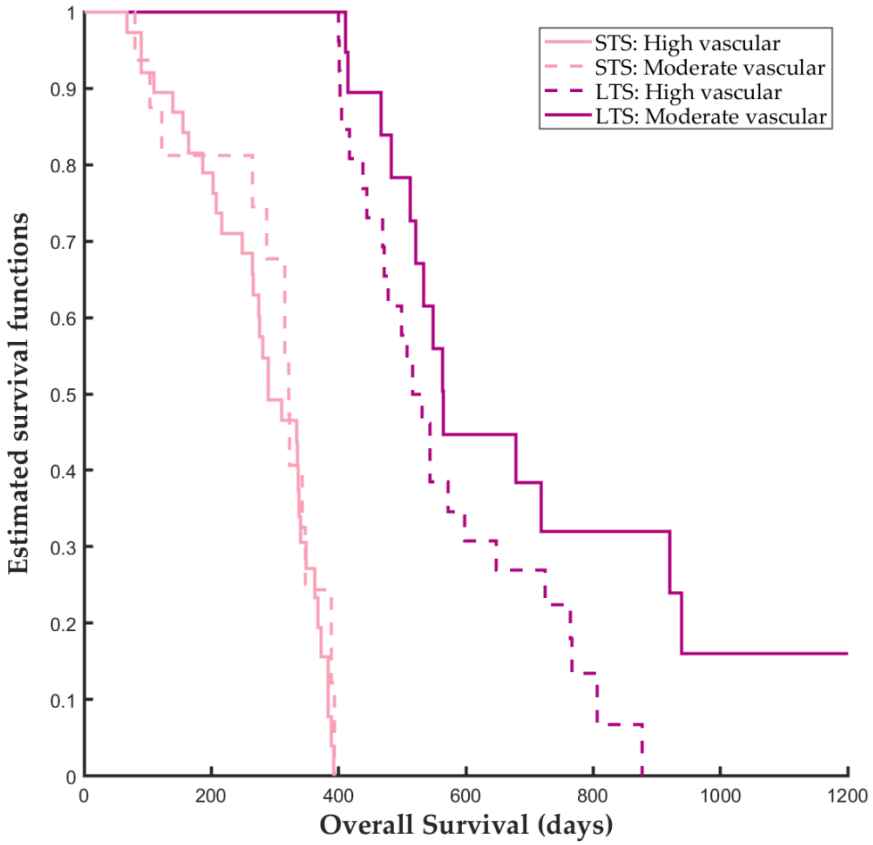

Figure 6.4. Kaplan Meier curves for the STS group (dotted purple lines) and for the LTS group (solid green lines).

6.4. Discussion

This study of the differential effect of vascularity in LTSs and STSs with glioblastoma *IDH*-wildtype is based on the data from multicentre clinical trial NCT03439332[2] and included 99 patients with glioblastoma *IDH*-wildtype. We found that the beneficial effect of having a moderate $rCBV_{mean}$ can only be observed in patients surviving more than 400 days, ie those included in the LTS group. In addition, we also found significant stratification capacity of $rCBV_{mean}$ for the entire cohort, although the difference in OS between vascular groups was higher for the LTS (1.7 versus 2.9 months). We did not find an association between the $rCBV_{mean}$ biomarker and patient OS for the STS group. These results are compatible with previous studies in which the effect of vascularity was evaluated[2,68]. In our study we went a step further to analyze whether the beneficial effect of having moderate

vascularity in the HAT habitat is constant over time and if it is present in both long- and short-survival groups.

A possible explanation for the association of vascularity with survival in LTSs may rely on how the influence of vascularity increases significatively after approximately 400 days from diagnosis (Figure 6.2). This implies that, from that time, LTS patients with a moderate vascular signature will have longer survival than those patients with a high vascular signature. By contrast, in the STS group there are unknown factors that lead to poor survival, and tumor vascularity does not represent a variable that influences survival.

For the LTSs, vascularity marks the tumor behaviour, thus the $rCBV_{mean}$ image marker can be used as prognostic biomarker at an advanced stage, allowing a more accurate decision making from this time. In fact, we found a much higher HR than the one reported in our previous study, which included both glioblastoma *IDH1*/2-wildtype and astrocytoma *IDH*-mutant grade 4 (HR: 1.19 versus 1.05, respectively)[2]. This may suggest that the prognostic value of this vascular biomarker is more accurate and clinically relevant for the *IDH*-wildtype LTS group, rather than the entire population of glioblastoma patients.

Moreover, the different influence of tissue vascularity on survival between the LTS and STS groups may be also influenced by several clinical factors[166,167]. Comorbid conditions, such as cardiovascular or pulmonary diseases[166], or early deaths caused by treatment complications, could hide the effect of vascularity on OS in the STS group, whereas for the LTS group the significant effect of the vascularity becomes apparent, revealing a strong association with patient OS. Comparing the distributions of main demographics (age and gender) and clinical characteristics (type of resection, completeness of standard treatment), we did not find significant differences between the groups.

Moreover, it is well known that patients with the methylated *MGMT* promoter benefit most from treatment with temozolomide[168], an integral component of the standard treatment for glioblastoma patients[19]. We analyzed the distributions of patients with methylated and non-methylated *MGMT* in each group, as well as the completeness of the Stupp treatment. No significant differences were observed in this regard, suggesting that these variables do not impact the observed effect of vascularity on survival.

Furthermore, the results of the combined analysis of the rCBV and the *MGMT* methylation status are consistent with the uniparametric analyzes, so the *MGMT* methylation status does not seem to be affecting the differential influence of vascularity between LTSs and STSs. In addition, we have found that the *MGMT* methylation status, as for rCBV, seems to be relevant not at the beginning of the

disease, but from 300-350 days onwards. Hence, it is consistent not to observe an influence of the state of methylation from the initiation, since the benefit produced by *MGMT* methylation is associated with treatment with temozolomide. However, the combination of these two factors (rCBV and *MGMT* methylation) improves their association with patient survival both for LTSs and for the entire cohort, and p-values were found to be lower than in the uniparametric analysis.

Other molecular factors, however, might also influence our results. The influence of telomerase reverse transcriptase (*TERT*) promoter mutation on survival of glioblastoma patients has been suggested by several authors. More than 90% of GBM are *IDH-wildtype*; amongst them, about 80% have mutations on the *TERT* promoter, which confers a worse prognosis. In two studies[169,170], the negative impact of *TERT* promoter mutations on survival of patients with glioblastoma *IDH*-wildtype becomes visible only after approximately 400 days of evolution; before this point, survival curves overlapped. Thus, the distribution of TERT mutations in our patient series could help understand the different influence of vascular biomarkers on the LTS and STS groups. Of note, the molecular profiles of *IDH*-wildtype and TERT mutation have been associated with the classical and mesenchymal subtypes[169,171], of which the latter is associated with active angiogenesis[171,172].

Our study has some limitations. First, more detailed clinical information on completion of treatment and the second line treatment type, comorbidities and treatment complications would have helped to explain our results and would have allowed a more thorough discussion about this aspect. Moreover, *MGMT* promoter methylation status was unknown in 40% of patients, and other molecular features, such as TERT promoter mutation status, were not recorded. The lack of extensive clinical and molecular information is due to the retrospective nature of the study. Thus, for future studies, we aim to analyze the association between the molecular profile of tumors and patients' clinical factors with the imaging markers and the effect of vascularity on survival. The combined information may provide a better understanding of the influence of vascular biomarkers on the evolution of glioblastoma. Furthermore, despite having a considerably large total cohort (99 patients), the high rCBV-LTS group only includes 12 patients. Finally, the estimated thresholds calculated to define the different vascular groups are statistical values and not parameters that can be used in the clinic yet.

Related to further work, image-based vascular biomarkers have proven their ability to guide anti-angiogenic therapy for glioblastoma [173], but this therapy only benefits specific populations of glioma patients [173]. Lui *et al.*[149] used MRI features to define a subgroup of glioblastoma patients with higher angiogenic activity and better response to the antiangiogenic treatment. Based on the main results of our study, it

would be worth studying whether only the group of LTSs with high values of $rCBV_{mean}$ at HAT would be the best responders to antiangiogenic treatment.

6.5. Conclusions

In conclusion, in our study we found that a moderate $rCBV_{mean}$ level in the HAT habitat is associated with prolonged survival in patients with glioblastoma, particularly in a cohort of 45 glioblastoma *IDH*-wildtype patients that survive more than 400 days. For the long-surviving group, the vascular $rCBV_{mean}$ image marker can differentiate patients with moderate vascularity and longer OS from patients with high vascularity and shorter OS. However, this association between vascularity and patient survival was not found for patients who did not survive more than 400 days. Therefore, we propose the use of $rCBV_{mean}$ in HAT as a clinically relevant prognostic marker for LTSs with glioblastoma *IDH*-wildtype. This biomarker could be used as a potential target for randomized clinical trials that focused on this group of patients.

In addition, this study was the first study proposing that influence of *MGMT* methylation on survival is also dependent on treatment stage. This factor was significantly associated with OS only for long-term survivors. A more detailed study analyzing the combined association of *MGMT* methylation on survival and response to TMZ is included in chapter 7 of this thesis.

PART III

Treatment Responses Assessment

Chapter 7

Towards personalized Temozolomide treatment considering tumor vascularity and *MGMT* methylation status

The key role of tumor vascularity and its close relationship with survival of astrocytoma patients have been analyzed and demonstrated in this thesis (part I and II). It is well known that a higher vascularity allows a greater supply of oxygen and nutrients to the tumor cells and, therefore, a faster tumor progression.
In this chapter we evaluate the implication of tumor vascularity on the benefit of chemotherapy treatment. For this purpose, the combination of vascular biomarkers with the methylation status of the *MGMT* gene, which is closely associated with the response to temozolomide (TMZ) chemotherapy, has been analyzed. In chapter 6, it was demonstrated that association between *MGMT* methylation and overall survival varies through patient treatment, being significantly relevant after 400 days from diagnosis. This study analyzing the combined effect of *MGMT* methylation and tumor vascularity was defined considering that preliminary results.

Currently the number of standard temozolomide cycles recommended in the guidelines for patients with astrocytoma grade 4 is six. However, number of TMZ cycles has been matter of debate and the final decision to continue adjuvant treatment is the decision of the oncologist based on their experience and local circumstances. This results in subjective treatment selection based on observational factors.

The results of the studies included in this chapter open the possibility of designing a more personalized treatment approach, allowing an optimal selection of the number of TMZ cycles for each patient. On the other hand, those who would not benefit from a greater number of TMZ cycles would improve their quality of life by avoiding adverse effects and toxicity, opening possibilities to alternative treatments.

The contents of this chapter were published in the journal publications P1 (Álvarez-Torres, Cancers, 2021a), P7(Fuster-Garcia, Eur Rad, 2021) and presented in P5 (ISMRM 2022) – thesis contribution C4.

7.1. Introduction

Glioblastoma patients remain a devastating prognosis of 12–15 months from diagnosis[10,135] despite an intrusive treatment including tumor resection, radiotherapy, and concomitant and maintenance chemotherapy with temozolomide[19]. This standard treatment, proposed by Stupp in 2005[19], was demonstrated to be the most effective in terms of overall survival but, due to strong interpatient heterogeneity, it is not equally efficient for all patients[26].

Several studies have evaluated the efficacy of this treatment depending on several conditions as extend of tumor resection, age[174], the methylation of the *MGMT* promoter gene[175], dose of temozolomide[176–182], the addition of new agents[183–185], or the device tumor treating fields [186–192], that in fact is the only modification that has proven to increase survival.

The optimal number of cycles of TMZ in the maintenance phase has also been a matter of debate[193,194]. This is due to the heterogeneity of uses or interpretation of the term 'maintenance' or 'adjuvant therapy' in a disease such as glioblastoma where surgery seldom achieves a complete resection. The number of cycles administered is clearly variable in the clinical setting or even in the different trials[195]. The only prospective trial assessing the role of extending temozolomide further than six cycles is a randomized phase II trial that did not demonstrate differences in progression-free survival or overall survival[176]. The European Association of Neuro-oncology guidelines recommend six cycles of maintenance therapy[196]. The same treatment for all patients with glioblastoma has been demonstrated in-effective. The availability of robust markers to characterize interpatient heterogeneity, and, therefore, to discriminate different subgroups could lead to a more personalized medicine approach. In this line, imaging markers derived from MRI and combined with the capabilities of artificial intelligence can provide individually specific variations of the Stupp treatment. This would allow better prognosis and facilitate the clinical decision-making for patient treatment in a non-invasive way and without additional cost[197–201].

Currently, glioma classification, decision making, and management of glioblastoma are still based on molecular biomarkers[10,202–205]. One of the most relevant biomarkers, related with the Stupp treatment efficacy, is *MGMT* methylation status[206], present in approximately 50% of glioblastomas[207]. *MGMT* removes alkyl groups from guanine in the DNA, potentially counteracting the therapeutic efficacy of alkylating chemotherapeutics, such as temozolomide, in tumor cells[168,205]. Methylation of the promoter region of *MGMT* might lead to transcriptional repression and a decreased *MGMT* protein expression[168,205]. It is associated with an improved response to

temozolomide chemotherapy and longer overall survival of glioblastoma patients [10,202–205].

A recent study with a multicenter cohort of 96 glioblastoma patients[5] concluded that *MGMT* methylation may benefit overall survival only in patients with moderately vascularized glioblastomas, defined by MRI perfusion-based marker, such as rCBV. This study opened the possibility of investigating vascularity as a determinant factor, in combination with methylation status, on the benefit of temozolomide cycles.

In this study, we aimed to evaluate the combined effect of *MGMT* methylation and tumor vascularity on patient survival, assessing the performance of the proposed rCBV threshold for patient stratification. We also assessed the implications of the association between *MGMT* methylation and vascularity on the benefit of extending temozolomide treatment in different groups of glioblastoma patients.

7.2. Material and Methods

7.2.1. Patient information

For this study, 123 glioblastoma patients were included from the GLIOCAT database[208], which includes patients from the following six centers from Cataluña, Spain: (I) Instituto Catalán de Oncología (ICO) de Badalona (Barcelona), (II) Hospital del Mar (Barcelona), (III) Hospital Clínic (Barcelona), (IV) ICO Hospitalet (Barcelona), (V) ICO Girona (Girona), and (VI) Hospital Sant Pau (Barcelona). A Material Transfer Agreement was approved by all the participating centers and an acceptance report was issued by the Ethical Committee of each center.

The inclusion criteria were: (a) adult patients (age >18 years) with histopathological confirmation of glioblastoma; diagnosed between June 2007 and May 2015, (b) with access to the preoperative MRI studies, including: pre- and post-gadolinium T1-weighted, T2-weighted, Fluid-Attenuated Inversion Recovery (FLAIR), and Dynamic Susceptibility Contrast (DSC) T2*-weighted perfusion sequences; (c) with *MGMT* methylation status information, (d) with a minimum survival of 30 days and, (e) with tumor resection.

Patients still alive at readout were considered censored observations. The date of censorship was the last date of contact with the patient or, if not available, the date of the last MRI exam.

The patient cohort included in this study is totally independent from that which was analyzed in the previous study[5].

7.2.2. MRI

Standard-of-care MR examinations were obtained for each patient before surgery, including pre- and post-gadolinium-based contrast agent enhanced T1-weighted MRI, as well as T2-weighted, FLAIR T2- weighted, and DSC T2* perfusion MRI.

MRI Processing and Vascular Marker Calculation

To process the MRIs and calculate the imaging vascular markers, we used the Hemodynamic Tissue Signature (HTS) method[67,68], freely accessible at the ONCO-habitats platform at www.oncohabitats.upv.es, accessed on 04/06/2020. The HTS is an automated unsupervised method developed to describe the heterogeneity of the enhancing tumor and edema tissues at morphological and vascular levels, and to calculate robust biomarkers with prognostic and patient stratification capabilities. This method includes the following four phases (Figure 7.1):

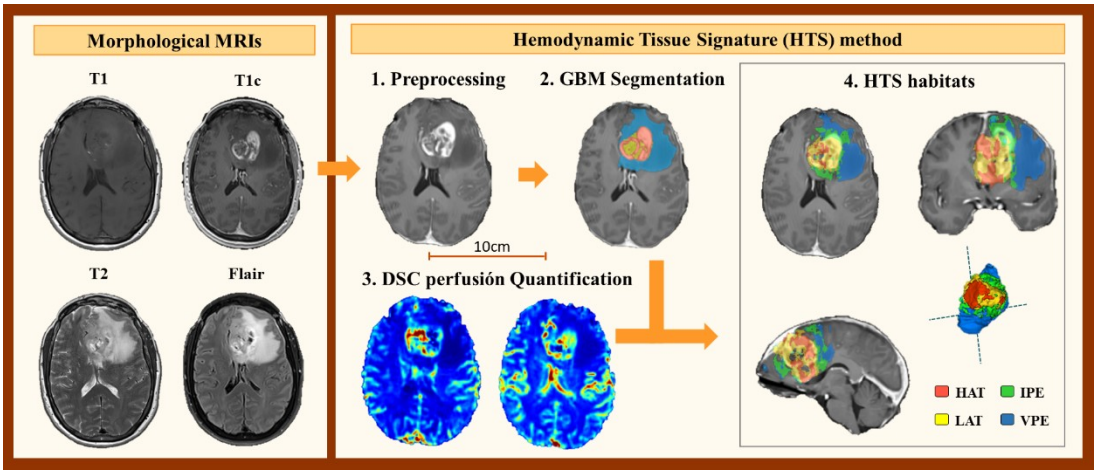

Figure 7.1. Hemodynamic Tissue Signature (HTS) method, including the four phases: 1. Preprocessing of morphological MRIs (T1, T1c, T2, and Flair); 2. Glioblastoma tissue segmentation; 3. DSC perfusion quantification; and 4. HTS vascular habitats. HAT: High Angiogenic Tumor, LAT: Low Angiogenic Tumor, IPE: Infiltrated Peripheral Edema, and VPE: Vasogenic Peripheral Edema.

1. MRI Pre-processing. This phase includes voxel isotropic resampling of all MR im-ages, correction of the magnetic field in homogeneities and noise, rigid intra-patient MRI registration, and skull-stripping.

2. Glioblastoma tissue segmentation. It is performed using an unsupervised segmentation method, which implements a state-of-the-art deep-learning 3D CNN, which takes as input the T1c, T2, and Flair MRIs. This method is based on DCA-

SVFMM, which consists of a clustering algorithm that combines Gaussian mixture modeling with continuous Markov Random Fields to take advantage of the self-similarity and local redundancy of the images.

3. DSC perfusion quantification. In this phase, biomarkers such as the relative rCBV maps, as well as rCBF or MTT, are calculated for each patient. T1-weighted leakage effects are automatically corrected using the Boxerman method[114], while gamma-variate curve fitting is employed to correct for T2 extravasation phase. rCBV maps are calculated by numerical integration of the area under the gamma-variate curve. The AIF is automatically quantified with a divide and conquer algorithm.

4. Hemodynamic Tissue Signature and Vascular Habitats. The HTS provides an automated unsupervised method to describe the heterogeneity of the enhancing tumor and edema tissues, in terms of the angiogenic process located at these regions. We consider four sub-compartments for the glioblastoma, two within the active tumor: HAT and LAT habitats, and two within the edema: the IPE and VPE. These four habitats are obtained by the unsupervised analysis of perfusion patterns, which is carried out through the Directional Class Adaptative Spatially Varying Finite Mixture Model (DCA-SVFMM) algorithm. Such algorithm is an extension of the classic FMM specially focused on image data, which incorporates a continuous Markov Random Field on the spatial coefficients of the model to capture the self-similarity and local redundancy of the images. The clustering consists of two stages: (a) a two-class clustering of the whole enhancing tumor and edema ROIs and (b) a two-class clustering performed using only the rCBV and rCBF data within the ROIs obtained in stage a to detect the different vascular behaviors expressed by the glioma.

A more detailed description of the methodology is included in chapter 2, subsection 2.4.3 and in references [67,68]. In addition, the HTS method and the vascular biomarkers were validated in an international multicenter study and results were published in [2].

To validate the combined effect of *MGMT* methylation and vascularity, we used the $rCBV_{max}$ calculated in the HAT habitat, since it is shown to be the most relevant prognostic marker calculated with the HTS method[2,67,68] and it was used in the previous study to define the vascular groups[5].

Moderate- and High-Vascular Groups

The entire cohort was divided in two groups according to the tumor vascularity: the moderate-vascular group and the high-vascular group. To determine these groups, we carried out the analysis independently using three different thresholds (th) of the HAT $rCBV_{max}$:

I) The threshold proposed in the literature[5] (th = 10.7). It was calculated as the median $rCBV_{max}$ of 96 patients included in an international multicenter study.

II) The median $rCBV_{max}$ of the current study cohort (th = 9.1). Calculated from the 123 patients included in the present study.

III) The combined threshold of both cohorts (th = 9.8). It is calculated considering the 219 patients from two independent multicenter studies.

The purpose to evaluate these three different thresholds is to validate the previous results and the threshold proposed in the literature [5] with an independent multi-center cohort; but also to analyze the stratification capability of the HAT $rCBV_{max}$ when using the specific threshold calculated from the current study cohort. Finally, proposing a combined threshold calculated from both independent cohorts with 219 patients will allow most reproducible results.

7.2.3. DNA extraction and assessment of MGMT methylation

DNA was extracted from two 15-µm sections of FFPE tissue using the QIAamp DNA Mini Kit (QIAGEN GmbH, Hilden, Germany), following the manufacturer's protocol. In cases with less than 50% of tumor cells, the tumor tissue was macro-dissected manually. Then 500 ng of extracted DNA was subjected to bisulfite treatment using the EZ DNA Methylation-Gold Kit (Zymo Research Corporation, Irvine, CA, USA). DNA methylation patterns in the CpG island of the *MGMT* gene were determined by methylation-specific PCR (MSP) using primers specific for either methylated or modified non-methylated DNA, as previously described[209].

7.2.4. Statistical Analyses

Dataset description: differences between methylated and unmethylated *MGMT* groups

We described the main demographic, clinical, and molecular variables for the entire cohort and for methylated and unmethylated *MGMT* populations. The analyzed variables for each population were: gender, age at diagnosis, survival times, extent of tumor resection, completeness of concomitant chemotherapy, number of adjuvant temozolomide cycles, *IDH1* mutation status, and $rCBV_{max}$ at HAT habitat. Possible differences in the distributions of these variables for the populations with methylated and unmethylated *MGMT* were assessed using Mann–Whitney U test (for ordinal or con-tinuous variables) or Fisher exact test (for nominal variables) in

MATLAB R2017b (MathWorks, Natick, MA, USA). The significance level used in all the statistical analyses was 0.05.

Association between MGMT Methylation, Tumor Vascularity and Patient Survival

To validate the previous results published in[5], which showed a significant correlation between *MGMT* methylation status with overall survival only for those patients with moderate vascularized tumors, we carried out the Uniparametric Cox proportional hazard regression. These analyses were carried out for the entire cohort, and independently for the methylated and unmethylated *MGMT* groups and using the three studied thresholds. The proportional hazard ratios (HRs) with a 95% confidence interval (CI), as well as the associated p-values are reported.

Survival Differences between Groups According to Tumor Vascularity and MGMT Methylation Status

Kaplan Meier test was carried out to evaluate the different effect on survival of *MGMT* methylation status, depending on tumor vascularity and, the Log rank was used to determine any statistical differences between the estimated survival functions of the different *MGMT* methylation populations, both at moderate- and high-vascular groups. The number of patients included in each group, the median OS rates of each group, the differential OS, and the p-values are reported.

The following results were carried out using the (III) combined threshold (th = 9.8), since authors consider it as the most robust threshold because its calculation was derived from data of 214 patients from two different multicenter datasets and could generate more repeatable results.

Benefit of Adjuvant Temozolomide Cycles in Different Groups of Glioblastoma Patients

To analyze the combined effect of *MGMT* methylation and the number of adjuvant temozolomide cycles on survival, a Multiparametric Cox regression analysis was carried out including *MGMT* methylation status and number of temozolomide cycles for the entire cohort, and independently for the moderate- and high-vascular groups. The number of temozolomide cycles was a continuous variable with a minimum of 0 to a maximum of 12 cycles.

In addition, to study differences in patient survival associated with the number of administered temozolomide cycles, a boxplot was carried out for each group (defined by *MGMT* methylation status and tumor vascularity).

7.3. Results

7.3.1. Study cohort

This study includes data from 123 patients with primary glioblastoma (Table 7A.1).

Table 7.1. Demographic, clinical, and biological characteristics of the entire cohort, and the groups with methylated and unmethylated *MGMT*. p-values derived from Mann–Whitney (MW) test or Fisher exact (FE) test analyzing differences between methylated and unmethylated *MGMT*.

Variables	Entire Cohort	Methylated *MGMT* Population	Unmethylated *MGMT* Population	*p*-Values (MW/FE)
Number of patients	123	67	56	-
Gender				
-% females	41.5	43.3	39.2	0.7150
Age at diagnosis (years)				0.8973
-Mean	60	62	58	
-Range	(32,80)	(33,80)	(32,77)	
Overall Survival (months)				0.1214
-Mean	20.2	22.4	17.6	
-Median	17.1	19.3	15.5	
-Range	(2.7,72.8)	(2.7,71.6)	(2.7,72.8)	
Extent of Resection (#patients)				0.4524
-Complete	45	27	18	
-Partial	78	40	38	
Concomitant chemotherapy (#patients)				0.3788
-Complete	110	58	52	
-Incomplete	13	9	4	
Adjuvant chemotherapy (number of cycles)				0.4435
-Mean	4	5	4	
-Median	5	5	4	
-Range	(0,12)	(0,12)	(0,12)	
IDH1 mutation status				1.0000
-Mutated	2	1	1	
-Wild type	93	51	42	
-Unknown	28	15	13	
HAT $rCBV_{max}$				0.4150
-Mean	9.77	9.49	10.10	
-Median	9.10	9.53	8.87	
-Range	(3.39, 21.80)	(3.39, 16.93)	(3.49, 21.8)	

Any variable was found as statistically different between methylated and un-methylated *MGMT* groups ($p < 0.05$), suggesting that any of these variables affect the results of the rest of survival and stratification analyses.

7.3.2. Lack of benefit of Temozolomide for MGMT methylated patients with high vascular tumors

Uniparametric Cox Regression Analysis

Table 7.2 includes the results of the Uniparametric cox regression analyses for the entire cohort and for the moderate- and high-vascular groups, generated with different proposed cut off thresholds: (I) the threshold proposed in the preliminary study[5], (II) the median HAT $rCBV_{max}$ of the current study cohort, and (III) the threshold calculated with the combination of both cohorts (n = 214 patients).

Table 7.2. Uniparametric Cox regression results for the entire cohort, and for the moderate- and high-vascular groups, using different proposed cut off thresholds: (I) the threshold proposed in the preliminary study [ref], (II) the median $rCBV_{max}$ of the present study cohort, and (III) the combined threshold calculated with data of both populations (n = 214 patients).

Association *MGMT* Methylation–Overall Survival		**#patients**	**HR [95% CI]**	***p*-Value**
Analyzed thresholds	Entire cohort	123	1.58 [1.06, 2.35]	0.0247 *
(I) Th. proposed in[5] = 10.7	Moderate rCBV	80	1.70 [1.04, 2.79]	0.0353 *
	High rCBV	43	1.36 [0.69, 2.67]	0.3734
(II) Th. study cohort = 9.1	Moderate rCBV	61	**2.40** [1.34, 4.31]	0.0032 *
	High rCBV	62	1.04 [0.60, 1.80]	0.9008
(III) Th. combined = 9.8	Moderate rCBV	71	**2.01** [1.19, 3.41]	0.0095 *
	High rCBV	53	1.09 [0.59, 2.00]	0.7894

* Th.: threshold; HR: Hazard Ratio; CI: Confidence Interval.

The Uniparametric Cox results show a significant association between the *MGMT* methylation status and patient overall survival (OS) for the entire cohort of 123 patients. However, when this association is analyzed individually for the moderate- and high-vascular groups, we only found significant results for the group of patients with moderate rCBV, regardless of the threshold used. By contrast, we did not find

a significant association for the group with high rCBV. These results are repeated for all the vascular groups generated with the three analyzed thresholds, although they are more patent when using the specific threshold of the study cohort, yielding higher HR and lower p-value.

Kaplan Meier and Log Rank Test

Kaplan Meier results for the entire cohort and for the moderate- and high-vascular groups are included in Table 7.3.

Table 7.3. Kaplan Meier results for the entire cohort, and for the moderate- and high-vascular groups, generated by the combined cut off threshold (9.8), when comparing the populations with methylated and unmethylated *MGMT*.

Survival rates according to *MGMT* methylation and tumor vascularity	**Number of Patients**			**Kaplan Meier Results**			
Kaplan-Meier Analysis	**Total**	**Meth. *MGMT***	**Unmeth. *MGMT***	**Median OS Meth. *MGMT***	**Median OS Unmeth. *MGMT***	**|OS|**	***p*-value**
Entire cohort	123	67	56	578	462	114	0.0220 *
Moderate rCBV	71	46	34	641	467	174	0.0129 *
High rCBV	53	21	22	454	461	7	0.9119

* Meth. *MGMT*: methylated *MGMT*; Unmeth. *MGMT*: unmethylated *MGMT*; OS: overall survival

The Kaplan Meier results showed significant differences in survival for the entire cohort ($p < 0.05$) depending on the *MGMT* methylation status. However, these differences in survival time were more significant (lower p-value) and more patent (higher difference in survival days) for the moderate-vascular group. For this group, we found significant differences ($p = 0.0129$) in median survival between the populations with methylated *MGMT* and with unmethylated *MGMT* (641 vs. 467 days, respectively), with a difference in OS of 174 days. By contrast, we did not find any difference in survival for the high-vascular group, independently of their *MGMT* methylation status.

This differential effect of *MGMT* methylation depending on tumor vascularity is also illustrated in Figure 7.2, which shows the Kaplan Meier survival curves for each vascular group and for each *MGMT* population. The Kaplan Meier curves using the

other two proposed thresholds are included in Figures S7.1.A and S7.1.B of the Supporting Information.

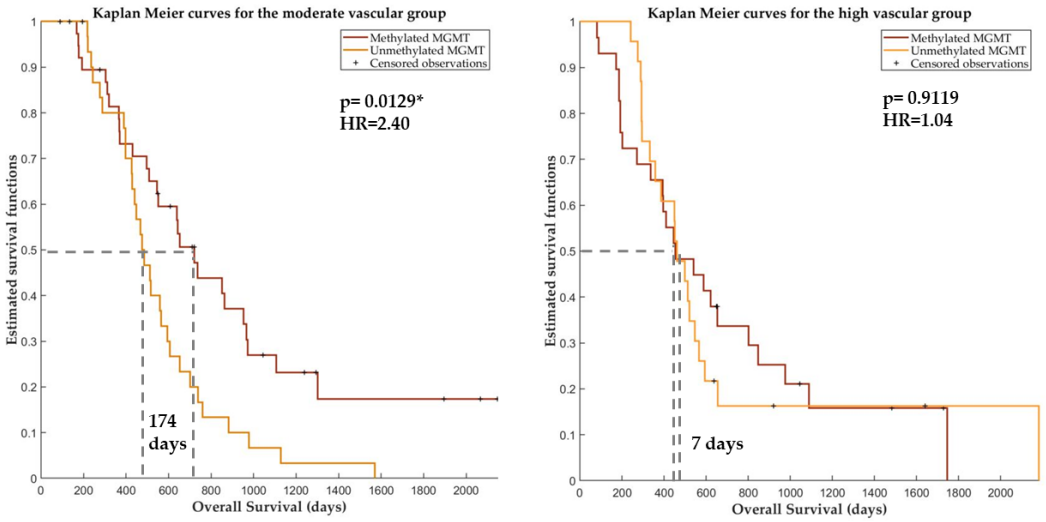

Figure 7.2. Kaplan Meier curves for the moderate-vascular group (left) and for the high-vascular group (right) depending on the *MGMT* methylation status. * Significant p-values: < 0.05.

The Kaplan Meier curves reaffirm the results that the influence of *MGMT* methylation on survival time is only for the moderate vascular group, since only for this group are the survival functions significantly different.

7.3.3. Benefit of adjuvant Temozolomide cycles in different groups of glioblastoma patients

Multiparametric Cox Regression Analysis

Multiparametric Cox results for the entire cohort, and independently for the moderate- and high-vascular groups, including hazard ratios, Cis, and p-values are shown in Table 7.4.

Table 7.4. Multiparametric Cox regression results for the entire cohort, and for the moderate- and high-vascular groups, analyzing the combined correlation between the *MGMT* methylation status and the number of adjuvant Temozolomide-cycles with the overall survival.

Covariables	HR [95% CI] *MGMT*	*p*-Value
Entire cohort		
***MGMT* status**	1.53 [0.96, 2.43]	0.0727
TMZ cycles	0.78 [0.70, 0.85]	<0.0001 *

Moderate rCBV		
***MGMT* status**	1.75 [1.08, 4.20]	0.0416 *
TMZ cycles	0.78 [0.66, 0.90]	<0.0001 *
High rCBV		
MGMT status	1.03 [0.56, 1.92]	0.9121
TMZ cycles	0.77 [0.68, 0.87]	<0.0001 *

A significant correlation between the number of temozolomide cycles and patient survival was found for the entire cohort, and for the moderate- and high-vascular groups. Nonetheless, only for the moderate vascular group a significant correlation for both variables (*MGMT* methylation status and number of temozolomide cycles) was found. These results suggest that the combined effect of these two clinical variables is more relevant for survival time for those patients with moderate tumor vascularity.

Additionally, Figure 7.3 shows a boxplot per each following group, with survival times depending on the number of adjuvant temozolomide cycles administered:

a) Moderate vascularity + methylated *MGMT*

b) Moderate vascularity + unmethylated *MGMT*

c) High vascularity + methylated *MGMT*

d) High vascularity + unmethylated *MGMT*

We can see that for the unmethylated *MGMT* populations (in green and in red), median survival rates do not overcome 700 days in any case, independently from adjuvant temozolomide cycles.

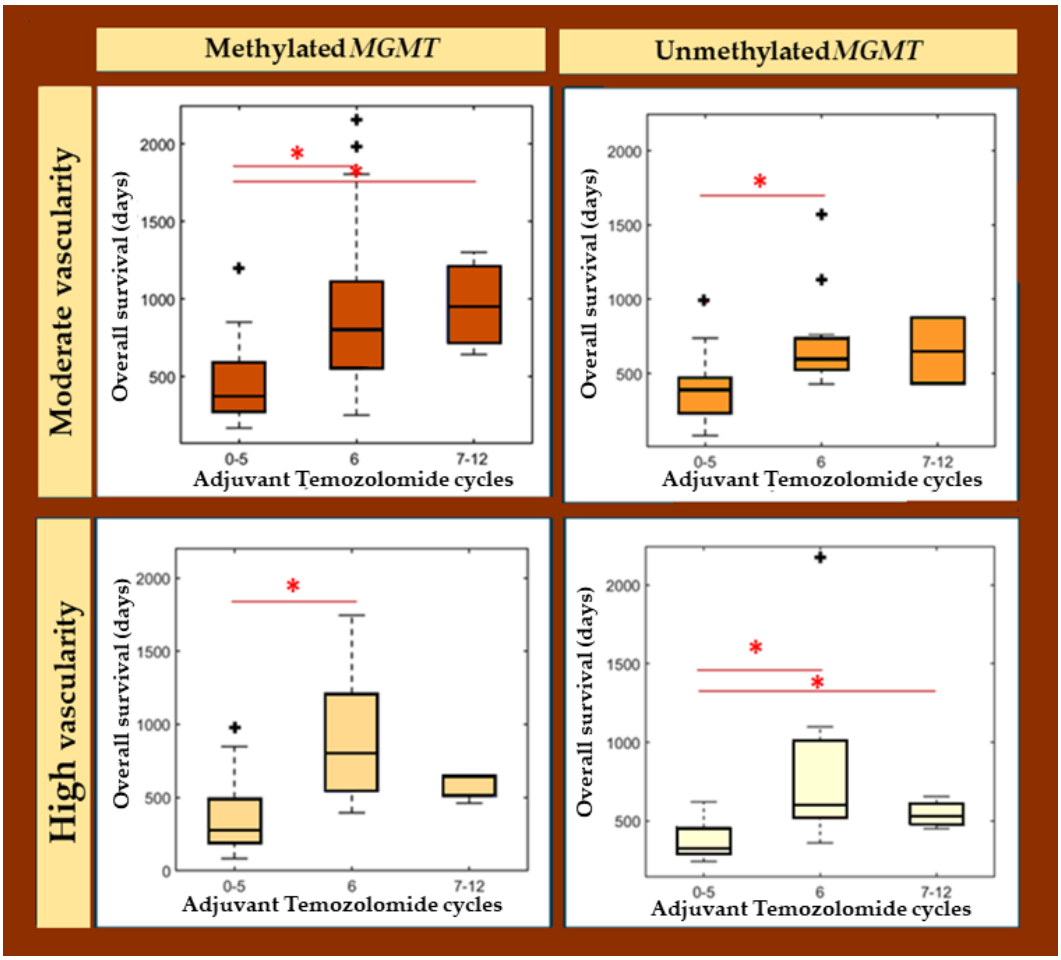

Figure 7.3. Boxplots analyzing the differences in overall survival according to the administered number of adjuvant Temozolomide cycles (1–5, 6, and 7–12) for different populations: patients with moderate vascularity and methylated *MGMT* (top left), patients with moderate vascularity and unmethylated *MGMT* (top right), patients with high vascularity and methylated *MGMT* (bottom left), and patients with high vascularity and unmethylated *MGMT*. * Significantly differences between groups (* in black). Data points beyond the whiskers are shown with + (in red).

By contrast, different tendencies could be appreciated for the methylated *MGMT* populations. In the case of patients with moderate vascularity, median survival rates seem to increase with higher number of temozolomide cycles, being the highest median OS for the group with more than six temozolomide cycles.

However, the tendency seems different for the high vascular group. Although patients that completed the standard six-cycle treatment, presented a higher survival rate, to administer more than six cycles do not seem to provide a beneficial effect, even an adverse one.

7.4. Discussion

With the present study, we aimed to evaluate the lack of benefit of temozolomide for *MGMT* methylated patients with high vascular glioblastoma, since previous results published in[5] concluded that the combined effect of *MGMT* methylation and moderate vascularity of the tumor causes a benefit in glioblastoma patient OS. For this purpose, we have analyzed data from an independent and larger cohort than in[5]. In addition, the previously proposed threshold has been validated and we propose an upload to be more generalizable in future studies, since it has been calculated with data from 214 patients. Finally, we aimed to investigate the potential benefit of increasing the number of adjuvant TMZ cycles in different groups of glioblastoma patients according to their *MGMT* methylation status and tumor vascularity.

To achieve our main purposes, we used an independent and major multicenter cohort of 123 glioblastoma patients. Our results validate the hypothesis proposed in[208], since we have found significant associations ($p < 0.05$) between *MGMT* methylation status and patient survival only for the moderate vascular group of patients, but not for the high vascular group ($p > 0.05$). This is, prognosis of patients with a moderate vascular tumor will be affected by *MGMT* methylation status, while survival times for the high vascular group do not differ, independently of the *MGMT* methylation status. This evidence is also shown when analyzing the Kaplan Meier results: for the moderate-vascular group there is a significant difference ($p < 0.005$) of 174 days in median survival depending on presenting methylated or unmethylated *MGMT*, while for the high-vascular group there are not significant differences in survival. That is, there is a lack of benefit of temozolomide for *MGMT* methylated patients with high vascular glioblastomas.

Some clinical studies have been developed with the purpose of analyzing the effect of increasing the number of adjuvant temozolomide cycles [176–182], six cycles being considered as the standard[19] One meta-analysis[193] and a retrospective large cohort analysis[194] found no benefits on OS but a possible improvement in progression free survival. The only randomized phase II trial did not show any benefit in those parameters for the fact of continuing temozolomide for further than six cycles. Anyway, this was only a phase II trial with a small number of patients, and it may be that a particular subgroup of patients gets benefits from continuing temozolomide treatment, as our preliminary results suggest.

Considering previous results, which opened the possibility to investigate the different effect of temozolomide in particular subgroups, we explored the benefit of increasing the number of temozolomide cycles depending on their specific *MGMT* status and vascular profile. We investigated the correlation between the number of

temozolomide cycles and *MGMT* status for the high- and moderate-vascular groups and we found that only for the moderate-vascular group, both variables were significantly associated with patient survival. We hypothesize that tumors with a lower vascularization could be potentially less aggressive, with a lower prevalence of molecular aberrations that may confer resistance to alkylating agents in the presence of a methylated *MGMT*. Additionally, a high tumor vascularity could be related with a faster progression, hindering the damaging effect of temozolomide on tumor cells. In this sense, advanced MRI-based methodologies can complement molecular analysis to help in glioblastoma characterization and therapy selection[4,209,210].

Furthermore, we analyzed, in an observational way, the survival patterns of each group (defined by *MGMT* status and vascularity) and with different number of administered temozolomide cycles (<6, 6 or >6). We found specific survival tendencies for each group of patients when administering different number of temozolomide cycles. The group of patients with methylated *MGMT* and moderate vascularity was observed as the only one that benefits from more than six temozolomide cycles. Additionally, we want to highlight the low number of patients who received more than six temozolomide cycles, being less than 10% of the entire cohort. This fact is probably due to the retrospective nature of our cohort when more than six cycles were administered in some centers before the evidence generated in subsequent studies[5,176].

These are preliminary results but considering the interest in deciding more individual treatments for glioblastoma patients, future prospective studies could be relevant to analyze the beneficial effect of providing more than six cycles of temozolomide for selected groups of patients. Knowing the marked interpatient heterogeneity, a more personalized approach to treat glioblastoma patients appears to be a potential solution to overcome the heterogeneity and prolonged overall survivals.

The main limitation of this study is the lack of a randomized strategy to provide more than six cycles of adjuvant temozolomide to patients. This is due to the observational and retrospective nature of the study. Assuming that association does not imply causation, our results of analyzing the prognostic effect of temozolomide cycles should be interpreted with caution. In addition, despite the sample size is large enough comparing with previous studies; the comparison of the effect of different number of TMZ cycles could be affected by a small size in some groups of patients, since 12 different groups have been analyzed. However, differences in survival tendencies among groups seem to exist, and future prospective studies could validate these results. These limitations are only referred to the second objective of the study.

7.5. Conclusions

In conclusion, our results demonstrate the lack of benefit of extending temozolamide treatment in those patients with high vascular glioblastoma, even presenting *MGMT* methylation. In addition, we have validated the previously proposed threshold (th = 10.7) as useful to stratify patients in terms of vascularity and with significant differences in survival, and we proposed an upload threshold, calculated with both cohorts, (th = 9.8) to be more generalizable in future studies. Finally, we found preliminary results related with the potential benefit of increasing the number of adjuvant temozolomide cycles only for a particular group of patients with *MGMT* methylation and moderate vascularity, which represents almost a 40% of the study entire cohort. Authors consider clinically relevant a future prospective study analyzing the beneficial effect of providing more than six temozolomide cycles in the group of patients with moderate vascularity and methylated *MGMT*. Positive results could lead us to a more personalized decision making in glioblastoma treatment, in particular during the chemotherapy stage, allowing prolonged survival times in patients with methylated *MGMT* and moderate vascular tumors and avoiding toxicity in patients with high vascular tumors.

Chapter 8

Glioblastomas *IDH*-wildtype located in left cerebral hemisphere present most advantageous immune response to anti-PD-1 treatment

Immunotherapy has emerged as one of the most promising therapies to lengthen the prognosis of patients. Therapies targeting checkpoints such as anti-PD1 have been shown to be very effective but in a very low percentage of patients. Therefore, in order to select the group of patients who would benefit from this treatment, it is necessary to characterize tumors in deep. Genomic and immune profiles associated with response to anti-PD1 treatment have been found. However, to determine these patterns, very advanced and expensive techniques are used, making it impossible to implement them in the clinic.
Finding easy-to-determine characteristics that improve predictive models of response to therapies could significantly improve the selection of patients who may benefit from these novel immunotherapies.

The contents of this chapter correspond with thesis contribution C5 and the study was performed during the international research stay at Rabadan Lab (Columbia University, NY, USA).

8.1. Introduction

In 2019, Zhao *et al.*[211] published an article revealing that immune and genomic profiles correlated with response to programmed cell death protein-1 inhibitor (anti-PD1) immunotherapy in glioblastoma *IDH*-wildtype, one of the most promising treatments in last decades in a variety of tumors[212–214]. This study opens the possibility to generate and improve predictive models to select patients more likely to benefit from this immunotherapy. However, to know these specific tumor profiles that characterize responders, a great variety of techniques were used, including genomic, transcriptomic and single cells sequencing. The time, effort and economic costs of this methodology makes unfeasible its use in clinics for each patient, making necessary the definition of variables easier to determine to select patients more advantageous to benefit from immunotherapy treatment.

Zhao [211] found that a higher density of immune infiltration correlated with response to anti-PD1 in glioblastoma patients, as well as specific mutations and transcriptomic signatures both in responders and non-responders. Considering that previous

studies in animal and human models suggest the existence of different immune microenvironments between two cerebral hemispheres[215–221], we hypothesize that tumor location could be relevant to predict response to immunotherapy with anti-PD1. There is no evidence of differences in survival according to tumor hemisphere in glioblastoma patients treated with the Stupp treatment[222]. However, there is a lack of studies analyzing differences in immune activity in both hemispheres in the presence of a tumor or analyzing potential difference in response to immunotherapies.

In this study, we present the results of analyzing differences in responses to anti-PD1 treatment in patients with glioblastoma depending on tumor hemisphere, as well as its association with overall survival. In addition, the molecular basis underlying these differences were analyzed from a genomic, transcriptomic, and immune approaches.

8.2. Material and Methods

8.2.1. Patient Information

The study cohort was conformed with 42 patients treated with PD1 inhibitor treatment (anti-PD1) derived from two centers: Columbia University (n = 23) and Northwestern University (n = 19) with proper IRB approval at each institution. Informed consent was obtained from all patients, and this study complied with all relevant ethical regulations. Before providing anti-PD1, all patients were treated as regularly with chemo- and radiotherapy.

In addition, we included a control cohort of 224 patients only treated with the Stupp treatment from the public database TCGA-GBM.

The baseline patient characteristics and the workflow of both cohorts are found in Supplementary Table 8.1 and Figure 8.1A.

8.2.2. Sequencing and mapping

On average, 100-fold exome-wide target coverage was achieved for all of the sequenced tumor samples, and 60-fold for matched blood normal samples. High-quality reads for these samples were mapped by Burrows-Wheeler Aligner (BWA)[223] to the hg19 human genome assembly with default parameters. All mapped reads were then marked for duplicates by Picard to eliminate potential duplications.

8.2.3. Somatic mutations

To identify somatic mutations from WES data for samples from patients with glioblastoma, we applied the variant-calling software SAVI2 (statistical algorithm for variant frequency identification), which is based on an empirical Bayesian method. SAVI2 was able to assess mutations by simultaneously considering multiple tumor samples, as well as their corresponding RNA samples, if available. Only variants with a mutant allele frequency of 5% or greater were included for further analysis. More detailed information is included in Appendix E.

8.2.4. Analysis of copy number changes

CNVkit[224] was used to detect copy number changes from whole exome sequencing data. More detailed information about CNVkit is included in Appendix E.

8.2.5. Gene expression analysis

Paired-end transcriptome reads were processed using STAR[225] aligner based on the Ensembl GRCh37 human genome assembly with default parameters. Normalized gene expression values were calculated by featureCounts[226] as RPKM. ssGSEA was performed using the R package GSVA[227]. We compared the transcriptomic profiles of the two tumor groups using ssGSEA based on 5 collections of annotated gene sets from the Molecular Signature Database v6.0 (C2 curated gene sets, C4 computational gene sets, C6 oncogenic gene sets, and C7 immunologic gene sets). The differentially-enriched gene sets between the responders and non-responders were defined by an effect size of GSVA score differences being greater than 0.8 and a t-test p value of less than 0.01.

8.2.6. Quantitative multiplex immunofluorescence (qmIF) analysis

Formalin-fixed, paraffin-embedded (FFPE) tumor samples were collected for each sample and Hematoxylin and Eosin (H&E) slides were reviewed by a neuropathologist (PC) to confirm presence of tumor. Opal multiplex staining was performed on FFPE immunoblank slides for CD3 (T cells), CD8 (cytotoxic T lymphocytes (CTLs)), CD68 (microglia/ macrophages), HLA-DR (activation marker), PD-L1 (immunosuppression marker), and SOX2 (tumor marker)[228,229]. Images were acquired using Vectra™ (PerkinElmer) for whole slide scanning, and multispectral images (MSI) were acquired for all areas with at least 99% tissue, using inForm™ software (PerkinElmer) to unmix and remove autofluorescence. MSIs were analyzed

using inForm™ software and R to evaluate density of immune phenotypes within the tumor microenvironment.

8.2.7. Statistical Analysis

All statistical analysis were performed with Matlab and R. For survival analyses we used Uniparametric Cox regression analysis and Kaplan Meier test. To compare differences in location frequencies between populations we used the two-sided Wilcoxon rank sum test. P-values were adjusted for multiple comparisons with the Benjamini-Hochberg (FDR) method, and statistical significance was assessed at a threshold of 0.05.

8.3. Results

8.3.1. Evaluation of demographic and clinical features as predictors of anti-PD1 response

We studied a retrospective cohort of 42 adult patients with glioblastoma treated with PD-1 inhibitors (pembrolizumab or nivolumab), hereinafter referred to as anti-PD1, upon tumor relapse. In addition, to compare with a control cohort, we used the public dataset TCGA-GBM, including 224 patients with glioblastoma treated with the Stupp treatment. Baseline patient characteristics of both cohorts can be found in Figure 8.1.

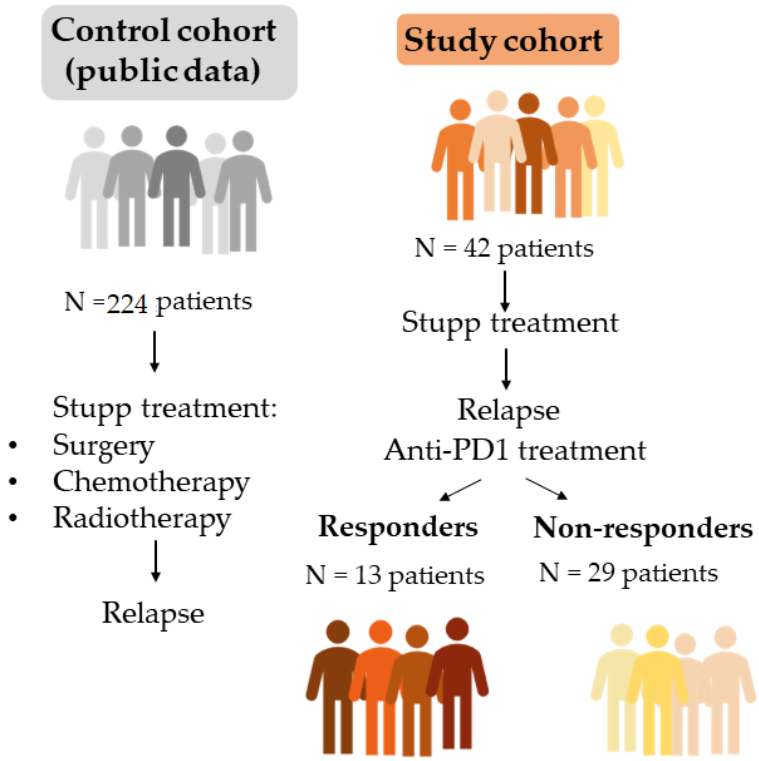

Figure 8.1. Workflow of both cohorts: study cohort treated with anti-PD1 after glioblastoma relapse (n = 42), and control cohort only treated with the Stupp treatment (n = 224).

Patients treated with anti-PD-1 were classified as responders or non-responders according to the following two criteria:

1. Tissue sampled during surgery after anti-PD-1 treatment showed a remarkable inflammatory response and low density of tumor cells.
2. Tumor volumes were stable or shrinking after six months from anti-PD1 treatment (assessed by MRI).

Finally, from the 41 patients treated with anti-PD1, 13 were considered as responders and 28 as non-responders (Figure 8.1).

In order to get a deeper knowledge about responders' profiles, we analyzed the independent correlation between demographic and clinical features with anti-PD1 response. The assessed variables were age, sex, tumor hemisphere, tumor location (frontal, temporal, parietal or other location, including thalamus and cerebellum) and KPS at anti-PD1 start.

Univariate correlation analysis revealed that the most associated demographic or clinical variable with anti-PD1 response was tumor hemisphere (rho = 0.298, p =

0.055) (Figure 8.2). In particular, presenting the tumor at the left hemisphere was correlated with a positive response to anti-PD1.

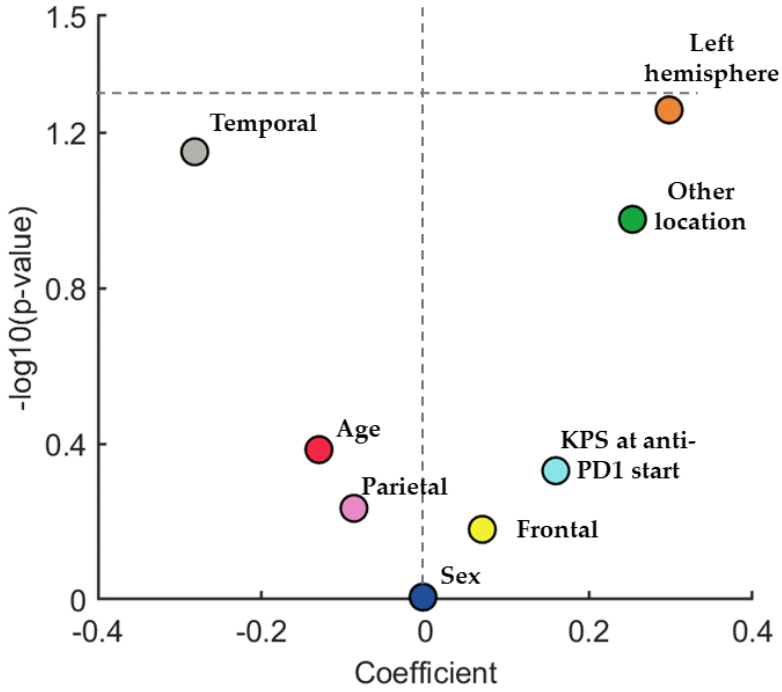

Figure 8.2. Univariate correlation analysis between anti-PD1 response and demographic and clinical variables.

8.3.2. Patients with glioblastoma located at the left cerebral hemisphere are more likely to respond to anti-PD-1 treatment

We found well balanced frequencies of tumors in each cerebral hemisphere for the study cohort and the control cohort, with 53.7% and 48.0% of tumors located at left hemisphere respectively. By contrast, focusing on responders to anti-PD-1 there is a significant higher proportion of tumors located at the left hemisphere (76.9%) comparing with the control group (Wilcoxon rank sum test, $p = 0.0402$*). Differences in response rates between tumors located at left and right hemisphere are illustrated in Figure 8.3.

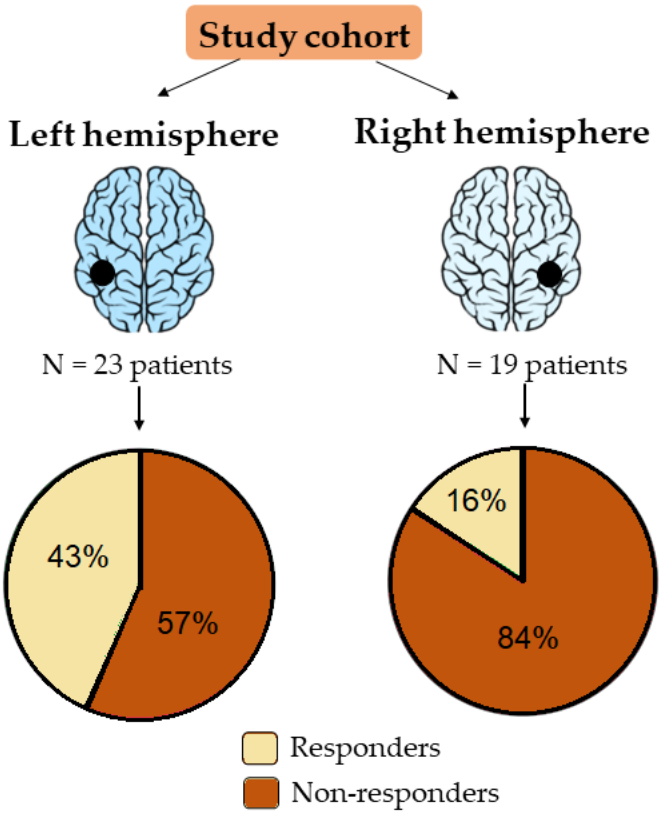

Figure 8.3. Frequencies of response to anti-PD1 treatment for the study cohort divided according to tumor hemisphere.

8.3.3. Lack of benefit in terms of overall survival when providing anti-PD1 to patients with glioblastoma located at the right hemisphere

To compare the benefit in overall survival (OS) of providing the anti-PD-1 treatment depending on the tumor location (left vs. right hemisphere), Uniparametric Cox regression analysis and Kaplan Meier test were carried out for the entire cohort (266 patients, of which 41 were treated with anti-PD-1).

A significant association between OS and providing the anti-PD-1 treatment was found for the entire cohort ($p = 00.28$, HR = 1.81). However, when stratifying the entire cohort according to brain location, we found that providing the anti-PD-1 to patients with tumors located at the right hemisphere did not result in a significant benefit in OS ($p = 0.2651$, HR = 1.35). On the contrary, the benefit of providing the anti-PD-1 treatment was significantly higher for those patients with the tumor located at the left hemisphere ($p = 0.0026$, HR = 2.40).

Patients with tumors located at left hemisphere presented a median survival 340 days longer when the anti-PD1 treatment was provided. However, patients with

tumors located at right hemisphere only presented a median OS of 95 days longer. These results are illustrated with the Kaplan Meier curves in Figure 8.4 (which also include p-values).

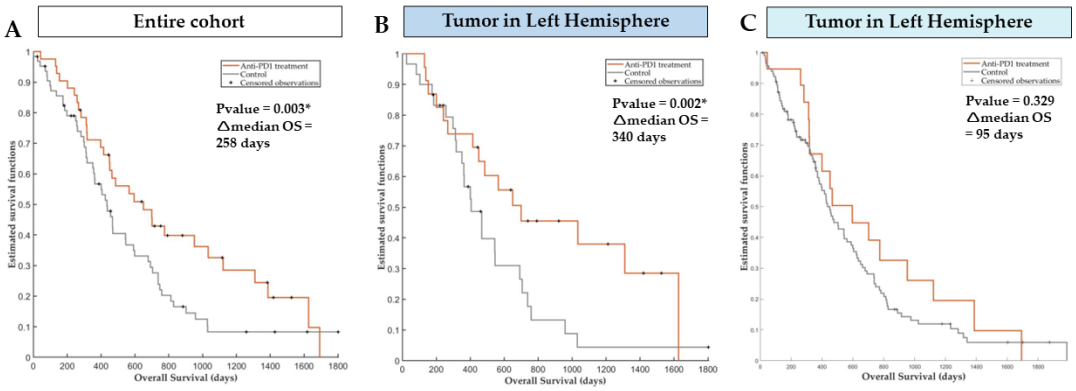

Figure 8.4. A) Kaplan Meier curves for the entire cohort (n = 266) divided by treatment (anti-PD1 or control), **B)** for the group of patients with glioblastoma located at the left hemisphere (n = 130) divided by treatment (anti-PD1 or control), and **C)** for the group of patients with glioblastoma located at the right hemisphere (n = 136) divided by treatment (anti-PD1 or control).

8.3.4. Molecular basis of differences in survival and anti-PD1 response between tumors located at the right and left hemispheres

Transcriptomic differences between tumors located at right and left hemispheres

We performed a gene expression analysis across a total of 12,368 gene sets from MSigDB comparing between samples from right and left tumors. The main top gene sets differentially enriched for each group are shown in Figure 2 (p-value <0.05).

It is important to highlight that we observed that the ratio *MOLT4* (immature T cells)/ *CAL1* (plasmacytoid dendritic cells) was enriched in samples from tumors located at the right hemisphere. By contrast, this gene set was downregulated in tumors located at the left hemisphere, suggesting a higher expression of plasmacytoid dendritic cells, which play a critical role in mediating innate and adaptive immune response (Figure 8.5).

Furthermore, we found a higher expression of a gene set related with the regulation of estrogen in the group of patients with tumors in the left hemisphere, being the hormonal environment suggested as key in some type of cancers.

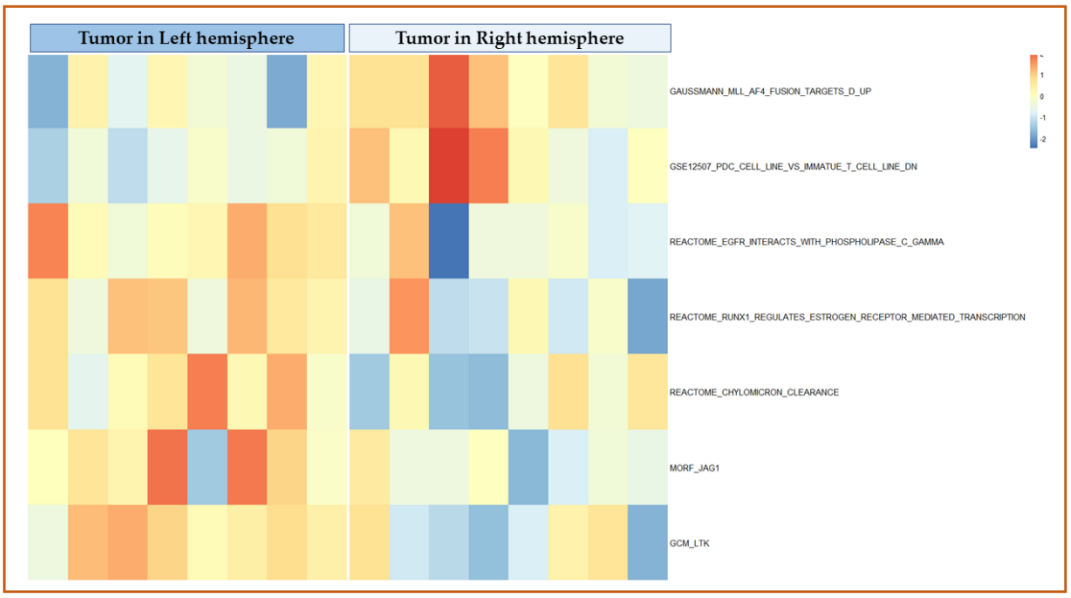

Figure 8.5: Heatmap showing the top gene sets differentially enriched in tumors located in the left hemisphere versus tumors located in the right hemisphere.

8.3.5. Genomic differences between tumors located at right and left hemispheres

We analyzed if mutations previously described as relevant for immunotherapy response, as well as other typically present in glioblastoma, were significantly enriched in tumors located in either right or left tumors.

From the 32 tumors with genomic data, we found 13 tumors with *PTEN* mutation: 4 among the 15 left tumors (26.7%) and 9 among the 17 right tumors (52.9%), being *PTEN* mutation significantly enriched in tumors located in the right hemisphere (Wilcoxon rank sum test, p = 0.0412). This mutation was previously reported as significantly enriched in patients with glioblastoma which did not respond to anti-PD1 treatment[9], being coherent with our results. This difference was not found for the control cohort.

Additionally, for the study cohort we found that tumors located at right hemisphere presented a higher proportion of copy number alterations in the following genes comparing with tumors located at the left hemisphere: *CDKN2A/B*, *CDK4/6*, *RB1*, *EGFR* and *PTEN* (40.0% vs. 11.8% for *CDK4/6*; 73.3% vs. 41.2% for *CDKN2A/B*; 40.0% vs. 17.6% for *RB1*, 53.3% vs. 41.2% for *EGFR* and 40.0% versus 17.6% for *PTEN*). Although individually, these differences did not reach statistical differences (p = 0.074, p = 0.075, 0.175, 0.175 and 0.155, respectively), the proportion of patients presenting these five alterations at the same tumor was significantly enriched in right tumors (Wilcoxon rank sum test, p = 0.010) (5 from 15) versus left tumors (0 from 17).

These differences in alterations depending on tumor laterality are illustrated in Figure 8.6.

These alterations have been previously described as associated with shorter survivals and correlated with therapy responses in patients with gliomas [222,230–233]. Kaplan Meier curves differentiating survival depending on the presence or absence of these five alterations are included in supporting material in Appendix E.

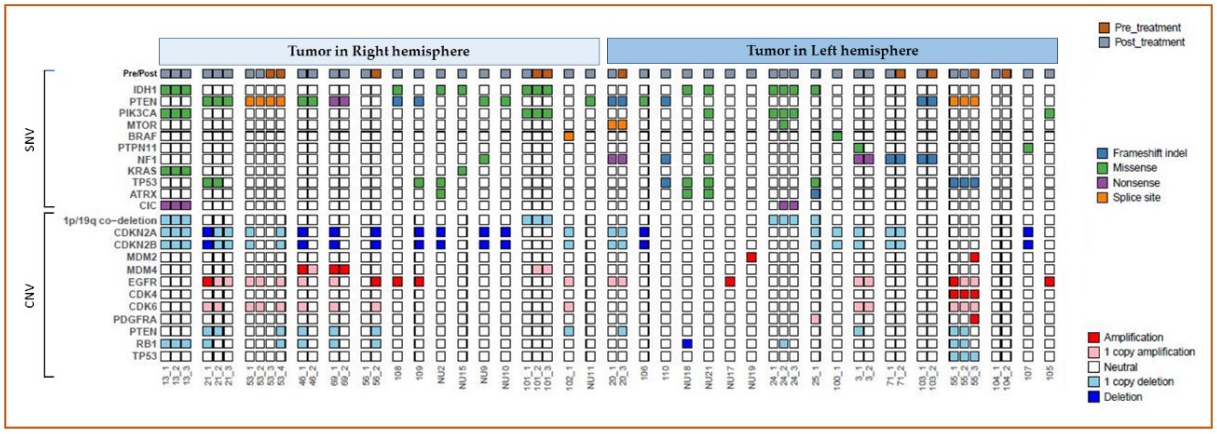

Figure 8.6: Genetic profiles of the study cohort (n = 32 patients) stratified according to the tumor hemisphere: 15 patients with glioblastoma located at right hemisphere and 17 patients with tumor located at left hemisphere.

8.3.5. Differences in immune cells infiltration between tumors located at right and left hemispheres

We analyzed density of immune cells for tumors located at right and left hemispheres before and after immunotherapy. We found higher cell density of CD3+HLA-DR+ T cells (Figure 8.7A), and CD68+HLA−DR−PDL1+ macrophages (Figure 8.7B) when comparing pre- and post-treatment samples only for left tumors, although these differences did not reach statistical significance.

By contrast, in tumors located at the right hemisphere, PDL1- tumor cells showed an increase in cell density after immunotherapy (Figure 8.7C).

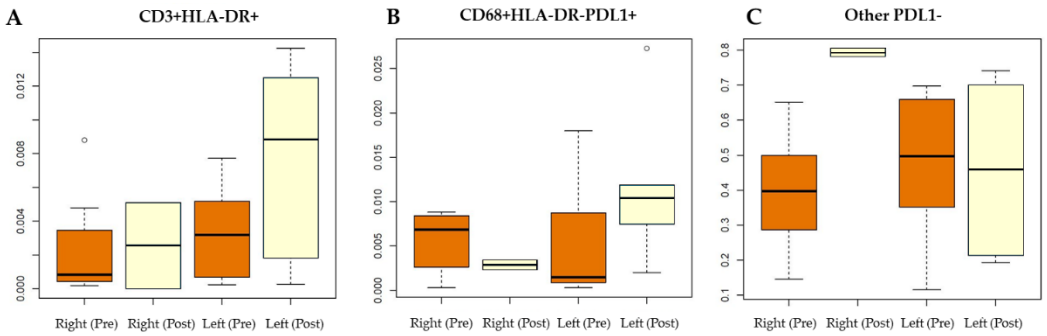

Figure 8.7. Boxplot showing differences in cell density of different types of cells between right and left hemisphere before and after anti-PD1 treatment.

Additional transcriptomic analyses are included in Extended Data Figure 2.

Our results suggest a higher infiltration of some immune cell types after anti-PD1 treatment for those tumors located at the left hemisphere, but not for glioblastomas located at right hemisphere. In addition, PDL1- tumor cell density seems to be increased after anti-PD1 treatment in tumors located at the right hemisphere after anti-PD1 treatment. It is important to remark than more potential differences may occur in the tumor microenvironment, which was not studied in this work.

8.3.6. Tumor hemisphere is more correlated with anti-PD1 response than *PTEN* mutation and specific CNVs detected

Multiparametric correlation analyses with anti-PD-1 response were performed for *PTEN* mutations, CNVs in *CDKN2A/B*, *CDK4/6*, *RB1*, *EGFR* and *PTEN* and for tumor hemisphere (Table 3).

Referred to the correlation between the anti-PD-1 response with the rest of variables, the highest coefficient, and the lowest p-value (close to 0.05) were yielded for tumor hemisphere, suggesting that it is the most correlated variable to predict the response to anti-PD-1.

In addition, tumor hemisphere is significantly correlated with the presence of *PTEN* mutation and CNVs in *CDKN2A/B*, *CDK4/6*, *RB1*, *EGFR* and *PTEN* being more prevalent in tumors located in the right hemisphere (table 8.1).

Table 8.1. Uniparametric correlation results among PTEN mutation, alterations in copy number variations, tumor hemisphere and response to anti-PD1

	PTEN mutation	*5 CNVs	Hemisphere	Response to Anti-PD-1
PTEN mutation	rho = 1.00 p =1.000	rho = 0.39 **p =0.011***	rho = 0.32 **p =0.037***	rho = -0.11 p =0.472
*5 CNVs	rho = 0.39 **p =0.011***	rho = 1.00 p =1.000	rho = 0.40 **p =0.0079***	rho = -0.25 p =0.116
Hemisphere	rho = 0.32 **p =0.037***	rho = 0.40 **p =0.0079***	rho = 1.00 p =1.000	rho = -0.30 p =0.055
Response to Anti-PD-1	rho = -0.11 p =0.472	rho = -0.25 p =0.116	rho = -0.30 p =0.055	rho = 1.00 p =1.000

*5 CNVs referred to presenting copy number variations of *CDKN2A/B*, *CDK4/6*, *RB1*, *EGFR* and *PTEN* at the same tumor.

8.4. Discussion

We have found that patients with glioblastoma located at left cerebral hemisphere have a more significant probability to respond to anti-PD-1 treatment than patients with the tumor located at the right hemisphere. These differences in response influence patient survival, presenting longer overall survival (OS) those patients with the tumor located at the left hemisphere when anti-PD-1 treatment is provided. When stratifying the cohorts by tumor hemisphere, we found a significant difference in survival between patients treated with anti-PD-1 and the control cohort for the group with tumors located at the left hemisphere (with a median benefit of 258 days when providing the immunotherapy). By contrast, none difference in survival was found for patients with the tumor located at the right hemisphere, suggesting a lack of benefit of providing this immunotherapy for this group of patients. As far as we know, this is the first study that has investigated the potential impact of tumor hemisphere for response to anti-PD-1 treatment in patients with glioblastoma.

The lack of studies analyzing differences in immunity between cerebral hemispheres in the presence of a tumor, as well as the novelty of these immunotherapies, make challenging the comparison with previous studies. However, some previous works in animal and human models studied the correlation between hemispheric lateralization and immune activity. All collectively concluded that a relationship between left-hemisphere and stronger immunity seem to exist[215–221].

In 2002, Neveu PJ[215] affirmed that immune defects observed after brain lesions in humans depend on the side of the lesion. They suggested a more active function of T-cell mitogenesis, IL-1 production, NK cell activity and macrophage alteration in normal left hemisphere, being these functions reduced after a lesion in this hemisphere. By contrast, these functions did not change after right lesions. Furthermore, in 2011, Sumner R *et al.*[216] published a review article including 11

articles analyzing the correlation between hemispheric lateralization and the immune function in humans. They concluded that all the analyzed studies point to a relationship between left-hemisphere and stronger immunity. In addition, in 2012 other review article tried to explain the correlation between brain asymmetry and immunity. They mentioned that that left hemispheric influences enhance the reactivity of different T-cell dependent immune mechanisms and, in general, immune functions under physiological conditions, whereas right hemispheric influences have a predominantly immunosuppressive effect[217,218]. More recently, in 2021, AbdelRazek M [219] studied a cohort of patients with strictly unilateral relapsing primary angiitis and the potential differences in the immune response between the cerebral hemispheres. They hypothesized that a functional difference in immune responses between the right and left brain may exist, caused by such discrepancies as basal levels of cytokines, asymmetric distribution of microglia, and differences in modulation of the systemic immune functions18. However, they stated that this was speculative.

Our main conclusion is that patients with tumors located at left hemisphere respond better to immunotherapy which is correlated with a benefit in survival, being coherent with all these previous studies. This conclusion is supported by the analysis of differences at genomic, transcriptomic, and immune levels between tumor samples from glioblastoma located at left and right hemispheres.

Related with the transcriptomic differences, we found a significant lower expression of a gene set related with estrogen regulation in samples of right tumors. Surprisingly, in a study carried out by Ramadhani *et al.*[221] found that the risk of breast cancer is 39% higher in left-handed women (which is correlated with a right hemisphere dominance). The authors hypothetically explained the association between handedness and breast cancer by influences of intrauterine sex hormonal, including estrogens. In addition, samples from tumors located at the left hemisphere, which respond better to anti-PD1, showed a lower expression of the ratio MOLT4 (immature T cells)/ CAL1 (plasmacytoid dendritic cells)[234]. This suggests a higher number of plasmacytoid dendritic cells in left tumors, which play a critical role in mediating innate and adaptive immune response. Interestingly, a previous study which studied multiple myeloma cells found that pDCs expressed high surface levels of PDL1. Therefore, a better response to anti-PD1 could be related with a more effective blockade of this immune checkpoint in tumors with a higher number of pDCs cells (tumors located in the left hemisphere according to our study). However, we did not find differences in CD83+ expression, which encodes dendritic cells, between tumor samples from both hemispheres.

Although previous studies found differences in immunity between hemispheres in presence of a lesion13-19, it is certain that differences in gene expression between

healthy cerebral hemispheres was studied in a previous work and they did not show positive results26. Authors hypothesized that it may be that the basis for lateralization of function involves more subtle changes in specific cellular components or is more related to functional connectivity patterns than molecular differentiation.

We also found several differences in cell density of both tumor and immune cells between hemispheres, although none of these differences reach statistical significance. We found higher cell density of CD3+HLA-DR+ T cells, and CD68+HLA−DR−PDL1+ macrophages when comparing pre- and post-treatment samples only for left tumors. This is, in tumors located at left hemisphere seem to be a change in immune cells composition after providing the anti-PD1 treatment. By contrast, in tumors located at the right hemisphere, PDL1- tumor cells showed an increase in cell density after immunotherapy, suggesting the inefficacy of the treatment in these tumors.

Furthermore, we analyzed if the tumor hemisphere was correlated with an enrichment of mutations. We found that *PTEN* mutations are significantly more predominant in tumors located at right hemisphere. This alteration was previously described as significantly more frequent in non-responders to anti-PD1 treatment[211]. Alterations in *CDKN2A/B*, *CDK4/6*, *RB1*, *EGFR* and *PTEN* were also more frequent in right-tumor samples, being significantly more prevalent the alteration of these four genes at same tumor in tumors located at the right hemisphere. Both *PTEN* mutation and CNVs of these genes have been described previously as associated with poor prognosis in gliomas and/or correlated with worse response to therapies [222,230–233].

The main limitation of this study is the reduced size of the responder group (only conformed by 13 patients). This is cause of the low proportion of patients with glioblastoma which respond to the anti-PD1 treatment. In addition, future works analyzing immune differences in samples taken from the tumor microenvironment of both hemispheres are needed to define in deep the immune differences in response to immunotherapy.

8.5. Conclusions

In conclusion, this is the first study proposing the potential relevance of tumor cerebral hemisphere, to select patients with glioblastoma more likely to respond to anti-PD1 treatment. Differences in response to anti-PD1 according to the cerebral hemisphere, may be caused by a correlation between brain asymmetry and immunity previously demonstrated in several studies. In addition, our findings in

differential immune, genomic, and transcriptomic differences can support our main conclusion, although it must be taken with caution and must be validated. Positive results in future studies could provide a precious knowledge to improve the selection of patients to receive immunotherapies by using an extremely easy-to-determine tumor characteristic. We encourage other research groups to consider this work to validate these findings with independent cohorts of glioblastoma patients treated with anti-PD1.

Part IV

Clinical Studies Implementation and Datasets Creation

Chapter 9

Clinical studies and protocols design and implementation

The low prevalence of astrocytomas grade 4 as well as the short survival rates make it difficult to collect data for research. The three previous pillars included in this thesis address tumor characterization, patient prognosis and treatment response. All of them must be based on biomedical data derived from tumors and patients. Therefore, a fundamental part of this thesis has been the design and implementation of clinical studies that allow the collection of the necessary data to perform the analyses. Data from 650 patients treated at 18 international hospitals have been collected during this thesis, constituting a relevant dataset.

On the other hand, to validate the MRI-DSC biomarkers calculated in the habitats delineated by the vascular heterogeneity assessment method, it is necessary to study their differences at the biological level. For this purpose, the *BIOhabitats* study has been initiated and a clinical protocol has been designed for the collection and analysis of biological samples from each tumor and edema habitat. This protocol has been approved by the Ethical Committee of the Universitat Politècnica de València and it is currently implemented in two national reference hospitals.

The contents of this chapter correspond with thesis contributions C6 and C7.

9.1. Design and implementation of the *BIOhabitats* study (NCT05375318)

9.1.1 Background

As previously defined in *section 2.6*. of chapter 2, the ONCOhabitats platform provides an unsupervised method to describe the heterogeneity of the enhancing tumor and edema areas in terms of the angiogenic process located at these regions. The following four habitats are automatically delineated for each patient: 1) the HAT habitat, which refers to the high angiogenic enhancing tumor part of the tumor, 2) the LAT habitat, which refers to the less angiogenic enhancing tumor area of the tumor, 3) the IPE habitat, which refers to the potentially infiltrated peripheral edema, and 4) the VPE habitat, which refers to the vasogenic peripheral edema of the tumor[67,68]. This methodology has been validated at multicenter level (work included in chapter 5).

Furthermore, relevant associations have been found between the perfusion markers and clinical-routine biomarkers, such as *IDH* mutation[4,123], *MGMT* methylation[1,5], molecular subtype[8] or microvessel area[4].

Considering these promising results and, in order to develop a decision support system based on pixel level Artificial Intelligent models for deciding treatment in high-grade glioma, it is necessary to develop a prospective study and to validate at biological level the vascular habitats defined by the ONCOhabitats method.

To conclusively validate the ability of this methodology to analyze the angiogenic processes intrinsic to the tumor, as well as their association with the molecular, histopathological and immunological profile, a prospective study has been initiated at two Spanish hospitals. Biological samples from the different habitats will be collected during standard surgeries for their posterior analysis.

9.1.2. Participating centers

The Biomedical Data Science Laboratory of the Universitat Politècnica de València is the coordinator of the BIOhabitats study. Two Spanish hospitals are collaborating in the development of the study: Hospital Clínico Universitario de Valencia (Valencia) and the Hospital Universitario 12 de Octubre (Madrid). The Neurosurgery, Radiology and Anatomic Pathology departments of both hospitals are involved.

9.1.3. Study Design

The *BIOhabitats* study is single-arm, prospective, non-interventional study. The main aim is to provide training data necessary for the development of a clinically validated decision support system based on pixel level Artificial Intelligent (AI) models for deciding treatment in glioblastoma, referred to here as called ALBATROSS, and to evaluate its performance. For that, the software will assess the health status of glioma patients for personalized therapy planning and follow-up by means of a set of AI models and address high-level clinical questions in different phases of glioma patient management.

Information related with regulatory and ethics status is included in appendix F.

9.1.4. Hypothesis and objectives

The main hypothesis leading to the design of the *BIOhabitats* study are as follows:

I. Since the tumor and edema HTS habitats (HAT, LAT, IPE and VPE) have been proven as different in relation to their hemodynamic and vascular behavior[2,68],

we hypothesize that these are habitats are also significantly different at the vascular, tissular, cellular and molecular level.

II. Significant associations between the perfusion imaging markers calculated with the HTS methodology and both molecular and histopathological markers (useful in prognosis, monitoring, and evaluation of therapies) have been found in previous studies[5,8,99]. Therefore, we hypothesize that relevant associations between the imaging markers and clinical-routine biomarkers, such as molecular and histopathological markers, exist.

III. Preliminary studies have shown associations between the perfusion imaging markers and molecular markers related with the immune action/suppression[235]. In addition, previous works have demonstrated that immune and genomic correlates of response to immunotherapy treatments, such as anti-PD-1, in glioblastom[211]a. Therefore, to find correlations between these immune and genomic signatures with perfusion imaging markers can be useful for decision making and evaluation of immunotherapies.

IV. Preliminary retrospective studies have demonstrated robust association between the perfusion imaging markers calculated at high and low angiogenic habitats and patient overall survival[2,68]. We hypothesize that these robust associations between the perfusion imaging markers and survival times will be demonstrated with a prospective study.

In relation with the presented hypothesis, the main purposes of this study are:

I. To assess that the four habitats within the tumor (HAT and LAT) and edema (IPE and VPE) in high-grade glioma are different at vascular, tissular, cellular and molecular levels.

II. To analyze the associations between the perfusion imaging markers and relevant molecular markers at the HTS habitats for high-grade glioma diagnosis, prognosis/aggressiveness, progression and/or prediction.

III. To analyze the associations between the perfusion imaging markers and immune markers at the HTS habitats useful in immunotherapy evaluation and/or patient selection.

IV. To prospectively validate the prognostic capacity (association with OS and PFS) and stratification capacity of the perfusion imaging markers calculated at the HTS habitats.

9.1.5. Methodology

Selection Criteria

The cohort will be formed by patients diagnosed with Astrocytoma, Grade 4, cIMPACT-NOW: update 6[10] classification during one year since the beginning of the study (estimated dates: 1st of March of 2021 to 1st of June of 2022). The inclusion and exclusion criteria were defined as follow:

Inclusion criteria

Adult patients (18 years at diagnosis), with Astrocytoma, Grade 4, cIMPACT-NOW: update 6 classification with histopathological/genetic confirmation who undergo the Stupp treatment. It is essential the access to complete pre-operative MRI studies, including:

- Pre gadolinium T1-weighted MRI
- Post gadolinium T1-wighted MRI
- T2-weighted MRI
- T2-Fluid-Attenuated Inversion Recovery (FLAIR)
- Dynamic Susceptibility Contrast (DSC) T2*-weighted perfusion sequences
- Diffusion Weighted Imaging (DWI)

In addition, patients must undergo surgery with the possibility to collect samples from different regions of the tumor to be included in the study.

Exclusion criteria

Patients presenting the following diseases or conditions will be excluded of the study, since clinical outcomes can be influenced by them.

- Congestive heart failure within 6 months prior to study entry (New York Heart Association >= Grade 3)
- Uncontrolled or significant cardiovascular disease, including:
  - Myocardial infarction and transient ischemic attack or stroke within 6 months prior to enrollment
  - Uncontrolled angina within 6 months
  - Diagnosed or suspected congenital long QT syndrome
  - Any history of clinically significant ventricular arrhythmias (such as ventricular tachycardia, ventricular fibrillation, or Torsades de pointes)
  - Clinically significant abnormality on electrocardiogram (ECG)
  - Pulmonary disease including or greater than grade 2 dyspnea or laryngeal edema, grade 3 pulmonary edema or pulmonary hypertension according to CTCAE 4.03

Variables

The following variables were defined as mandatory to be collected for the correct course of the project.

Tables 9.1-9.5. includes the different types of variables that will be collected during the clinical study.

Table 9.1. Socio-demographic variables.

Socio-demographic data	
Variable	**Units/categories**
Age at diagnosis	Years old
Sex	female/male/other
Ethnicity	self-reported ethnicity group: Asian, Black, White, Other/Unknown

Table 9.2. Clinical variables.

Clinical data	
Variable	**Units/categories**
Date of preoperative MRI study	dd/mm/yyyy
Date of surgery	dd/mm/yyyy
KPS at diagnosis	0-100
Date of recurrence	dd/mm/yyyy
Previous Diabetes / hypertension / dyslipidemia	Yes/no
Date of exitus	dd/mm/yyyy

Table 9.3. Treatment-related variables.

Treatment-related data	
Variable	**Units/categories**
Surgery	
Resection	Total/Subtotal/No
Volume of resected tumor	cm^3
Remaining tumor after surgical resection	% of entire tumor
Nurosurgery report	observations
Radio- and chemotherapy	

Completeness	Complete/incomplete/no /only RT/only CT
Radiotherapy	Gy
Complete Concomitant TMZ	Yes/No
Adjuvant TMZ cycles	0-12
Second-line treatments	
Bevacizumab	Yes/No
Date of first BVZ dosis	dd/mm/yyyy
Immunotherapy	Yes/No
Type of immunotherapy	Anti-PD1/others
Corticosteroids	Yes/No

Table 9.4. Image findings.

Imaging data	
Variable	**Units/categories**
Location	
Lobe	Frontal/Parietal/Occipital/Temporal/Other (Thalamus/Cerebellum,Brain Stem)
Subventricular tumor	Yes/No
Hemisphere	Right/Left
Observations	discontinuation, adherence, compliance, modifications of the treatment, etc (text)
Preoperative, post-radiotherapy and follow-up MRIs	
Pre-gadolinium Spoiled Gradient Echo T1-weighted exam	
Post-gadolinium Spoiled Gradient Echo T1-weighted exam	
Fast Spin Echo T2-weighted exam	
FLAIR exam	
T2*-weighted DSC Perfusion MRI*	

*Preferred sequence and protocol for DSC:

- Gradient Echo-Echo Planar Image (GE-EPI)
- TE/TR = 30ms / 1-1.2 seconds
- Flip angle = 72°
- Reps = 120 (# of images per slice, collected over time)

- Slice thickness = 4-5mm
- FOV = 22-24cm, Matrix = 962
- After approximately 1 minute of baseline collection, inject a bolus of Gd-chelated contrast agent, typically 0.1mmol/kg at 3-5cc/sec.

Table 9.5. Histopathological analysis

Histopathological data	
Variable	**Units/categories**
For one sample of the tumor	
Necrosis	Yes/No
Microvascular proliferation	Yes/No
For each sample of habitats	
Volume of the sample	mm^3
Number of tissue sections	value
Area of tissue sections	
Neoplasic cellularity	Proportion (%)
Cytologic atypia	High/Low
Mitosis	Number
Reactive gliosis	Yes/No
Edema	Yes/No
Microvessel area	μ2
Glomeruloid vessels	Yes/No

The molecular profile for at least one of the collected will be collected, including the alteration status of the following genes: *IDH*, *EGFR*, *TERT*, *P53*, *ATRX*, *H3 G34* mutations, and *MGMT* methylation.

In addition, the molecular status pf the following genes for each of the collected samples (at least one for habitat) will be collected:

- PD-L1 expression (value)
- CD4+/CD8+ expression (value)
- CD68+/CD163+ expression (value)
- CD20+/CD3+ expression (value)
- Mutational burden (value)*
- PTEN loss/mutation (yes/no, yes/no)*
- PIK3CA mutation (yes/no, yes/no)*

- MAPK pathway alterations (PTPN11, BRAF)*
- PDGFA mutation/amplification (yes/no)
- Vimentin expression (value)
- PDGFRA amplification (yes/no)
- HIF pathways activation (yes/no)
- PI3 kinase pathway activation (yes/no)
- PDGFRA pathway activation (yes/no)
- HIF-1 expression (value)
- VEGF expression (value)
- VEGFR expression (value)
- Description of the techniques used to define the molecular profile (IHC, sequencing, RNAseq, microarray, others)

Tasks

The development of the study includes the following tasks (T):

T1. Patient selection and inclusion. The study cohort will be formed according to the selection criteria defined in the study design subsection of the protocol. Considering the number of glioblastoma patients treated at the collaborating hospital per year, it is estimated that the cohort will consist of between 60 and 80 patients.

T2. Preoperative MRI study collection. After the inclusion of each patient in the study, the complete preoperative MRI study (defined in the variables subsection) will be sent to the BDSLab group, previously anonymized and making it impossible to identify the patient. For the exchange of previously anonymized data, a secure server of the UPV will be used.

T3. HTS and segmentation masks generation. From the MRI studies of each patient, the classic segmentation masks (which define active tumor, edema and necrosis) and the masks of the four vascular habitats (HAT, LAT, IPE and VPE) will be obtained using the HTS methodology, included in the ONCOhabitats site.

T4. Planification of sample collection. In no case will the clinical routine followed by patients be altered. For this reason, sampling will be done during the surgery of the tumor that is included in the standard Stupp treatment. In order to agree on the points (regions) from which the samples will be taken, a pre-surgery planning session will be established. The neurosurgeon and the radiologist, together with the BDSLab researchers, will decide the optimal points from which to take the samples of the tumor and the peripheral edema. The most appropriate locations will be

established using the masks obtained previously and considering the values of blood perfusion in each habitat and the accessibility to that area during the resection.

T5. Surgery and sample collection. Patients included in the study will follow the usual procedure, which includes resection of the tumor at an early stage. During surgery, tumor samples will be taken from the previously chosen locations, which will consist of at least one 1 cm3 block for each habitat (HAT, LAT, IPE, VPE). In the case of easily accessible tumors, 2-3 blocks will be collected in the habitats where it is possible. To facilitate the location of the sampling points, the masks of the vascular habitats may be included in the neuronavigator. The samples will be labeled to know which habitat they belong to and to define the location as precisely as possible.

Figure 9.1. includes an example of a standard surgery of a patient with astrocytoma grade 4. The photography was taken in the Hospital Clinico Universitario de Valencia during the surgery of a patient included in the *BIOhabitats* study. The masks with the tumor and edema habitats delineated with the HTS method are included in the neuronavigator to orientate neurosurgeons during the sample collection of each habitat.

T6. Histopathological and molecular analyses. The samples collected from each habitat will be analyzed in order to define the histopathological and molecular characteristics of each zone, considering what was defined in the variables subsection of the protocol.

T7. Data collection and management. Socio-demographic and clinical data, results of the histopathological and molecular analyses will be sent to the BDSLab, for their correct processing and analysis preparation. Patient follow-up data will be periodically updated to include MRI studies, recurrence dates, second line treatments, exitus date, etc. In any case, the information provided to the researchers will be previously anonymized, preventing the identification of the patients.

T8. Data and statistical analysis. When the inclusion of patients is completed on the date indicated (January 1st, 2022), and all the indicated data have been collected, the in-depth study of the data and the appropriate statistical analyses will be carried out, including: Uniparametric and multiparametric cox regression, Kaplan Meier test, Mann Whitney test and others, to analyze the associations defined in the objectives section.

T9. Publication and dissemination of results. Publication the results and conclusions of the study in high-impact journals and dissemination in national and international congresses.

The following table 9.6 summarizes the tasks of the study, and the responsible(s) institution(s) for its adequate development. It should be noted that during all phases,

the BDSLab researcher María del Mar Álvarez Torres will support the collaborating hospitals.

Table 9.6. Tasks and responsible institutions included to implement the *BIOhabitats* study.

	Tasks	Responsible institutions
TASK 1	Patient selection and inclusion	Hospitals
TASK 2.1	Preoperative MRI study	Hospitals
TASK 2.2	Collection and processing of MRI study	BDSLab (Universitat Politècnica de València)
TASK 3	HTS and segmentation masks generation	BDSLab (Universitat Politècnica de València)
TASK 4	Planification of sample collection	Hospitals & BDSLab (Universitat Politècnica de València)
TASK 5	Surgery and sample collection	Hospitals
TASK 6	Histopathological and molecular analyses	Hospitals
TASK 7	Data collection and management	BDSLab (Universitat Politècnica de València)
TASK 8	Data and statistical analysis	BDSLab (Universitat Politècnica de València)
TASK 9	Publication and dissemination of results.	BDSLab (Universitat Politècnica de València) and Hospitals (coordinated by BDSLab)

9.1.6. Implementation

Included patients

At the date of submission of this thesis, data from 42 patients have been initially transferred to evaluate their inclusion in the study.

Use of habitats masks during surgery

The habitat masks have been successfully included in the neuronavigator at the two participating hospitals. This constitutes a relevant achievement, since it is the first time that the ONCOhabitats results are used in hospitals. Figure 9.1 illustrates the sample collection from each vascular habitat during one standard surgery guided by the masks included in the neuronavigator.

Figure 9.1. Sample collection guided by the habitats masks included in the neuronavigator during the standard surgery of a patient with astrocytoma grade 4.

Histopathological analyses

The anatomic pathology service of each hospital is responsible of performing the histopathological analysis of the samples of each habitat (Figure 9.2A) and of the rest of the tumor (Figure 9.2B) collected during surgery.

Tumor tissue after exeresis was fixed in formaldehide 10% and paraffine embedded. Paraffin-embedded tumor sections of 3 μm in thickness were deparaffinised,and stained with Hematoxilin-Eosin. The antigen retrieval was done with a pressure cooker in citrate buffer at high pH (Dako, Glostrup, Denmark). Immunohistochemical study was done using an automatised system Dako OMNIS (Dako) with monoclonal antibodies: IDH1 R132H (clone H09, dilution 1/50, Dianova), ATRX (clone AX1, dilution 1/50, Dianova) and P53 (clone DO-7, prediluted, Dako). Only nuclear staining with or without cytoplasmic staining in tumor cells was considered positive. Only the intense nuclear staining of IDH1 R132H with positive external control was considered as mutated pattern of IDH1 R132H. Only the complete loss of nuclear staining of ATRX with positive internal control was considered as mutated pattern of ATRX. Only the intense nuclear staining of p53 in >10% of tumoral cells with positive external control was considered as mutated pattern of p53. Molecular study was carried out using Oncomine Childhood ADN/ARN panel (ThermoFisher) and Easy PGX Ready IDH1-2 (Diatech Pharmacogenetics).

At time of this thesis writing, histopathological data from each habitat of 10 patients have been collected.

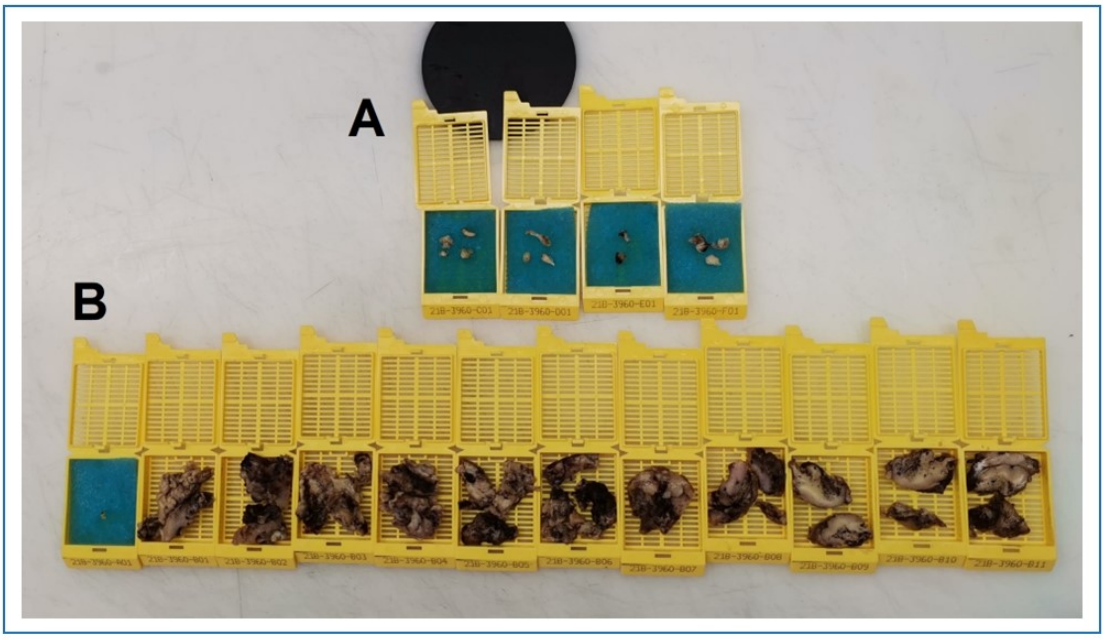

Figure 9.2. A) Samples collected from each tumor and edema habitat defined by the ONCOhabitats method during standard surgery. B) Resected astrocytoma grade 4.

Figure 9.3 includes an example of the main histopathologic features of each tumor and edema habitat defined by ONCOhabitats, and figure 9.4 shows some examples of stained slides viewed under the microscope. They show typical histopathologic features of grade 4 astrocytomas such as: MVP, endothelial glomeruloid hyperplasia, strong cellular atypia, and mitosis.

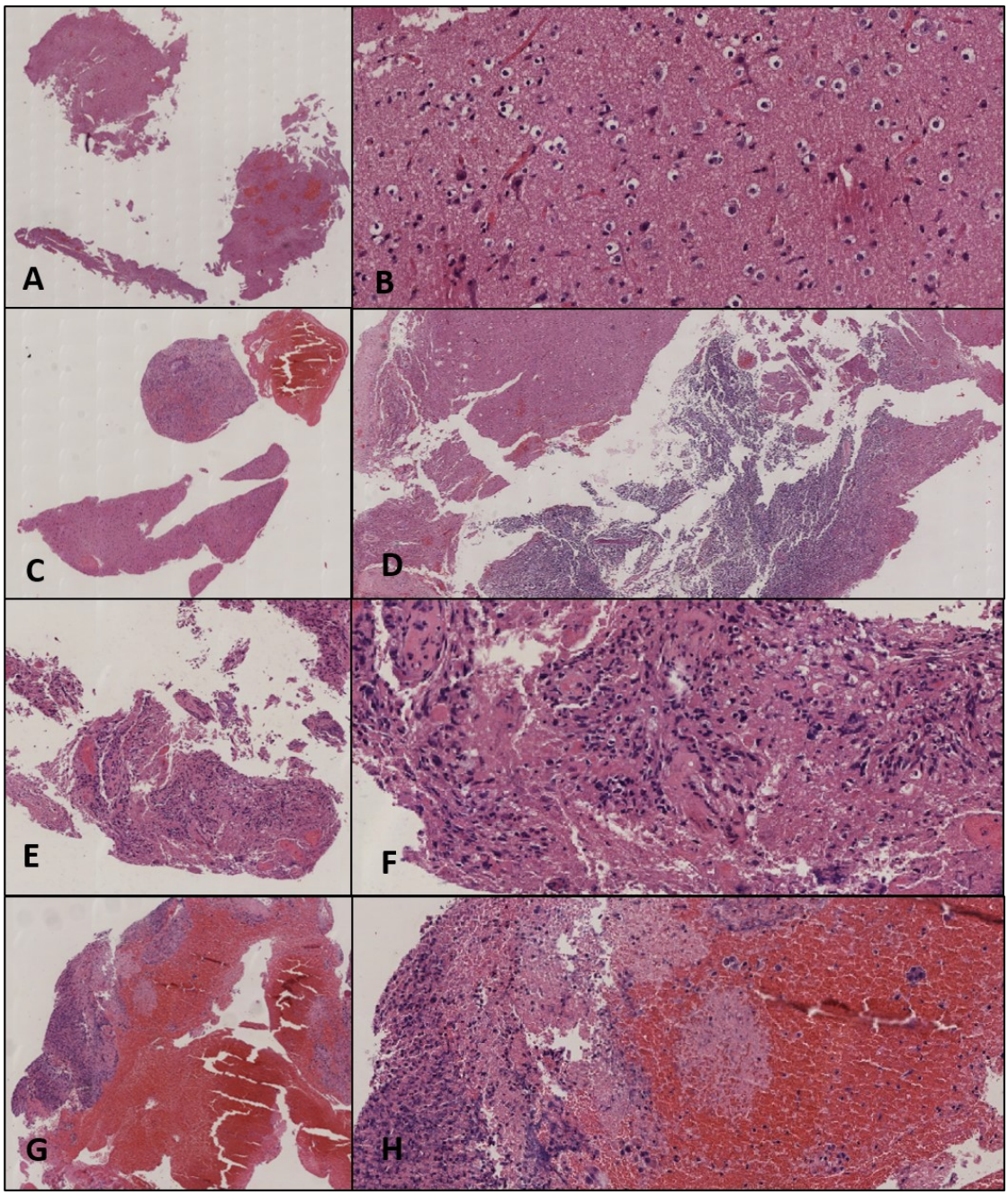

Figure 9.3. Histopathologic main features of different habitats. **A-B)** Vasogenic Peripheral Edema (VPE). Non tumor. Gliosis, oedema and haemorrhagia (HE, 10X, 100X). **C-D)** Infiltrated peripheral edema (IPE). 50% Healthy brain tissue and 50% astrocytoma (upper

area)(HE, 10X, 100X). **E-F)** High angiogenic Tumor (HAT). Highly cellular areas and hypervascularity (HE, 10X, 100X). **G-H)** Low Angiogenic Tumor (LAT). Necrosis and haemorrhagia with scantly neoplastic cells. (HE, 10X, 100X)

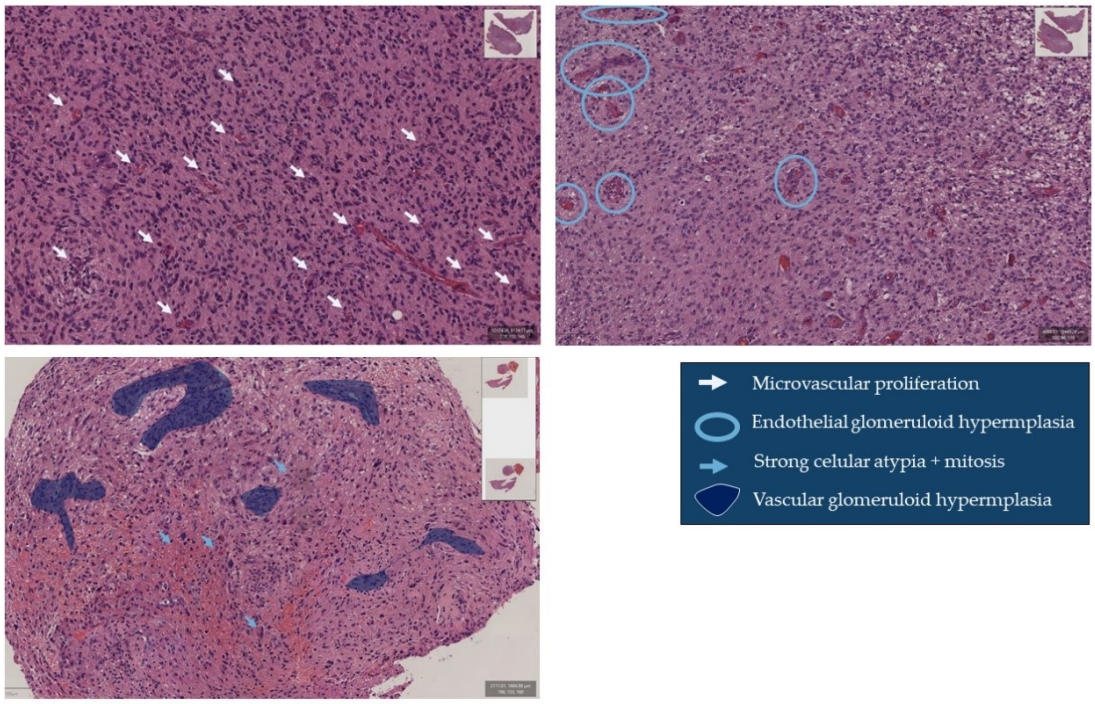

Figure 9.4. Stained slides from the samples of the vascular tumor and infiltrated peripheral edema habitats showing hallmarks of astrocytoma grade 4, including microvascular proliferation, endothelial and vascular glomerualoid hyperplasia, strong cellular atypia and mitosis.

9.1.7. Conclusions

The clinical protocol proposed by UPV in collaboration with two Spanish hospitals for sample collection of each habitat delineated with the ONCOhabitats method has been successfully implemented. Patient recruitment is still in process. Positive results of the histopathological and molecular analyses would allow the biologic confirmation and validation of the vascular habitats. In addition, this study has supposed the first time of the use of the ONCOhabitats method during surgeries.

9.2. Other clinical studies and datasets

Subsection 1.1.1 from chapter 1 of this thesis includes a brief description of the clinical studies coordinated by the BDSLab, as well as the collected datasets in

collaboration with other centers. Table 9.1 represents a summary of the main characteristics of each generated dataset.

At the time of writing this thesis, data have been collected from a total of 780 patients treated in 18 hospitals, and it is estimated that at the end of the two clinical studies that are in progress, the number will rise to more than 1,000.

Table 9.1. Main characteristics of each collected dataset during the thesis, including type of study, type of data, status, number of patients, coordinator, collaborating centers and derived publications.

	Type of study	Type of data	Status	# patients	Coordinator	Centers*
BIOhabitats	Multicenter, prospective, low-interventional	MRI, clinical, biological samples of each habitat	In proccess	(42) 70-100	BDSLab	Hospital Clinico de Valencia y Hospital 12 de Octubre
MTS4UP	Multicenter, retrospective, observational	MRI, clinical	Finished	305	BDSLab	7 European centers
ALBATROSS	Multicenter, prospective, observational	MRI, clinical	In proccess	(40) 200-250	BDSLab	7 European centers
GLIOCAT	Retrospective, observational	MRI, clinical, molecular	Finished	302	GLIOCAT	6 centers of Cataluña
Columbia U	Prospective, interventional	Clinical, genomic, transcriptomic	Finished	42	Columbia University	Columbia University and Northwestern University
GEINO-Mol	Single-center, observational	MRI, molecular	Finished	49	Hospital Universitario y Politecnico La Fe	Hospital Universitario y politecnico La Fe

*The number of patients indicated in those datasets that are in process is the expected at the end of the recruitment stage. *Numbers between brackets indicate the number of patients included at date of the writing of this chapter (April 2022).

Chapter 10
Concluding remarks and recommendations

This chapter summarizes the concluding remarks related with the defined research questions and the proposed specific objectives. In addition, in this chapter we provide a guideline with recommendations for continuing the scientific research based on this work.

10.1. Concluding remarks

Astrocytoma grade 4 still being one of the most lethal tumors mainly due to its extensive heterogeneity at intratumor, interpatient and temporal levels. The capability of non-invasive biomarkers to provide relevant information for tumor characterization, as well as to improve prognostic and treatment response models, is an invaluable aid in combating this devastating disease. This thesis has contributed to the state-of-the-art in Neuro-oncology, Medical Imaging, Histopathology and Molecular Biology. The scientific publications in top-ranked journals and international conferences derived from this thesis endorse the research carried out in these fields.

Part I. Tumor characterization and classification

CR1. MRI-DSC perfusion biomarkers calculated at vascular habitats from the presurgical stage can contribute to astrocytoma grade 4 classification, since they are associated with vascular structures derived from microvascular proliferation. It has been demonstrated the correlation between the MRI-DSC biomarkers with the presence, quantity and area of microvessels, structures typically characterized at histopathological level after tumor sample collection.

This concluding remark responds to the research question RQ1, covers the objective O1 and was derived from the work in publication P4 (chapter 3).

CR2. Glioblastoma *IDH*-wildtype and astrocytoma *IDH*-mutant grade 4 present different vascularity and can be differentiate using DSC-MRI

perfusion biomarkers calculated at vascular habitats from the presurgical stage. Differences in vascularity are also evident at transcriptomic level, being the following vascular genes overexpressed in glioblastoma *IDH*-wildtype: *EFEMP2*, *SLC2A10*, *MDK* and *TMBIM*. In addition, *BMP2* and *STOX1*, genes related with better outcomes were enriched in astrocytomas *IDH*-mutant grade 4. The studies conducted in Chapter 4 includes the results of analyzing the association between imaging biomarkers and *IDH* mutation, as well as the correlation with specific transcriptomic patterns according to the astrocytoma type.

This concluding remark responds to the research question RQ2, covers the objective O3 and was derived from the work in publications P5 and P9.

Part II. Patient prognosis and stratification

CR3. The association between MRI-DSC biomarkers calculated at vascular habitats from the presurgical stage with patient survival is robust at international and multicenter level. In addition, the MRI-DSC biomarkers are reproducible when using a multicenter setting with different clinical and MRI acquisition protocols. Chapter 5 includes the results derived from the main expected outcome of the MTS4UP multicenter clinical study (CS1).

This concluding remark responds to the research questions RQ3 and RQ4, covers the objectives O3 and O4 and was derived from the work in publications P2 and P6.

CR4. Tumor vascularity presents different influence on survival in long- and short-term survivors of astrocytoma grade 4. The MRI-DSC biomarkers are more clinically relevant for prognosis for long-term survivors with *IDH*-wildtype glioblastoma. The study conducted in Chapter 6 demonstrated the robust association between imaging biomarkers and survival in those patients with a survival longer than 400 days. However, this association between vascularity and patient survival was not found for short-term survivors, suggesting that other factors, such as molecular alterations or comorbid diseases, may be more relevant than tumor vascularity at early stages.

This concluding remark responds to the research question RQ5, covers the objective O4 and was derived from the work in publication P3.

Part III. Treatment response assessment

CR5. Patient response to Temozolomide treatment in terms of survival is influenced by tumor vascularity. Specific subgroups of patients with moderate vascularity and *MGMT* methylated would benefit most from extending TMZ treatment. In this sense, MRI-DSC biomarkers calculated from the presurgical stage have been shown as useful to characterize tumor vascularity and stratifying patients.

This concluding remark responds to the research question RQ6, covers the objective O5 and was derived from the works in publication P6, P7 and P8.

CR6. Easy-to-determine clinical and imaging features, such as the brain hemisphere in which the tumor is located, were proven helpful for selecting patients with astrocytoma grade 4 who can benefit from the immunotherapy with anti-PD-1.

This concluding remark responds to the research question RQ7, covers the objective O6 and was derived from the work included in chapter Ch9.

Part IV. Clinical studies implementation and datasets creation

CR7. It is feasible to design and implement a clinical protocol to validate biologically (molecular, cellular and histopathological levels) the four tumor and edema habitats defined by imaging with the HTS method.

CR8. The collection of retrospective and prospective data of different nature (MRI, clinical, molecular, histopathologic data) from a remarkable cohort of patients at international level is a challenging but feasible contribution. This allows the development of multidisciplinary preclinical studies for addressing complex problems including tumor characterization, patient prognosis and therapy selection.

Concluding remarks 7 and 8 respond to the research question RQ8, covers the objectives O8 and O9 and the associated results include datasets D1-D5.

Summarizing, clinical, molecular, and imaging biomarkers have been investigated in this thesis, concluding that they can present relevant applications for astrocytoma grade 4 characterization and classification, patient prognosis estimation and predicting treatment response. Understanding the high heterogeneity of these aggressive malignancies constitutes a key element in advancing the design of effective therapies, and therefore, in improve patient prognosis and quality of life. To continue the study and research of this neoplasm combining different

perspectives it essential, including its pathology, the underlying molecular and genetic processes, its immunology, and neuroimaging.

There have been no significant changes in the treatment of patients with these aggressive tumors in the last two decades. With the advances of this thesis, we offer tools easily applicable in the clinic that can contribute to change the paradigm of "one fits all" to a more personalized medicine strategy.

10.2. Recommendations and future directions

To help combat these aggressive brain tumors, it is needed to acquire a multimodal data-guided approach. Understanding its origin, evolution and heterogeneity requires analyzing a vast amount of complex multidisciplinary medical information derived from the tumor and the patient. Under this scenario, the progress to treat these lethal diseases lies in the development of integrated data models, with the final purpose of acquiring personalized and, consequently more effective, therapies for each patient. The proposed non-invasive biomarkers and the research findings performed in this thesis contributes significantly to the state-of-the-art in the research and clinical fields. In addition, it can support the development of future multimodal data integrated models. In this sense, the following recommendations are suggested and the future directions in the research of astrocytomas grade 4.

R1. It has been demonstrated the potential application of MRI-DSC biomarkers to support the estimation of the two first classification criteria from the presurgical stage: microvascular proliferation and *IDH* mutation. We encourage its use as a supporting tool for CNS tumor classification mainly for those inoperable tumors, and for the most complex and uncertain diagnoses.

R2. Specific genes related with vascular processes have been differentially enriched between glioblastoma *IDH*-wildtype and astrocytoma *IDH*-mutant grade 4. These specific transcriptomic profiles can explain differences in tumors progression velocities, survival times and therapy responses. Although it is needed deep analyses, these genes can be proposed as targets for specific novel therapies for each type of high-grade astrocytoma, as well as to select patients who benefit from antiangiogenics. Continue to deepen characterizing the intratumor heterogeneity of tumor and edema regions at multiple levels will allow a better understanding of the nature and evolution of these lethal tumors. For this purpose, the biological samples taken during the *BIOhabitats* study (presented in chapter 9) will be analyzed at the molecular level, both the genome and transcriptome, as well as at the histopathological level.

R3. Vascular architecture, processes and behavior strongly influences the progression velocity and aggressiveness of the astrocytoma, influencing patient survival. MRI-DSC biomarkers can measure underlying vascularity and can help estimating patient prognosis treated at different international centers.

This is a highly desirable property to conduct large cross-sectional multicenter studies, where the conclusions of the experiments must be extrapolable to the entire population. Therefore, we encourage to use these biomarkers to improve clinical prognostic models and to select patients for randomized studies, although future prospective studies are needed to validate its relevance for the clinical use.

R4. Tumor vascularity and genetic alterations, such as *MGMT* methylation, present different influence on patient survival over time. Clinical factors, including comorbid conditions or early deaths caused by treatment complications, could hide the effect of vascularity on survival in early stages, whereas in later tumor stages, vascularity seems to mark tumor behavior.

To acquire more accurate planification of patient follow-up and to predict tumor progression, it is needed to analyze in deep the temporal heterogeneity and evolution of these tumors. In this regard, we propose the MRI-DSC biomarkers to estimate influence over time using presurgical studies. In addition, they could be used as a potential target for randomized clinical trials that focused on patients considered as long survivors.

R5. The optimal number of cycles of temozolomide in the maintenance phase still being a matter of debate, being this number clearly variable in the clinical setting or even in the different trials. Predictive biomarkers would help to select a more personalized TMZ treatment for each patient. *MGMT* methylation is determinant for patient response, allowing a longer lasting effect of TMZ when this gene is methylated. However, this unique variable is not enough to select an optimal number of adjuvant cycles. We have demonstrated that lower tumor vascularity is an essential biomarker to allow an efficient effect of TMZ. We propose to use MRI-DSC biomarkers to acquire a more personalized TMZ treatment through the selection of the optimal number of cycles.

R6. Only a reduced proportion of patients with astrocytoma grade 4 respond to the PD1 inhibitor. Specific genomic and immune profiles have been discovered as associated with response. However, the economic cost, and the complexity of the methodologies, do not allow to implement in clinics at this time. In this sense, easy-to-determine characteristics associated with anti-PD-1 response could help to select patients who can benefit from this immunotherapy. The relevance of the

cerebral lateralization in immune and molecular processes on tumor progression has been demonstrated. These results must be validated in future studies. Positive results would imply that brain lateralization is key to improve models for selecting patients who benefit from this novel immunotherapy.

R7. The low prevalence of astrocytoma grade 4 makes challenging to collect a remarkable amount of data to analyze and perform scientific studies. In addition, it is almost impossible for individual research groups to analyze the different sources of information available for a patient, i.e. imaging, demographic data, electronic health records, molecular profiling, including genomic, transcriptomic and immune data, histopathologic data, etc. In this regard, we encourage research groups specialized in particular topics, making an effort to provide open data, as well as to collaborate and create robust international networks with complement expertise. Collaborative studies will facilitate the development of effective multimodal data integrated models to select personalized treatment for each patient with this lethal tumor.

Bibliography

1. Álvarez-Torres, M. D. M., Fuster-García, E., Balaña, C., Puig, J. & García-Gómez, J. M. Lack of benefit of extending temozolomide treatment in patients with high vascular glioblastoma with methylated mgmt. *Cancers (Basel)* **13**, (2021).

2. Álvarez-Torres, M. del M. *et al.* Robust association between vascular habitats and patient prognosis in glioblastoma: An international multicenter study. *Journal of Magnetic Resonance Imaging* **51**, 1478–1486 (2020).

3. Álvarez-Torres, M. del M. *et al.* Differential effect of vascularity between long- and short-term survivors with IDH1/2 wild-type glioblastoma. *NMR in Biomedicine* **34**, (2021).

4. Álvarez-Torres, M. del M. *et al.* Local detection of microvessels in IDH-wildtype glioblastoma using relative cerebral blood volume: an imaging marker useful for astrocytoma grade 4 classification. *BMC Cancer* **22**, (2022).

5. Fuster-Garcia, E. *et al.* MGMT methylation may benefit overall survival in patients with moderately vascularized glioblastomas. *European Radiology* **31**, 1738–1747 (2021).

6. Henriksen, O. M. *et al.* High-Grade Glioma Treatment Response Monitoring Biomarkers: A Position Statement on the Evidence Supporting the Use of Advanced MRI Techniques in the Clinic, and the Latest Bench-to-Bedside Developments. Part I: Perfusion and Diffusion Techniques. *Frontiers in Oncology* **12**, (2022).

7. Booth, T. C. *et al.* High-Grade Glioma Treatment Response Monitoring Biomarkers: A Position Statement on the Evidence Supporting the Use of Advanced MRI Techniques in the Clinic, and the Latest Bench-to-Bedside Developments. Part 2: Spectroscopy, Chemical Exchange Saturation, Multiparametric Imaging, and Radiomics. *Frontiers in Oncology* **11**, (2022).

8. Chelebian, E., Fuster-Garcia, E., Álvarez-Torres, M. del M., Juan-Albarracín, J. & García-Gómez, J. M. Higher vascularity at infiltrated peripheral edema differentiates proneural glioblastoma subtype. *PLOS ONE* **15**, e0232500 (2020).

9. Stoyanov, G. S. & Dzhenkov, D. L. On the Concepts and History of Glioblastoma Multiforme - Morphology, Genetics and Epigenetics. *Folia Med (Plovdiv)* **60**, 48–66 (2018).

10. Louis, D. N. *et al.* The 2021 WHO classification of tumors of the central nervous system: A summary. *Neuro-Oncology* **23**, 1231–1251 (2021).

11. Louis, D. N. *et al.* The 2016 World Health Organization Classification of Tumors of the Central Nervous System: a summary. *Acta Neuropathologica* vol. 131 803–820 Preprint at https://doi.org/10.1007/s00401-016-1545-1 (2016).

12. Tamimi, A. & Juweid, M. *Glioblastoma*. (Codon Publications, 2017). doi:10.15586/codon.glioblastoma.2017.

13. Crocetti, E. *et al.* Epidemiology of glial and non-glial brain tumours in Europe. *European Journal of Cancer* **48**, 1532–1542 (2012).

14. Gladson, C. L., Prayson, R. A. & Liu, W. M. The pathobiology of glioma tumors. *Annual Review of Pathology: Mechanisms of Disease* vol. 5 33–50 Preprint at https://doi.org/10.1146/annurev-pathol-121808-102109 (2010).

15. Aldape, K. *et al.* Glioma through the looking GLASS: Molecular evolution of diffuse gliomas and the Glioma Longitudinal Analysis Consortium. *Neuro-Oncology* **20**, 873–884 (2018).

16. Brennan, C. W. *et al.* The somatic genomic landscape of glioblastoma. *Cell* **155**, 462 (2013).

17. McLendon, R. *et al.* Comprehensive genomic characterization defines human glioblastoma genes and core pathways. *Nature* **455**, 1061–1068 (2008).

18. Ceccarelli, M. *et al.* Molecular Profiling Reveals Biologically Discrete Subsets and Pathways of Progression in Diffuse Glioma. *Cell* **164**, 550–563 (2016).

19. Stupp, R. *et al. Radiotherapy plus Concomitant and Adjuvant Temozolomide for Glioblastoma*. www.nejm.org.

20. Han, S. *et al.* IDH mutation in glioma: molecular mechanisms and potential therapeutic targets. *British Journal of Cancer* vol. 122 1580–1589 Preprint at https://doi.org/10.1038/s41416-020-0814-x (2020).

21. Badur, M. G. *et al.* Oncogenic R132 IDH1 Mutations Limit NADPH for De Novo Lipogenesis through (D)2-Hydroxyglutarate Production in Fibrosarcoma Sells. *Cell Reports* **25**, 1018-1026.e4 (2018).

22. Dang, L. *et al.* Cancer-associated IDH1 mutations produce 2-hydroxyglutarate. *Nature* **462**, 739–744 (2009).

23. Ward, P. S. *et al.* The Common Feature of Leukemia-Associated IDH1 and IDH2 Mutations Is a Neomorphic Enzyme Activity Converting α-Ketoglutarate to 2-Hydroxyglutarate. *Cancer Cell* **17**, 225–234 (2010).

24. Das, S. & Marsden, P. A. Angiogenesis in Glioblastoma. *New England Journal of Medicine* **369**, 1561–1563 (2013).

25. Weis, S. M. & Cheresh, D. A. Tumor angiogenesis: Molecular pathways and therapeutic targets. *Nature Medicine* vol. 17 1359–1370 Preprint at https://doi.org/10.1038/nm.2537 (2011).

26. Soeda, A. *et al.* The evidence of glioblastoma heterogeneity. *Scientific Reports* **5**, 7979 (2015).

27. Hu, L. S., Hawkins-Daarud, A., Wang, L., Li, J. & Swanson, K. R. Imaging of intratumoral heterogeneity in high-grade glioma. *Cancer Letters* vol. 477 97–106 Preprint at https://doi.org/10.1016/j.canlet.2020.02.025 (2020).

28. Becker, A. P., Sells, B. E., Jaharul Haque, S. & Chakravarti, A. Tumor heterogeneity in glioblastomas: From light microscopy to molecular pathology. *Cancers* vol. 13 1–25 Preprint at https://doi.org/10.3390/cancers13040761 (2021).

29. LemCrossed D Sign©e, J. M., Clavreul, A. & Menei, P. Intratumoral heterogeneity in glioblastoma: Don't forget the peritumoral brain zone. *Neuro-Oncology* **17**, 1322–1332 (2015).

30. Patel, A. P. *et al.* Single-cell RNA-seq highlights intratumoral heterogeneity in primary glioblastoma. *Science (1979)* **344**, 1396–1401 (2014).

31. Comba, A. *et al.* Uncovering Spatiotemporal Heterogeneity of High-Grade Gliomas: From Disease Biology to Therapeutic Implications. *Frontiers in Oncology* vol. 11 Preprint at https://doi.org/10.3389/fonc.2021.703764 (2021).

32. Akbari, H. *et al.* Pattern analysis of dynamic susceptibility contrast-enhanced MR imaging demonstrates peritumoral tissue heterogeneity. *Radiology* **273**, 502–510 (2014).

33. Palpan Flores, A. *et al.* Assessment of Pre-operative Measurements of Tumor Size by MRI Methods as Survival Predictors in Wild Type IDH Glioblastoma. *Frontiers in Oncology* **10**, (2020).

34. Henker, C., Kriesen, T., Glass, Ä., Schneider, B. & Piek, J. Volumetric quantification of glioblastoma: experiences with different measurement techniques and impact on survival. *Journal of Neuro-Oncology* **135**, 391–402 (2017).

35. Iliadis, G. *et al.* Volumetric and MGMT parameters in glioblastoma patients: Survival analysis. *BMC Cancer* **12**, (2012).

36. Schoenegger, K. *et al.* Peritumoral edema on MRI at initial diagnosis: An independent prognostic factor for glioblastoma? *European Journal of Neurology* **16**, 874–878 (2009).

37. Wu, C. X. *et al.* Peritumoral edema on magnetic resonance imaging predicts a poor clinical outcome in malignant glioma. *Oncology Letters* **10**, 2769–2776 (2015).

38. Simpson, J. R. *et al.* ??*Clinical Original Contribution INFLUENCE OF LOCATION AND EXTENT OF SURGICAL RESEaION ON SURVIVAL OF PATIENTS WITH GLIOBLASTOMA MULTIFORME: RESULTS OF THREE CONSECUTIVE RADIATION THERAPY ONCOLOGY GROUP (RTOG) CLINICAL TRIALS*. *Radumon Oncology Biol Phys* vol. 26 (1993).

39. Larjavaara, S. *et al.* Incidence of gliomas by anatomic location. *Neuro-Oncology* **9**, 319–325 (2007).

40. Jeremic, B. *et al. Influence of extent of surgery and tumor location on treatment outcome of patients with glioblastoma multiforme treated with combined modality approach*. *Journal of Neuro-Oncology* vol. 21 (1994).

41. Peters, O., Gnekow, A. K., Rating, D. & Wolff, J. E. A. Impact of location on outcome in children with low-grade oligodendroglioma. *Pediatric Blood and Cancer* **43**, 250–256 (2004).

42. Gempt, J. *et al.* Factors influencing neurocognitive function in patients with neuroepithelial tumors. *Scientific Reports* **7**, (2017).

43. Baumann, C. *et al.* Delay in diagnosing patients with right-sided glioblastoma induced by hemispheric-specific clinical presentation. *Journal of Neuro-Oncology* **146**, 63–69 (2020).

44. de Palma, M., Biziato, D. & Petrova, T. v. Microenvironmental regulation of tumour angiogenesis. *Nature Reviews Cancer* vol. 17 457–474 Preprint at https://doi.org/10.1038/nrc.2017.51 (2017).

45. Gerstner, E. R. *et al.* Antiangiogenic agents for the treatment of glioblastoma. *Expert Opinion on Investigational Drugs* vol. 16 1895–1908 Preprint at https://doi.org/10.1517/13543784.16.12.1895 (2007).

46. Mahase, S. *et al.* Hypoxia-Mediated Mechanisms Associated with Antiangiogenic Treatment Resistance in Glioblastomas. *American Journal of Pathology* vol. 187 940–953 Preprint at https://doi.org/10.1016/j.ajpath.2017.01.010 (2017).

47. Huang, W. J., Chen, W. W. & Zhang, X. Glioblastoma multiforme: Effect of hypoxia and hypoxia inducible factors on therapeutic approaches (review). *Oncology Letters* vol. 12 2283–2288 Preprint at https://doi.org/10.3892/ol.2016.4952 (2016).

48. Xue, W. *et al.* Aberrant glioblastoma neovascularization patterns and their correlation with DCE-MRI-derived parameters following temozolomide and bevacizumab treatment. *Scientific Reports* **7**, (2017).

49. Heddleston, J. M., Li, Z., Hjelmeland, A. B. & Rich, J. N. *The Hypoxic Microenvironment Maintains Glioblastoma Stem Cells and Promotes Reprogramming towards a Cancer Stem Cell Phenotype*.

50. Dimberg, A. The glioblastoma vasculature as a target for cancer therapy. *Biochemical Society Transactions* **42**, 1647–1652 (2014).

51. Hanahan, D. & Weinberg, R. A. Hallmarks of cancer: The next generation. *Cell* vol. 144 646–674 Preprint at https://doi.org/10.1016/j.cell.2011.02.013 (2011).

52. Kim, J. *et al.* Spatiotemporal Evolution of the Primary Glioblastoma Genome. *Cancer Cell* **28**, 318–328 (2015).

53. Garrett, A. M., Lastakchi, S. & McConville, C. The personalisation of glioblastoma treatment using whole exome sequencing: A pilot study. *Genes (Basel)* **11**, (2020).

54. Ülgen, E. *et al.* Sequential filtering for clinically relevant variants as a method for clinical interpretation of whole exome sequencing findings in glioma. *BMC Medical Genomics* **14**, (2021).

55. Tsimberidou, A. M., Fountzilas, E., Bleris, L. & Kurzrock, R. Transcriptomics and solid tumors: The next frontier in precision cancer medicine. *Seminars in Cancer Biology* (2020) doi:10.1016/j.semcancer.2020.09.007.

56. Reed, M. R. *et al.* A functional precision medicine pipeline combines comparative transcriptomics and tumor organoid modeling to identify bespoke treatment strategies for glioblastoma. *Cells* **10**, (2021).

57. van Timmeren, J. E., Cester, D., Tanadini-Lang, S., Alkadhi, H. & Baessler, B. Radiomics in medical imaging—"how-to" guide and critical reflection. *Insights into Imaging* vol. 11 Preprint at https://doi.org/10.1186/s13244-020-00887-2 (2020).

58. Chaddad, A. *et al.* Radiomics in glioblastoma: Current status and challenges facing clinical implementation. *Frontiers in Oncology* vol. 9 Preprint at https://doi.org/10.3389/fonc.2019.00374 (2019).

59. Aftab, K. *et al.* Radiomics for precision medicine in glioblastoma. *Journal of Neuro-Oncology* vol. 156 217–231 Preprint at https://doi.org/10.1007/s11060-021-03933-1 (2022).

60. Sun, R. *et al.* A radiomics approach to assess tumour-infiltrating CD8 cells and response to anti-PD-1 or anti-PD-L1 immunotherapy: an imaging biomarker, retrospective multicohort study. *The Lancet Oncology* **19**, 1180–1191 (2018).

61. Pope, W. B. & Brandal, G. Conventional and advanced magnetic resonance imaging in patients with high-grade glioma. *Quarterly Journal of Nuclear Medicine and Molecular Imaging* vol. 62 239–253 Preprint at https://doi.org/10.23736/S1824-4785.18.03086-8 (2018).

62. Tofts, Paul. *Quantitative MRI of the brain : measuring changes caused by disease*. (Wiley, 2003).

63. Duda, R. O. & Hart, P. E. *PATTERN CLASSIFICATION AND SCENE ANALYSIS*.

64. Gonzalez, R. C., Woods, R. E. & Prentice Hall, P. *Digital Image Processing Third Edition Pearson International Edition prepared by Pearson Education*.

65. *of their individual structures for total intracranial volume (Kesslak et al*.

66. Despotović, I., Goossens, B. & Philips, W. MRI segmentation of the human brain: Challenges, methods, and applications. *Computational and Mathematical Methods in Medicine* vol. 2015 Preprint at https://doi.org/10.1155/2015/450341 (2015).

67. Juan-Albarracín, J., Fuster-Garcia, E., García-Ferrando, G. A. & García-Gómez, J. M. ONCOhabitats: A system for glioblastoma heterogeneity assessment through MRI. *International Journal of Medical Informatics* **128**, 53–61 (2019).

68. Juan-Albarracín, J. *et al.* Glioblastoma: Vascular Habitats Detected at Preoperative Dynamic Susceptibility-weighted Contrast-enhanced Perfusion MR Imaging Predict Survival. *Radiology* **287**, 944–954 (2018).

69. Mangla, R. *et al.* Changes in relative cerebral blood volume 1 month after radiation-temozolomide therapy can help predict overall survival in patients with glioblastoma. *Radiology* **256**, 575–584 (2010).

70. Jain, R. *et al.* Outcome prediction in patients with glioblastoma by using imaging, clinical, and genomic biomarkers: Focus on the nonenhancing component of the tumor. *Radiology* **272**, 484–493 (2014).

71. Lev, M. H. *et al. Glial Tumor Grading and Outcome Prediction Using Dynamic Spin-Echo MR Susceptibility Mapping Compared with Conventional Contrast-Enhanced MR: Confounding Effect of Elevated rCBV of Oligodendroglimoas*. http://xray.bsd.uchicago.

72. Cha, S. *et al.* Dynamic, contrast-enhanced perfusion MRI in mouse gliomas: Correlation with histopathology. *Magnetic Resonance in Medicine* **49**, 848–855 (2003).

73. Cagney, D. N. *et al.* The FDA NIH Biomarkers, EndpointS, and other Tools (BEST) resource in neuro-oncology. *Neuro-Oncology* **20**, 1162–1172 (2018).

74. Wen, P. Y. *et al.* Updated response assessment criteria for high-grade gliomas: Response assessment in neuro-oncology working group. *Journal of Clinical Oncology* vol. 28 1963–1972 Preprint at https://doi.org/10.1200/JCO.2009.26.3541 (2010).

75. Booth, T. C. *et al.* A Position Statement on the Utility of Interval Imaging in Standard of Care Brain Tumour Management: Defining the Evidence Gap and Opportunities for

Future Research. *Frontiers in Oncology* vol. 11 Preprint at https://doi.org/10.3389/fonc.2021.620070 (2021).

76. Ellingson, B. M. *et al.* Baseline pretreatment contrast enhancing tumor volume including central necrosis is a prognostic factor in recurrent glioblastoma: Evidence from single- and multicenter trials. *Neuro-Oncology* **19**, 89–98 (2017).

77. Patel, P. *et al.* MR perfusion-weighted imaging in the evaluation of high-grade gliomas after treatment: A systematic review and meta-analysis. *Neuro-Oncology* vol. 19 118–127 Preprint at https://doi.org/10.1093/neuonc/now148 (2017).

78. Schmainda, K. M. *et al.* Multisite concordance of DSC-MRI analysis for brain tumors: Results of a National Cancer Institute Quantitative Imaging Network Collaborative Project. *American Journal of Neuroradiology* **39**, 1008–1016 (2018).

79. Hu, L. S. *et al.* Correlations between perfusion MR imaging cerebral blood volume, microvessel quantification, and clinical outcome using stereotactic analysis in recurrent high-grade glioma. *American Journal of Neuroradiology* **33**, 69–76 (2012).

80. Prah, M. A. *et al.* Spatial discrimination of glioblastoma and treatment effect with histologically-validated perfusion and diffusion magnetic resonance imaging metrics. *Journal of Neuro-Oncology* **136**, 13–21 (2018).

81. Connelly, J. M. *et al.* Magnetic Resonance Imaging Mapping of Brain Tumor Burden: Clinical Implications for Neurosurgical Management: Case Report. *Neurosurgery Open* **2**, (2021).

82. Iv, M. *et al.* Perfusion MRI-based fractional tumor burden differentiates between tumor and treatment effect in recurrent glioblastomas and informs clinical decision-making. *American Journal of Neuroradiology* **40**, 1649–1657 (2019).

83. Hoxworth, J. M. *et al.* Performance of standardized relative CBV for quantifying regional histologic tumor burden in recurrent high-grade glioma: Comparison against normalized relative CBV using image-localized stereotactic biopsies. *American Journal of Neuroradiology* **41**, 408–415 (2020).

84. Can, T. Introduction to Bioinformatics. in *miRNomics: MicroRNA Biology and Computational Analysis* (ed. Yousef Malik and Allmer, J.) 51–71 (Humana Press, 2014). doi:10.1007/978-1-62703-748-8_4.

85. Bashiardes, S. *et al. PROTOCOL PUBLISHED IN ASSOCIATION WITH COLD SPRING HARBOR LABORATORY Direct genomic selection*. *NATURE METHODS* | vol. 2 http://www.nature.com/naturemethods (2005).

86. McLendon, R. *et al.* Comprehensive genomic characterization defines human glioblastoma genes and core pathways. *Nature* **455**, 1061–1068 (2008).

87. Ng, K., Kim, R., Kesari, S., Carter, B. & Chen, C. C. Genomic profiling of glioblastoma: Convergence of fundamental biologic tenets and novel insights. *Journal of Neuro-Oncology* vol. 107 1–12 Preprint at https://doi.org/10.1007/s11060-011-0714-2 (2012).

88. Tang, J., He, D., Yang, P., He, J. & Zhang, Y. Genome-wide expression profiling of glioblastoma using a large combined cohort. *Scientific Reports* **8**, (2018).

89. Chu, Y. & Corey, D. R. RNA sequencing: Platform selection, experimental design, and data interpretation. *Nucleic Acid Therapeutics* **22**, 271–274 (2012).

90. Verhaak, R. G. W. *et al.* Integrated Genomic Analysis Identifies Clinically Relevant Subtypes of Glioblastoma Characterized by Abnormalities in PDGFRA, IDH1, EGFR, and NF1. *Cancer Cell* **17**, 98–110 (2010).

91. Park, J. *et al.* Transcriptome profiling-based identification of prognostic subtypes and multi-omics signatures of glioblastoma. *Scientific Reports* **9**, (2019).

92. Yin, W. *et al.* Expression profile analysis identifies a novel five-gene signature to improve prognosis prediction of glioblastoma. *Frontiers in Genetics* **10**, (2019).

93. Cao, M. *et al.* A four-gene signature-derived risk score for glioblastoma: prospects for prognostic and response predictive analyses. *Cancer Biology and Medicine* **16**, 595–605 (2019).

94. Zhao, J. *et al.* Immune and genomic correlates of response to anti-PD-1 immunotherapy in glioblastoma. *Nature Medicine* **25**, 462–469 (2019).

95. Clark, T. G., Bradburn, M. J., Love, S. B. & Altman, D. G. Survival Analysis Part I: Basic concepts and first analyses. *British Journal of Cancer* vol. 89 232–238 Preprint at https://doi.org/10.1038/sj.bjc.6601118 (2003).

96. Emmerson, J. & Brown, J. M. Understanding Survival Analysis in Clinical Trials. *Clinical Oncology* vol. 33 12–14 Preprint at https://doi.org/10.1016/j.clon.2020.07.014 (2021).

97. Cox, D. R. Regression Models and Life-Tables. *Journal of the Royal Statistical Society: Series B (Methodological)* **34**, 187–202 (1972).

98. Louis, D. N. *et al.* cIMPACT-NOW update 6: new entity and diagnostic principle recommendations of the cIMPACT-Utrecht meeting on future CNS tumor classification and grading. *Brain Pathology* **30**, 844–856 (2020).

99. Wu, H. *et al.* Vascular habitat analysis based on dynamic susceptibility contrast perfusion MRI predicts IDH mutation status and prognosis in high-grade gliomas. *European Radiology* **30**, 3254–3265 (2020).

100. Ziyad, S. & Iruela-Arispe, M. L. Molecular Mechanisms of Tumor Angiogenesis. *Genes and Cancer* **2**, 1085–1096 (2011).

101. Ling, C. *et al.* Endothelial cell hypertrophy and microvascular proliferation in meningiomas are correlated with higher histological grade and shorter progression-free survival. *Journal of Neuropathology and Experimental Neurology* **75**, 1160–1170 (2016).

102. Sharma, S., Sharma, M. C. & Sarkar, C. Morphology of angiogenesis in human cancer: A conceptual overview, histoprognostic perspective and significance of neoangiogenesis. *Histopathology* vol. 46 481–489 Preprint at https://doi.org/10.1111/j.1365-2559.2005.02142.x (2005).

103. Pathak, A. P. *et al.* MR-derived cerebral blood volume maps: Issues regarding histological validation and assessment of tumor angiogenesis. *Magnetic Resonance in Medicine* **46**, 735–747 (2001).

104. Chakhoyan, A. *et al.* Validation of vessel size imaging (VSI) in high-grade human gliomas using magnetic resonance imaging, image-guided biopsies, and quantitative immunohistochemistry. *Scientific Reports* **9**, (2019).

105. Sadeghi, N. *et al.* Apparent diffusion coefficient and cerebral blood volume in brain gliomas: Relation to tumor cell density and tumor microvessel density based on stereotactic biopsies. *American Journal of Neuroradiology* **29**, 476–482 (2008).

106. Liang1, L. & Ge1, Y. *Downloaded from www.ajronline.org by 62*. (1998).

107. Folkerth, R. D. *Histologic Measures of Angiogenesis in Human Primary Brain Tumors*. (2004).

108. Donahue, K. M. *et al.* Utility of simultaneously acquired gradient-echo and spin-echo cerebral blood volume and morphology maps in brain tumor patients. *Magnetic Resonance in Medicine* **43**, 845–853 (2000).

109. Li, X., Tang, Q., Yu, J., Wang, Y. & Shi, Z. Microvascularity detection and quantification in glioma: a novel deep-learning-based framework. *Laboratory Investigation* **99**, 1515–1526 (2019).

110. Hochberg, F. H. & Rosen, B. R. *Cerebral Blood Volume Maps of Gliomas: Comparison with Tumor Grade*.

111. Weibel ER. Estimation of basic Stereologic parameters: theoretical foundations of stereology. *Academic Press* **2**, (1980).

112. Essig, M. *et al.* Perfusion MRI: The five most frequently asked technical questions. *American Journal of Roentgenology* vol. 200 24–34 Preprint at https://doi.org/10.2214/AJR.12.9543 (2013).

113. Puchalski, R. B. *et al.* An anatomic transcriptional atlas of human glioblastoma. *Science (1979)* **360**, 660–663 (2018).

114. Boxerman, J. L., Schmainda, K. M. & Weisskoff, R. M. *Relative Cerebral Blood Volume Maps Corrected for Contrast Agent Extravasation Significantly Correlate with Glioma Tumor Grade, Whereas Uncorrected Maps Do Not*. www.ajnr.org.

115. Álvarez-Torres, M. del M., Chelebian, E., Fuster-Garcia, E., Juan-Albarracin, J. & García-Gómez, J. M. ONCOhabitats results for Ivy Glioblastoma Atlas Project (Ivy Gap): Segmentation and Hemodynamic Tissue Signature. Preprint at (2021).

116. Birner, P. *et al.* Vascular Patterns in Glioblastoma InfluenceClinical Outcome and Associate with Variable Expression of Angiogenic Proteins: Evidence for Distinct Angiogenic Subtypes. *Brain Pathology* **13**, 133–143 (2003).

117. Ohgaki, H. & Kleihues, P. The definition of primary and secondary glioblastoma. *Clinical Cancer Research* vol. 19 764–772 Preprint at https://doi.org/10.1158/1078-0432.CCR-12-3002 (2013).

118. Yan, H. *et al. IDH1 and IDH2 Mutations in Gliomas A bs tr ac t*. *N Engl J Med* vol. 360 (2009).

119. Mirchia, K. & Richardson, T. E. Beyond IDH-mutation: Emerging molecular diagnostic and prognostic features in adult diffuse gliomas. *Cancers* vol. 12 1–22 Preprint at https://doi.org/10.3390/cancers12071817 (2020).

120. Christians, A. *et al.* The prognostic role of IDH mutations in homogeneously treated patients with anaplastic astrocytomas and glioblastomas. *Acta Neuropathologica Communications* **7**, (2019).

121. Popovici-Muller, J. *et al.* Discovery of AG-120 (Ivosidenib): A First-in-Class Mutant IDH1 Inhibitor for the Treatment of IDH1 Mutant Cancers. *ACS Medicinal Chemistry Letters* **9**, 300–305 (2018).

122. Kaminska, B., Czapski, B., Guzik, R., Król, S. K. & Gielniewski, B. Consequences of IDH1/2 mutations in gliomas and an assessment of inhibitors targeting mutated IDH proteins. *Molecules* vol. 24 Preprint at https://doi.org/10.3390/molecules24050968 (2019).

123. Wu, H. *et al.* Vascular habitat analysis based on dynamic susceptibility contrast perfusion MRI predicts IDH mutation status and prognosis in high-grade gliomas. *European Radiology* **30**, 3254–3265 (2020).

124. Robinson, M. D., McCarthy, D. J. & Smyth, G. K. edgeR: A Bioconductor package for differential expression analysis of digital gene expression data. *Bioinformatics* **26**, 139–140 (2009).

125. Carbon, S. *et al.* The Gene Ontology resource: Enriching a GOld mine. *Nucleic Acids Research* **49**, D325–D334 (2021).

126. Ashburner, M. *et al. Gene Ontology: tool for the unification of biology The Gene Ontology Consortium**. http://www.flybase.bio.indiana.edu (2000).

127. Korotkevich, G. *et al.* Fast gene set enrichment analysis. doi:10.1101/060012.

128. Sawlani, R. N. *et al.* Glioblastoma: A method for predicting response to antiangiogenic chemotherapy by using MR perfusion imaging - Pilot study. *Radiology* **255**, 622–628 (2010).

129. Wang, L. *et al.* EFEMP2 is upregulated in gliomas and promotes glioma cell proliferation and invasion. *Int J Clin Exp Pathol* **8**, (2015).

130. Cheng, C. H. *et al.* Mutations in the SLC2A10 gene cause arterial abnormalities in mice. *Cardiovascular Research* **81**, 381–388 (2009).

131. Filippou, P. S., Karagiannis, G. S. & Constantinidou, A. Midkine (MDK) growth factor: a key player in cancer progression and a promising therapeutic target. *Oncogene* vol. 39 2040–2054 Preprint at https://doi.org/10.1038/s41388-019-1124-8 (2020).

132. Gao, L. *et al.* TMBIM1 promotes EMT by stimulating autophagic degradation of E-cadherin via AMPK/mTOR/ULK1 axis in human gliomas. (2022) doi:10.21203/rs.3.rs-1403508/v2.

133. Zhou, K. *et al.* A new glioma grading model based on histopathology and Bone Morphogenetic Protein 2 mRNA expression. *Scientific Reports* **10**, (2020).

134. Jin, F. Q., Jin, L. & Wang, Y. L. Downregulation of STOX1 is a novel prognostic biomarker for glioma patients. *Open Life Sciences* **16**, 1164–1174 (2021).

135. Gately, L., McLachlan, S., Dowling, A. & Philip, J. Life beyond a diagnosis of glioblastoma: a systematic review of the literature. *Journal of Cancer Survivorship* vol. 11 447–452 Preprint at https://doi.org/10.1007/s11764-017-0602-7 (2017).

136. Bae, S. *et al.* Radiomic MRI phenotyping of glioblastoma: Improving survival prediction. *Radiology* **289**, 797–806 (2018).

137. Jensen, R. L. *et al.* Preoperative dynamic contrast-enhanced MRI correlates with molecular markers of hypoxia and vascularity in specific areas of intratumoral microenvironment and is predictive of patient outcome. *Neuro-Oncology* **16**, 280–291 (2014).

138. Demerath, T. *et al.* Mesoscopic imaging of glioblastomas: Are diffusion, perfusion and spectroscopic measures influenced by the radiogenetic phenotype? *Neuroradiology Journal* **30**, 36–47 (2017).

139. Jena, A. *et al.* Glioma recurrence versus radiation necrosis single-session multiparametric approach using simultaneous O-(2-18F-fluoroethyl)-L-tyrosine PET/MRI. *Clinical Nuclear Medicine* **41**, e228–e236 (2016).

140. Price, S. J. *et al.* Multimodal MRI can identify perfusion and metabolic changes in the invasive margin of glioblastomas. *Journal of Magnetic Resonance Imaging* **43**, 487–494 (2016).

141. Chang, Y. C. C. *et al.* Delineation of Tumor Habitats based on Dynamic Contrast Enhanced MRI. *Scientific Reports* **7**, (2017).

142. Cui, Y. *et al.* Prognostic imaging biomarkers in glioblastoma: Development and independent validation on the basis of multiregion and quantitative analysis of MR images. *Radiology* **278**, 546–553 (2016).

143. Fuster-Garcia, E. *et al.* Improving the estimation of prognosis for glioblastoma patients by MR based hemodynamic tissue signatures. *NMR in Biomedicine* **31**, (2018).

144. Abramson, R. G. *et al.* Methods and Challenges in Quantitative Imaging Biomarker Development. *Academic Radiology* vol. 22 25–32 Preprint at https://doi.org/10.1016/j.acra.2014.09.001 (2015).

145. O'Connor, J. P. B. *et al.* Imaging biomarker roadmap for cancer studies. *Nature Reviews Clinical Oncology* **14**, 169–186 (2017).

146. Wetzel, S. G. *et al.* Relative cerebral blood volume measurements in intracranial mass lesions: Interobserver and intraobserver reproducibility study. *Radiology* **224**, 797–803 (2002).

147. Schnack, H. G. *et al.* Reliability of brain volumes from multicenter MRI acquisition: A calibration study. *Human Brain Mapping* **22**, 312–320 (2004).

148. de Guio, F. *et al.* Reproducibility and variability of quantitative magnetic resonance imaging markers in cerebral small vessel disease. *Journal of Cerebral Blood Flow and Metabolism* vol. 36 1319–1337 Preprint at https://doi.org/10.1177/0271678X16647396 (2016).

149. Liu, T. T. *et al.* Magnetic resonance perfusion image features uncover an angiogenic subgroup of glioblastoma patients with poor survival and better response to antiangiogenic treatment. *Neuro-Oncology* **19**, 997–1007 (2017).

150. Hirai, T. *et al.* Prognostic value of perfusion MR imaging of high-grade astrocytomas: Long-term follow-up study. *American Journal of Neuroradiology* **29**, 1505–1510 (2008).

151. Hambardzumyan, D. & Bergers, G. Glioblastoma: Defining Tumor Niches. *Trends in Cancer* vol. 1 252–265 Preprint at https://doi.org/10.1016/j.trecan.2015.10.009 (2015).

152. Artzi, M. *et al.* Differentiation between vasogenic-edema versus tumor-infiltrative area in patients with glioblastoma during bevacizumab therapy: A longitudinal MRI study. *European Journal of Radiology* **83**, 1250–1256 (2014).

153. Verhaak, R. G. W. *et al.* Integrated Genomic Analysis Identifies Clinically Relevant Subtypes of Glioblastoma Characterized by Abnormalities in PDGFRA, IDH1, EGFR, and NF1. *Cancer Cell* **17**, 98–110 (2010).

154. Ostrom, Q. T. *et al.* CBTRUS Statistical Report: Primary brain and other central nervous system tumors diagnosed in the United States in 2010-2014. *Neuro Oncol* **19**, v1–v88 (2017).

155. Burgenske, D. M. *et al.* Molecular Profiling of Long-Term IDH-wildtype Glioblastoma Survivors. doi:10.1093/neuonc/noz129/5539012.

156. Kong, X. *et al.* CD34 over-expression is associated with gliomas' higher WHO grade. *Medicine (United States)* vol. 95 e2830 Preprint at https://doi.org/10.1097/MD.0000000000002830 (2016).

157. Michaelsen, S. R. *et al.* Molecular profiling of short-term and long-term surviving patients identifies CD34 mRNA level as prognostic for glioblastoma survival. *Journal of Neuro-Oncology* **137**, 533–542 (2018).

158. Krex, D. *et al.* Long-term survival with glioblastoma multiforme. *Brain* **130**, 2596–2606 (2007).

159. Costa, E. *et al.* Long-term survival after glioblastoma resection: hope despite poor prognosis factors. *Journal of Neurosurgical Sciences* **63**, (2019).

160. Walid, M. S. *Prognostic Factors for Long-Term Survival after Glioblastoma*. *The Permanente Journal/ Fall* vol. 12 www.emedicine. (2008).

161. Stringfield, O. *et al.* Multiparameter mri predictors of long-term survival in glioblastoma multiforme. *Tomography* **5**, 135–144 (2019).

162. Zhou, M. *et al.* Radiologically defined ecological dynamics and clinical outcomes in glioblastoma multiforme: Preliminary results. *Translational Oncology* **7**, 5–13 (2014).

163. Bian, Y. *et al.* Effect of radiochemotherapy on the cognitive function and diffusion tensor and perfusion weighted imaging for high-grade gliomas: A prospective study. *Scientific Reports* **9**, (2019).

164. Saini, J. *et al.* Comparative evaluation of cerebral gliomas using rCBV measurements during sequential acquisition of T1-perfusion and T2-perfusion MRI. *PLoS ONE* **14**, (2019).

165. Scheike, T. H., Zhang, M.-J. & Shang, M.-J. *Board of the Foundation of the Scandinavian Journal of Statistics An Additive-Multiplicative Cox-Aalen Regression Model*. *Source: Scandinavian Journal of Statistics* vol. 29 (2002).

166. Fisher, J. L., Palmisano, S., Schwartzbaum, J. A., Svensson, T. & Lönn, S. Comorbid conditions associated with glioblastoma. *Journal of Neuro-Oncology* **116**, 585–591 (2014).

167. Field, K. M., Rosenthal, M. A., Yilmaz, M., Tacey, M. & Drummond, K. Comparison between poor and long-term survivors with glioblastoma: Review of an Australian dataset. *Asia-Pacific Journal of Clinical Oncology* **10**, 153–161 (2014).

168. Mansouri, A. *et al.* MGMT promoter methylation status testing to guide therapy for glioblastoma: Refining the approach based on emerging evidence and current challenges. *Neuro-Oncology* **21**, 167–178 (2019).

169. Eckel-Passow, J. E. *et al.* Glioma Groups Based on 1p/19q, IDH , and TERT Promoter Mutations in Tumors . *New England Journal of Medicine* **372**, 2499–2508 (2015).

170. Killela, P. J. *et al. Mutations in IDH1, IDH2, and in the TERT promoter define clinically distinct subgroups of adult malignant gliomas*. *Oncotarget* vol. 5 www.impactjournals.com/oncotarget/.

171. Phillips, H. S. *et al.* Molecular subclasses of high-grade glioma predict prognosis, delineate a pattern of disease progression, and resemble stages in neurogenesis. *Cancer Cell* **9**, 157–173 (2006).

172. Liu, S. *et al.* Molecular and clinical characterization of CD163 expression via large-scale analysis in glioma. *OncoImmunology* **8**, (2019).

173. Kong, Z. *et al.* Imaging biomarkers guided anti-angiogenic therapy for malignant gliomas. *NeuroImage: Clinical* vol. 20 51–60 Preprint at https://doi.org/10.1016/j.nicl.2018.07.001 (2018).

174. Perry, J. R. *et al.* Short-Course Radiation plus Temozolomide in Elderly Patients with Glioblastoma. *New England Journal of Medicine* **376**, 1027–1037 (2017).

175. Hegi, M. E. *et al. MGMT Gene Silencing and Benefit from Temozolomide in Glioblastoma*. www.nejm.org.

176. Balana, C. *et al.* A phase II randomized, multicenter, open-label trial of continuing adjuvant temozolomide beyond 6 cycles in patients with glioblastoma (GEINO 14-01). *Neuro-Oncology* **22**, 1851–1861 (2020).

177. Bhandari, M. *et al.* Comparative study of adjuvant temozolomide six cycles versus extended 12 cycles in newly diagnosed glioblastoma multiforme. *Journal of Clinical and Diagnostic Research* **11**, XC04–XC08 (2017).

178. Barnett, A. *et al.* Efficacy of Extended Adjuvant Temozolomide Cycle Duration in Newly Diagnosed Glioblastoma: Four-year experience of a single major tertiary care institution (P2.6-035). *Neurology* **92**, (2019).

179. Chen, S. & Visintini, S. SUMMARY WITH CRITICAL APPRAIS AL Extended Dosing of Adjuv ant Temozolomide in Adults with Newly D iagnosed High Grade Gliomas Authors.

180. Roldán Urgoiti, G. B., Singh, A. D. & Easaw, J. C. Extended adjuvant temozolomide for treatment of newly diagnosed glioblastoma multiforme. *Journal of Neuro-Oncology* **108**, 173–177 (2012).

181. Hirono, S. *et al.* Feasibility study of finalizing the extended adjuvant temozolomide based on methionine positron emission tomography (Met-PET) findings in patients with glioblastoma. *Scientific Reports* **9**, (2019).

182. Gilbert, M. R. *et al.* Dose-dense temozolomide for newly diagnosed glioblastoma: A randomized phase III clinical trial. *Journal of Clinical Oncology* **31**, 4085–4091 (2013).

183. Gilbert, M. R. *et al.* A Randomized Trial of Bevacizumab for Newly Diagnosed Glioblastoma. *New England Journal of Medicine* **370**, 699–708 (2014).

184. Chinot, O. L. *et al.* Bevacizumab plus Radiotherapy–Temozolomide for Newly Diagnosed Glioblastoma. *New England Journal of Medicine* **370**, 709–722 (2014).

185. Weller, M. *et al.* Rindopepimut with temozolomide for patients with newly diagnosed, EGFRvIII-expressing glioblastoma (ACT IV): a randomised, double-blind, international phase 3 trial. *The Lancet Oncology* **18**, 1373–1385 (2017).

186. Mehta, M., Wen, P., Nishikawa, R., Reardon, D. & Peters, K. Critical review of the addition of tumor treating fields (TTFields) to the existing standard of care for newly diagnosed glioblastoma patients. *Critical Reviews in Oncology/Hematology* vol. 111 60–65 Preprint at https://doi.org/10.1016/j.critrevonc.2017.01.005 (2017).

187. Liu, Y. *et al.* Clinical efficacy of tumor treating fields for newly diagnosed glioblastoma. *Anticancer Research* **40**, 5801–5806 (2020).

188. Stupp, R. *et al.* Effect of tumor-treating fields plus maintenance temozolomide vs maintenance temozolomide alone on survival in patients with glioblastoma a randomized clinical trial. *JAMA - Journal of the American Medical Association* **318**, 2306–2316 (2017).

189. Lassman, A. B., Joanta-Gomez, A. E., Pan, P. C. & Wick, W. Current usage of tumor treating fields for glioblastoma. *Neuro-Oncology Advances* **2**, (2020).

190. Fabian, D. *et al.* Treatment of glioblastoma (GBM) with the addition of tumor-treating fields (TTF): A review. *Cancers* vol. 11 Preprint at https://doi.org/10.3390/cancers11020174 (2019).

191. Rominiyi, O. *et al.* Tumour treating fields therapy for glioblastoma: current advances and future directions. *British Journal of Cancer* vol. 124 697–709 Preprint at https://doi.org/10.1038/s41416-020-01136-5 (2021).

192. Davies, A. M., Weinberg, U. & Palti, Y. Tumor treating fields: a new frontier in cancer therapy. *Ann N Y Acad Sci* **1291**, 86–95 (2013).

193. Blumenthal, D. T. *et al.* Is more better? the impact of extended adjuvant temozolomide in newly diagnosed glioblastoma: A secondary analysis of EORTC and NRG Oncology/RTOG. *Neuro-Oncology* **19**, 1119–1126 (2017).

194. Gramatzki, D. *et al.* Limited role for extended maintenance temozolomide for newly diagnosed glioblastoma. *Neurology* **88**, 1422–1430 (2017).

195. Balañá, C. *et al.* Should we continue temozolomide beyond six cycles in the adjuvant treatment of glioblastoma without an evidence of clinical benefit? A cost analysis based on prescribing patterns in Spain. *Clinical and Translational Oncology* **16**, 273–279 (2014).

196. Weller, M. *et al.* EANO guidelines on the diagnosis and treatment of diffuse gliomas of adulthood. *Nature Reviews Clinical Oncology* **18**, 170–186 (2021).

197. Sinigaglia, M. *et al.* Imaging-guided precision medicine in glioblastoma patients treated with immune checkpoint modulators: research trend and future directions in the field of imaging biomarkers and artificial intelligence. *EJNMMI Research* vol. 9 Preprint at https://doi.org/10.1186/s13550-019-0542-5 (2019).

198. Colombo, M. C. *et al.* Towards the personalized treatment of glioblastoma: Integrating patient-specific clinical data in a continuous mechanical model. *PLoS ONE* **10**, (2015).

199. Sotoudeh, H. *et al.* Artificial intelligence in the management of glioma: Era of personalized medicine. *Frontiers in Oncology* vol. 9 Preprint at https://doi.org/10.3389/fonc.2019.00768 (2019).

200. Medical imaging in personalised medicine: a white paper of the research committee of the European Society of Radiology (ESR). *Insights into Imaging* **2**, 621–630 (2011).

201. Schork, N. J. Artificial Intelligence and Personalized Medicine. in 265–283 (2019). doi:10.1007/978-3-030-16391-4_11.

202. McDonald, K. L., Aw, G. & Kleihues, P. Role of biomarkers in the clinical management of glioblastomas: What are the barriers and how can we overcome them? *Frontiers in Neurology* vol. 3 JAN Preprint at https://doi.org/10.3389/fneur.2012.00188 (2013).

203. Hottinger, A. F., Homicsko, K., Negretti, L., Lhermitte, B. & Stupp, R. Decision making and management of gliomas: Practical considerations. *Annals of Oncology* **23**, (2012).

204. Staedtke, V., Dzaye, O. D. a. & Holdhoff, M. Actionable Molecular Biomarkers in Primary Brain Tumors. *Trends in Cancer* vol. 2 338–349 Preprint at https://doi.org/10.1016/j.trecan.2016.06.003 (2016).

205. Szopa, W., Burley, T. A., Kramer-Marek, G. & Kaspera, W. Diagnostic and therapeutic biomarkers in glioblastoma: Current status and future perspectives. *BioMed Research International* vol. 2017 Preprint at https://doi.org/10.1155/2017/8013575 (2017).

206. Stupp, R. *et al.* Effects of radiotherapy with concomitant and adjuvant temozolomide versus radiotherapy alone on survival in glioblastoma in a randomised phase III study: 5-year analysis of the EORTC-NCIC trial. *The Lancet Oncology* **10**, 459–466 (2009).

207. Wick, W. *et al.* MGMT testing—the challenges for biomarker-based glioma treatment. *Nature Reviews Neurology* **10**, 372–385 (2014).

208. Pineda, E. *et al.* Glioblastoma gene expression subtypes and correlation with clinical, molecular and immunohistochemical characteristics in a homogenously treated cohort: GLIOCAT project. *Journal of Clinical Oncology* **37**, 2029–2029 (2019).

209. Esteller, M., Hamilton, S. R., Burger, P. C., Baylin, S. B. & Herman, J. G. Inactivation of the DNA repair gene O6-methylguanine-DNA methyltransferase by promoter hypermethylation is a common event in primary human neoplasia. *Cancer Res* **59**, 793–7 (1999).

210. Wu, J. *et al.* Radiological tumour classification across imaging modality and histology. *Nature Machine Intelligence* **3**, 787–798 (2021).

211. Zhao, J. *et al.* Immune and genomic correlates of response to anti-PD-1 immunotherapy in glioblastoma. *Nature Medicine* **25**, 462–469 (2019).

212. Wolchok, J. D. *et al.* Nivolumab plus Ipilimumab in Advanced Melanoma. *New England Journal of Medicine* **369**, 122–133 (2013).

213. Garon, E. B. *et al.* Pembrolizumab for the Treatment of Non–Small-Cell Lung Cancer. *New England Journal of Medicine* **372**, 2018–2028 (2015).

214. Ansell, S. M. *et al.* PD-1 Blockade with Nivolumab in Relapsed or Refractory Hodgkin's Lymphoma. *New England Journal of Medicine* **372**, 311–319 (2015).

215. Neveu, P. J. *CEREBRAL LATERALIZATION AND THE IMMUNE SYSTEM*. (2002).

216. Sumner, R. C., Parton, A., Nowicky, A. v., Kishore, U. & Gidron, Y. Hemispheric lateralisation and immune function: A systematic review of human research. *Journal of Neuroimmunology* vols. 240–241 1–12 Preprint at https://doi.org/10.1016/j.jneuroim.2011.08.017 (2011).

217. Stoyanov, Z., Decheva, L., Pashalieva, I. & Nikolova, P. Brain asymmetry, immunity, handedness. *Central European Journal of Medicine* vol. 7 1–8 Preprint at https://doi.org/10.2478/s11536-011-0121-2 (2012).

218. Barn6oud, P., Neveu, P. J., Vitiello, S., Morm6de, P. & le Moal, M. *Brain neocortex immunomodulation in rats*. (1988).

219. AbdelRazek, M. A. *et al.* Unilateral Relapsing Primary Angiitis of the CNS: An Entity Suggesting Differences in the Immune Response Between the Cerebral Hemispheres. *Neurology(R) neuroimmunology & neuroinflammation* **8**, (2021).

220. Fu, Q. L. *et al.* Brain interleukin asymmetries and paw preference in mice. *Neuroscience* **116**, 639–647 (2003).

221. Ramadhani, M. K. *et al.* Innate left handedness and risk of breast cancer: Case-cohort study. *British Medical Journal* **331**, 882–883 (2005).

222. Lu, V. M. *et al.* The prognostic significance of CDKN2A homozygous deletion in IDH-mutant lower-grade glioma and glioblastoma: a systematic review of the contemporary literature. *Journal of Neuro-Oncology* vol. 148 221–229 Preprint at https://doi.org/10.1007/s11060-020-03528-2 (2020).

223. Mertes, F. *et al.* Targeted enrichment of genomic DNA regions for next-generation sequencing. *Briefings in Functional Genomics* vol. 10 374–386 Preprint at https://doi.org/10.1093/bfgp/elr033 (2011).

224. Talevich, E., Shain, A. H., Botton, T. & Bastian, B. C. CNVkit: Genome-Wide Copy Number Detection and Visualization from Targeted DNA Sequencing. *PLoS Computational Biology* **12**, (2016).

225. Dobin, A. *et al.* STAR: Ultrafast universal RNA-seq aligner. *Bioinformatics* **29**, 15–21 (2013).

226. Liao, Y., Smyth, G. K. & Shi, W. FeatureCounts: An efficient general purpose program for assigning sequence reads to genomic features. *Bioinformatics* **30**, 923–930 (2014).

227. Hänzelmann, S., Castelo, R. & Guinney, J. *GSVA: gene set variation analysis for microarray and RNA-Seq data*. *BMC Bioinformatics* vol. 14 http://www.biomedcentral.com/1471-2105/14/7http://www.bioconductor.org.Background (2013).

228. Carter, S. L. *et al.* Absolute quantification of somatic DNA alterations in human cancer. *Nature Biotechnology* **30**, 413–421 (2012).

229. Yoshihara, K. *et al.* Inferring tumour purity and stromal and immune cell admixture from expression data. *Nature Communications* **4**, (2013).

230. Ma, S. *et al.* Prognostic impact of CDKN2A/B deletion, TERT mutation, and EGFR amplification on histological and molecular IDH-wildtype glioblastoma. (2020) doi:10.1093/noajnl/vdaa126/5908751.

231. Li, M. *et al. CDK4/6 inhibition is more active against the glioblastoma proneural subtype*. vol. 8 www.impactjournals.com/oncotarget (2017).

232. Goldhoff, P. *et al.* Clinical Stratification of Glioblastoma Based on Alterations in Retinoblastoma Tumor Suppressor Protein (RB1) and Association With the Proneural Subtype. *Journal of Neuropathology & Experimental Neurology* **71**, 83–89 (2012).

233. Hobbs, J. *et al. Paradoxical Relationship Between the Degree of EGFR Amplification and Outcome in Glioblastomas*. www.R-project.org (2012).

234. Ray, A. *et al.* Targeting PD1-PDL1 immune checkpoint in plasmacytoid dendritic cell interactions with T cells, natural killer cells and multiple myeloma cells. *Leukemia* vol. 29 1441–1444 Preprint at https://doi.org/10.1038/leu.2015.11 (2015).

235. Reynes G *et al.* Marcadores moleculares, inmunológicos y de imagen en glioblastoma primario. Datos preliminares. GEINO 2019. in *Simposio anual del Grupo Español de Investigación en Neuro-Oncología (GEINO)* (2019).

Appendix A

Supplemental material of Chapter 3

Table S3.1. Information about the Magnetic Resonance Imaging (MRI) acquisition parameters.

MRI Modalities	TR (ms)	TE (ms)	Flip angle	Slice Thickness (mm)	Number of temporal positions
T1c	1940	10	12	5	
T2	3200	90	90	2-3	-
FLAIR	11000	140	90	2-3	-
DSC	1500	25	60	5	48

Table S3.2. Demographic, clinical and MRI-related data of included patients with *IDH*-wildtype glioblastoma (n=17) and *IDH*-mutant astrocytoma (n=2)

	IDH-wildtype glioblastoma	*IDH*-mutant astrocytoma
Median age (years old)	61	41
Gender (#F;#M)	8; 9	2; 0
Initial KPS	90	100
Median Weight (kg)	95.0	79.8
Median Height (cm)	173.0	173.0
Tumor location (#right; #left)	13; 4	1; 1
#patients with complete chemotherapy/#patients with incomplete chemotherapy	15/17	2/2
#patients with complete radiotherapy/#patients with incomplete radiotherapy	16/17	2/2

Table S3.3. Comparative table with previous studies reported in literature related with the correlation between perfusion MRI and vascular features defined by histopathological analyses.

	Human cohort	#Patients	#Tissue samples	Diagnostic MRI[a]	Spatial corregistration [b]	Continuous histopathologic variable[c]
Aronen HJ *et al.*; 1994 [14]	✓	5 WHO IV (+14 other gliomas)	Not specified	✗	✗	✗

Cha S *et al.*; 2003 [17]	✗	34 mice	34	NA	✗	✗
Chakhoyan *A et al.*; 2019 [18]	✓	4 WHO IV (+7 WHO III)	Not specified. 1-3 per tumor	✗	✓	✓
Hu LS *et al.*; 2012 [8]	✓	12 WHO IV (+12 other gliomas)	21	✗	✓	✓
Pathak AP *et al.*; 2001 [10]	✗	12 rats with gliosarcoma	Over 3 slices per tumor	NA	✓	✓
Sadegui N *et al.*; 2008 [19]	✓	2 WHO IV (+17 other gliomas)	8	✗	✓	✓
Sugahara T *et al.*; 1998 [20]	✓	11 WHO IV (+19 other gliomas)	Not specified	✗	✓	✗
Present study	✓	17 WHO IV	73	✓	✓	✓

Diagnostic MRI[a]: Use of the initial MRI study performed as standard in the diagnosis of glioblastoma; **Spatial corregistration**[b]: Spatial corregistration between the MR images and the tissue samples; **Continuous histopathologic variable**[c]**:** Area/volume of microvascular structures; **NA**: Not aplicable.

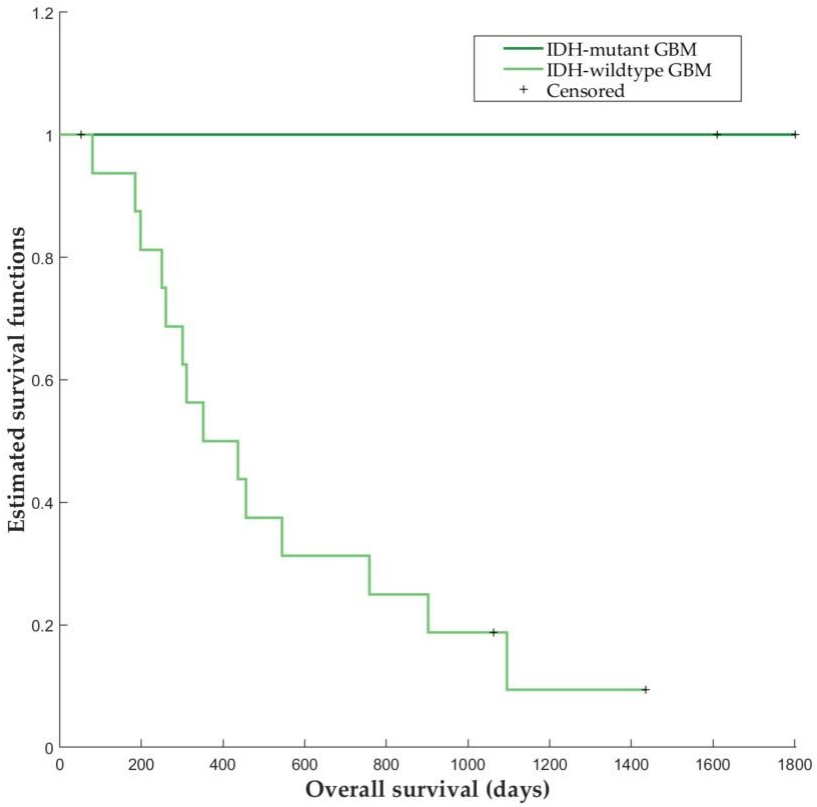

Figure S3.1. Kaplan Meier curves with the estimated survival functions for IDH-wildtype and IDH-mutant glioblastoma patients from the Ivy GAP database included in the study.

Appendix B

Supplemental material of Chapter 4

Table S4.1. Vascular key terms selected to filter genes of interest.

Vascular terms
vascular
vasculature
blood vessel
microvessel
angiogenesis
hypoxia
necrosis
capillary
glomerulus
glomerular

Table S4.2. Differences in rCBV between *IDH*-mutant astrocytoma and *IDH*-wildtype glioblastoma, and Mann Whitney results.

	***IDH*-mutant astrocytoma (n = 16)**	***IDH*-wildtype glioblastoma (n = 283)**	**Mann Whitney test results**
	Median [min, max]	Median; [min, max]	p-value
HAT-rCBV$_{mean}$	4.6 [2.2, 9.1]	6.9 [2.8, 20.0]	0.0007*
HAT-rCBV$_{median}$	4.7 [2.0, 9.1]	6.5 [2.3, 18.4]	0.0005*
HAT-rCBV$_{max}$	7.4 [3.4, 20.2]	11.0 [4.2, 34.2]	0.0010*
LAT-rCBV$_{mean}$	2.5 [1.1, 3.9]	3.5 [1.1, 9.6]	0.0002*
LAT-rCBV$_{median}$	2.5 [1.1, 3.9]	3.4 [1.2, 9.6]	0.0002*
LAT-rCBV$_{max}$	4.1 [1.5, 6.0]	5.3 [2.2, 15.7]	0.0002*

Significant difference: $p<0.05$*

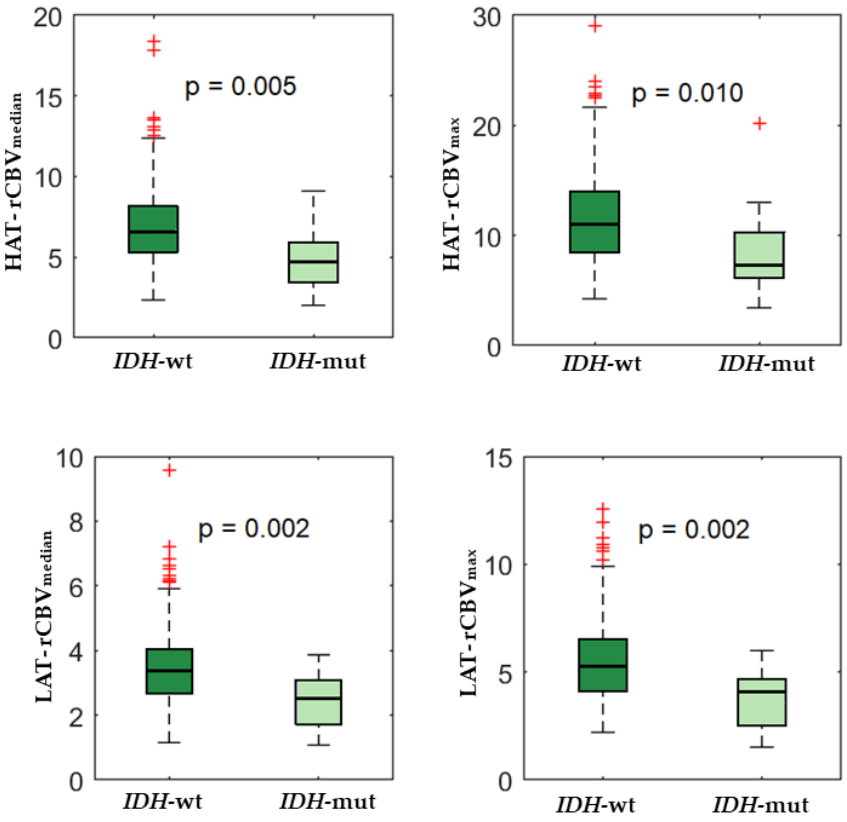

Figure S4.1. Boxplot showing differences in perfusion ($rCBV_{mean}$ and $rCBV_{median}$ at HAT and LAT habitats) between glioblastomas *IDH*-wildtype and astrocytomas *IDH*-mutant grade 4.

Appendix C

Supplemental material of Chapter 5

Table S5.1. Summary of the magnetic resonance imaging (MRI) acquisition parameters per center.

	MFS		TR (ms)	TE (ms)	Matrix (mm)	Slice thickness (mm)	FOV (cm^2)	Number of dynamics
H Ribera[a]	1.5T	T1	25	4.6	268x268	0.9	24x24	-
		T2	2000	120	320x199	5.0	23x18.3	-
		FLAIR	1100	140	256x164	6.0	23x18.3	-
		DSC	1650	40	116x116	2.2	24x24	80
H Manises[b]	1.5T	T1	500	20	304x241	5.0	24x24	-
		T2	2000	120	304x228	5.0	24x24	-
		FLAIR	11000	140	256x209	6.0	24x24	-
		DSC	836	30	128x128	5.0	24x24	40
C Barcelona[c]	3.0T	T1	12	4.68	256x256	1.0	24x24	-
		T2	3000	80	256x256	5.0	24x24	-
		FLAIR	9000	164	256x256	5.0	24x24	-
		DSC	1550	32	128x128	5.0	24x24	50
H Vall d'Hebron[d]	3.0T	T1	253	2.64	320x180	4.0	22x16.5	-
		T2	6100	91	512x326	4.0	22x17.5	-
		FLAIR	9000	68	320x288	4.0	22x19.8	-
		DSC	1450	45	128x128	5.0	23x23	60
AO Parma[e]	3.0T	T1	8.18	8.18	256x256	1.0	24x24	-
		T2	6500	65.90	160x160	4.0	24x24	-
		FLAIR	12000	96.72	384x224	4.0	24x24	-
		DSC	1500	30	128x128	4.0	24x24	60
CH Liège[f]	1.5T	T1	13	4.76	256x218	1.0	25x25	-
		T2	5000	109	384x384	5.0	23x23	-
		FLAIR	9000	90	256x173	5	23x23	-
		DSC	1460	47	128x128	5	23x25	50
Oslo UH[g]	3.0T	T1	5.2	2.3	512x512	1.0	25.6x25.6	-
		T2	3800	84	896x896	3.0	22.0x22.0	-
		FLAIR	4800	325	512x512	0.9	25.6x25.6	-
		DSC	1500	25/105	128x128	5.0	25.6x25.6	100

Hospital de la Ribera[a]; Hospital de Manises[b]; Clinic de Barcelona[c]; Hospital Vall d'Hebron[d]; Azienda Ospedaliero-Universitaria di Parma[e]; Centre Hospitalier Universitaire de Liège[f]; Oslo University Hospital[g]; MFS: Magnetic Field Strength; TR: Repetition Time; TE: Echo Time; FOV:

Field of View; T1: pre gadolinium T1-weighted; T1c: post gadolinium T1-weighted; T2: T2-weighted, FLAIR: FLuid-Attenuated Inversion Recovery; DSC: Dynamic Susceptibility Contrast

Table S5.2. Summary of patients excluded and included per hospital.

	H Ribera[a]	H Manises[b]	C Barcelona[c]	H Vall d'Hebron[d]	AO Parma[e]	CH Liège[f]	Oslo UH[g]	*TOTAL*
Initial	10	14	28	34	42	34	34	196
Excluded	3	0	5	2	2	1	2	15
Included	7	14	25	33	40	33	32	**184**

Hospital de la Ribera[a]; Hospital de Manises[b]; Clinic de Barcelona[c]; Hospital Vall d'Hebron[d;] Azienda Ospedaliero-Universitaria di Parma[e]; Centre Hospitalier Universitaire de Liège[f]; Oslo University Hospital[g]

Table S5.3.1. Results of the pair-wise Mann Whitney analyses for HAT markers

	Hospital de la Ribera	*Hospital de Manises*	*Clinic de Barcelona*	*Hospital Vall d'Hebron*	*Azienda Ospedaliero-di Parma*	*Centre Hospitalier de Liège*	*Oslo University Hospital*
Hospital de la Ribera		0.3139	0.6816	0.1762	0.1937	0.4765	0.0959
Hospital de Manises			0.0363*	0.6170	0.7899	0.1111	0.7292
Clinic de Barcelona				0.0258*	0.0124*	0.2091	0.0017*
Hospital Vall d'Hebron					0.6063	0.1302	0.1584
Azienda Ospedaliero-di Parma						0.0504	0.3557
Centre Hospitalier de Liège							0.0085*

Table S5.3.2. Results of the pair-wise Mann Whitney analyses for LAT markers

	Hospital de la Ribera	*Hospital de Manises*	*Clinic de Barcelona*	*Hospital Vall d'Hebron*	*Azienda Ospedaliero-di Parma*	*Centre Hospitalier de Liège*	*Oslo University Hospital*
Hospital de la Ribera		0.0932	0.3384	0.1445	0.0914	0.2401	0.0135*
Hospital de Manises			0.1243	0.6170	0.7003	0.2794	0.5586
Clinic de Barcelona				0.1317	0.932	0.5300	0.0103*
Hospital Vall d'Hebron					0.7690	0.3832	0.0844
Azienda Ospedaliero-di Parma						0.2423	0.1392
Centre Hospitalier de Liège							0.0228*

Table S5.3.3. Results of the pair-wise Mann Whitney analyses for IPE markers

	Hospital de la Ribera	*Hospital de Manises*	*Clinic de Barcelona*	*Hospital Vall d'Hebron*	*Azienda Ospedaliero-di Parma*	*Centre Hospitalier de Liège*	*Oslo University Hospital*
Hospital de la Ribera		0.0932	0.0917	0.1016	0.2500	0.1349	0.1383
Hospital de Manises			0.8262	0.6170	0.2910	0.7011	0.3457
Clinic de Barcelona				0.8752	0.3771	0.9624	0.5253
Hospital Vall d'Hebron					0.2949	0.9387	0.6227
Azienda Ospedaliero-di Parma						0.2848	0.7296
Centre Hospitalier de Liège							0.6698

Table S5.3.4. Results of the pair-wise Mann Whitney analyses for VPE markers

	Hospital de la Ribera	*Hospital de Manises*	*Clinic de Barcelona*	*Hospital Vall d'Hebron*	*Azienda Ospedaliero-di Parma*	*Centre Hospitalier de Liège*	*Oslo University Hospital*
Hospital de la Ribera		0.0676	0.0754	0.0299*	0.1937	0.0462*	0.4103
Hospital de Manises			1.0000	0.8615	0.2030	0.8433	0.0678
Clinic de Barcelona				0.8260	0.2275	0.9374	0.0546
Hospital Vall d'Hebron					0.0931	0.8174	0.0160*
Azienda Ospedaliero-di Parma						0.1117	0.5595
Centre Hospitalier de Liège							0.0280*

Table S5.4. Cox regression results obtained by performing the analysis with the OS and $rCBV_{max}$ data from each center.

		Hospital de la Ribera	*Hospital de Manises*	*Clinic de Barcelona*	*Hospital Vall d'Hebron*	*Azienda Ospedaliero-di Parma*	*Centre Hospitalier de Liège*	*Oslo University Hospital*
#patients		7	14	25	33	40	33	32
HAT	HR	1.00	1.04	1.10	1.10	1.07	0.98	1.09
	CIs	[0.84,1.20]	[0.96, 1.13]	[0.96, 1.28]	[0.98, 1.23]	[0.98, 1.18]	[0.86,1.12]	[1.00, 1.20]
LAT	HR	1.08	1.11	1.07	1.33	1.11	0.96	1.15
	CIs	[0.64, 1.81]	[0.89, 1.37]	[0.79, 1.44]	[0.98, 1.80]	[0.95, 1.30]	[0.77, 1.28]	[0.97, 1.36]
IPE	HR	1.95	1.76	1.01	1.73	1.40	1.10	1.54
	CIs	[0.5, 7.65]	[0.80, 3.89]	[0.61, 1.65]	[0.65, 4.61]	[0.97, 2.01]	[0.64, 1.90]	[0.92, 2.57]

Appendix D

Supplemental material of Chapter 7

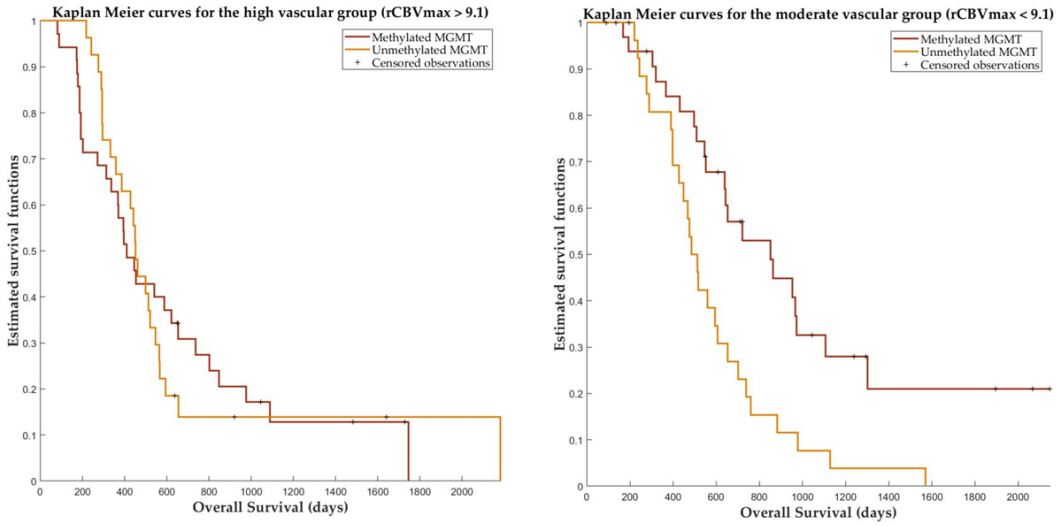

Figure S.7.1. Kaplan Meier curves for the moderate vascular group (left) and for the high vascular group (right) depending on the *MGMT* methylation status. Vascular groups are defined by the threshold of the study cohort: median $rCBV_{max}$ (th = 9.1).

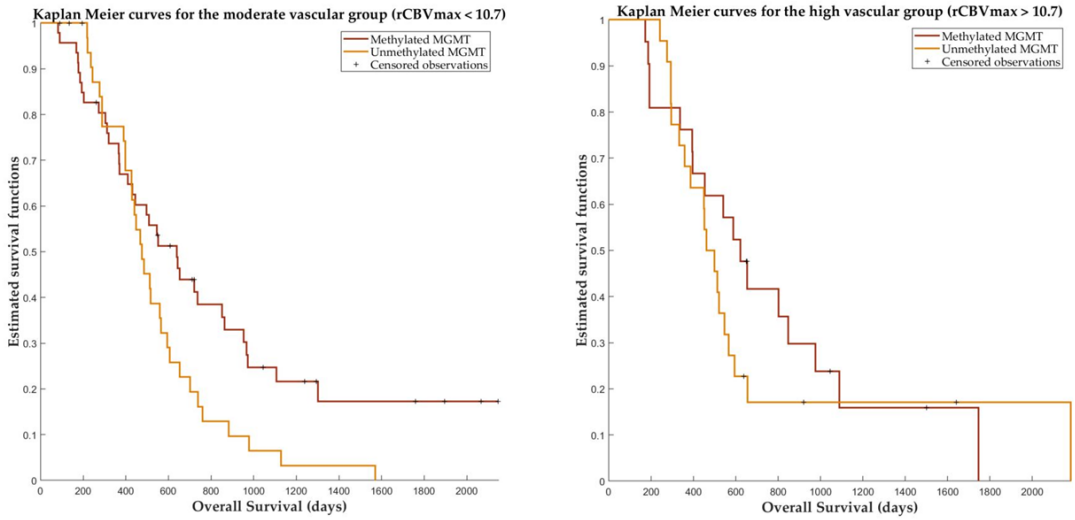

Figure S.7.2. Kaplan Meier curves for the moderate vascular group (left) and for the high vascular group (right) depending on the *MGMT* methylation status. Vascular groups are defined by the threshold proposed in the previous study (49) (th = 10.7).

Appendix E

Supplemental material of Chapter 8

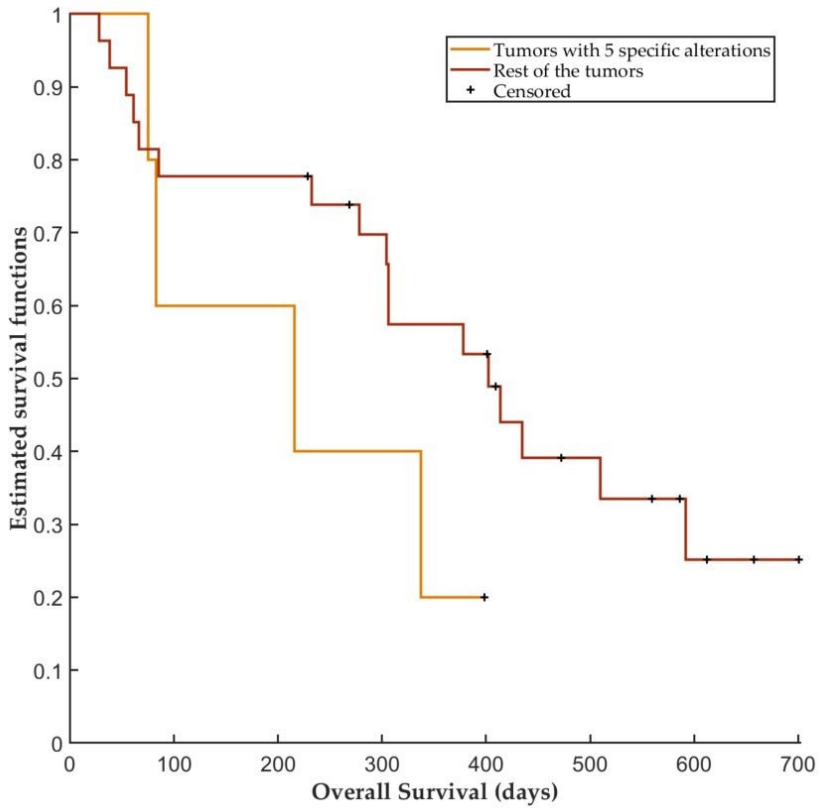

Figure S.8.1. Kaplan Meier curves for the group of patients with the five following alterations in the same tumor: *CDKN2A/B, CDK4/6, RB1, EGFR and PTEN,* and for the rest of the patients.

Somatic mutations

To identify somatic mutations from WES data, the variant-calling software SAVI2 was applied. Specifically, we first generated a list of variant candidates by successively eliminating positions without variant reads, positions with low sequencing depth, positions that were biased for one strand, and positions that contained only low-quality reads. Then, the numbers of high-quality reads for forward-strand reference alleles, reverse-strand reference alleles, forward-strand nonreference alleles, and reverse-stand non-reference alleles were calculated at the remaining candidate positions to build the prior and the posterior distribution of mutation allele fraction. Finally, somatic mutations were identified on the basis of the posterior distribution of differences in mutation allele fraction between normal and tumor samples.

CNVkit[224]

This kit uses both the targeted reads and the nonspecifically captured off-target reads to infer copy number evenly across the genome. This combination achieves exon-level resolution in targeted regions to detect copy number changes. It can be inferred copy

number at equivalent to 100-kilobase resolution genome-wide from a platform targeting as few as 293 genes. After normalizing read counts to a pooled reference, an evaluation and correction from three sources of bias that explain most of the extraneous variability in the sequencing read depth: GC content, target footprint size and spacing, and repetitive sequences. CNVkit is freely available from https://github.com/etal/cnvkit.

Appendix F

Supplemental material of Chapter 9

Regulatory / Ethics status

This prospective low-interventional clinical study falls under the Regulation EU No 2017/745 (Medical Device Regulation) as the intention is the creation of a software for medical applications.

The study includes several additional diagnostic procedures that are added on top of the normal practice: advanced MRI, questionnaires, neuropsychological assessment, use of investigational medicinal products – radiopharmaceuticals.

Therefore, the study falls under the EU regulation No 536/2014. The additional diagnostic procedures will be performed during the standard follow-up intervals and thus not leading to major increase of the diagnostic time or the number of visits in the hospital and thus not presenting a major additional burden to the patient, thus justifying the low-interventional status of the study. For each clinical centre a local approval will be needed of the respective university ethics committees. Ethics approval must be granted.

II. Scientific advice / protocol assistance

EUnetHTA is to-date not involved, e.g. through their Early Dialogues Process, but the authors consider applying for advice to check details of the protocol.

III. Qualification advice

This is not a pharmacological intervention study, which would need EMA-guided qualification advice to assess treatment effects measures.

Ethical issues

The study will be developed according to the Declaration of Helsinki about ethical principles for clinical research in humans. By the other hand, the study will be following Good Clinical Practices Guidelines and The International Conference on Harmonisation (ICH) and regulatory requirements of the institutions involved.

According to the design of the study –an observational, prospective study, patients will be informed through the informed consent form, which must be signed in order to be included in the study. Furthermore, all personal data collected will be properly anonymized and identified by a code. Only the main researcher in each center involved could identify that code with clinical records. Treatment, communication and data cession of all participants will be managing according to the General Data Protection Regulation (GDPR).

Study protocol will be approved by ethical committees' authorities including ethical committees of the centers involved in the study like the Universitat Politècnica de

València. Results of the study will be published according to STROBE declaration in a relevant scientific journal.